Nano to Micro Scale Modeling of Hydrate Phase Transition Kinetics

Khuram Baig

Thesis for the degree of philosophiae doctor (PhD)
at the University of Bergen

2017

I. Scientific Environment

This scientific work was performed at the Department of Physics and Technology, Faculty of Mathematics and Natural Sciences, University of Bergen. The PhD thesis is developed under the supervision of Professor Bjørn Kvamme and co-supervision of Tatiana Kuznetsova.

This research was financially supported by the Research Council of Norway and industrial partners through the following projects:

- SSC-RAMORE, "Subsurface storage of CO2 - Risk assessment, monitoring and remediation", project number: 178008/I30
- FME-SUCCESS, project number: 804831
- PETROMAKS, "CO2 injection for extra production", project number: 801445
- Research Council of Norway, project number: 224857
- STATOIL ASA, contract number: 4502354080

II. Acknowledgements

Though only my name appears on the cover of this dissertation, a great many people who in one way or another have contributed to its production. I owe my gratitude to all those people who have made this dissertation possible and because of whom my PhD experience has been one that I will cherish forever. First and foremost, my utmost gratitude goes to my supervisor Professor Bjørn Kvamme for having faith in me and giving me the opportunity to work under him. His wide spectrum of knowledge, logical ways of thinking and personal attention have been of great value to me. The thesis would not have been completed without his immense support, advice and constructive feedback during the production of this thesis. I am deeply grateful to him for the long discussions that helped me sort out the technical details of my work. I always felt very comfortable while discussing problems with him because of his positive and friendly attitude as well as prompt feedback.

I would take this opportunity to thank my co-supervisor Professor Tatiana Kuznetsova, who helped me in dealing with challenges related to the use of computational resources available in the university. I also thank her for the guidance regarding computer related problems and paper writing.

I sincerely acknowledge the grant and support from the Research Council of Norway, STATOIL ASA and various industrial partners. I would also like to thank the Department of Physics and Technology at the University of Bergen for providing me with an academic environment where I could perform my research activities.

Here, I also want to acknowledge some of my colleagues who supported me in my work in one way or another. I am pleased to thank my colleague Muhammad Qasim, who shared the office with me and was deeply involved during my work and helped me to improve my programing skills. I also wish to thank Ashok Chejara, Mohammad Taghi Vafaei, Bjørnar Jensen and Khaled Jemai for providing a very good environment. I would also like to thank my friends Adil Rasheed and Attique ur Rehman for providing valuable feedback and special Asian foods during the end moments of thesis compilation.

My deepest thank goes to my family members for their persistent love and support. I am thankful to my father Aslam Baig, mother Farhat Aslam, father in-law Muhammad Akram and mother in-law Zahida Akram for their prayers and their continued support during the critical and difficult times. Finally, my sincere and deepest thanks to my dearest wife Sana and sweetest daughter Minsa, whose love and sacrifices always provided me extra energy and strength. I am very thankful to God for giving me such a nice and loving family.

III. List of Publications

Reviewed publications in scientific journals

K. Baig, B. Kvamme, T. Kuznetsova, and J. Bauman, Impact of water film thickness on kinetic rate of mixed hydrate formation during injection of CO2 into CH4 hydrate, AIChE Journal, Volume 61, Issue 11, 2015, pp. 3944–3957 (**Paper 7**)

B. Kvamme, M. Qasim, K. Baig and P. H. Kivelä, J. Bauman, Hydrate phase transition kinetics from Phase Field Theory with implicit hydrodynamics and heat transport, International Journal of Greenhouse Gas Control, Volume 29, 2014, pp. 263-278 (**Paper 6**)

B. Kvamme, K. Baig, M. Qasim and J. Bauman, Thermodynamics and Kinetic Modeling of CH4/CO2 Hydrates Phase transitions, International Journal of Energy and Environment, Volume 7, Issue 1, 2013, pp. 1-8 (**Paper 4**)

M. Qasim, K. Baig, B. Kvamme and J. Bauman, Mix Hydrate formation by CH4-CO2 exchange using Phase Field Theory with implicit Thermodynamics, International Journal of Energy and Environment, Volume 6, Issue 5, 2012, pp. 479-487 (**Paper 5**)

M. Qasim, B. Kvamme, and K. Baig, Phase field theory modeling of CH4/CO2 gas hydrates in gravity fields, International Journal of Geology, Volume 5, Issue 2, 2011, pp. 48-52 (**Paper 1**)

Publications in conference proceedings with review system

K. Baig, B. Kvamme and T. Kuznetsova, The Impact of Water Film Thickness on the Rate of Mixed Hydrate Formation, In Proceedings from the 8th International Conference on Gas Hydrates (ICGH8-2014), Beijing, China, 28 July - 1 August, 2014.

P. H. Kivelä, K. Baig, M. Qasim and B. Kvamme, Phase Field Theory Modeling of Methane Fluxes from Exposed Natural Gas Hydrate Reservoirs, American Institute of Physics Conference Proceedings, Volume 1504, Issue 1, 2012, pp. 351-363

B. Kvamme, K. Baig, M. Qasim and J. Bauman, Thermodynamic and Kinetic Modeling of Phase Transitions for CH4/CO2 Hydrates, In Proceedings from the 9th international conference on Heat and Mass transport, Harvard, Cambridge, USA, January 25-27, 2012, pp. 229-235

M. Qasim, K. Baig and B. Kvamme, Phase Field Theory modeling of Phase transitions involving hydrate, In Proceedings from the 9th international conference on Heat and Mass transport, Harvard, Cambridge, USA, January 25-27, 2012, pp. 222-228 (**Paper 3**)

M. Qasim, B. Kvamme and K. Baig, Modeling Dissociation and Reformation of Methane and Carbon Dioxide Hydrate using Phase Field Theory with implicit hydrodynamics, In Proceedings from the 7th international conference on gas hydrate (ICGH7), Edinburgh, Scotland, July 17, 2011- July 21, 2011, 9 pages (**Paper 2**)

Bjørn Kvamme, Khuram Baig, Jordan Bauman and Pilvi-Helinä Kvelä, Thermodynamics and Kinetic Modeling of CH4/CO2 Exchange in Hydrates, In Proceedings from the 7th international conference on gas hydrate (ICGH7), Edinburgh, Scotland, July 17, 2011- July 21, 2011, 9 pages

M. Qasim, B. Kvamme and K. Baig, Phase Field Theory Modeling of CH4/CO2 Gas Hydrates in Gravity Fields, In Proceedings from the European Conference of Chemical Engineering, Puerto De La Cruz, Tenerife, November 30-December 2, 2010, pp. 164-167

Oral and Poster Presentations

M. Zarifi, B. Kvamme and K. Baig, Hydrate phase transition kinetics using phase field theory including mineral impact, 65th Canadian Chemical Engineering Conference, Calgary, Canada, October 4–7, 2015.

K. Baig, B. Kvamme and T. Kuznetsova, The Impact of Water Film Thickness on the Rate of Mixed Hydrate Formation, In Proceedings from the 8th International Conference on Gas Hydrates (ICGH8-2014), Beijing, China, 28 July - 1 August, 2014.

B. Kvamme, K. Baig, M. Qasim and J. Bauman, Thermodynamic and Kinetic Modeling of Phase Transitions for CH4/CO2 Hydrates, Oral presentation at the 9th international conference on Heat and Mass transport, Harvard, Cambridge, USA, January 25-27, 2012

M. Qasim, K. Baig and B. Kvamme, Phase Field Theory modeling of Phase transitions involving hydrate, Oral presentation at the 9th international conference on Heat and Mass transport, Harvard, Cambridge, USA, January 25-27, 2012

Bjørn Kvamme, Khuram Baig, Jordan Bauman and Pilvi-Helinä Kvelä, Thermodynamics and Kinetic Modeling of CH4/CO2 Exchange in Hydrates, Oral presentation at the 7th international conference on gas hydrate (ICGH7), Edinburgh, Scotland, July 17, 2011- July 21, 2011

M. Qasim, B. Kvamme and K. Baig, Modeling Dissociation and Reformation of Methane and Carbon Dioxide Hydrate using Phase Field Theory with implicit hydrodynamics, Poster presentation at the 7th international conference on gas hydrate (ICGH7), Edinburgh, Scotland, July 17, 2011- July 21, 2011

M. Qasim, B. Kvamme and K. Baig, Phase Field Theory Modeling of CH4/CO2 Gas Hydrates in Gravity Fields, Oral presentation at the European Conference of Chemical Engineering, Puerto De La Cruz, Tenerife, November 30-December 2, 2010

IV. Abbreviations

CH4	Methane
C2H6	Ethane
C2H8	Propane
CMG	Computer Modelling Group
CNG	Compressed Natural Gas
CO2	Carbon Dioxide
DFT	Density Functional Theory
GHs	Gas Hydrates
LNG	Liquefied Natural Gas
NGHs	Natural Gas Hydrates
PFC	Phase Field Code
PFM	Phase Field Model
PFT	Phase Field Theory
MPI	Message Passing Interface
N2	Nitrogen
RCB	Retraso Code Bright
STARS	Steam Thermal and Advanced Processes Reservoir Simulator

V. List of Figures

VI. Table of Contents

1 Motivation

With the United Nations predicting a rapid increase in population and an increasing standard of living in developing countries led by China and India, energy demand is bound to grow rapidly. According to the International Energy Outlook 2013, the world energy consumption will increase from 534000 trillion BTU to 820000 trillion BTU by 2040 (E.I.A, 2013). As the world's carbon emission is expected to have the highest increase within the next two decades, adopting non-carbonized energies could minimize emissions to zero by the end of this century thereby restricting the global temperature rise to less than 2 degrees Celsius (Buffett & Zatsepina, 2000).

While there is a huge focus on renewable energy sources, it will take decades before they can replace high carbon concentrated fossil fuels to fulfill energy demands and carbon reduction requirements. According to energy outlook 2014, a major share of energy will be produced from carbon based sources like gas, oil, and coal at least till the mid of this century (ExxonMobil, 2014). Amongst the three sources, natural gas (NG) is the least poisoning and therefore, most suitable to replace coal as a primary source of energy thereby reducing CO2 emissions in the foreseeable future (E.I.A, 2013; IEA, 2015).

Unconventional sources of NG (tight gas, shale gas, and coal bed CH4) are already commercially viable and can strike a balance between supply and demand in the energy market. The huge boost in shale gas in the USA has turned the country into a net gas exporter rather than a huge importer. Another alternative that has huge potential are gas hydrates (GHs). They are present in large quantities in arctic regions under the permafrost and in oceanic sediments along the continental margins around the world. These reserves are enough to fulfill the future energy demands for a long time to come. Some estimates indicate that if just one thousandth part of the entire CH4 hydrate reserves is extracted that will be enough for meeting global energy demand for one year. (Nakicenovic, 2002).

Countries with limited conventional resources but with huge hydrate reserves like Japan, which is the second largest consumer of oil has negligible resource of a gas and therefore, the import is of the order of 98% of their fossil fuel needs. However, Japan is actively exploiting its own new energy resources like solar, wind, and GHs (Okuda, 2005). BSR results shown the presence of huge amounts of GHs reserves in the country (mainly distributed in the southwestern islands trench, Nankai Trough, Boso Peninsula East, the Kuril Trench, Japan sea east edge, Tatar Trough, and Okhotsk region). The spreading area is about 44,000 km^2 and total reserves is 40-63 times the national gas consumption (BP p.l.c., 2013; METI, 2001; Okuda, 1993; Satoh, et al., 1996). Japan Oil, Gas, and Metals National Corporation ("JOGMEC", Headquarter: Minato-ku, Tokyo, President: Hirobumi Kawano) conducted an offshore production test in the first phase off the coasts of Atsumi and Shima peninsulas using the depressurization method and confirmed production of 120000 cubic meters of CH4 gas from CH4 hydrate layers. Japan now plans to proceed with the second offshore production tests which are scheduled to be undertaken in the first half of 2017 (JOGMEC, 2013; JAPEX, 2016). Likewise Taiwan, whose average annual NG consumption is about 10 billion cubic meters and has 97.75% of its energy supply imported from abroad due to shortages of traditional energy resources (Bureau of Energy MOEA, 2015) can become self-sufficient if all (approximately 2.7 trillion cubic meters) of the hydrate resources present in Tainan-Pingtung coast is exploited (Weng, et al., 2013). These reserves can provide Taiwan with CH4 gas for the next 270 years, according to the existing reserves along the southwestern Taiwan seas. Conventional hydrocarbon is also declining in India and the country is looking for ways to exploit its huge hydrate reserves. China is also investing heavily in research targeted towards the exploitation of natural gas hydrates (NGHs) in land and marine areas. The country has an estimated amount of 107.7 trillion cubic meters of gas reserves in the form of hydrates and provided that these reserves are completely exploited, can provide NG for 749 years (Lu, 2015). Several other countries which are in a similar situation also have substantial offshore CH4 resources trapped in hydrates.

An interesting option for use of hydrate as a phase is storage of CO2 in the form of hydrate, like for instance in depleted hydrocarbon reservoirs that have proven cap rock

sealing and conditions of temperature and pressure that facilitate the CO2 hydrate formation. Injection of CO2 into NGHs filled sediments is yet another option. This method not only helps to reduce the climate emissions of greenhouse gases but also provides an interesting solution to produce CH4 from *in situ* GHs to fulfill the global energy needs. This hydrate production technology offers a win-win situation since released CH4 gas may compensate even more than the storage costs since the conversion is thermodynamically self-driven. The cost of CO2 injection and associated infrastructure (including transport to the actual site) is the only cost. CO2 forms a more stable hydrate than CH4 hydrate under the same thermodynamic conditions over a large range of temperatures and pressures. A mixed hydrate where CO2 stabilizes part of the structure (large cavities) and CH4 is filling the other part (mainly small cavities), is more stable compared to only CH4 hydrate over all ranges of temperature and pressure. The production of methane from GHs through the exchange process maintains the mechanical stability of the geologic formation. (Ors & Sinayuc, 2014; Chong, et al., 2015).

Besides storing CO2 in GHs reservoirs, there have been promising developments in the geological storage of CO2, which is a feasible alternative for reducing CO2 emissions into the atmosphere. These efforts also include storing CO2 as hydrate in the colder aquifers where temperature and pressure conditions are within the hydrate stability regions (e.g. northern parts of the North Sea and Barents Sea). The assessment of the potential GHs production requires predictions of their complex behavior. The reliability and accuracy of these predictions hinge on the availability of robust numerical simulators that describe the dominant processes and phenomena. The complexity of processes involved during GHs production like formation, dissociation, and reformation in reservoirs are motivating factors for developing a new reservoir simulator. This will give the possibility of studying the kinetics of CH4 and CO2 hydrates. Thermodynamic modeling of hydrate is one of the complex features in reservoirs as will be discussed in the coming chapters. Most hydrates that form or dissociate in industry or in nature are in situations of non-equilibrium and requires a great deal of modelling efforts and computational resources.

Through the scientific work documented in this thesis and the associated publications, we have developed a new approach for non-equilibrium theory of hydrates and a related Phase Field Theory (PFT) for modeling the kinetics of hydrate phase transitions. Non-equilibrium thermodynamics is very crucial to imitate the fact that hydrates in nature or in industry in most cases cannot reach any state of thermodynamic equilibrium. The Phase Field Model (PFM) is further extended to contain implicit heat transport and hydrodynamics which makes it possible to examine kinetic rates in systems of competing phase transitions of hydrate formation and hydrate dissociation. To the best of our knowledge, the current PFM is the most advanced theoretical treatment used for Nano to Micro scale studies of hydrate phase transition dynamics.

2 Introduction

NGHs are crystalline structures composed of water and gas molecules like CH4, CO2 and H2S. The water molecules form cage like structures due to hydrogen bonding, termed as cavities. Under suitable conditions of temperature and pressure (high pressure and low temperature), guest (CH4, CO2, etc.) molecules with favorable shapes and sizes can occupy these cavities (Koh, et al., 2011). A brief historical background of hydrate discovery, their structure and characteristics are described in sections 2.1 and 2.2 respectively.

Huge deposits of GHs are present at several locations around the world in permafrost areas and subsea (section 2.3). In subsea occurrences, the integrity of sealing structures of clay or shale traps the hydrate from contact with water that is under saturated with CH4. Similar sealing may be present in permafrost, but in these areas, even the thick ice layer provides tight sealing. The ice layer by itself is of course not inert with respect to the hydrate water and corresponding trapped hydrate formers inside the hydrate cavities. But in most cases these systems have developed over geological time scales and entered a state of stationary situation.

The thermodynamic instability of hydrates in contact with under saturated phases (water or gas) leads to dissociation of hydrate and corresponding leakages of CH4 into the oceans and eventually into the air. This is a huge concern due to the greenhouse nature of CH4, which might be roughly 25 times worse than CO2. Some of the climate hazards of CH4 are briefly discussed in section 2.3.1. In some cases, the hydrate instabilities can lead to disastrous dissociation scenarios causing landslides. A brief overview is given in section 2.3.2. Another important aspect of *in situ* hydrate is it being a huge source of trapped energy. NGHs deposits are therefore, an attractive unconventional source of fossil fuel for some countries. A brief overview of this aspect is given in section 2.3.3.

Existence of GHs rich in CH4 in abundance is a good motivation for creating safe techniques for CH4 flow out of the geological formation. Some most commonly proposed and studied techniques are briefly discussed in section 2.4.

The current industry concerns related to NGHs are discussed in section 2.5. Undesired formation of hydrates during transport and processing of hydrocarbons containing water has been a huge motivation for hydrate research in the past and is still a big concern for the oil and gas industry. A brief overview of the most important aspects is given in section 2.5.1. But besides the problems with hydrate formation there are also attractive possible industrial uses of the GHs. CH4 trapped inside hydrate is very dense packing so large volumes of CH4 can be encapsulated in a crystalline form. Therefore, storage and transport of CH4 and CO2 in the form of hydrate is one area for the utilization of hydrate as a phase. This, as well as some other uses of the GHs as a phase for industrial processes, is briefly described in section 2.5.2.

2.1 History of Hydrates

Historically, NGHs were discovered by Sir Humphrey Davy in 1810, when he noticed that a solid was formed above the ice point from a solution of chlorine gas and water known as oxymuriatic gas. It is speculated that before Davy's experiments, Priestly might had unintentionally produced SO2 hydrates. The GHs did not get much fame during the era and remained as a part of laboratory experiments, until 1934. (Koh, et al., 2011)

In 1934 an American chemist named E.G. Hammerschmidt discovered GHs in a pipeline (above the water freezing point) formed from the left over water after construction. Since then, lots of research has been done to predict and prevent hydrate formation in equipment and pipelines during processing or transport. Since the mid-1960s, the discovery of NGHs in deep oceans and permafrost regions has revolutionized the research in this field (Sloan & Koh, 2008).

2.2 Hydrate Structures

It is important to know that GHs are not chemical compounds since the encaged molecules are not bonded to the lattice. Actually, water molecules are held together by hydrogen bonds and mainly non-polar attractions to encaged molecules. These gas

molecules must fit into the water cavities (cages) in terms of volume. This work focuses on the guest molecules CO2 and CH4. Both the molecules form structure-I hydrate which is composed of two polyhedral (pentagonal dodecahedron and tetrakaidecahedron) formed by hydrogen-bonded water molecules as shown in Figure 2-1. The pentagonal dodecahedron normally known as 5^{12} (small cavity) has 12 pentagonal faces with equal edge lengths and equal angles. The tetrakaidecahedron has 12 pentagonal and 2 hexagonal faces and hence are known as $5^{12}6^2$ (large cavity). The two small cages are situated at the center of a unit cell (see Figure 2-1) and have one water molecule at each of its 20 vertices. Each large cavity consists of 24 water molecules and overall there are 46 water molecules per unit cell with an average length of 12.01Å. The length is normally treated as constant over the limited range of temperatures relevant for industrial hydrate occurrences. There are 2 small and 6 large cavities per unit cell giving a small to large cavity ratio of 1:3. Molecules (guest) having a diameter between 4.2 and 6Å such as CH4, CO2, C2H6 and H2S can form structure-I hydrates. (Sloan & Koh, 2008)

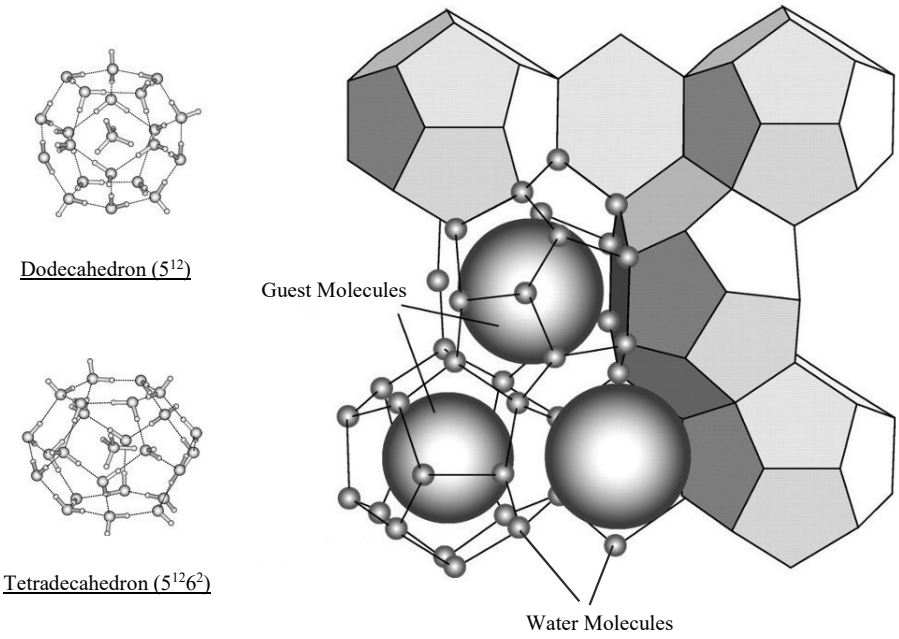

Figure 2-1:The unit cell of hydrate structure-I, and the cavities constituting the structure. (adopted from Grimme, et al. (2007) & Maslin, et al. (2010))

If we assume that all the cavities are filled with guest molecules, the mole percent of water would be 85 %. The repulsive nature of the guest molecules prevents hydrate cavities from collapses, either in a large quantity of neighboring cavities or in the cavity itself. The guest molecules also have some attraction towards water molecules, but it is the repulsion that is more important to maintain cavity expansion. In comparison to ice and liquid, hydrates have very different properties (like thermal conductivity, thermal expansion, and electrical conductivity). Hydrates can exist at temperatures higher than 0^{o}C and high pressures, which is the reason that the presence of water in hydrocarbon flows has been a problem in the oil and gas industry. The discussion is now narrowed down to focus only on CO2 and CH4. CO2 cannot stabilize into small cavities due to its size and shape compared to the available volume in the symmetric small cavity. There are some literatures available which provide evidence that CO2 may enter into the small cavities (Circone, et al., 2003) but available experimental evidences from different groups are not entirely consistent as

these findings are fairly recent. In this work our focus is on modeling leading to simplified kinetic models for hydrates in porous media related to hydrate formation using injection of CO2. It is still unverified whether CO2 filling in small cavities will really be significant under the dynamic flow conditions during those types of scenarios. So, within the scope of this work, CO2 is neglected in small cavities. On the other hand, CH4 can enter both small and large cavities, but CO2 out competes CH4 in the occupation of the large cavities in terms of mixed hydrate as CO2 has a larger stabilization impact on these cavities.

2.3 Hydrates in Nature

GHs in nature may occur on land in connotation with permafrost regions and below the seafloor in marine sediments. In contrast, GHs in a marine environment are likely to occur in continental margin sediments (Kvenvolden & Lorenson, 2001). The GHs appear to be filling up spaces between the grains and within the cracks and gaps in sediments on deep water continental shelves where the conditions lie within the GHs stability region. Such sediments may not have a high average saturation of GHs, this can be explained by the very small pore size and low permeability in clay-rich sediments hindering the mobility of both water and gas (both these components are essential for the formation of hydrates). GHs mostly occur in high concentrations in the sand units and are largely absent from the mud sequences (Tsuji, et al., 2009; Boswell & Collett, 2011; Boswell, et al., 2009). In the case of permafrost, GHs occurrences are identified in sand rich units deposited in onshore and near shore environments, typical examples are the occurrences in Alaska and Canada. The coexistence of thermogenic and biogenic gases at the Alaska North slope leads to two general scenarios for GHs formation 1) pre-existing gas reservoir converted into hydrates after favorable changes in temperature and pressure 2) gas migrated upwards into the stability zone leading to hydrate formation (Carman & Hardwick, 1983; Masterson, et al., 2001; Lorenson, et al., 2008; Dai, et al., 2011). The saturation of GHs in Mount Elbert site is around 60 – 75% based on the analyses of well-log data (Lee & Collett, 2011) and pore water geochemistry (Torres, et al., 2011). The upward

migration of deep thermogenic gases together with shallower biogenic gases gets trapped within the current GHs stability zone and changed into GHs bearing sediments well before the existence of permafrost. Preexisting free gas and high conductivity faults can explain the high hydrate saturations found on the North Slope (Dai, et al., 2011). Gibbs phase rule together with the consequences from the 1st and 2nd laws of thermodynamics explicates that GHs in sediments are thermodynamically in a state of non-equilibrium. This fact will be further explained in section 2.3.2.

2.3.1 Impact on climate

As mentioned earlier, NGHs are spread around the world containing huge amounts of CH4 gas. The GHs reservoirs are metastable and dynamic therefore, formation and dissociation of NGHs are continuous phenomena controlled by three factors; temperature, pressure, and concentration.

Hydrates of CH4 and/or CO2 are not thermodynamically stable due to Gibbs Phase rule (see section 2.3.2). From a thermodynamic point of view, the reason is simply that the water structure on hydrate surfaces are not able to obtain optimal interactions with surfaces of calcite, quartz, and other reservoir minerals. The impact of this is that hydrates are separated from the mineral surfaces by fluid channels. The sizes of these fluid channels are not known, and are basically not even unique in the sense that it depends on the local fluxes of all the fluids in addition to the surface thermodynamics. Stability of NGHs reservoirs therefore, depends on sealing or trapping mechanisms like that in ordinary oil and gas reservoirs. Many hydrate reservoirs are in a dynamic state where hydrates are leaking from top through the contact with groundwater/seawater which is under saturated with CH4. The seafloor at the sites of gas leakage in the Gulf of Mexico (MacDonald, et al., 1994) is a typical example in which GHs were breached. Some of the released CH4 from these GHs reserves is consumed by biological organisms that in result releases CO2 through biologically catalyzed Sulphur reactions. The large portion of the releasing CO2 will dissolve in the aqueous phase and may result in precipitation of solid carbonates. The presence of carbonates/bicarbonates ion effects the seawater PH which will become vital for the

existence of life (Boetius & Suess, 2004; Luff, et al., 2005). However, some of the CH4 remaining as CH4 gas can end up in the environment depending on the water depth and CH4 concentration in seawater (Yamamoto, et al., 2009). This is supported by field measurements done on the Santa Barbara site in California, where 50% of the CH4 emitted from large leakage site at a water depth around 20 to 70 m reaches the atmosphere (Kvenvolden & Harbaugh, 1983). According to this evidence, it was projected that only two fifths of the CH4 can reach the atmosphere from such a large submarine seepage (Kvenvolden, et al., 2001). CH4 is a very effective greenhouse gas (GHG). Although it is less abundant in the atmosphere it can be more than 20 times lethal in comparison to CO2 (Beget & Addison, 2007). Furthermore, enormous amount of CH4 is contained in a relatively small amount of hydrates ($1m^3$ of fully saturated CH4 hydrate contains approximately $164m^3$ of CH4 gas at standard condition of pressure and temperature) (Archer, 2007; Sloan & Koh, 2007; Max, et al., 2006). And since, CH4 hydrates are so abundant on the earth, dissociation of even a small fraction of it can cause catastrophic changes in the climate over even a small-time scale. Fortunately, most of the hydrates exist at depths where they are unaffected from the surface climate changes due to global warming for at least a time period of the order of 100 decades or longer (Archer, 2007).

2.3.2 Geo hazard

Beside a threat to the climate, GHs are also a submarine geo hazard (Xu & Germanovich, 2006; Nixon & Grozic, 2007). Submarine landslides and slope failures can be triggered by GHs dissociation (Sultan, et al., 2004; Locat & Lee, 2002). Study of GHs suggests its close relationship with the occurrences of landslides on the continental slope where GHs commonly form resulting in slope instability (McIver, 1982). One of the largest submarine landslides is the Storegga slide off the coast of Norway. It was probably triggered by a process involving GHs dissociation (Bouriak, et al., 2000) about 8000 years ago that covered a total volume of nearly 5000 km^3 and travelled from the western coast of Norway to the south of Iceland (Harbitz, 1992).

GHs cannot be stable in porous sediments due to Gibbs Phase rule, since temperature and pressure are always given in all local positions of a hydrate reservoir. Any number of degrees of freedom (no. of components - no. of phases + 2) other than two means that equilibrium is never possible. This will be the case with all hydrates in sediments. So, any deficit in trapping (shale and clay) will lead to hydrate dissociation through interactions with under saturated phases. The dissociation of hydrates may cause significant weakening of the sediment as shown in the studies on the strength of hydrates and hydrate saturated media performed by different researchers (Winters, et al., 2001; Cameron, et al., 1990; Parameswaran, et al., 1989) decreasing the resistance capability of the slope. GHs binds together with sediment particles and/or fills the voids preventing the potential compaction processes in the GHs stability region. Therefore, the hydrate dissociation may generate an under consolidated soil with a significant weakening of the soil. Another effect of hydrate dissociation on the slope failure is due to the release of water and free gas resulting in a significant volume expansion (approximately 100% expansion at 1000 meters water depth due to dissociation). If there are no channels through which excess water and gas can escape, an excess pore pressure will be generated. The excess pore pressure depends on the solubility of the dissolved gas (ratio of CH4 to water in the hydrate phase is around 150 times greater than the solubility of the dissolved gas) (Sultan, et al., 2004). Hence the dissociation of GHs will release a huge amount of CH4, much higher than the solubility of the dissolved CH4 gas. The effective stress greatly reduced due to the presence of excess pressure may reduce the slope's ability to resist the driving forces acting upon it. (Xinpo & Siming, 2012)

2.3.3 Gas hydrates as energy source

Estimated organic carbon bound in GHs vary depending on who is reporting the numbers. The estimates from US Geological Survey are frequently referred to. These numbers indicate that the carbon contained in worldwide hydrate reservoirs are twice the amount of carbon found in all known conventional fossil fuels worldwide (Collet, 2002; Demirbas, 2010). NGHs reserves around the world contain NG resources up to

50 times the conventional petroleum reserves, with as much as 2500 – 20,000 trillion cubic meters of CH4 (IEA, 2008).

NGHs are considered a potential source of energy mainly consisting of CH4 gas and they are present in the Arctic regions under the permafrost and in the oceanic sediments along the continental margins where suitable thermodynamic conditions prevail. GHs can provide energy with a little emission of CO2 into the environment (Lu, 2015; Moridis, et al., 2011; Letcher, 2014; Ruppel, 2011; Johnson, 2014). Over 230 potential reserves have been found globally in permafrost at depths ranging from 130 to 1100 m, and in offshore below mean sea level at continental margins between 800 to 4000 m water depth (Lu, 2015). These natural reserves could potentially meet global energy needs for the next 1000 years (Demirbas, 2010). This is a huge motivation for advanced research in this field.

2.4 Recovery Methods

NG can be produced from NGHs either by thermodynamic destabilization of the clathrate structure, yielding liquid water and gaseous CH4, or by exchanging the CH4 molecule with another guest molecule. The focus of this scientific work is the utilization of the novel method of exchanging CH4 with CO2 for the production of NG from hydrates. The motivation cannot be fully understood without understanding the challenges associated with other methods.

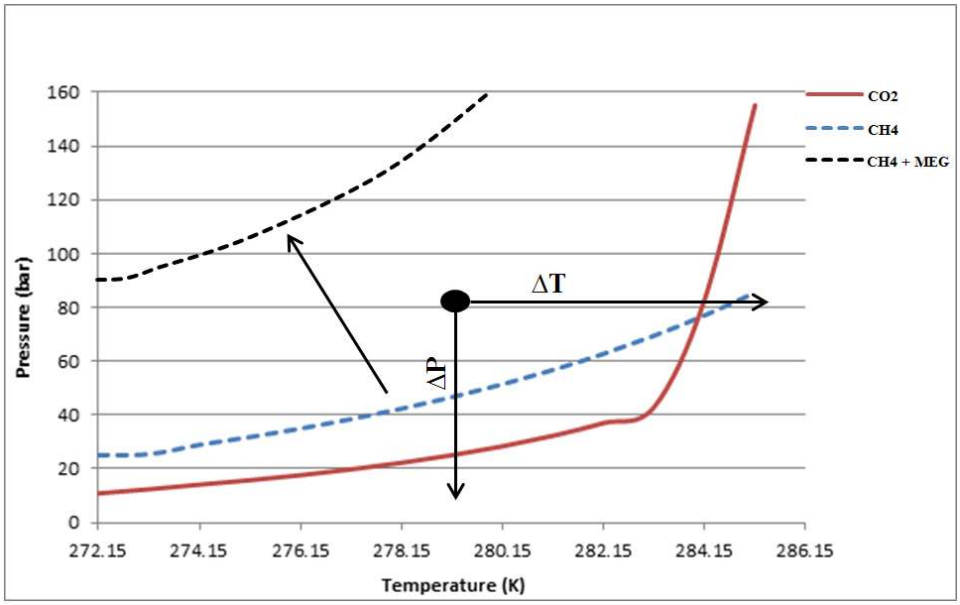

Figure 2-2: Schematic diagram of Natural gas hydrate recovery techniques.

The key production approaches to dissociate clathrate hydrates are 1) thermal stimulation: The hydrate temperature is raised above the stability point by using continuous energy source (hot brine injection, steam injection, cyclic steam injection, fire flooding, and electromagnetic heating) to dissociate, 2) depressurization: This technique involves lowering the hydrate pressure below the stability point resulting in rapid hydrate dissociation but with an associated drop in the hydrate temperature, and 3) inhibitor injection: The injection of an organic or inorganic compound (salts & alcohols like Ethylene glycol (MEG)) that shifts the hydrate stability point to lower temperatures for isobaric conditions. Inhibitor injection could require additional inhibitor or a heat source to compensate the decrease in hydrate temperature with dissociation. Figure 2-2 shows a schematic illustration of these production methods.

Based on these approaches, numerous tests were carried out around the world to extract the energy stored in GHs. Thermal stimulation tests were conducted in 2002 by the Japex, JNOC, and GSC (Huenges, et al., u.d.), and depressurization tests to produce CH4 from hydrate were conducted in 2008 by JOGMEC and NRCan in the Canadian Arctic off the Mackenzie Delta (Smith, u.d.). The extraction of CH4 from

hydrates under the seafloor was considered in Japan (MH21 Research Consortium, u.d.; Uchida & Tsuji, 2004). The first marine production is being tested by the MH21 research consortium to confirm the decompression procedure for the recovery of CH4 gas from GHs from 2012 to 2013 (MH21 Research Consortium, u.d.). Even though there are many challenges for practical recovery of CH4 hydrates, several major proposals presently being investigated include thermal treatment (Cranganu, 2009), depressurization (Liu Y, et al., 2009) and inhibitor addition (Demirbas, 2010). All these methods are based on promoting GHs dissociation by external stimulation. They are so far not used for commercial production of CH4 due to the related economic and potential environmental threats, except for Messoyakha field in Russia (Makogon, 1997). Production from Messoyakha field was originally set up as a conventional gas field and the existence of GHs was first known when they, along a timeline could see pressure increase again in contrast to pure conventional fields that would of course show a pressure decrease along the timeline (Makogon, 1997).

The natural occurrence for CO2 clathrate is an indication of the potential for hydrate sequestration of CO2. Even though CO2 clathrates are not naturally as plentiful as those of CH4, their occurrence forms the basis of an unconventional approach to producing gas by exchange of CO2 with CH4 in the hydrate structures. This unconventional concept has several potential benefits over the conventional methods: 1) maintaining mechanical stability of the geologic formation as CO2 hydrate is more stable than CH4 hydrate (Figure 2-2), and 2) storing CO2 helps in reducing GHGs emissions thereby, contributing to climate stability.

Water surrounding the hydrate will first be displaced by liquid CO2 during the injection process into the pores because of a higher affinity of minerals (compared to hydrates) towards water. This also depends on the wetting properties of the minerals. As an example, first few water layers adsorbed on hematite may have lower chemical potential by 2-4 kJ/mole than that of liquid water (Kvamme, et al., 2012). The free gas (if existing) *in situ* will dissolve to some extent in the injected CO2 if the mineral surface is CO2 wetted. In this case, the greater amount of the *in situ* water will surround the hydrate core inside the pores. The diffusion of CO2 into hydrate depends

on the diffusion rate of CO2 into porous medium depending on the properties of the medium like pore sizes, pore connections and porosity (Mu, et al., 2008). The conversion of CO2 into mix hydrate is directed by two mechanisms: The injected CO2 on contacting with residual liquid water in porous media will form pure CO2 hydrate, since hydrate formation is an exothermic process and the heat released (57.98kJ/mole) is larger than the heat required CH4 hydrate dissociation (54.49kJ/mole) (Chong, et al., 2015; Kvamme, et al., 2014). This heat will contribute to dissociate the surrounding CH4 hydrate. When all the residual water is consumed, then the conversion process will be governed by a solid state exchange mechanism which is substantially slower in comparison to the first mechanism (Kvamme, et al., 2014; Baig, et al., 2015). This hydrate exchange process is also possible with injection of CO2 and N2 mixture as also demonstrated in a field trial which was completed successfully in the Ignik Sikumi GHs field in Alaska North slope in 2012 (NETL, 2012).

2.5 Industrial Aspects of Hydrates

The focus of this thesis is on hydrates in porous media and the aspects of hydrate stability and dynamics of importance for CH4 production from hydrate, as well as on the storage of CO2 in hydrates. Nevertheless, industrial problems did fund a substantial portion of experimental data and theoretical development so a few words on industrial aspects is mentioned here.

2.5.1 Hydrate formation as an industrial problem

Water will always follow the hydrocarbon streams since the water is always produced along with the hydrocarbons. During processing of hydrocarbons, natural temperatures may be down to -22 C for dry gas with limited C2+ of value and down to -70 C in plants in which the C2+ is significant and/or contains valuable components like C2H6 or C3H8 which can be polymerized for manufacture of plastic products.

Pressure during processing is high. Typical units of hydrate formations in such a plant are connecting pipelines, expanders, and separators. Transport of NG or CO2

containing water through pipelines is typically at a pressure of 50 to 300 bars. With a maximum seafloor temperature in the North Sea around 6 ºC the whole transport line might be at a risk of plugging due to hydrate formation if the water content of the gas is too high. Additional pathway for hydrate formation in the pipeline is the presence of rust on the walls which provides water adsorption sites. Formed hydrate can partially or completely block pipelines. If the blockage is not removed quickly then high pressure can build up inside the pipeline leading to it collapse, thus causing serious risk to the safety of operating personnel, equipment, and surrounding environment. It costs billions of dollars annually to the petroleum industry to prevent and inhibit hydrate formation. Offshore operations additionally cost approximately US$1.6 million per kilometer on the insulation of subsea pipelines to prevent hydrates. (Jassim & Abdi, 2008)

2.5.2 Use of hydrate as a phase for industrial processes

The discovery of GHs have increased interest significantly towards GHs and initiated fundamental research. The main focus was two-fold, avoiding the formation of hydrates in pipelines and studying the dynamics of *in situ* naturally occurring GHs. Besides, the GHs can also be useful in many ways to industries, like gas separation, transportation, and storage of NG.

2.5.2.1Gas separation

Global warming caused by emissions of GHGs into the atmosphere due to anthropogenic activities, the most commonly known gas, which plays a major role in global warming is CO2. The most economical technique in comparison to other conventional techniques which is used to reduce emissions of CO2 into the environment is Carbon Capture & Storage (CCS) technique. According to International Energy Agency (IEA) the total cost of proposed target climate changes control will increase by up to 70% if CCS is not used by 2050 (IEA, 2008). One of the promising CCS process that could be integrated into the existing plants can be separation and capture of CO2 from flue gas (usually CO2/CO/N2 mixture emitted by steel making plant) streams. This process involves mixing of flue gas with water under

hydrate forming temperature and pressure conditions which will form hydrate containing CO2 and then this hydrate is separated and dissociated to recover CO2 by means of depressurization and/or heating. (Yang, et al., 2013; Herri, et al., 2014)

As the hydrate formation process involves high pressure and low temperature, the process becomes very costly, so main studies done until now (Herri, et al., 2014; Duc, et al., 2007) is to find thermodynamic additives to reduce the operating pressure under which hydrates can stabilize. The CO2 selectivity is another important factor to be considered for gas separation. Since flue gas contains huge amounts of N2 due to combustion with air so removal of CO2 from flue gas can be partly done with hydrate since the ratio of CO2/N2 in hydrate can be 3:1 with N2 occupying small cavities and CO2 the large ones, while the original flue gas CO2/N2 was with ratio 1:8.5 that will result in a substantial upconcentration of CO2. A promoter (Tetrahydrofuran, Cyclopentane, alkyls ammonium salts, etc.) can enter into the hydrate cavity to stabilize the hydrate structure under mild conditions of temperature and pressure and increase the selectivity of CO2 into hydrate formation and other gases remains as in gas or liquid form (Herri, et al., 2014).

2.5.2.2 Transportation and storage of natural gas

NG is a cleaner fuel than other highly consumed fossil fuels and according to International Energy Outlook 2016 it accounts for the largest increase in world primary energy consumption. But their sources are often located very far away from the end user so that it becomes a major concern to develop efficient transport and storage technologies for NG. Due to the presence of CH4 as the main component of NG whose boiling point is about -162ºC under 1 bar pressure, it becomes more difficult to store and transport (Sun, et al., 2004). The liquefied natural gas (LNG) and compressed natural gas (CNG) are the most frequently used and developed methods for the transport and storage of NG. The usage of these methods depends on the scale of development and distance from the markets. In general, LNG and CNG processes are economically feasible for NG storage with a sizeable volume and long distance transportation. However, extreme operating temperature (around -163ºC for LNG) and high pressure (around 200 bars for CNG) are required, which can make these

technologies economically less favorable for small or medium sized fields, storage, and transportation. The storage of NG as hydrates can be another alternative technique providing volumetric gain as one volume of hydrate can store around 150-180 volumes of NG (Makogon, 1997; Khokhar, et al., 1998). This will be safer and more cost effective in comparison to LNG and CNG.

Chugoku Electric Power Co., Inc. (CEP) and Mitsui Engineering & Shipbuilding Co. Ltd. (MES), constructed a NGHs production plant with a capacity of 5 tons per day in the Yanai LNG-based power station located in the west side of Japan, where they have demonstrated that they could supply NG in the form of hydrates to power generation plant and a housing complex through land transportation in 2009. The storage and transportation of NG in the form of hydrate involve 5 major steps, 1) synthesis of hydrate formation in the presence of water, 2) dewatering and pelletizing, 3) storing in modified vessels after refrigeration and depressurization, 4) transportation and 5) regasification of NGHs to supply it to power plants and local market. The first step involves a continuous formation of 10% NGHs slurry by stirring a mixture of water and gas with gas bubbling in the high pressure vessel at temperature 277K and 5.3 MPaG of high pressure. Then this slurry is carried off to the de-watering process and further converted to NGHs pellets with 75% NGHs. These pellets are refrigerated from 277K to 253K and de-pressurized from 5.3 MPaG to atmospheric pressure for storage in already refrigerated vessels at the same temperature 253K. It is then transported to power plants and a housing complex about a hundred kilometers from the production plant. On arrival, the NGHs pellets are re-gasified in the same containers and the gas is taken out from the top and water from the bottom of the vessel. Furthermore, MES has been developing NGHs carrier to establish the total supply chain of NGHs, for marine transportation, which enables to spread the use of NG around the world as they claimed. (Watanabe, et al., 2008; Nakai & Mitsui Engineering & Shipbuilding Co., Ltd., 2012)

3 Scientific Method

Abundance of NG, its easy exploitability compared to shale gas and rapidly declining conventional fossil fuels have led many to attempt the modeling of hydrate dynamics in sediments. Modelling the complex nature of hydrates in sediments is a challenging task. It involves modelling processes like GHs formation, dissociation, and reformation which are the important factors for developing new reservoir simulators. As mentioned earlier, the hydrates in sediments cannot achieve equilibrium. This can be seen from all the independent thermodynamic variables in a system of hydrate inside porous media versus conservation laws and conditions of thermodynamic equilibrium. Even in the most trivial case of hydrate former in a separate gas phase, liquid water and hydrate, Gibbs phase rule implies that only one independent thermodynamic variable can be fixed for equilibrium to reach. And since two independent variables are locally defined by hydrostatics, hydrodynamics and geothermal gradients, the system is over-specified. Mineral surfaces add additional phases to the balance since they serve as potential nucleation surfaces for hydrates increasing the complexity of the system. The partial charge distribution on atoms in the mineral surface is incompatible with partial charges on oxygens and hydrogens in hydrate water inhibiting the further hydrate formation.

It is quite obvious that the inner core of any reservoir model is a multi-scale problem. Phase transitions are nano-scale processes controlled by dynamics across a thin interface (typically 0.8 to 1.5 nm), coupled to hydrodynamic scales by porous media flow (pore-scale, mm) and reservoir flow (Darcy flow) connecting pores throughout the reservoir (km scale). Density Functional Theory (DFT) in the classical statistical mechanical regime links changes in atomistic structures to phase transition kinetics. And since atomistic structures are directly coupled to free energy through the canonical ensemble in statistical mechanics then a formulation based on free energies is more appealing since it is more directly linked to the transport of mass and energy. For this reason, PFT has been chosen as the scientific method in this work. The theory utilized in this work is briefly described in section 3.2 and in more detail in chapter 4.

However, since this work is part of a multi-scale modeling approach, a brief overview of present generations of hydrate reservoir simulators is given in the next section.

3.1 Hydrates in Sediments and Modeling Challenges

One of the numerical models for calculation of GHs distribution and volume in the sediments was suggested by Davie & Buffet (2001). This numerical model considers CH4 production by conversion of organic material (main source of carbon supply to the hydrate stability region) in sediment. Hydrate formation and dissociation are controlled by local thermodynamic conditions such that if the dissolved CH4 concentration increases from equilibrium concentration then hydrate will form and if it decreases then some of the formed hydrate will dissociate to maintain the equilibrium concentration. It was concluded that the model is more sensitive to sedimentation rate, biological productivity, and amount & quality of organic material (e.g. low sedimentation rates and very high sedimentation rates both result in small hydrate volume due to reduced supply of carbon that is available to bacteria). The results were compared against observation data from actual sites and the accuracy of their predicted results was shown to be dependent on the available data of sedimentation rate and organic content (Davie & Buffett, 2001).

A new module for the TOUGH2 simulator was proposed by Moridis et al. (2003) named EOSHYDR2 which was designed to model hydrate behavior under both sediments and laboratory conditions. TOUGH2 is a 3D software for multicomponent and multiphase flow simulation for subsurface purposes. EOSHYDR2 can handle up to nine components (CH4 GHs, water, CH4 present as native and from hydrate dissociation, a 2nd native and dissociated hydrocarbon, water soluble inhibitors, salt, and heat as pseudo-component). It can handle up to four phases of gas, liquid, ice, and hydrate phase. For hydrate formation and dissociation, EOSHYDRA2 includes both equilibrium and kinetic models. They performed four test cases of CH4 production while only using equilibrium model due to the lack of enough suitable data necessary for the parameters of the kinetic model. They concluded that both thermal stimulation and depressurization can produce substantial quantity of gas from CH4 hydrate and

further suggested that a combination of the two can be the most desirable approach. (Moridis, 2003)

Kowalsky & Moridis (2007) used the same model to compare the kinetic and equilibrium approaches. It was concluded that the kinetic model is useful for the simulation of short-term and core scale systems based on the accuracy related to the kinetic model as mentioned earlier while equilibrium model can also be used for larger scale simulations. Sun & Mohanty (2006) studied the formation and dissociation of hydrates in permeable media and developed a 3D simulator to accomplish the study using Kim & Bishnoi1 (1987) kinetic model. The model also accounted for the equilibrium phase transitions using five phases (salt precipitate, hydrate phase, an aqueous phase, ice, and gas phase) and four components (i.e. CH4, water, salt, and hydrate), and also considered ice melting and water freezing. Furthermore, the mass transport, molecular diffusion and heat transport were implicitly solved. Later on, the simulator was upgraded by Phirani et al. (2010) through the inclusion of CO2 as a new component and CO2 hydrate as a new phase. Another study was conducted on CH4 production by Ahmadi et al. (2004) where a 1D model was developed based on the depressurization approach for the dissociation of GHs while neglecting the Joule-Thomson effect and the water flow in the reservoir. The equilibrium conditions were used at the dissociation front and heat of dissociation, convection, and conduction in the gas phase as well as in the hydrate phase was included (Ahmadi, et al., 2004). Liu et al. (2009) also used a similar approach to study hydrate decomposition process in porous media and developed a 1D model considering heat and mass transfer in both gas and hydrate phase while using moving front to separate the two phases. Stationary water phase was assumed and it was concluded that the model under-predicts gas production in wells and over-predicts dissociation front locations. Another conclusion was that the production rate is significantly affected by well-pressure and reservoir permeability. (Liu Y, et al., 2009)

Uddin et al. (2008) introduced a new kinetic model to study the production of CH4 gas while injecting CO2 into the CH4 hydrate reservoir for storage of CO2. To accomplish this conversion study, the model was coupled to CMG STARS (Steam

Thermal and Advanced Processes Reservoir Simulator) simulator. The simulator was developed by the Computer Modeling Group (CMG) Limited (CMG Ltd., 2007) to utilize it for modeling three phase flow, multicomponent fluids, and *in situ* combustion process. Uddin et al. (2008) studied the dynamics of hydrate formation and dissociation and concluded that the kinetic rate is constant and permeability has a significant effect on the dissociation.

Another hydrate simulator provided by National Energy Technology Laboratories (NETL) is known as HydrateResSim (HRS) which is the only open-source simulator available for public use. This code is written in FORTRAN and can only simulate equilibrium and kinetic models of CH4 hydrate formation and dissociation. The software accounts for CH4, water, hydrate, and inhibitors components as well as liquid, gas, ice, and hydrate phases. This software can perform hydrate dissociation by using depressurization, thermal stimulation, inhibitor injection and combination of the first two techniques (ΔP & ΔT). This simulator was further improved by Garapati et al. (2013) to account for CO2 and N2 components and the implementation of equilibrium surface, the equilibrium pressure and hydrate number which is a function of temperature and pressure. This software named as Mix3HydrateResSim because it can handle the ternary mixture (CH4 + CO2 + N2) and allows modelling of Ignik Sikumi No. 1 field test trial during which CO2+N2 mixture was injected to produce CH4 gas while storing CO2 into the hydrate (Garapati, et al., 2013). A 1D simulation was used to exchange CH4 hydrate with CO2+N2 mixture followed by depressurization technique using a single well. It was concluded that the released CH4 gas from the hydrate during depressurization process reforms CH4 hydrate. A comparison with Ignik Sikumi field test showed that a huge amount of water and gas was produced due to the solid hydrate production which is not stable. Therefore, simultaneous injection of CO2+N2 mixture and removal of CH4 gas was suggested and found that the amount of N2 produced was higher in the field trial data than from Mix3HydrateResSim model. Gamwo & Liu (2010) also used HydrateResSim model for 3 components (CH4, water and hydrate) and 4 phases (Gas, aqueous, ice and hydrate). The TOUGH-HYDRATE simulator was used to validate the studied model and concluded that the code was suitable for simulating CH4 hydrate behavior and

kinetic approach usually under-predicts hydrate dissociation compared to the equilibrium approach. (Gamwo & Liu, 2010)

One of the most important concepts that is missing in almost all these efforts is the fact that hydrates in nature which form or dissociate are not capable of reaching true equilibrium due to Gibbs phase rule when temperature and pressure are locally defined at a given depth. In such situations, a system will strive towards lowest free energy possible under the constraints of heat and mass transport. Such situation requires lot of resources and efforts in the modeling and simulation (Moridis, et al., 2013).

Further, hydrate phase transitions are nano-scale processes happening across a thin (in order of 1.2 nm) interface between the hydrate core and the surrounding fluids. It is therefore extremely important to understand the coupled dynamics from nano-scale to micro-scale (diffusion to hydrodynamics) and all the way up to macro-scale. All the theories and models presented above fails to address the challenge. The current work proposes appropriate models for thermodynamics and phase transitions at nano-scale coupled with hydrodynamics, briefly discussed in the next section. This will lay the basis for the kinetic quantification at pore scale that is necessary for the implementation into reservoir modeling tools.

3.2 Kinetic and Thermodynamics Models

PFT is the only appropriate theory to model the phase field transition kinetics as well as capable of providing a detailed insight into the interface dynamics of any two co-existing phases. PFT is basically derived from Density Functional Theory (DFT) which is also limited in geometry as the kinetics of the phase transition is proportional to the changes in molecular structures through the interface from the old to the new phase and furthermore, the free energy is directly related to the molecular structures which is the main reason for the development of PFT. In PFT the molecular structures are replaced with free energies limited only by the scale of the thermodynamic description and conversely, the phase transition will be proportional to the thermal

fluctuations of the interface and capillary waves which are linked to at least some nano scale processes. (Evans & Sluckin, 1980; Tarazona & Evans, 1984)

Another complication arises when the release rate is faster than the capacity of the surroundings to dilute the dissociated molecules. In such a situation bubbles or droplets will form affecting the phase transition rate and necessitating the inclusion of gravity forces in the model. To incorporate these effects, it was necessary to add hydrodynamics to the model. For this purpose, Navier Stokes equations were coupled with the PFT (details will follow in the papers attached). During the hydrate formation and dissociation heat transport is very fast compared to mass transport at the interface of hydrate and surrounding fluids dominated by liquid. If the dissociation rate is very fast, the escaping paths of the releasing gas are hindered by the surrounding obstacles like hydrate, clay or a gas layer may act as a thermal insulator limiting the heat transport.

During such situations heat transport dynamics can have a significant affect on the kinetics of hydrate dissociation. Hence a heat transport model is implemented into the PFT. Furthermore, the existing thermodynamic model is improved to account for non-equilibrium thermodynamics. Detailed descriptions of fluid and aqueous phases are applied and the improved thermodynamic model is implemented into the PFT. This is the main contribution of this PhD Thesis. The next two chapters are explicitly dedicated to explain the proposed kinetic theory and residual thermodynamics implicitly coupled with hydrodynamic and heat transport.

4 Phase Field Theory

PFT is a kinetic theory derived from free energy minimization under the constraints of mass and heat transport dynamics and molecular structures which are connected to free energies through statistical mechanics (Elder, et al., 2007). The hydrodynamics is implicitly implemented into the three components PFT which is important in situations where the dissociation rate of hydrate is faster than the solubility of CH4 into the surrounding water hence free CH4 gas form bubbles and affect the phase transition kinetics. The implicit heat transport is also implemented in three components PFT for the situation where heat from new hydrate formation will contribute to the dissociation of CH4 hydrate. During the dissociation process, heat transport is about 2 to 3 orders of magnitude faster than mass transport in liquid water and hydrate system, but it will be slow through gas layers or gas bubbles. The two sections 4.1 and 4.2 explain two and three components PFT collected from PhD work (Svandal, 2006) and Kvamme et al. (2009) as well other publications referred to during the sections of this chapter.

4.1 Two Component Phase Field Theory

The PFT in this section deals with one guest and water. The scalar phase field $\phi(x,t)$ represents the solidification of hydrate and the local solute concentration of the guest represented by $c(x,t)$. The field parameter ϕ is varied continuously in the range from 0 to 1. Here ϕ value 0 represent solid, 1 is used for liquid phase and intermediate values correspond to the interface between the two phases. The starting point of the field model is a free energy functional. For a system of two components undergoing a phase transition the functional is given by:

$$F = \int d^3r \left(\frac{\varepsilon_\phi^2 T}{2} |\nabla\phi|^2 + f(\phi, c) \right) \tag{4.1}$$

This is an integration of free energy density $f(\phi, c)$ and the gradient term (ensures the correction in free energy density due to the fluctuations in phases at the interface) over

the system volume. There is a more general expression for the total free energy functional to include the changes in temperature due to the fluctuations in concentration at the interface and is given as:

$$F = \int d^3r \left(\frac{\varepsilon_\phi^2 T}{2} |\nabla \phi|^2 + \frac{\varepsilon_c^2 T}{2} |\nabla c|^2 + f(\phi, c) \right) \tag{4.2}$$

The free energy density function is given as

$$f(\phi, c) = WTg(\phi) + \big(1 - p(\phi)\big) g_L + p(\phi) g_S \tag{4.3}$$

Where $p(\phi) = \phi^3(10 - 15\phi + 6\phi^2)$ and obviously $p(0) = 0$ and $p(1) = 1$. Therefore, this function switches on and off the liquid g_L and solid g_S free energy densities contribution respectively in the overall free energy density. The double well form of $f(\phi, c)$ is included with free energy scale $W = (1 - c)W_A + cW_B$. Where subscript A is used here for water and B is used for some guest molecule. The function $g(\phi) = \phi^2(1 - \phi)^2/4$ decides the ratio of contribution depending on the value of ϕ. The concentration c is the mole fraction of guest component and formulated as the fraction of the guest component to total with the assumption that the molar volume is constant where mole fraction concentration and the volume concentration are related by $c_m = c_v v_m$, where $v_m$is the average molar volume.

It is assumed that the system evolves in time so that its total free energy decreases to derive the kinetic model. This assumption is consistent with the following model. The simplest form of the evolution that ensures the minimization of the free energy can be derived as follows provided the phase field is not conserved:

$$\dot{\phi} = M_\phi \left\{ \nabla \left(\frac{\partial f}{\partial \Delta \phi} \right) - \frac{\partial f}{\partial \phi} \right\} \tag{4.4}$$

Where M_ϕ is the phase field mobility and $M_\phi > 0$ and the expression $M_\phi = (1 - c)M^A + cM^B$ will allow dependency of M_ϕ on composition, while $M^A = \big(1 - p(\phi)\big)M^A_{solid} + p(\phi)M^A_{fluid}$ and $M^B = \big(1 - p(\phi)\big)M^B_{solid} + p(\phi)M^B_{fluid}$. For

the conserved quantity, the flux may be associated to the concentration. Using the classical linear irreversible thermodynamics, it is assumed that near equilibrium the flow is linearly proportional to the force that drives it and we write it as

$$\dot{c} = \nabla\left\{\nabla M_c\left[\frac{\partial f}{\partial c} - \nabla\left(\frac{\partial f}{\partial \Delta c}\right)\right]\right\} \tag{4.5}$$

M_ϕ is the associated concentration field mobility and to recreate the Fick's Law in the bulk phase, M_c is related to diffusivity by the expression $M_c = c(1-c)\frac{v_m}{RT}D$ with D is the diffusion coefficient that in order to allow for coefficient diffusivities in the solid and liquid can be expressed as $D = D_S + p(\phi)(D_L - D_S)$. The model parameters ε_ϕ, W_A, W_B, M^A and M^B can be provided by measurable quantities. It is possible to relate the phase field mobility to diffusivity but is expected to be more complex and also reflect dynamic characteristics of the water rearrangement. Molecular dynamics simulations can be one method for obtaining more insight into this and might even be able to provide a tool for estimating values for the mobility.

4.2 Three Component Phase Field Theory

The extension from two components to three components is necessary to deal with the mix hydrate formation and dissociation processes. The extension to more than two components and two phases is straightforward, but as per requirement only the extension to three components will be discussed here. The equation (4.2) can then be extended as:

$$F = \int d\underline{r}\left\{\frac{\varepsilon_\phi^2 T}{2}|\nabla\phi|^2 + \sum_{i,j=1}^{3}\frac{\varepsilon_{i,j}T}{4}(c_i\nabla c_j - c_j\nabla c_i)^2 + f_{bulk}(\phi, c_1, c_2, c_3)\right\} \tag{4.6}$$

This is integrated over the system volume and the subscripts i and j run over three components. The bulk free energy density is described as,

$$f_{bulk} = WTg(\phi) + \big(1 - p(\phi)\big)g_S(c_1, c_2, c_3) + p(\phi)g_L(c_1, c_2, c_3) \tag{4.7}$$

With g_S and g_L, the free energies of solid and liquid in a similar way as for equation (4.2). The equations of motion are defined the same way as for the two components, but one needs to be careful in measuring the phase field mobility since it now depends on the source of the components crossing the interface during the phase transition. For example, the mobility of CO2 is different into hydrate from supersaturated aqueous phase and CO2/CH4 phase. This can be taken care by letting the mobility be a function of the concentrations.

5 Thermodynamics and Kinetic of Phase Transition

This chapter treats the development of the precise and consistent thermodynamic model needed for the PFT modeling. This chapter will initially explain the equilibrium thermodynamics in section 5.1. The description of thermodynamic properties of fluids, aqueous and hydrate phases are described in sections 5.2, 5.3 and 5.4 respectively. The last section 5.5 explains the formation and dissociation kinetics related to GHs.

5.1 Equilibrium Thermodynamics

The theory for equilibrium thermodynamics is based on revised adsorption theory due to (Kvamme & Tanaka, 1995) and (van der Waals & Platteeuw, 1959). The expression of the chemical potential of water in hydrate is:

$$\mu_w^H = \mu_w^{O,H} - \sum_i RT v_i \ln\left(1 + \sum_j h_{ij}\right) \tag{5.1}$$

This equation is derived from the macro canonical ensemble under the constraints of a constant amount of water, corresponding to an empty lattice of the actual structure. Details of the derivation are given elsewhere (Kvamme & Tanaka, 1995) and will not be repeated here. $\mu_w^{O,H}$ is the chemical potential for water in an empty hydrate structure and h_{ij} is the cavity partition function of component j in cavity type i. The first sum is over cavity types, and the second sum is over components j going into cavity type i. Here v_i is the number of types i cavities per water molecule. For hydrate structure-I, there are 3 large cavities and 1 small per 23 water molecules, $v_l = 3/23$ and $v_s = 1/23$. In the classical use of equation (5.1), the cavity partition functions are integrated under the assumption that the water

molecules are fixed and normally also neglecting interactions with surrounding guest molecules. This may be adequate for small guest molecules with weak interactions. On the other hand, molecules like CO2 are large enough to have a significant impact on the librational modes of the water molecules in the lattice. An alternative approach (Kvamme & Tanaka, 1995) is to consider the guest movements from the minimum energy position in the cavity as a spring, and evaluate the free energy changes through samplings of frequencies for different displacements in the cavity. A molecule like CH4 will, as expected, not have a significant impact on the water movements (Kvamme & Tanaka, 1995; Qasim, 2013). CO2 on the other hand, will change water chemical potential by roughly 1 kJ/mole at 0°C when compared to the assumption of undisturbed fixed water molecules. The cavity partition function may thus be written as:

$$h_{ij} = e^{\beta\left(\mu_j^H - \Delta g_{ji}^{inc}\right)} \tag{5.2}$$

Where Δg_{ji}^{inc} now is the effect of the inclusion of the guest molecule *j* in the cavity of type *i*, which as indicated above is the minimum interaction energy plus the free energy of the oscillatory movements from the minimum position. At hydrate equilibrium the chemical potential is equal to that of the chemical potential of the guest molecule in its original phase (chemical potential of dissolved CO2 or CH4 for the case of hydrate formation from aqueous solution). Equation (5.2) can be inverted to give the chemical potential for the guest as a function of the cavity partition function:

$$\mu_j^H = \Delta g_{ji}^{inc} + RT \ln h_{ij} \tag{5.3}$$

Equation (5.3) is basically derived from an equilibrium consideration but may be

used as an approximation for bridging chemical potential to composition dependency. The relation between the filling fraction, the mole fractions, and the cavity partition function is:

$$\theta_{ji} = \frac{x_{ji}}{v_i(1 - x_T)} = \frac{h_{ji}}{1 + \sum_j h_{ji}} \tag{5.4}$$

Here x_T is the total mole fraction of all the guests. It is assumed that CO2 can only fit into the larger cavities, and unless some other guest molecule is present, the small cavities will then all be empty. For more detail follow paper 6 attached to this thesis.

5.2 Fluid Thermodynamics

The free energy of the fluid phase is assumed to have:

$$G_L^{Fluid} = \sum_{r=c,m,w} x_r \mu_r^{Fluid} \tag{5.5}$$

where μ_r^{Fluid} is the chemical potential of the fluid phase. The lower concentration of water in the fluid phase and its corresponding minor importance for the thermodynamics results in the following form of water chemical potential with some approximation of fugacity and activity coefficient:

$$\mu_w^{Fluid} = \mu_w^{ideal\ gas}(T, P) + RT \ln(y_w) \tag{5.6}$$

Where $\mu_w^{idea\ \ gas}(T, P)$ chemical potential of water in ideal gas and y_w is the mole fraction of water in the fluid phase and can be calculated as:

$$y_w = \frac{x_w \gamma_w(T, P, \bar{x}) P_w^{sat}(T)}{\varphi_w(T, P, \bar{y})} \tag{5.7}$$

The vapour pressure can be calculated using many available correlations but better of the simplest formulations is given by Van der Waals & Platteeuw (1959) as a fit to the simple equation:

$$\ln(P) = V_A - \frac{V_B}{T + V_C} \tag{5.8}$$

The temperature of the system is obviously available and $V_A = 52.703$, $V_B = -3146.64$ and $V_C = 5.572$. Further, the fugacity and the activity coefficient are approximated to unity merely because of the very low water content in fluid phase and its corresponding minor importance for the thermodynamics of the system. Hydrate formation directly from water in gas is not considered as significant within the systems discussed in this work. A separate study reveals that hydrate formation from water dissolved in CO2 may be feasible from a thermodynamic point of view (Kvamme, et al., 2013) but more questionable in terms of mass transport in competition with other hydrate phase transitions. The water phase is close to unity in water mole fraction. Raoult's law is therefore accurate enough for our purpose. The chemical potential for the mixed fluid states considered as:

$$\mu_i^{Fluid} = \mu_i^{id.gas,pure} + RT\ln(y_i) + RT\ln\varphi_i(T, P, \bar{y}) \tag{5.9}$$

Where i represents CH4 or CO2. The fugacity coefficients of component i in the mixture is calculated using the Soave Redlich Kwong (SRK) equation of state (EOS) (Soave, 1972). Detail description is given in Paper 4 attached to this thesis.

5.3 Aqueous Thermodynamics

The free energy of the aqueous phase can be written as:

$$G_L^{aqueous} = \sum_{r=c,m,w} x_r \mu_r^{aqueous} \tag{5.10}$$

The chemical potential $\mu_r^{aqueous}$ for components c (CO2) and m (CH4) dissolved into the aqueous phase is described by nonsymmetric excess thermodynamics:

$$\mu_i = \mu_i^{\infty}(T) + RT\ln(x_i\gamma_i^{\infty}) + v_i^{\infty}(P - P_o) \quad (5.11)$$

μ_i^{∞} is the chemical potential of component i in water at infinite dilution, γ_i^{∞} is the activity coefficient of component i in the aqueous solution and v_i^{∞} is the partial molar volume of the component i at infinite dilution. The chemical potentials at infinite dilution as a function of temperature are found by assuming equilibrium between fluid and aqueous phases $\mu_i^{Fluid} = \mu_i^{aqueous}$. This is done at varying low pressures where the solubility is very low and the gas phase is close to ideal gas using experimental values for the solubility and extrapolating the chemical potential down to a corresponding value for zero concentration. The chemical potential of water can be written as:

$$\mu_w = \mu_w^{pure\ liquid}(T) + RT\ln(1 - x)\gamma_w + v_w(P - P_o) \quad (5.12)$$

where $\mu_w^{pure\ liquid}$ is pure water chemical potential and v_w is the molar volume of water. The strategy for calculating activity coefficient is given by Svandal et al. (2006b). A more accurate description for calculating the activity coefficients is given in paper 4 attached to this thesis.

5.4 Non-equilibrium Thermodynamics

The PFT model presented in this work has dynamically varying local densities, temperatures, concentrations and the constraints on the system is the pressure. Unlike our earlier PFT models (van der Waals & Platteeuw, 1959; Svandal, et al., 2006b), which were isothermal, non-equilibrium thermodynamics (Kvamme, et al., 2013) are implemented implicitly into the PFT model. This accounts for the changes (due to changes in local conditions and possibly competing phase transitions) in free energies of all co-existing phases. Case examples based on the conversion of CH4 hydrate into CO2 hydrate or mixed CO2-CH4 hydrate are presented. The conversions have two primary mechanisms. In the first mechanism, CO2 creates a new hydrate from free water in the porous media and the released heat dissociates the *in situ* CH4 hydrate. This mechanism is primarily dominated

by mass transport rates through fluid phases. The second mechanism, which is a much slower solid state phase transition, is a direct conversion of the *in situ* CH4 hydrate with the CO2. The first mechanism implies heat release as well as heat consumption and complex coupled behavior of mass and heat transport around the hydrate core. Also note that the fluid thermodynamics and aqueous thermodynamics outside of equilibrium is trivial in contrast to hydrate, for which the thermodynamic model is derived from statistical mechanics based on the equilibrium between hydrate and fluid phases. For this reason we expand the thermodynamic properties of hydrate by a first order Taylor-expansion. This is considered accurate enough since the rate limiting kinetic contributions are expected to be in the mass transport according to earlier studies (Svandal, 2006; Kvamme, et al., 2009; Kavanaugh & Trussell, 1980). First of all note that the mass is conserved in the PFT. The thermodynamics has to be developed in terms of gradients in all directions (P, T, mole-fractions) without conservation of mole-fractions in order to obtain the appropriate relative local driving forces and also avoid double conservation constraints in the free enrgy minimalization. This scientific work is limited to three components, where CH4 is the additional component with CO2 and water. This can be directly extended to more components through straightforward extensions of the equilibrium and supersaturation thermodynamics, and appropriate adjustment of the PFT. As the thermodynamic changes are outlined here, the primary additional change in the PFT model is in the free energy of the thermal fluctuations (Svandal, 2006; Conti, 1997; Conti, 2000) as function of concentrations, which is mathematically trivial. Supersaturations of fluid phases is straightforward and not different from Svandal et al. (2006) and Kvamme (2003).

The Gibbs free energy of the hydrate phase is written as a sum of the chemical potentials of each component (Svandal, 2006; Kvamme, 2003),

$$G_H = \sum_r x_r \mu_r^H \tag{5.13}$$

where μ_r^H and x_r is chemical potential and mole fraction of component r respectively. G_H is the free energy of hydrate. In the earlier work due to Svandal et al. (2006) a simple interpolation in mole-fractions was used between pure CH4 hydrate and pure CO2 hydrate, which was considered as sufficient to theoretically illustrate the exchange concept under PFT. This will of course not reproduce the absolute minimum in free energy for a mixed hydrate in which CH4 occupies portions of the small cavities and increases stability over pure CO2 hydrate. The expression for free energy gradients with respect to mole fraction, pressure, and temperature is:

$$G_H^{EXP} = G^{EQ} + \sum_r \left.\frac{\partial G_H}{\partial x_r}\right|_{P,V,T,x_{i\neq r}} (x_r^{act} - x_r^{EQ}) + \left.\frac{\partial G_H}{\partial P}\right|_{T,V,\vec{x}} (P^{act} - P^{EQ}) + \left.\frac{\partial G_H}{\partial T}\right|_{P,V,\vec{x}} (T^{act} - T^{EQ}) \tag{5.14}$$

Here G_H^{EXP} is the free energy of hydrate away from equilibrium and the superscripts EQ and act represent the corresponding states at equilibrium and actual states respectively. Paper 4 attached to this thesis provides a detail derivation of three partial derivatives given in equation (5.14).

5.5 Hydrate Formation and Dissociation

The most important and challenging question about hydrates is regarding the formation and dissociation of hydrates. These processes are very complex and require deeper understanding. The hydrate formation is generally a three-step process involving nucleation, growth followed by induction. Nucleation is a microscopic stochastic phenomenon where small clusters of water and guest grow together and disperse again until some nuclei have grown to a critical size. This size is the defining moment where the net gain of the growth outcompetes the penalty of pushing on the surroundings to get space. It is very difficult to observe the dynamics of the nucleation process as this process involves huge quantities of molecules. Once the critical size is attained the monotonic growth occurs provided that the clusters are not dominated by

competing clusters with more favorable free energy. In contrast to this primary nucleation process, a third stage, which is not as well defined in terms of physics, is the onset of massive growth. The induction time is the time from the first detectable evidence of the onset of massive growth. This definition is not unique since the actual detection of first onset massive growth point depends on what method is used for detecting that point (pressure change, laser, and visual). Temperature, pressure, and available mass will affect the induction time. (Sloan & Koh, 2008)

Deviations from equilibrium are either super-saturated if the free energy benefit is favorable in terms of hydrate formation or sub-saturated if the conditions favor hydrate dissociation. The higher the super saturation the lower the induction time normally is. But generally speaking, the system can be super saturated in some independent thermodynamic variables and sub saturated in other independent thermodynamic variables, which implies competing phase transitions of hydrate formation and hydrate dissociation. Of course, the absolute necessity for nucleation to occur is the saturation of water with a guest. But normally the solubility of guest molecules is limited and therefore, the formation is mostly observed on the vapor-water interface. The lower the free energy change, the more rapid is the hydrate formation, although the mass transport part of the kinetics often dominates the overall kinetic rate.

There are two hypotheses about nucleation presented by Sloan & Fleyfel (1991) and by Kvamme (1996). The first hypothesis suggests that water molecules form clusters around guest molecules and then these clusters combine to form unit cells. When the size of the collective clusters reaches a critical size, then it grows. On the contrary the work by Kvamme (1996) proposes that gas molecules form first partial and then complete cages around the adsorbed species. The clusters then join and grow on the vapor side of the surface until the critical size is achieved. Further, nucleation is generally divided into two types, homogeneous and heterogeneous nucleation. The homogenous nucleation means that all the hydrate components are extracted from a single phase like for instance hydrate formation from a liquid solution. Hydrate formation on a gas/water interface is an example of heterogeneous nucleation in which the components come from two different phases. The heterogeneous nucleation can

also happen on solid surfaces from adsorbed water and adsorbed hydrate formers, or from adsorbed water and hydrate former from a separate phase outside. After nucleation stage has resulted in hydrate crystals of critical size, the crystals will grow unconditionally, except for completion of mass with other hydrate crystals which have reached levels of lower free energy. In those cases, less stable hydrate cores may be consumed at the cost of further growth of the more stable ones. There are also other exceptions related to non-equilibrium which will not be discussed in detail. Unconditional growth in a non-equilibrium system is only possible if the impact of all gradients of independent thermodynamic variables (temperature, pressure, concentrations) in free energy change is negative.

In order to illustrate the mechanisms behaving the two stages, it can be useful to look at very simple theories like the classical nucleation theory. If the cluster (nucleus) is considered a complete sphere, then bulk free energy change involved in the phase transition ΔG , can be formulated as:

$$\begin{aligned} \Delta G &= \Delta G_s + \Delta G_v \\ &= 4\pi r^2 \sigma + \frac{4}{3}\pi r^3 \Delta g_v \end{aligned} \tag{5.15}$$

Δg_v is the free energy change per unit volume and σ is the interfacial tension. The terms ΔG_s (surface free energy) is positive and decreases whereas ΔG_v (volume free energy) is negative and increases. This implies ΔG passes through a maximum at any radius r that corresponds to the critical size. This nucleus with maximum radius is called the critical nucleus. The critical size is the turning point when the free energy gains of the phase transition turns over to dominate the total free energy change over the free energy penalty of pushing away “old phases” in order to give space for the hydrate phase. At stages before the critical nucleus size is reached, the competition between the penalty term and the gain term results in nuclei growth as well as nuclei decay. As for kinetic rates, corresponding flux of hydrate growth in classical theory is given by a mass transport flux multiplied by a Boltzmann factor of the total free energy change. Associated heat transport requires a heat transport model but the consistent

enthalpy changes are trivially obtained from equation (5.15) through a classical thermodynamic relationship. (Sloan & Koh, 2008)

During growth, mass and heat transfer become increasingly important, especially on the aqueous-vapor interface where transport across hydrate is rate limiting unless hydrate films are broken by shear forces during the flow. Modeling of hydrate kinetics has historically been very much dominated by the industrial funding of hydrate projects. Experimental activities have dominated and the modeling has often been empirical fitting to some function of super-cooling conditions. Other directions have been using different empirical concepts from chemical engineering, which practically relates mass transport constants to a sum over different stages believed to be mass transport limiting. Thermodynamic driving forces are often modeled as fugacity differences between equilibrium and real state. A more detailed, but not necessarily complete, review may be found in chapter 3 in the book from Sloan & Koh (2008).

Dissociation of hydrates in porous media for NG production can be promoted by several different means, each having in common that the energy for breaking bonds must be provided. The dissociation is an endothermic process and therefore heat must be provided from external sources to break hydrogen bonds between water molecules and interaction forces between guest and water molecules of the hydrate lattice to decompose. The methods mainly applied for dissociation of *in situ* NGHs are depressurization, thermal stimulation, and inhibitors injection. Further details are discussed in section 2.4.

6 Numerical Implementation

This chapter will explain the strategies used for developing the Phase Field Code (PFC). The first section 6.1 gives a brief overview of the original code on which the work presented in this thesis is built upon. The second section explains extension of the code to include hydrodynamic coupling, non-equilibrium thermodynamics and heat transport.

6.1 Phase Field Code and Limitations

The original version of the PFC was first programmed and tested by Tamasz Puztai. It was first used by László Gránásy for the hydrate system in collaboration with Bjørn Kvamme (Kvamme, et al., 2003). The governing differential equations in time and three dimensional space are up to second and fourth order with respect to phase parameter (from equation (4.4)) and concentration (from equation (4.5)) respectively. The differential equations were solved with semi-implicit Euler method for marching in time and using finite difference method for discretization on uniform structured grid in space. The code is parallelized using Message Passing Interface (MPI).

Two sources of computational resources have been applied in this project. A cluster located at the Department of Physics and Technology, University of Bergen consisting PC clusters with overall 24 nodes and 192 cores with about 1 GB communication memory. The other facility is a Cray supercomputer at the University of Bergen containing 696 nodes. Each node has two 16-core AMD "Interlagos" processors (2.3 GHz) and 32 GB memory. The total number of cores is 22272.

The code lacked modules to compute free energy and its gradients. These quantities were computed separately at constant temperature and pressure to create tables which were used for integrating the governing equations during simulations.

This method for supplying thermodynamics restricted the free energy changes to mole fraction dependencies in different phases at constant temperature and pressure which is appropriate for isothermal simulations without hydrodynamics as applied in earlier

studies. These have been fair assumptions in earlier studies of solid state CH4/CO2 exchange (limited heat exchange) and homogeneous hydrate formation from solution which is rate limited by mass transport where heat transport is 2 – 3 orders of magnitudes faster than the rate of mass transport. The exchange of CH4 hydrate into CO2 hydrate can also occur through the formation of new CO2 hydrate from free water and injected CO2. This hydrate formation can occur when CO2 encounters free water available along the pore walls and also on liquid water surrounding the hydrate core. The latter case involving complex temperature behavior around the hydrate surface is discussed in papers 6 & 7 attached to this thesis. The absence of hydrodynamics in the code limits the applicability of the model to exchange processes dominated by diffusion.

Implementation of hydrodynamics will not only open up avenues for studies of hydrate system under pressure changes (like hydrate production through pressure reduction) but also the impact of local bubble formations on hydrate phase transitions. Addressing these constraints is important to accomplish heat transport and impact of local changes in densities. An overview of the main calculation sequence is given in the form of a simplified flow chart (Figure 6-1). The following section will further

discuss all the extensions made to this code and a detailed flow chart (Figure 6-2) at the end will provide a full picture of the extended PFC algorithm.

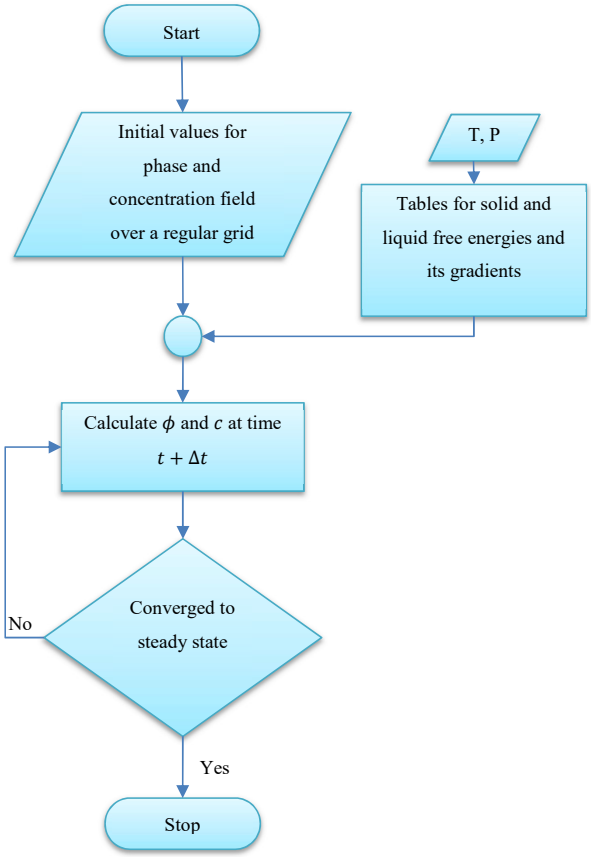

Figure 6-1:PFT simulation algorithm's flow chart

Concentration gradients in each direction with respect to each volume coordinate are estimated by discrete forward and backward approximations using the local grid concentrations at each time step, and similar for integration of the phase field according to equation (4.4).

6.2 Extension of the Code

Three major contributions of this work are implementation of; 1) Hydrodynamics 2) Non-equilibrium thermodynamics and 3) Heat transport.

6.2.1 Implementation of Hydrodynamics

The kinetic rates in the cases of formation and dissociation processes towards under saturated phases will depend on how fast the processes occur. These processes are diffusion controlled and the kinetic rate is not dependent on hydrodynamics if the dissociation rate per hydrate former is slower than self-diffusion into the surrounding phase. On the other hand if the dissociation is faster than the ability of surroundings to dilute the released molecules then the hydrodynamics needs to be included. For this purpose, the Navier Stokes equations, along with the continuity equation for density change due to flow are introduced and coupled with the PFT. The detail may be found in the papers attached to this thesis. The Navier Stokes equations are discretized on a finite cubic grid and using finite difference method and semi-implicit Euler method for marching in time. Furthermore, the variation in density across the system (most importantly on the interface of any two coexisting phases) is a continual phenomenon dependent on the phase transitions is also modelled and implemented, the details of which can be found in the papers attached to this thesis.

6.2.2 Implementation of Non-equilibrium Thermodynamics

In the total set of independent thermodynamic variables there may be several competing phase transitions of significance in the total distribution of different co-existing phases. For a given phase transition (hydrate formation or dissociation) the minimum criteria is that the free energy change is negative and at least exceeds the barrier due to the work required for creating a new phase (penalty of giving space), which is proportional to the interface free energy. But a given phase transition will only proceed unconditionally as long as the impact of all the gradients of free energy changes from independent thermodynamic variables imply lower free energy. The non-equilibrium situation also implies that hydrates formed from different phases will

have different free energies since the chemical potentials of guest molecules will be different. In some cases, water also will have different chemical potentials as water molecules may come from liquid water extracted from gas or from water adsorbed on solid surfaces. The above implication of non-equilibrium requires a kinetic concept based on a universal reference state for free energy as well as a concept for minimizing free energy under constraints of mass- and heat transport.

At first residual thermodynamics was implemented in MATLAB to calculate free energy and their derivatives at discrete points saved in the form of tables which were then used to interpolate values in the PFC. In next step thermodynamics was implemented in the PFC that allows calculating the free energy at each time step with locally varying temperature and pressure. Which eventually enabled us to evaluate the heat transfer model which is discussed in the next section. It is worth mentioning that mass conservation is not used in thermodynamic part as it is covered in PFT and each grid of the simulation represent each phase of the system (hydrate or fluid or aqueous phase).

6.2.3 Implementation of Heat Transport

Heat transport is very rapid compared to mass transport, especially at the interface of hydrate and surrounding liquid due to the formation and / or dissociation of hydrate, which is dominated by the liquid. Released CH4 from hydrate dissociation will be at low density typically between 200 - 400 kg/m^3 for reservoirs that are not very deep. If the dissociation rate is very fast and the escape paths for released gas is constrained by surrounding hydrate clay or other escape rate reducing factors then, a gas layer surrounding the dissociating zone may serve as a thermal insulator and heat transport dynamics can have an important impact on the kinetics of hydrate dissociation. So far, the thermal fluctuations are estimated using a simple heat conductivity equation. This is based on the level of current state of interpretation of experimental data in different laboratories around the world and considered adequate enough at this stage. The apparent conductivity reported by different groups will as such be a “lumped” value that also contains impact of heat convection. More rigorous models can be

implemented at later stages. See the attached papers for more detailed description and parameters applied in the examples used to illustrate the theory. The extended code can be explained by the flow chart in Figure 6-2.

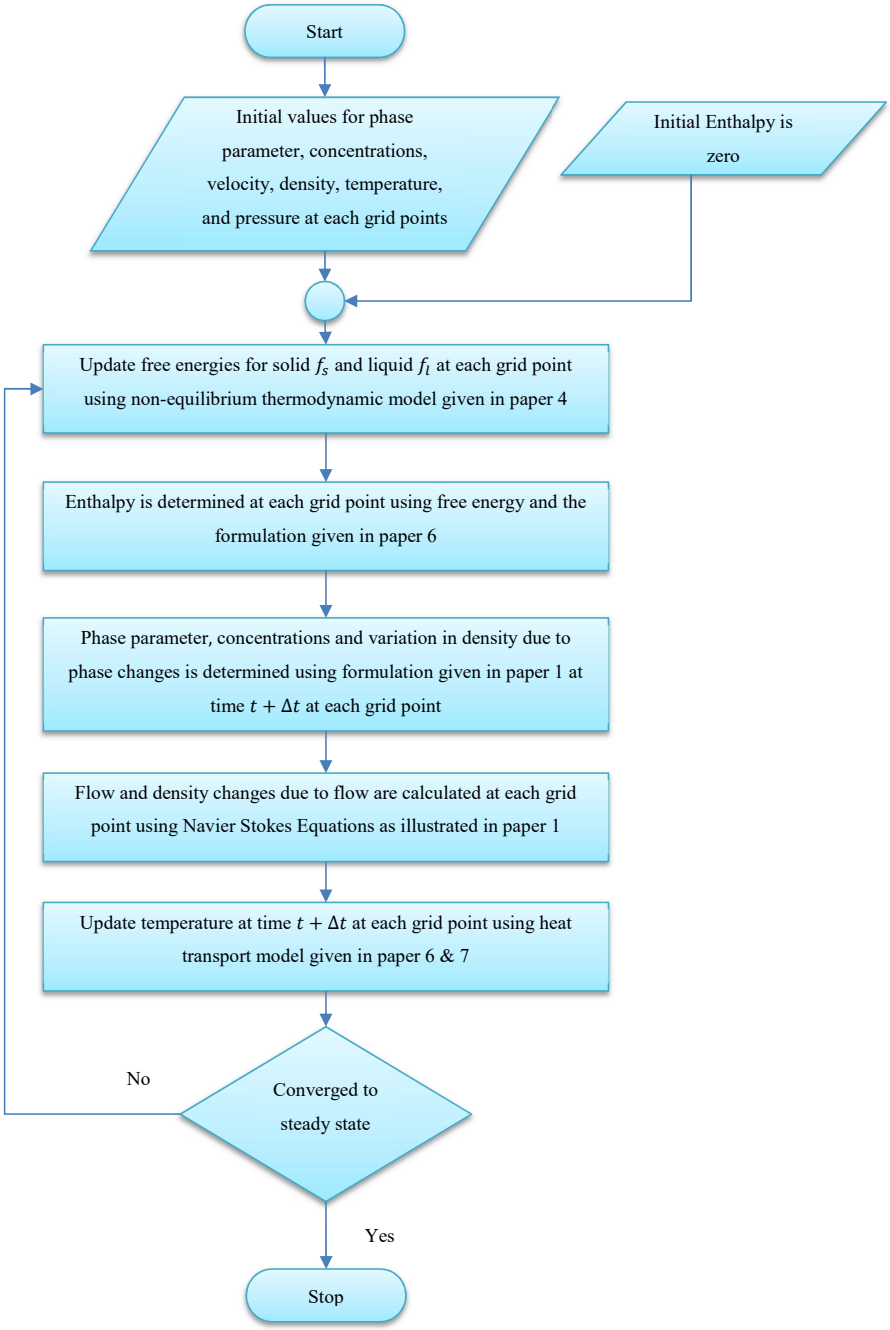

Figure 6-2: Detailed flow sheet of modified PFC

7 Summary of Papers

The progress of the scientific work and corresponding achievements are presented through international publications and presentations. A complete publication list is given at the beginning of the thesis and a selection of 7 papers is included here. Brief reviews of these papers are summarized from sections 7.1-7.7 while the papers are attached at the end of the thesis.

7.1 Phase Field Theory Modeling of CH4/CO2 Gas Hydrates in Gravity Fields

NGHs are thermodynamically unstable in reservoirs due to the interaction with surrounding mineral surfaces, under saturated water, and hydrate formers. This simply means that hydrate formation and dissociation can occur from different phases and different thermodynamic driving forces. If the dissociation rate is faster than the ability of the surrounding fluids to dissolve the released gas, the gas will remain as free gas on the interface and eventually will form bubbles. The proper implementation of hydrodynamics is therefore necessary and will provide a deeper insight into the hydrate kinetics involved during formation and dissociation processes.

In this paper the hydrodynamic model is coupled with PFT. The primary focus is to implement the density of all phases based on relative compositions and calculation of releasing gas existing in the form of bubbles which can escape through empty channels resulting in a more accurate calculation of gas flux. CH4 hydrate density is calculated using the formulation given by Sloan et al. (Sloan & Koh, 2008). The SRK equation of state is used to calculate the compressibility factor for the fluid phase (CO2 and/or CH4) (Soave, 1972) while the density of the water phase is kept constant and approximated independent of dissolved CH4 and / or CO2. It is worth to mention that the SRK equation of state may not reproduce the liquid densities accurately and expected accuracy of the liquid CO2 densities is likely to be within 5% for the conditions studied. This result is based on other research related to CO2 aquifer storage accompanied within the same research group and compared to more accurate

equation of state by Span & Wagner (1996). At this level of theoretical development this is not a critical factor and more appropriate density equation can be implemented at later stages. Further details regarding property calculations are given in the paper.

For the fluid phases containing variable relative amounts of CH4 and CO2 this will be crucial for three cases 1) Dissociation of mixed hydrates of 2 components (CH4, CO2) and the potential for free gas formation, 2) simulations of the exchange process between CH4 and CO2 during injection of CO2 into GHs, and 3) hydrate dissociation during lowering pressure which is not yet explored. In the second case above, an important and crucial question is to what extent the released CH4 will dissolve into CO2 versus the extent of separate CH4 bubbles escaping due to buoyancy. In this paper results for dissociation of CH4 hydrate are discussed. Simulation studies for exchange process follow in Paper 2.

7.2 Modeling Dissociation and Reformation of Methane and Carbon Dioxide Hydrate using Phase Field Theory with Implicit Hydrodynamics

The main objective of this paper is to extend the coupling of Navier-Stokes equations from two components to three components and to examine some of the mechanisms involved in the exchange of CO2 with CH4 in the hydrate. CO2 cannot enter into small cavities due to its size and shape compared to the available volume in the symmetric small cavity. There are some literature available which provide evidence that CO2 may enter into the small cavities (Ripmeester, et al., 1987) but available experimental evidences from different groups are not entirely consistent. It is still unverified that CO2 filling in small cavities will really be significant under the dynamic flow conditions during those types of scenarios. Within the scope of this work, CO2 is neglected in small cavities. On the other hand, CH4 can enter both small and large cavities, but CO2 will outcompete CH4 in occupation of the large cavities in terms of mixed hydrate as CO2 has a larger stabilization impact in these cavities. The resulting mixed hydrate (CO2-CH4) will be more stable than the original CH4 hydrate. Within the limited simulation time it is observed that 60% of initial CH4 in hydrate was

exchanged. The simulation was terminated for publication while the exchange process still going on, so the final exchange percentage is unverified and also the corresponding progress in the exchange rate.

7.3 Phase Field Theory Modeling of Phase Transitions Involving Hydrate

As discussed in paper 2, conversion of CH4 hydrate into CO2 hydrate is an interesting win-win situation for energy production combined with a safe long term storage of CO2. As described theoretically and verified experimentally, the CO2 is able to induce and proceed with a solid exchange process, but this is a slow process due to solid state mass transport limitations. On the other hand, a faster process is going through the formation of a new hydrate from injected CO2 and residual pore water. Hydrate in contact with liquid water will establish an interface towards it. The viscosity of structure water is higher than the liquid water and interface layer is fairly thin (in the order of 1 nm) similar towards mineral surfaces. Addition of CO2 into hydrate filled pores will have highest permeability in pore channels filled with water and/or gas. To investigate this behavior, a more realistic model is considered in this paper by inserting a thin water layer between CH4 hydrate and CO2 fluid. It is found that the percentage of exchange increases in comparison to the observed CH4/CO2 exchange in paper 2.

7.4 Thermodynamic and Kinetic Modeling of CH4/CO2 Hydrates Phase Transitions

Paper 4 focuses on modifications in the free energy calculations. As mentioned earlier GHs in reservoirs are unstable towards under saturated surrounding medium. Changes in global temperatures also change the stability regions of the accumulations of GHs worldwide. The fact that hydrates can never reach equilibrium in porous media, and formation can occur from different phases, as well as dissociate according to different thermodynamic driving forces imposes very complex phase transition dynamics. The dynamics of these transitions are solutions to coupled differential equations of mass transport, heat transport and phase transition kinetics. The availability of free energy

as a function of temperature, pressure, and the composition of all components in all phases in thermodynamic states outside of equilibrium is therefore essential in kinetic models based on minimization of free energy. Inspired by the facts above, this publication presents an extended adsorption theory for hydrate, SRK equation of state (Soave, 1972) for CH4/CO2 fluid thermodynamics and solubilities of these components in water. The model allows for the calculation of free energy of super saturated phases along all the different gradients with respect to saturation (mole fractions, pressure, and temperature). By implementing this in the PFT model, it is possible to study the effect of hydrate coming in contact with an under saturated surrounding phase as shown in paper 5.

7.5 Mix Hydrate Formation by CH4-CO2 Exchange using Phase Field Theory with Implicit Thermodynamics

Paper 5 illustrates the exchange process with similar example, as in paper 3. The thermodynamic model used in paper 4 is implemented in the PFC. The simulation results are useful in the modeling and optimization of the production of CH4 from hydrate reservoir as well as long term storage of CO2 in CH4 hydrate reservoir. As expected, it was observed that CO2 concentration in the hydrate increases and that of CH4 decreases with time. After most of hydrate cavities are filled with CO2, the simulation shows a rapid dissociation. This is due to the hydrate being in contact with an under saturated phase. Simulation results show almost a 90% exchange of CO2 with CH4 in large cavities.

7.6 Hydrate Phase Transition Kinetics from Phase Field Theory with Implicit Hydrodynamics and Heat Transport

Paper 6 adopts a new approach for non-equilibrium theory of hydrate together with a PFT for simulation of phase transition kinetics. In this scientific work an extended PFT model is presented which considers hydrodynamics and heat transport model.

As discussed earlier, conversion of CH4 hydrate into mixed (CO2&CH4) hydrate is a very interesting win-win situation of energy production and safe long term storage of GHG CO2. This conversion will tend towards a solid exchange process which is a slow process due to solid state mass transport limitations. On the other hand, a substantially faster process is going through the injection of CO2, which in contact with residual pore water form a new hydrate and releases significant amount of heat helping in dissociation of *in situ* CH4 hydrate. This makes the conversion process faster. But the formation of CO2 hydrate in the vicinity of the hydrate core will add heat to some portions of the surface which will increase the local temperature, while dissociating regions will show a decrease in temperature due to extraction of heat from the surrounding by CH4 hydrate core. Another reason for heat transport implementation is in those regions of the system which contains non-polar gas phase having low heat conductivity and low heat convection. This will have an impact on the distribution of released heat as well as transport of heat towards the dissociating regions. At this stage, a simplified heat conduction model is used for heat transport dynamics.

There are no nano scales experimental data available that can be used to verify theoretical estimates so different model systems are applied for demonstrations. The model was used to study the conversion of CH4 hydrate into mix hydrate (CH4-CO2-hyd) using three initial hydrate pore sizes; 150x150 Å, 500x500 Å and 5000x5000 Å. All hydrates are assumed to be of solid spherical shape with different sizes making it easier to demonstrate the impact of curvature. Mineral surfaces are considered to be water wetting in all three systems. The initial process was fast in all the three systems since it was dominated by the formation of new CO2 hydrate and subsequent CH4 hydrate dissociation from releasing heat. The smaller system showed a faster exchange process from CH4 hydrate over to mixed hydrate than the larger one. The smaller system formed unstable mix hydrate; this instability is caused by under saturated fluid phases around the hydrate and secondly, because of significant losses of the initial CH4 hydrate core before reaching the maximum mix hydrate core. On the other hand, the larger system behaved differently by reaching a steady state situation faster than the two smaller systems.

7.7 Impact of Water Film Thickness on Kinetic Rate of Mixed Hydrate Formation during Injection of CO2 into CH4 hydrate

The main purpose of this paper is the conversion of CH4 hydrate into either CO2 hydrate or mixed CO2-CH4 hydrate to investigate the relative impact of the two mechanisms. The efficiency of the mechanism based on the formation of new CO2 hydrate depends on the amount of liquid water surrounding the *in situ* CH4 hydrate, and the corresponding contact between the injected CO2 and liquid water. We have therefore investigated three CH4 hydrate systems (2D square geometry of same size 5000 x 5000 Å) surrounded by varying amounts of initial liquid water (5Å, 50Å, and 70Å) and having the same initial solid spherical CH4 hydrate core (radius of 1136 Å).

Simulations found that the kinetic rate of conversion increases with increasing thickness of the initial free water phase. The result clearly shows that the kinetic rate of conversion increases proportionally with respect to the amount of liquid water surrounding the CH4 hydrate initially. After the surrounding liquid is converted into CO2 and CO2/CH4 mixed hydrate all systems end up with a slow rate proportional to the solid state mass transport mechanism.

8 Conclusions

Through the scientific work documented in this thesis, a new kinetic theory is developed for hydrates in porous media using PFT with corresponding residual thermodynamics, hydrodynamics, and heat transport in a closed system under constant pressure. The theory, valid for kinetic progresses is implemented as a c-simulator which can handle competing hydrate phase transitions of formation and dissociation in non-equilibrium systems. A relevant example is the case of mixed hydrate (CO2 and CH4) formation during CO2 sequestration process in GHs.

The derivation of a complete and consistent thermodynamic model for the three phase system consisting of fluid, aqueous and hydrate phases is applied. It is worth noting that the mass is conserved in the PFT. The thermodynamic model is developed in terms of gradients (Pressure, Temperature, mole-fractions) in all directions without the conservation of mole-fractions to obtain the appropriate relative local driving forces and also to avoid double conservation constraint in the free energy minimization.

The PFM with accurate description of implicit thermodynamics, hydrodynamics, and heat transport is used to illustrate the exchange of CO2 with CH4 hydrate and form mixed hydrate accompanied by dissociation. In particular, the implicit implementation of thermodynamics in the PFC makes it possible to calculate the free energies with changing temperature. This is important for an accurate implementation of the heat transport model. The theory, not limited to study the CO2-CH4 exchange process in hydrates, is the focus of this thesis. To save CPU time, simulations were conducted in 2D geometry although the PFC can solve in 3D. The 2D assumption is sufficient for the simple crystal morphology. The use of initial spherical hydrate cores is considered good enough at this stage of theoretical development but can be adopted to more realistic geometries at a later stage. The initial spherical symmetry is also expected to be fairly symmetrical in 2D so substantial differences are not expected in 3D simulations. An initial setup is considered for disk shaped hydrate in the center surrounded by thin water strip and liquid CO2 in a square geometry. The insertion of

water strip between CH4 hydrate and liquid CO2 speeds up the exchange process. After the completion of the exchange process, the resulting hydrate starts to dissociate due to undersaturation of CO2 at the interface. This study is useful in the modeling and optimization of the production of NG from CH4 hydrate as well as CO2 storage.

Simulations using three different sized systems and hydrate disks show that the initial exchange process is fast in all the three systems since it is dominated by the rapid initial formation of CO2 hydrate and subsequent dissociation of CH4 hydrate from the released heat. The exchange process is faster in smaller systems compared to the larger systems with little of the original hydrate remaining. As shown in the previous studies, the smallest system was completely dissociated (due to under saturated surrounding water) after it reaches almost full exchange in 5.6 ns. On the other hand, the larger system behaves differently and takes 64 ns for full exchange with more of the original core remaining.

The injection of CO2 into CH4 hydrate to form mix hydrate is aided by two primary mechanisms. The fastest mechanism involves the formation of CO2 hydrate on the interface between liquid water and the liquid CO2. The heat released from the formation of new hydrate helps to dissociate original CH4 hydrate. This simply indicates that the kinetics of the heat transport mechanism is proportional to the liquid state mass transport rate. The second mechanism is much slower due to the solid state transport of molecules through hydrate phase. For investigation of these complex hydrate phase transition, three examples with different water film thicknesses around the same sized hydrate cores placed in the center of square geometry are considered. As mentioned earlier, the initial process is fast in all the three systems due to the rapid formation of new CO2 hydrate and the rate of exchange increases with increasing water film thickness. This implies that thicker water film gives faster heat transport over longer durations. The exchange rate is governed by the slower solid state transport after the consumption of water film around hydrate core and all three systems reaches the same state accordingly.

9 Future Work

Development of PFT model is under progress and there are several possible future enhancements as will be discussed in the following sections. While the enhancements described below are extremely important it was not possible to implement them in this research work due to time constraints.

9.1 Improvement in Phase Field Code Simulation

PFT simulations are computationally expensive therefore, it needs to be made more efficient. The efficiency can be improved in two ways firstly, optimizing the numerical algorithms and secondly through the use of dynamically adaptive computational grid. Currently, the uniform structured grid used has limitations in properly representing the local regions and hence the interfacial dynamics are not captured accurately. Using dynamically adaptive grid will not only minimize the number of grid points but will also help in a better discretization of the critical zones (essentially across hydrate / fluid interfaces).

9.2 Improvement in PFT Model to Incorporate Salinity Effect

The current thermodynamic model in the PFT has been used assuming pure water system. It is important to implement the chemical potential of water as a function of salinity in the thermodynamic model since the presence of salt ions in the water will affect the chemical potential of the water as well as guest molecules solubility in the aqueous phase. Thermodynamic driving force for hydrate formation will be reduced in the presence of salt due to the reduction in water chemical potentials and this will affect the growth rate of hydrate. If the concentration of salt is high enough this will lead to dissociation of hydrate. The simplest way to include this is by a correction of the water chemical potential through the activity induced by the specific salinity in consideration. One limitation of this approach is that the ionic concentration will locally increase as a function of hydrate formation.

Another approach is to include salt, which will be inert with respect to hydrate phase transitions, as an additional component in the PFT. This latter modification would make it possible to study the impact of salt ion increase on the surrounding water during hydrate formation.

9.3 Imporvement in Hydrodynamics Model

The current hydrodynamics model ignores bubble merging. Dissociation of hydrate leads to a rapid release of CH4 in the form of bubbles which collide with each other and ultimately merge together. Proper implementation of hydrodynamics is needed to incorporate variations in local viscosity and interfacial tension through which local forces of collisions are analysed with respect to either bubble merging or bubble deformation. As mention earlier, the current PFT model is implemented on a uniform cartesian grid which is not effective for modelling merging, growth, and changes in shapes of bubbles. The grid system needs to be upgraded to a dynamically adaptive grid system (e.g. section 9.1) but the range of needed grid resolutions is different than in the regions around interfaces involved in the phase transitions. This new implementation is also expected to play a significant role in modelling a rising droplet surrounding by CO2 hydrate.

9.4 Phase Field Code Coupling with Retraso Code Bright (RCB)

The world is in a serious situation in its efforts to combat climate change. Climate change will have severe impacts globally in the absence of fully committed and urgent action towards the reduction of GHG (CO2) emissions according to the International Panel on Climate Change (IPCC). One option is to inject CO2 in cold aquifers for long term storage. The injected CO2 can form hydrate in contact with water under the upper regions of reservoirs where conditions of pressure and temperature are favourable. It is assumed that the hydrate film will be stable and will block the flow of CO2 in all directions in regions where hydrates are formed. However, this is not entirely true because hydrates formed in these reservoirs can be thermodynamically unstable due

to the presence of different concentrations of components in different phases. To study the formation of layers and its stability which can provide the desired sealing effects, it is important that the PFT is coupled to a reservoir simulator (RCB is one of the options). Direct implementation of PFT in reservoir simulators may not be feasible due to its computationally expensive nature. A more feasible way is to use PFT for systematic studies of specific pore structures representative of a given reservoir and then implement mathematically simplified parameterizations that reflect the main features of the phase transition dynamics into RCB.

The option of CO2 storage via the exchange of CH4 by CO2 in GHs, which was one of the main focus area of this work, is capable of solving two problems at once; that of energy production and of long term CO2 storage. The exchange takes place by two different mechanisms 1) faster exchange resulting from *in situ* dissociation due to substantial heat released by the new CO2 hydrate formation in contact with residual pore water. 2) slower solid-exchange process due to solid state diffusivity in the absence of free water. The developed PFT can estimate the kinetic rates of the exchange processes which can be utilized for a more accurate reservoir simulation.

9.5 Improvement in the Model to Incorporate Multiple Hydrates Effect and Multiple Occupancy

In the presence of more than one species of guest molecules, the most stable hydrate forms from the best hydrate formers and after its consumption a lesser stable hydrate forms from the rest of the guest molecules according to the first and second law of thermodynamics. As a consequence of this, a range of different hydrates form with less stability due to progressively increasing free energy. The multiple hydrates are treated as different phases.

This is very relevant with exchange process simulations with N2 and CO2 as this mixture has already been used in the Alaska Prudhoe bay. First CO2 dominates hydrate formation in the large cavities as it is the most stable hydrate former. Secondly, as the CO2 is completely consumed, N2 continues to penetrate in large

cavities and forms hydrate where there is more than one N2 in a single large cavity due to its size. It is worth mentioning that it is not clear what conditions are required for N2 to doubly occupy the large cavity. So implementation of N2 into the PFT model is a very useful option which would enable us to study N2-CH4 and N2-CO2 hydrate systems. Until now there are numerous experimental studies available for these systems, but almost no theoretical study. The current thermodynamic model described in this study is not valid for multiple occupancy but the required extension can be followed by the work done by Kvamme (2016) and Bauman (2015). Hence the kinetic theory that will handle the multiple occupancy situation would be achieved by the extension of PFT's free energy functional to 4 components as well as through the implicit implementation of the extended thermodynamics in the current PFC.

9.6 Improvement in Heat Transport Model and PFT

The current PFT model can handle dissociation of hydrates using reduction of pressure during which heat transport kinetics is often a limiting factor and a very complex problem since there are dynamically varying multiple phases (gas, liquid water, hydrate, minerals) in the system. Therefore, the parameters which are required to be implemented are the chemical potentials of different fluids adsorbed on these surfaces, specific enthalpies for solid materials, and thermal conductivities.

9.7 PFT for Non-spherical Cores

The PFT model can be extended to account for mineral pores in terms of pore geometry and mineralogy which enables us to study the aforementioned phenomena at pore scales creating new ways to examine heat transport mechanisms and rates for real systems. This extension will also be useful to study the effects of pore geometry on the formation of hydrates. As it is almost impossible to form hydrate in the nano-scale pore size due to the short length scale, so it is important to know the minimum pore size where hydrate formation begins and the pore size is no longer significantly affecting the hydrate stability.

References:

Ahmadi, G., Ji, C. & Smith, D. H., 2004. Numerical solution for natural gas production from methane hydrate dissociation. *Journal of petroleum science and engineering,* Volume 41, pp. 269-285.

Archer, D., 2007. Methane hydrate stability and anthropogenic climate change. *Biogeosciences Discussions,* Volume 4, pp. 521-544.

Baig, K., 2009. *Phase Field Theorey Modeling of CH4 and CO2 Fluxes from Exposed Natural Gas Hydrate reservoirs.* Bergen: BORA.

Baig, K., Kvamme, B., Kuznetsova, T. & Bauman, J., 2015. Impact of water film thickness on kinetic rate of mixed hydrate formation during injection of CO2 into CH4 hydrate. *AIChE Journal,* 61(11), p. 3944–3957.

Bauman, J. M., 2015. *Kinetic Modelling of Hydrate Formation, Dissociation, and Reformation,* Bergen: University of Bergen.

Beget, J. E. & Addison, J. A., 2007. Methane gas release from the Storegga submarine landslide linked to early Holocene climate change: a speculative hypothesis. *The Holocene,* 17(3), pp. 291-295.

Boetius, A. & Suess, E., 2004. Hydrate Ridge: a natural laboratory for the study of microbial life fueled by methane from near-surface gas hydrates. Chemical Geology 205, 291–310. *Chemical Geology,* Volume 205, p. 291–310.

Boswell, R. & Collett, T., 2011. Current perspectives on gas hydrate resources. *Energy and Environmental Science,* Volume 4, pp. 1206-1215.

Boswell, R. et al., 2009. Joint industry project Leg II discovers rich gas hydrate accumulations in sand reservoirs in the Gulf of Mexico, Fire in the Ice, US Department of Energy, Office of Fossil Energy. *National Energy Technology Laboratory,* Volume 9, pp. 1-5.

Bouriak, S., Vanneste, M. & Saoutkine, A., 2000. Inferred gas hydrates and clay diapirs near the Storegga Slide on the southern edge of the Vbring Plateau, offshore Norway. *Marine Geology,* 163(1-4), pp. 125-148.

BP p.l.c., 2013. *BP Statistical Review of World Energy June 2013.* [Online]
Available at: http://www.bp.com/content/dam/bp/pdf/statistical-review/statistical_review_of_world_energy_2013.pdf
[Accessed 28 September 2015].

Buffett, B. & Zatsepina, O., 2000. Formation of gas hydrate from dissolved gas in natural porous media. *Marine Geology,* 164(1-2), pp. 69-77.

Bureau of Energy MOEA, 2015. *Energy statistics handbook 2014, <http://web3.moeaboe.gov.tw/ECW/populace/content/wHandMenuFile.ashx?menu_id=682>*. s.l.:s.n.

Cameron, I., Handa, Y. & Baker, T., 1990. Compressive strength and creep behavior of hydrate-consolidated sand. *Canadian Geotechnical Journal,* Volume 27, pp. 255-258.

Carman, G. & Hardwick, P., 1983. Geology and regional setting of Kuparuk Oil Field, Alaska. *American Association of Petroleum Geologists Bulletin,* Volume 67, pp. 1014-1031.

Chong, Z. et al., 2015. Review of natural gas hydrates as an energy resource: Prospects and challenges. *Applied Energy,* Volume Available online 4 February 2015, ISSN 0306-2619, http://dx.doi.org/10.1016/j.apenergy.2014.12.061..

Circone, S. et al., 2003. CO2 Hydrate: Synthesis, Composition, Structure, Dissociation Behavior, and a Comparison to Structure I CH4 Hydrate. *J. Phys. Chem. B,* pp. 5529-5539.

CMG Ltd., 2007. *Computer Modeling Group Ltd..* [Online]
Available at: http://www.cmgl.ca/software/stars2016
[Accessed 7 June 2016].

Collet, T. S., 2002. Energy resource potential of natural gas hydrates. *Aapg Bull,* Volume 86, pp. 1971-92.

Conti, M., 1997. Solidification of binary alloys: Thermal effects studied with the phase-field model. *Physical Review A.,* Volume 55, pp. 765-771.

Conti, M., 2000. Thermal and chemical diffusion in the rapid solidification of binary alloys. *Physical Review E.,* Volume 61, pp. 642-650.

Coutinho, J. A. P., Kontogeorgis, G. M. & Stenby, E. H., 1994. Binary interaction parameters for nonpolar systems with cubic equations of state - a theoretical approach .1. CO2 hydrocarbons using SRK equation of state. *Fluid phase equilibria,* Volume 102, pp. 31-60.

Cranganu, C., 2009. In-situ thermal stimulation of gas hydrates. *Journal of Petroleum Science and Engineering,* Volume 65, pp. 76-80.

Dai, S., Lee, C. & Santamarina, J., 2011. Formation history and physical properties of sediments from the Mount Elbert Gas Hydrate Stratigraphic Test Well, Alaska North Slope. *Marine and Petroleum Geology,* Volume 28, pp. 427-438.

Davie, M. K. & Buffett, B. A., 2001. A numerical model for the formation of gas hydrates below the seafloor. *Journal of Geophysical Research,* 106(B1), pp. 497-514.

Demirbas, A., 2010. Methane Gas Hydrate: as a Natural Gas Source. In: *Methane Gas Hydrate.* London: Springer, pp. 113-160.

Demirbas, A., 2010. Methane hydrates as potential energy resource: part 2-methane production processes from gas hydrates. *Energy Convers Manage,* Volume 51, p. 1562–1571.

Duc, N. J., Chauvy, F. & Herri, J. M., 2007. CO2 Capture by Hydrate crystallization - A potential Solution for Gas emission of Steelmaking Industry. *Energy Conversion and Management,* Volume 48, p. 1313–1322.

E.I.A, U., 2013. *Annual energy outlook 2013,* Washington D.C.: U.S. Department of Energy.

E.I.A, U., 2013. *Carbon dioxide emissions coefficients,* Washington D.C: U.S. Department of Energy.

Elder, K. R. et al., 2007. Phase-field crystal modeling and classical density functinal theory of freezing. *Physical Review E,* Volume 75, p. 064107.

Evans, R. & Sluckin, T. J., 1980. A Density Functional Theory for Inhomogeneous Charged Fluids - Application to the Surfaces of Molten-Salts. *Molecular Physics,* 40(2), pp. 413-435.

ExxonMobil, 2014. *The outlook for energy: a view to 2040,* s.l.: s.n.

Gamwo, I. K. & Liu, Y., 2010. Mathematical modeling and numerical simulation of methane production in a hydrate reservoir. *Industrial & engineering chemistry research,* Volume 49, pp. 5231-5245.

Garapati, N., McGuire, P. & Anderson, B. J., 2013. *Modeling the Injection of Carbon Dioxide and Nitrogen into a Methane Hydrate Reservoir and the Subsequent Production of Methane Gas on the North Slope of Alaska.* Denver, Colorado, USA, s.n.

Grimme, S., Antony , J., Schwabea, T. & Mück-Lichtenfelda, C., 2007. Density functional theory with dispersion corrections for supramolecular structures, aggregates, and complexes of (bio)organic molecules. *Org. Biomol. Chem.,* Volume 5, pp. 741-758.

Gudmundsson, J. & Mork, M., 2001. *STRANDED GAS TO HYDRATE FOR STORAGE AND TRANSPORT.* Amsterdam, s.n.

Gudmundsson, J. S. & Børrehaug, A., 1996. *Frozen Hydrate for Transport of Natural Gas. In: Guillon O.* France: Toulouse, s.n.

Harbitz, C. B., 1992. Model simulations of tsunamis generated by the Storegga slides. *Marine Geology,* 105(1-4), pp. 1-21.

Herri, J. M. et al., 2014. Enhanced Selectivity of the Separation of CO2 from N2 during Crystallization of Semi-Clathrates from Quaternary Ammonium Solutions. *Oil & Gas Science and Technology – Rev. IFP Energies nouvelles,* 69(5), pp. 947-968.

Huenges, E., Henninges, J., Schrötter, J. & Erbas, K., n.d. *Spatial and temporal variation of temperature during a gas hydrate production.* [Online]
Available at: http://www-icdp.icdp-online.org/front_content.php?idart=1721
[Accessed 23 08 2015].

IEA, 2008. *Energy Technology Perspectives,* Paris: France: IEA.

IEA, 2008. *World Energy Outlook,* Paris: International Energy Agency.

IEA, 2015. *World Energy Outlook,* Paris: International Energy Agency.

JAPEX, 2016. *JAPEX Corporate Guide 2016.* [Online]
Available at: http://www.japex.co.jp/english/company/pdfdocs/library/JAPEX_CorporateGuide_e.pdf
[Accessed 18 December 2016].

Jassim, E. & Abdi, M. A., 2008. *A CFD-Based Model to Locate Flow Restriction Induced Hydrate Deposition in Pipelines", Manuscript OTC 19190.* Houston, Texas, USA, s.n.

JOGMEC, 2013. *Japan Oil, Gas and Metals National Corporation.* [Online]
Available at: http://www.jogmec.go.jp/english/news/release/release0110.html
[Accessed 18 December 2016].

Johnson, K., 2014. *Burning Ice and the Future of Energy. http://www.foreignpolicy.com/articles/2014/04/25/a_song_of_ice_and_fire_and_methane_hydrates.* [Online].

Kavanaugh, M. C. & Trussell, R. R., 1980. Design of aeration towers to strip volatile contaminants from drinking water. *J. Am. Water Works Assoc.,* Volume 72, pp. 684-692.

Khokhar, A. A., Gudmundsson, J. S. & Sloan, E. D., 1998. Gas storage in structure H hydrates. *Fluid Phase Equilib.,* Volume 150–151, p. 383–392.

Kim, H., Bishnoi, P., Heidemann, R. & Rizvi, S., 1987. Kinetics of methane hydrate decomposition. *Chemical engineering science,* Volume 42, pp. 1645-1653.

Koh, C. A., Sloan, E. D., Sum, A. K. & Wu, D. T., 2011. Fundamentals and Applications of Gas Hydrates. *Annual Review of Chemical and Biomolecular Engineerng,* Volume 2, pp. 237-257.

Kowalsky, M. B. & Moridis, G. J., 2007. Comparison of kinetic and equilibrium reaction models in simulating gas hydrate behavior in porous media. *Energy Conversion and Management,* Volume 48, pp. 1850-1863.

Kvamme, B., 1996. *A new theory for the kinetics of hydrate formation.* Toulose, France, In Proceedings from the second International Conference on Natural Gas, pp. 131-146.

Kvamme, B., 2003. Droplets of dry ice and cold liquid CO2 for self transport to large depths. *International Journal of Offshore and Polar Engineering,* Volume 13, pp. 1-8.

Kvamme, B., 2016. Thermodynamic Limitations of the CO2/N2 Mixture Injected into CH4 Hydrate in the Ignik Sikumi Field Trial. *Journal of chemical & engineering data,* Volume 61, pp. 1280-1295.

Kvamme, B., Baig, K., Qasim, M. & Bauman, J., 2013. Thermodynamic and Kinetic Modeling of CH4/CO2 Hydrates Phase transitions. *International Journal of Energy and Environment,* Volume 7, pp. 1-8.

Kvamme, B. et al., 2003. Kinetics of solid hydrate formation by carbon dioxide: Phase field theory of hydrate. *Physical chemistry chemical physics,* 9(6).

Kvamme, B. et al., 2007. Storage of CO2 in natural gas hydrate reservoirs and the effect of hydrate as an extra sealing in col aquifers. *International Journal of Greenhouse Gas Control,* Volume 1/2, pp. 236-246.

Kvamme, B., Kuznetsova, T. & Kivelæ, P. H., 2012. Adsorption of water and carbon dioxide on hematite and consequences for possible hydrate formation. *Physical Chemistry Chemical Physics,* 14(13), pp. 4410-4424.

Kvamme, B., Kuznetsova, T., Kivelæ, P. H. & Bauman, J., 2013. Can hydrate form in carbon dioxide from dissolved water?. *Phys. Chem. Chem. Phys.,* Volume 15, pp. 2063-2074.

Kvamme, B. et al., 2014. Hydrate Phase Transition Kinetics from Phase Field Theory with Implicit Hydrodynamics and Heat Transport. *Internation Journal of Green House Gas Control,* Volume 29, pp. 263-278.

Kvamme, B., Svandal, A., Buanes, T. & Kuznetsova, T., 2009. Phase field approaches to the kinetic modeling of hydrate phase transitions. In: *Natural gas hydrates—Energy resource potential and associated geologic hazards.* s.l.:AAPG Memoir 89, pp. 758-769.

Kvamme, B. & Tanaka, H., 1995. Thermodynamic stability of hydrates for ethene, ethylene and carbon dioxide. *J. Chem. Phys,* Issue 99, pp. 7114-7119.

Kvenvolden, K. A. & Harbaugh, J. W., 1983. Reassessment of the rates at which oil from natural sources enters the marine environment. *Marine Environmental Research,* Volume 10, p. 223–243.

Kvenvolden, K. A. & Lorenson, T. D., 2001. The global occurrence of natural gas hydrates. In: C. K. P. a. P. Dillon, ed. *Natural Gas Hydrates: Occurrence, Distribution, and Detection.* Washington, D. C.: American Geophysical Union, pp. 3-18.

Kvenvolden, K. A., Lorenson, T. D. & Reeburgh, W. S., 2001. Attention turns to naturally occurring methane seepage. *EOS Transactions,* Volume 82, p. 457.

Lee, M. & Collett, T., 2011. In-situ gas hydrate hydrate saturation estimated from various well logs at the Mount Elbert Gas Hydrate Stratigraphic Test Well, Alaska North Slope. *Journal of Marine and Petroleum Geology,* Volume 28, pp. 439-449.

Letcher, T. M., 2014. *Future Energy e Improved, Sustainable and Clean Options for Our Planet, second ed.* Boston: Elsevier.

Li, J. C. M., 1956. Clapeyron equation for multicomponent systems. *J. Chem. Phys.,* Volume 25, pp. 572-574.

Liu Y, Y., Strumendo, M. & Arastoopour, H., 2009. Simulation of methane production from hydrates by depressurization and thermal stimulation. *Industrial & Engineering Chemistry Research,* 48(5), p. 2451–2464.

Locat, J. & Lee, H. J., 2002. Submarin Landslides: Advances and Challenges. *Canadian Geotechnical Journal,* 39(1), pp. 193-212.

Lorenson, T., Collett, T. & Hunter, R., 2008. *Preliminary assessment of hydrocarbon gas source from the Mt. Elbert No.1 gas hydrate test well, Milne Pt, Alaska.* Vancouver, s.n.

Luff, R. et al., 2005. Simulation of long-term feedbacks from authigenic carbonate crust formation at cold vent sites. Chemical Geology 216, 157–174.. *Chemical Geology,* Volume 216, p. 157–174.

Lu, S., 2015. A global survey of gas hydrate development and reserves: Specifically in the marine field. *Renewable and Sustainable Energy Reviews,* Volume 41, p. 884–900.

MacDonald, I. R. et al., 1994. Gas hydrates that breaches the sea floor on the continental slope of the Gulf of Mexico. *Geology,* Volume 22, p. 699–702.

Makogon, Y. F., 1997. *Hydrates of Hydrocarbons.* Tulsa(Oklahama): Penn Well Publishing Company.

Maslin, M. et al., 2010. Gas hydrates: past and future geohazard?. *Philosophical Transactions of the Royal Society A: Mathematical,Physical and Engineering Sciences,* 368(1919), pp. 2369--2393.

Masterson, W. et al., 2001. Evidence for biodegradation and evaporative fractionation in West Sak, Kuparuk and Prudhoe Bay field areas, North Slope, Alaska. *Organic Geochemistry,* Volume 32, pp. 411-441.

Max, M. D., Johnson, A. H. & Dillon , W. P., 2006. *Economic geology of natural gas hydrate.* Dordrecht: Springer.

McIver, R. D., 1982. Role of naturally occurring gas hydrates in sediment transport. *AAPG Bulletin,* 66(6), pp. 789-792.

METI, 2001. *Japanese methane hydrate development plan,* s.l.: s.n.

MH21 Research Consortium, n.d. *MH21 First marine production test for methane hydrate.* [Online]
Available at: http://www.mh21japan.gr.jp/mh21/kss/
[Accessed 23 08 2015].

MH21 Research Consortium, n.d. *MH21 Japan's methane hydrate R&D program.* [Online]
Available at: http://www.mh21japan.gr.jp/english/infomation/558/
[Accessed 23 08 2015].

Moridis, G. J., 2003. Numerical studies of gas production from hydrates. *SPE Journal,* Volume 32, p. 359–370.

Moridis, G. J. et al., 2013. *Gas Hydrates as a Potential Energy Source: State of Knowledge and Challenges. In: J. W. Lee (ed.), Advanced Biofuels and Bioproducts.* s.l.:Springer.

Moridis, G. J. et al., 2011. Challenges, Uncertainties, and Issues Facing Gas Production from Gas Hydrates Deposits. *Society of Petroleum Engineers,* pp. 76-112.

Mu, D., Liu, Z. S., Huang , C. & Djilali, N., 2008. Determination of the effective diffusion coefficient in porous media including Knudsen effects. *Microfluidics Nanofluidics,* Volume 4, p. 257–260.

Nakai, S. & Mitsui Engineering & Shipbuilding Co., Ltd., 2012. *Development of Natural Gas Hydrate (NGH) Supply Chain.* Kuala Lumpur, World Gas Conference.

Nakicenovic, N., 2002. Methane as an energy source for the 21st century. *International Journal of Global Energy Issues (IJGEI),* 18(1), pp. 6-22.

NETL, 2012. *NETL.* [Online]
Available at: http://www.netl.doe.gov/research/oil-and-gas/methane-hydrates/co2_ch4exchange
[Accessed 25 September 2014].

NETL, 2012. *The U.S. Department of Energy's National Energy Technology Laboratory (NETL).* [Online]
Available at: http://www.netl.doe.gov/research/oil-and-gas/methane-hydrates/co2_ch4exchange
[Accessed 25 September 2014].

Nixon, M. F. & Grozic, J. L., 2007. Submarine slope failure due to gas hydrate dissociation: a preliminary quantification. *Canadian Geotechnical Journal,* 44(3), pp. 314-325.

Okuda, Y., 1993. Natural gas hydrate as future resources. *J Jpn Inst Eng,* Volume 6, pp. 425-435.

Okuda, Y., 2005. Geological and geophysical studies on gas hydrate in Japan. *ICOGS Asia-Pacific Newsl,* Volume 7, pp. 24-31.

Ors, O. & Sinayuc, C., 2014. An experimental study on the CO2–CH4 swap process between gaseous CO2 and CH4 hydrate in porous media, Journal of Petroleum Science and Engineering. *Journal of Petroleum Science and Engineering,* Volume 119, pp. 156-162.

Parameswaran, V. R., Paradis, M. & Handa, Y. P., 1989. Strength of frozen sand containing tetrahydrofuran hydrate. *Canadian Geotechnical Journal,* 26(3), pp. 479-483.

Phirani, J. & Mohanty, K. K., 2010. *Kinetic Simulation of CO2 Flooding of methane hydrates.* Florence, Italy, s.n.

Qasim, M., 2013. *Microscale modeling of natural gas hydrates in reservoirs.* PhD Thesis: University of Bergen.

Rajnauth, J., Barrufet, M. & Falcone, G., 2013. Potential Industry Applications Using Gas Hydrate Technology. *The West Indian Journal of Engineering,* 2(2), pp. 15-21.

Reid, R. C., Prausnitz, J. M. & Sherwood, T. K., 1977. *The properties of Gases and Liquids.* s.l.:s.n.

Ripmeester, J. A., Tse, J. S., Ratcliffe, C. I. & Powell, B. M., 1987. A new clathrate hydrate structure. *Nature 325,* Volume 135.

Ruppel, C., 2011. Methane Hydrates and the Future of Natural Gas. MITEI Natural Gas Report. *Supplementary Paper on Methane Hydrates,* pp. 1-25.

Sander, R., 1999. Modeling atmospheric chemistry: interactions between gas-phase species and liquid cloud/aerosols particles. *Surv. Geophys.,* Volume 20, pp. 1-31.

Satoh, M., Maekawa, T. & Okuda, Y., 1996. Estimation of amount of methane and resources of natural gas hydrates in the world and around Japan. *The Journal of the Geological Society of Japan,* 102(11), p. 959–971.

Sloan, E. D. & Fleyfel, F., 1991. A molecular mechanism for gas hydrate nucleation from ice. *AIChE Journal,* Volume 37, pp. 1281-1292.

Sloan, E. D. & Koh, C. A., 2007. *Clathrate Hydrates of Natural Gases.* 3rd ed. Boca Raton(Florida): CRC press.

Sloan, E. D. & Koh, C. A., 2008. Clathrate Hydrates of Natural Gases. In: 3rd ed. Boca Raton(Florida): CRC press, p. 721.

Smith, T., n.d. *Gas Hydrates-Not So Unconventional.* [Online]
Available at: http://www.geoexpro.com/articles/2009/02/gas-hydrates-not-so-unconventional
[Accessed 23 08 2015].

Soave, G., 1972. Equilibrium constants from a modified Redlich-Kwong equation of state. *Chemical Engineering Science,* Volume 27, pp. 1197-1340.

Soave, G., 1972. Equilibrium Constants from a Modified Redlich-Kwong Equation of State. *Chemical Engineering Science,* Volume 27, pp. 1197-1203.

Span, R. & Wagner, W., 1996. A New Equation of State for Carbon Dioxide Covering the Fluid Region from the Triple-Point Temperature to 1100 K at pressure up to 800 MPa. *Journal of Phys. Chem.,* 25(6), pp. 1509 - 1596.

Sultan, N., Cochonat, P., Foucher, J. P. & Mienert, J., 2004. Effect of gas hydrates melting on seafloor slope instability. *Marine Geology,* 213(1-4), pp. 379-401.

Sun, X. & Mohanty, K. K., 2006. Kinetic simulation of methane hydrate formation and dissociation in porous media. *Chemical Engineering Science,* Volume 61, pp. 3476-3495.

Sun, Z. et al., 2004. Investigation on Gas Storage in Methane Hydrate. *Journal of Natural Gas Chemistry,* Volume 13, pp. 107-112.

Svandal, A., 2006. *Modeling hydrate phase transitions using mean-field approaches.* PhD Thesis: University of Bergen.

Svandal, A., Kuznetsova, T. & Kvamme, B., 2006b. Thermodynamic properties and phase transitions in the H2O/CO2/CH4 system. *Phys Chem Chem Phys,* Volume 8, pp. 1707-1713.

Tarazona, P. & Evans, R., 1984. A Simple Density Functional Theory for Inhomogeneous Liquids - Wetting by Gas at a Solid Liquid Interface. *Molecular Physics,* 52(4), pp. 847-857.

Thomas, S. & Dawe, R. A., 2003. Review of ways to transport natural gas energy from countries which do not need the gas for domestic use. *Energy,* 28(14), pp. 1461-1477.

Torres, M. et al., 2011. Pore fluid geochemistry from the Mount Elbert Gas Hydrate Stratigraphic Test Well, Alaska North Slope. *Journal of Marine and Petroleum Geology,* Volume 28, pp. 332-342.

Tsuji, Y. et al., 2009. Methane-hydrate Occurrence and Distribution in the Eastern Nankai Trough, Japan: Findings of the Tokai-oki to Kumano-nada Methane-hydrate Drilling Program, in:T. Collett, A. Johnson, C. Knapp, and R. Boswell, eds.. *Natural gas hydrates – Energy resource potential and associated geologic hazards, AAPG,* Volume Memoir 89, pp. 228-249.

Uchida, T. & Tsuji, T., 2004. Petrophysical properties of natural gas hydrates-bearing sands and their sedimentology in the Nankai Trough. *Resource Geology,* Volume 54, pp. 79-87.

Uddin, M., Coombe, D., Law, D. & Gunter, B., 2008. Numerical studies of gas hydrate formation and decomposition in a geological reservoir. *Journal of energy resources technology,* Volume 130, pp. 032501-032514.

van der Waals, J. H. & Platteeuw, J. C., 1959. Clathrate solutions. *Advances in Chem. Phys,* Volume 2, pp. 1-57.

Watanabe, S., Takahashi, S. & Mizu, H., 2008. *A DEMONSTRATION PROJECT OF NGH LAND TRANSPORTATION SYSTEM.* Vancouver, British Columbia, Proceedings of the 6th International Conference on Gas Hydrates (ICGH6).

Weng, T. W., Lo, S. C., Huang, J. H. & Li, C. F., 2013. The general situation of the distribution and potential volume of gas hydrate in the south China. *Min Metall,* 57(2), pp. 56-70.

Wheeler, A. A., Boethinger, W. J. & McFadden, G. B., 1992. Phase field model for isothermal phase transitions in binary alloys. *Physical Review A,* Volume 45, pp. 7424-7439.

Winters, W. J. et al., 2001. *Relationships between frozen and gas hydrate-containing sediment.* Russia, s.n.

Xinpo, L. & Siming, H., 2012. Progress in stability analysis of submarine slopes considering dissociation of gas hydrates. *Environmental Earth Sciences,* 66(3), pp. 741-747.

Xu, W. & Germanovich, L. N., 2006. Excess pore pressure resulting from methane hydrate dissociation in marine sediments: A theoretical approach. *Journal of Geophysical Research,* 111(B1), pp. 1-12.

Yamamoto, A., Yamanaka, Y. & Tajika, E., 2009. Modeling of methane bubbles released from large sea-floor area: condition required for methane emission to the atmosphere. *Earth and Planetary Science Letters,* Volume 284, p. 590–598.

Yang, M. et al., 2013. Dynamic measurements of CO2 flow in water saturated porous medium at low temperature using MRI. *Energy Procedia,* Volume 37, p. 1267 – 1274.

Zheng, D. Q., Guo, T. M. & Knapp, H., 1997. Experimental and modeling studies on the solubility of CO2, CHCLF2, CHF3, C2H2F4 and C2H4F2 in water and aqueous NACL solutions under low-pressures. *Fluid Phase Equilib.,* Volume 129, pp. 197-209.

List of Papers Presented

M. Qasim, B. Kvamme, and K. Baig, Phase field theory modeling of CH4/CO2 gas hydrates in gravity fields, International Journal of Geology, Volume 5, Issue 2, 2011, pp. 48-52

M. Qasim, B. Kvamme and K. Baig, Modeling Dissociation and Reformation of Methane and Carbon Dioxide Hydrate using Phase Field Theory with implicit hydrodynamics, In Proceedings from the 7th international conference on gas hydrate (ICGH7), Edinburgh, Scotland, July 17, 2011- July 21, 2011, 9 pages

M. Qasim, K. Baig and B. Kvamme, Phase Field Theory modeling of Phase transitions involving hydrate, In Proceedings from the 9th international conference on Heat and Mass transport, Harvard, Cambridge, USA, January 25-27, 2012, pp. 222-228

B. Kvamme, K. Baig, M. Qasim and J. Bauman, Thermodynamics and Kinetic Modeling of CH4/CO2 Hydrates Phase transitions, International Journal of Energy and Environment, Volume 7, Issue 1, 2013, pp. 1-8

M. Qasim, K. Baig, B. Kvamme and J. Bauman, Mix Hydrate formation by CH4-CO2 exchange using Phase Field Theory with implicit Thermodynamics, International Journal of Energy and Environment, Volume 6, Issue 5, 2012, pp. 479-487

B. Kvamme, M. Qasim, K. Baig and P. H. Kivelä, J. Bauman, Hydrate phase transition kinetics from Phase Field Theory with implicit hydrodynamics and heat transport, International Journal of Greenhouse Gas Control, Volume 29, 2014, pp. 263-278

K. Baig, B. Kvamme, T. Kuznetsova, and J. Bauman, Impact of water film thickness on kinetic rate of mixed hydrate formation during injection of CO2 into CH4 hydrate, AIChE Journal, Volume 61, Issue 11, 2015, pp. 3944–3957

I

Paper 1

Phase field theory modeling of CH4/CO2 gas hydrates in gravity fields

M. Qasim, B. Kvamme, and K. Baig

International Journal of Geology, Volume 5, Issue 2, 2011, pp. 48-52

Phase field theory modeling of CH4/CO2 gas hydrates in gravity fields

M. Qasim, B. Kvamme[1], and K. Baig

***Abstract*—**Natural gas hydrates in reservoirs are thermodynamically unstable due to the interactions with surrounding fluids (aqueous, gas) and mineral surfaces. Depending on the local flow hydrate will dissociate as well as reform. If the dissociation rate is faster than the capacity of the surrounding fluids to dissolve the released gas, the gas will form bubbles. Depending on the rate of released gas and possible fracture patterns this may lead to venting of gas. The proper implementation of hydrodynamics will provide a deeper insight of the hydrate kinetics involved during dissociation and formation processes which involve hydrate former phase as smaller or larger bubbles or even continuous gas phase. In this work the phase field theory coupled with hydrodynamics model is implemented with variable density using the relative composition, phase field parameter and flow, which is an extension of our previous work which considers a constant density.

***Keywords*—**Phase field theory, Natural gas hydrate, Hydrodynamics, Dissociation, Hydrate.

I. Introduction

Gas hydrates are ice-like substances of water molecules encaging gas molecules (mostly methane) that form under specific pressure and temperature conditions within the upper hundred meters of the sub-seabed sediments. They occur worldwide and are a potential energy resource for the near future [1].

Natural gas hydrates are widely distributed in sediments along continental margins, and harbor enormous amounts of energy. Massive hydrates that outcrop the sea floor have been reported in the Gulf of Mexico [2]. Hydrate accumulations have also been found in the upper sediment layers of Hydrate ridge, off the coast of Oregon and a fishing trawler off Vancouver Island recently recovered a bulk of hydrate of approximately 1000kg [3]. Håkon Mosby Mud Volcano of Bear Island in the Barents Sea with hydrates are openly exposed at the sea bottom [4]. These are only few examples of the worldwide evidences of unstable hydrate occurrences that leaks methane to the oceans and eventually may be a source of methane increase in the atmosphere.

Hydrates of methane are not thermodynamically stable at mineral surfaces. From a thermodynamic point of view the reason is simply that water structure on hydrate surfaces are not able to obtain optimal interactions with surfaces of calcite, quarts and other reservoir minerals. The impact of this is that hydrates are separated from the mineral surfaces by fluid channels. The sizes of these fluid channels are not known and are basically not even unique in the sense that it depends on the local fluxes of all fluids in addition to the surface thermodynamics. Stability of natural gas hydrate reservoirs therefore depends on sealing or trapping mechanisms similar to ordinary oil and gas reservoirs. Many hydrate reservoirs are in a dynamic state where hydrate is leaking from top by contact with groundwater/seawater which is under saturated with respect to methane. Dissociating hydrate degasses as bubbles if dissociation rate is faster than dilution in surrounding fluids and/or surrounding fluid is supersaturated. The kinetic rate depends on mass transport dynamics as well as thermodynamic driving force. Phase field theory will be a power full tool to quantify this balance and provide basis for development of simplified models for reservoir modeling tools.

The primary focus in this work is to incorporate the density of all phases based on relative compositions and calculation of free gas exist in form of bubbles which can escape through empty channels and hence will be useful in calculation of an accurate natural gas flux.

II. Phase field theory

Phase field model follows the formulation of Wheeler et al. [5], which historically has been mostly applied to descriptions of the isothermal phase transition between ideal binary-alloy liquid and solid phases of limited density differences. The hydrodynamics effects were incorporated in a three components phase field theory by Kvamme et al. [6] through implicit integration of Navier stokes equation. The phase field ϕ is an order parameter describing the phase of the system as a function of spatial and time coordinates. The field ϕ is allowed to vary continuously on the range from solid to liquid.

The solid state is represented by the hydrate and the liquid state represents fluid and aqueous phase. The solidification of hydrate is described in terms of the scalar phase field $\phi(x_1, x_2, x_3)$ where x_1, x_2, x_3 represents the molar fractions of CH_4, CO_2 and H_2O respectively with obvious constraint on

Paper submitted October 29, 2010: Revised version submitted March 5, 2011. This work was supported financially by Norwegian research council under INJECT project and PETROMAKS project Gas hydrates on the Norwegian Research Council Sea-Svallbard margin (GANS, Project number. 175969/S30).

M. Qasim, is with the University of Bergen, Post box 7803, 5020 Bergen, Allegt. 55 Norway. (e-mail: Muhammad.Qasim@ift.uib.no).

B. kvamme[1], is with the University of Bergen, Post box 7803, 5020 Bergen, Allegt. 55 Norway (phone: +47-555-83310; e-mail: Bjorn.Kvamme@ift.uib.no).

K. Baig, is with the University of Bergen, Post box 7803, 5020 Bergen, Allegt. 55 Norway. (e-mail: kba062@ift.uib.no).

conservation of mass $\sum_{i=1}^{3} x_i = 1$. The field ϕ is a structural order parameter assuming the values $\phi = 0$ in the solid and $\phi = 1$ in the liquid [7]. Intermediate values correspond to the interface between the two phases. The starting point of the three component phase field model is a free energy functional [6],

$$\mathrm{F} = \int d\underline{r}\left(\frac{\varepsilon_\phi^2}{2}T(\nabla\phi)^2 + \sum_{i,j=1}^{3}\frac{\varepsilon_{xi,j}^2}{4}T\rho\big(x_i\nabla x_j - x_j\nabla x_i\big)^2 + f_{bulk}(\phi, x_1, x_2, x_3, T)\right), \quad (1)$$

which is an integration over the system volume, while the subscripts i, j represents the three components, ρ is molar density depends on relative compositions, phase and flow. The bulk free energy density described as

$$f_{bulk} = WTg(\phi) + \big(1 - p(\phi)\big)f_S(x_1, x_2, x_3, T) + p(\phi)f_L(x_1, x_2, x_3, T)\,. \quad (2)$$

The phase field switches on and off the solid and liquid contributions f_S and f_L through the function $p(\phi) = \phi^3(10 - 15\phi + 6\phi^2)$, and note that $p(\phi) = 0$ and $p(1) = 1$. This function was derived from density functional theory studies of binary alloys and has been adopted also for our system of hydrate phase transitions. The binary alloys are normally treated as ideal solutions. The free energy densities of solid and liquid is given by

$$f_S = G_S\rho_m^{hyd}\,, \quad (3)$$

$$f_L = G_L\rho_m^{L}\,. \quad (4)$$

The thermodynamics for the hydrate system is treated more rigorously and the free energy G_S and G_L are presented in thermodynamics section. Hydrate density ρ_m^{Hyd} is calculated using the formulation by Sloan et al. [8]

The liquid density ρ_m^{L} for fluid phase is calculated as

$$\bar{V}_L^{Fluid} = \sum_{i=1}^{3} x_i\bar{V}_i \qquad \rho_m^{L,Fluid} = \frac{1}{V_L^{Fluid}}\,, \quad (5)$$

where $\bar{V}_i$ represents the molar volume of *i*th component. The molar volume is calculated using gas law

$$\bar{V}_i = \frac{ZRT}{p} + \frac{nRT}{p}\left(\frac{\partial Z}{\partial n_i}\right)_{p,T,n_{i\neq j}}\,, \quad (6)$$

where p represents the pressure and Z is compressibility factor calculated using SRK equation of state. For simplicity to avoid partial molar volume at infinite dilution the density of liquid in aqueous phase is calculated as

$$V_L^{aqueous} = \sum_{i=1}^{2} x_i\bar{V}_i + x_3\bar{V}_3^0 \qquad \rho_m^{L,aqueous} = \frac{1}{V_L^{aqueous}}\,, \quad (7)$$

where $\bar{V}_3^0$ is the average molar volume of pure water. The function $g(\phi) = \phi^2(1-\phi^2)/4$ ensures a double well form of the f_{bulk} with a free energy scale $W = \left(1 - \frac{x_i}{v_m}\right)W_A + \frac{x_i}{v_m}W_B$ with $g(0) = g(1) = 0$, where v_m is the average molar volume of water. In order to derive a kinetic model we assume that the system evolves in time so that its total free energy decreases monotonically [7]. The usual equations of motion are supplemented with appropriate convection terms as explained by Tegze et al [9]. Given that the phase field is not a conserved quantity, the simplest form for the time evolution that ensures a minimization of the free energy is

$$\frac{\partial\phi}{\partial t} + (\vec{v}.\nabla)\phi = -M_\phi(\phi, x_1, x_2, x_3)\frac{\delta F}{\delta\phi}\,, \quad (8)$$

$$\frac{\partial x_i}{\partial t} + (\vec{v}.\nabla)x_i = \nabla.\left(M_{xi}(\phi, x_1, x_2, x_3)\nabla\frac{\delta F}{\delta xi}\right), \quad (9)$$

where $\vec{v}$ is the velocity, $M_{xi} = x_i(1 - x_i)\frac{1}{RT}D$ and $M_\phi = \left(1 - \frac{x_i}{v_m}\right)M^A + \frac{x_i}{v_m}M^B$ are the mobilities associated with coarse-grained equation of motion which in turn are related to their microscopic counter parts. Where $D = D_S + (D_L - D_S)p(\phi)$ is the diffusion coefficient. The detail may found elsewhere [6].

An extended phase field model is formed to account for the effect of fluid flow, density change and gravity. This is achieved by coupling the time evolution with the Navier Stokes Equations. An incompressible and viscous fluid is considered. The phase and concentration fields associates hydrodynamic equation as described by conti [10]-[12]

$$\frac{\partial\rho}{\partial t} = -\rho_m\nabla.\vec{v}, \qquad \rho\frac{\partial\vec{v}}{\partial t} + \rho(\vec{v}.\nabla)\vec{v} = \rho\vec{g} + \nabla.P. \quad (10)$$

Where $\vec{g}$ is the gravitational acceleration. ρ_m is the density of the system in hydrate (ρ_m^{Hyd}) and liquid (ρ_m^{L}). Further

$$P = \xi + \Pi. \quad (11)$$

is the generalization of stress tensor [10]-[13], ξ represents non-dissipative part and Π represents the dissipative part of the stress tensor.

III. Thermodynamics

The expression for chemical potential of water in hydrate is

$$\mu_3^H = \mu_3^{0,H} - \sum_i RT\Theta_i ln\left(1 + \sum_j h_{ij}\right), \qquad (12)$$

This equation is derived from the macro canonical ensemble under the constraints of constant amount of water, corresponding to an empty lattice of the actual structure. Details of the derivation are given elsewhere [14] and will not be repeated here. $\mu_3^{0,H}$ is the chemical potential for water in an empty hydrate structure and h_{ij} is the cavity partition function of component j in cavity type i. The first sum is over cavity types, and the second sum is over components j going into cavity type i. Here Θ_i is the number of type i cavities per water molecule.

A. Fluid Thermodynamics

The free energy of the fluid phase is assumed to have

$$G_L = \sum_{i=1}^{3} x_i \mu_i^{Fluid}, \qquad (13)$$

where μ_i^{Fluid} is the chemical potential of the ith component. The solubility of water is assumed to follow the Raoult's law. The lower concentration of water in the fluid phase and its corresponding minor importance for the thermodynamics results in the following form of water chemical potential with some approximation of fugacity and activity coefficient:

$$\mu_3^{Fluid} = \mu_3^{\infty} + RTln(y_3)\,, \qquad (14)$$

where μ_3^{∞} chemical potential of water at infinite dilution and y_3 is the mole fraction of water in the fluid phase. The chemical potential for the mixed fluid states considered as

$$\mu_i^{Fluid} = \mu_i^{SRK,pure} + RTln(y_3)\,, \qquad (15)$$

where i represents CH_4 or CO_2. The details are available in Svandal et al. [15].

B. Aqueous Thermodynamics

The free energy of the aqueous phase assumed as

$$G_L = \sum_{i=1}^{3} x_i \mu_i^{aqueous}, \qquad (16)$$

the chemical potential $\mu_i^{aqueous}$ of aqueous phase has the general form derived from excess thermodynamics

$$\mu_3^H = \mu_i^{\infty} + RTln(x_i \gamma_i^{\infty}) + v_i(P - P_0). \qquad (17)$$

μ_i^{∞} is the chemical potential of component i in water at infinite dilution, γ_i^{∞} is the activity coefficient of component i in the aqueous solution in the asymmetric convention (γ_i^{∞} approaches unity in the limit of x becoming infinitely small). The chemical potentials at infinite dilution as a function of temperature are found by assuming equilibrium between fluid and aqueous phases $\left(\mu_3^{Fluid} = \mu_3^{aqeouse}\right)$. This is done at low pressures where the solubility is very low, using experimental values for the solubility and extrapolating the chemical potential down to a corresponding value for zero concentration. The activity coefficient can be regressed by using the model for equilibrium to fit experimental solubility data. The chemical potential of water can be written as:

$$\mu_3 = \mu_3^p + RTln(1 - x)\gamma_3 + v_3(P - P_0), \qquad (18)$$

where μ_3^p is pure water chemical potential. The strategy for calculating activity coefficient is given in [15].

IV. RESULTS

The phase field model is implemented on a 2D geometry. This structure is used to dissociate circle of hydrate placed in the center surrounded by pure liquid water. The size of system is (500×500) grids with diameter of 200 grids for circular hydrate placed in the center as shown in Fig.1. One grid is equal to one angstrom (Å) and temperature (273.21 K) and pressure (63.90 bar) remain constant in the system. The values for temperature and pressure are taken at Nyegga cold seeps located on the edge of the Norwegian continental slope and the northern flank of the Storegga slide, on the border between two large oil/gas prone sedimentary basin – the Møre basin to the south and the Vøring basin to the north[16]-[17]. The temperature and pressure condition is well inside the stability region of CH_4. The standard value of 9.8 m/s^2 is assumed for gravity along the Y-axis of 2D geometry.

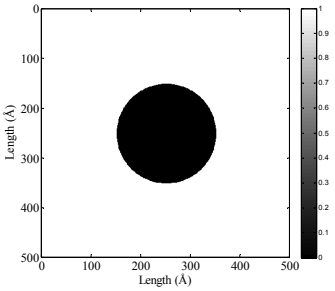

Fig. 1 Simulation at time zero, showing the initial picture of hydrate in black circle and liquid water in white with 500x500 Å and hydrate diameter of 200 Å.

The simulation is run to 3.6E+06 total time steps this corresponds to the time of 3.6 ns (Table.I).

Table. I The properties used to setup the simulations.

Total number of grid points	500×500
Corresponding area in m^2	2.5E-15
No. of time steps	3.6E+06
Total time in seconds	3.6E-09
CH_4 mole fraction in hydrate	0.14
Water mole fraction in liquid phase	1.0

The ratio between solid and liquid was taken as 1:2.5. This ratio is adjusted to achieve the stability.

The CH_4 concentration initially was adjusted to 0.14 in the hydrate assuming that all the cavities were filled with CH_4. The Fig.2(a) shows that the mole fraction is equals to the initial value which means that CH_4 has not yet diffused at time

zero. If the concentration of methane drops below the hydrate stability limit for the given temperature and pressure, a chemical potential driving force towards dissociation will arise as shown in Fig. 2(b) – 2(d). Also, these figures clearly indicate a non uniform dissociation of hydrate due to the effect of different velocities in different directions, which is a direct consequence of gravity.

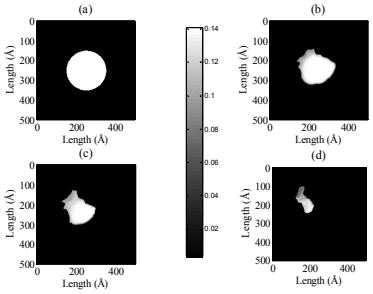

Fig. 2 The concentration profile, where a, b, c & d are 0, 1.225, 2.401 & 3.6 ns respectively.

The methane hydrate density is 5.089E+04 moles/m^3 and water density is 1000 kg/m^3 at time zero. The water density on the interface is decreasing due to the diffusion of dissociated methane from hydrate Fig.3. The dissociated gas may contain a fraction of free gas depending on the saturation of surrounding water with methane. The free gas exists in the form of bubbles which may escape in the environment through the empty channels.

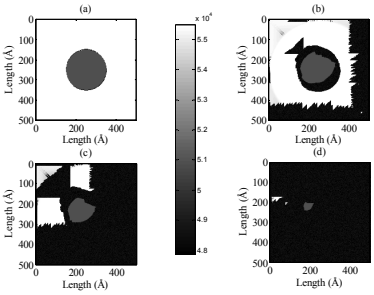

Fig. 3 Density of methane where a, b, c & d are 0, 1.225, 2.401 & 3.6 ns respectively.

The free gas is calculated by using the Raoult's law.

$$x_{CH_4} = \frac{y_{CH_4} f_{CH_4} P}{KH_{pc}}. \quad (19)$$

Where f_{CH_4} is the fugacity of methane, KH_{pc} is the Henry's constant in atm units at current temperature, P is the pressure of the system, y_{CH_4} is the concentration of methane containing free gas and x_{CH_4} is free gas concentration. The Henry's constant calculated using the formulation from [18].

$$KH_{pc} = K_H^{\Theta} exp\left(\frac{-\Delta_{soln}H}{R}\left(\frac{1}{T} - \frac{1}{T^{\Theta}}\right)\right). \quad (20)$$

Where K_H^{Θ} is the Henry's constant at temperature 298.15 K in M/atm, $\Delta_{soln}H$ is the enthalpy of the solution. The temperature dependence term is calculated as

$$\frac{-dlnk_H}{d(1/T)} = \frac{-\Delta_{soln}H}{R}. \quad (21)$$

The free gas calculation after dissociation of the CH_4 hydrate is shown in the Fig.4 (b) at some time instant when some hydrate is dissociated. The difference between CH_4 containing free gas can be seen from the values shown in color bars.

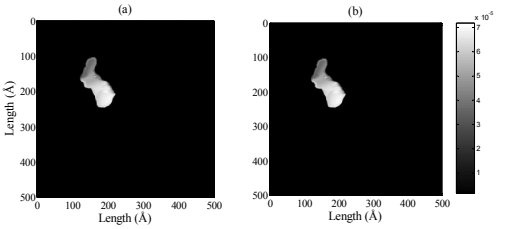

Fig. 4 Free gas profile, were (a) represents the methane concentration may contain free gas and (b) concentration of free gas.

The merging or deformation of bubbles depends on colliding force, elasticity and the interfacial energy of the bubbles. The criteria for potential merging or deformation may be found in literature. The thermo capillary and buoyancy forces drives the bubbles with velocity increasing with size and the square of the linear size respectively, thus large bubbles capture smaller bubbles [9]. Having the amount of free gas and velocity field, an improved and more realistic methane flux can be calculated than the previous work in Baig et al. [13].

V. DISCUSSION

Previous phase field models used for hydrate phase transitions dynamics like in Baig et al. [13] have been extended with more appropriate description of density dependencies in the phase field part as well as in the hydrodynamic parts. For the fluid phases containing variable relative amounts of CO_2 and CH_4 this will be crucial for two important cases. One case is the dissociation of mixed hydrates of these two components and the potential of free gas formation. The other important application is for simulations of the exchange process between CH_4 and CO_2 during injection of CO_2 into natural gas hydrate. In this case a crucial question is to what extent the released methane will dissolve into CO_2 versus the extent of separate methane bubbles escaping due to buoyancy. Simulation studies of these cases will follow in a subsequent paper and then related to experimental studies of the exchange process in porous media.

ACKNOWLEDGEMENT

This paper is a contribution to the Norwegian Research Council PETROMAKS project Gas hydrates on the Norwegian-Barents Sea-Svalbard margin (GANS, Norwegian Research Council Project No. 175969/S30). We are thankful for their financial support.

REFERENCES

[1] K. A. Kvenvolden, and B. W. Rogers, "Gaia's breath—global methane exhalations," *Marine and Petroleum Geology*, Vol.22, 2005, pp. 579-590.

[2] I. R. MacDonald, N. L. Guinasso , Jr., R. Sassen, J. M. Brooks, L. Lee and K. T. Scott**,** Gas hydrate that breaches the sea floor on the continental slope of the Gulf of Mexico, Aug. 1994, pp. 699-702.

[3] Rehder, G., S. H. Kirby, W. B. Durham, L. A. Stern, E. T. Peltzer, J. Pinkston, and P. G. Brewer, "Dissolution rates of pure methane hydrate and carbon-dioxide hydrate in undersaturated seawater at 1000-m depth," Geochimica et Cosmochimica Acta, Vol.68, Jan. 2004, pp. 285-292.

[4] A. V. Egorov, K. Crane, P. R. Vogt, A. N. Rozhkov, and P. P. Shirshov, "Gas hydrates that outcrop on the sea floor: stability models," Geo-Marine Letters, Vol.19, 1999, pp. 68-75.

[5] A. A. Wheeler, W. J. Boethinger, and G. B. McFadden, "Phase field model for isothermal phase transitions in binary alloys," Physical Review A, Vol. 45, May. 1992, pp. 7424-7439.

[6] B. Kvamme, A. Svandal, T. Buanes, and T. Kuznetsova, "Phase field approaches to the kinetic modeling of hydrate phase transitions," In Proc. Natural Gas Hydrates: Energy Resource Potential and Associated Geologic Hazards, Vancouver, BC, Canada, September 12-16, 2004.

[7] A. Svandal, "Modeling hydrate phase transitions using mean field approaches," University of Bergen, 2006, pp. 1-37.

[8] E. D. Sloan, and C. A. Koh, "Clathrate hydrates of natural gases (3rd ed.)," Boca Raton, FL: CRC Press, 2008.

[9] G. Tegze, and L. Gránásy, "Phase field simulation of liquid phase separation with fluid flow," Material science and engineering, vol. 413-414, Dec. 2005, pp. 418-422.

[10] M. Conti, "Density change effects on crystal growth from the melt," Physical Review, Vol.64, 2001, pp. 051601.

[11] M. Conti, and M. Fermani, "Interface dynamics and solute traping in alloy solidification with density change," Physical Review, Vol.67, 2003, pp. 026117.

[12] M. Conti, "Advection flow effects in the growth of a free dendrite," Physical Review, Vol. 69, 2004, pp. 022601.

[13] K. Baig, M. Qasim, P. H. Kivelä, and B. Kvamme, "Phase field theory modeling of methane fluxes from exposed natural gas hydrate reservoirs," American Institute of Physics, 2010, in press.

[14] B. Kvamme, and H. Tanaka, "Thermodynamic stability of hydrates for ethane, ethylene and carbon dioxide," J. Chem. Phys., Vol. 99, 1995, pp. 7114-7119.

[15] A. Svandal, T. Kuznetsova, and B. Kvamme, "Thermodynamic properties and phase transitions in the H2O/CO2/CH4 system," Fluid Phase Equilibria, Vol.246, 2006, pp. 177-184.

[16] Y. Chen, H. Haflidason, and J. Knies, "Methane fluxes from pockmarks areas in Nyegga, Norwegian sea," Internation Geology Conference, 2008.

[17] S. Bunz, J. Mienert, and C. Berndt, "Geological controls on the Storegga gas-hydrate system of the mid-Norwegian continental margin," Earth and planetary Science Letters, 209(3-4), 2003, pp. 291-307.

[18] R. Sander,"Modeling atmospheric chemistry: interactions between gas – phase species and liquid cloud/aerosol particles," Surveys in Geophysics, Vol.20, 1999, pp. 1-31.

Paper 4

Thermodynamics and Kinetic Modeling of CH4/CO2 Hydrates Phase transitions

B. Kvamme, K. Baig, M. Qasim and J. Bauman

International Journal of Energy and Environment, Volume 7, Issue 1, 2013, pp. 1-8

IV

Thermodynamic and Kinetic Modeling of CH4/CO2 Hydrates Phase transitions

B. Kvamme[1], K. Baig, M. Qasim and J. Bauman

***Abstract*—**Natural gas hydrates in reservoirs are thermodynamically unstable due to exposure to mineral surfaces and possibly undersaturated phases of water and hydrate formers. Changes in global temperatures also alter the stability regions of the accumulations of gas hydrates worldwide. The fact that hydrates in porous media never can reach equilibrium, and formation can occur from different phases, as well as dissociate according to different thermodynamic driving forces imposes very complex phase transition dynamics. These phase transitions dynamics are solutions to coupled differential equations of mass transport, heat transport and phase transition kinetics. The availability of free energy as functions of temperature, pressure and the composition of all components in all phases in states outside of equilibrium is therefore necessary in kinetic theories based on minimisation of free energy. For this purpose we have applied an extended adsorption theory for hydrate, SRK equation of state for methane/CO2 gas and solubilities of these components in water for the limit of water thermodynamics. The thermodynamic model is developed for calculation of free energy of super saturated phase along all different gradients (mole fractions, pressure and temperature) of super saturation.

***Keywords*—**Gas hydrates, Kinetic modeling, Phase transitions, Thermodynamics.

I. Introduction

GAS as hydrates are crystalline solids which occur when water molecules form a cage like structure around a non-polar or slightly polar (eg. CO2, H2S) molecule. These enclathrated molecules are called guest molecules and obviously have to fit into the cavities in terms of volume. In this work we focus on two specific guest molecules; carbon dioxide (CO2) and methane (CH4). Processing, transport and storage of carbon dioxide and potential hydrate formation is a timely issue. Natural gas is dominated by methane and processing as well as transport of methane involves conditions of hydrate stability in terms of temperature and pressure. In addition to methane from conventional hydrocarbon reservoirs huge amounts of methane is trapped inside water in the form of hydrates. Both of these guest molecules form structure I hydrate with water. Macroscopically, hydrates are similar in appearance to ice or snow. At sufficiently high pressure, hydrates are also stable at temperatures where ice cannot form. The encaged guest molecules are able to stabilize the hydrate through their interactions with the water molecules making up the cavity walls.

The description of hydrate phase thermodynamics typically follows the approach pioneered by van der Waal & Platteeuw [1]. A disadvantage of this simplified semi grand canonical ensemble result is that the empty clathrate were considered as rigid and unaffected by the inclusion of guest molecules. Another disadvantage in the typical engineering use of this is the lack of values for empty clathrate which have led to the use of chemical potential of liquid water (or ice) minus that of empty clathrate. This involves that a number of fundamental thermodynamic properties have been fitted empirically. An alternative form was derived by Kvamme & Tanaka [2] and examined using molecular dynamics simulations and two models for estimation of cavity partition function. The first was the classical integration over the Boltzmann factor for the cavity partition function using a rigid water lattice and the second one was a harmonic oscillator approach with full dynamics of all molecules and sampling of frequencies for displacements. An advantage of the latter approach is the sampling of frequencies that interferes with water lattice movements and reduces the stabilization of the cavity, which leads to approximately 1 kJ/mole difference in chemical potential of hydrate water at 0 ^{o}C compared to the classical rigid cavity integration for CO2. In contrast a small molecule like for instance methane does not significantly affect the water movements [2]. Empirical corrections are often introduced to correct for these effects as well as other shortcomings in the original van der Waal & Platteeuw formulation. An example of this is due to John & Holder [3]. The thermodynamic model is enhanced to calculate free energy of hydrate by inclusion of free energy gradient with respect to mole fraction, pressure and temperature. The use of these gradients will describe the phase transition kinetics in terms of the phase field theory (PFT) in presence of ice.

Carbon dioxide hydrate is more stable than methane hydrate

Paper submitted November 25, 2011: Revised version submitted January 2, 2012. This work was supported financially by The Research Council of Norway through the projects: “subsurface storage of CO2 – Risk assessment, monitoring and remediation”, Project number: 178008/I30, FME – SUCCESS, Project number: 804831, “CO2 injection for extra production”, Project number: 801445, PETROMAKS project Gas hydrates on the Norwegian-Barents Sea-Svalbard margin (GANS, Norwegian Research Council) Project number: 175969/S30 and INJECT “subsurface storage of CO2”, Project number: 805173.

B. kvamme[1], is with the University of Bergen, Post box 7800, 5020 Bergen, Allegt. 55 Norway (phone: +47-555-83310; e-mail: Bjorn.Kvamme@ift.uib.no).

K. Baig, is with the University of Bergen, Post box 7800, 5020 Bergen, Allegt. 55 Norway. (e-mail: kba062@ift.uib.no).

M. Qasim, is with the University of Bergen, Post box 7800, 5020 Bergen, Allegt. 55 Norway. (e-mail: Muhammad.Qasim@ift.uib.no).

J. Bauman is with the University of Bergen, Post box 7800, 5020 Bergen, Allegt. 55 Norway. (e-mail: Jordan.Bauman@ift.uib.no).

over a large range of conditions. Furthermore - the filling of methane in small cavities makes this mixed hydrate more stable at all conditions (fig.1).

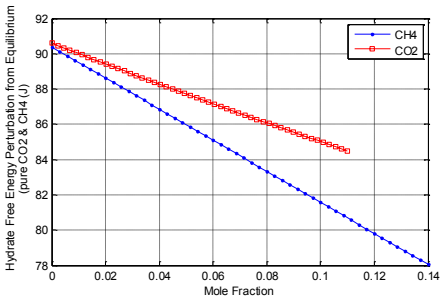

Figure 1: Perturbation due to pressure, temperature and composition gradients in CH4 and CO2 hydrate free energy from equilibrium.

This opens up for a novel technique for exploitation of methane form hydrates by injection of carbon dioxide. This is a win-win situation that also ensures long term storage of carbon dioxide as hydrate. And since pure carbon dioxide and pure methane both forms structure I it is straightforward to evaluate the changes in free energy as function of pressure and temperature in order to evaluate the thermodynamic control mechanisms.

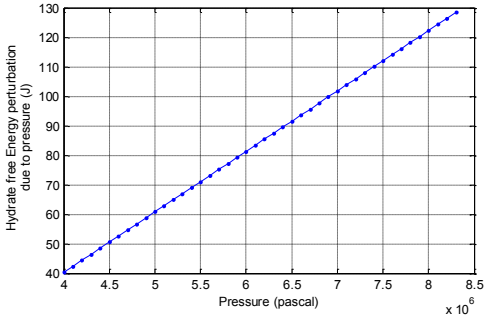

Figure 2: Perturbation in hydrate free energy from equilibrium due to pressure gradient term at constant temperature and composition.

Figure 2 shows the calculated free energy changes for mixed hydrate at constant temperature and constant mole fraction at different pressures in between 40 bar and 83 bar, this perturbation from equilibrium due to pressure gradient is increasing by increasing pressure.

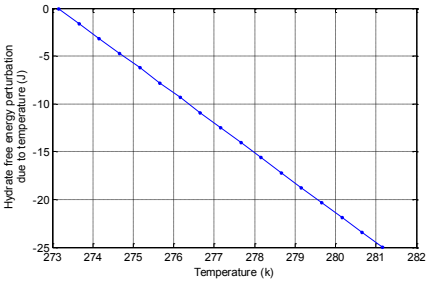

Figure 3: Perturbation in hydrate free energy from equilibrium due to temperature gradient at constant pressure of 20 bar and constant mole fraction.

Figure 3 shows the Free energy perturbation away from equilibrium is decreasing due to increase in temperature at constant pressure. Figure 4 is given to see the effect of temperature gradient on the free energy with variation in mole fractions at constant temperature and pressure.

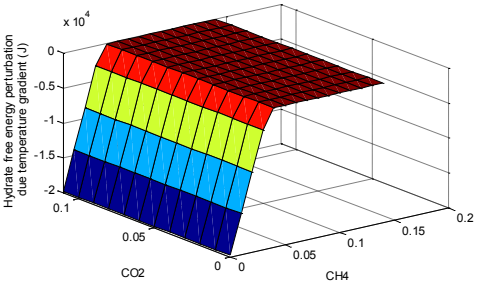

Figure 4: Perturbation in hydrate free energy perturbation from equilibrium with variation in compositions at constant temperature and pressure.

II. Hydrate Thermodynamics

The Gibbs free energy of the hydrate phase is written as a sum of the chemical potentials of each component [4].

$$G_H = \sum_{r=CO2,CH4,water} x_r \mu_r^H \qquad (1)$$

where μ_r^H and x_r is chemical potential and mole fraction of component r respectively. G_H is the free energy of hydrate. In the earlier work due to Svandal et al. [4] a simple interpolation in mole-fractions was used between pure CH4 hydrate and pure CO2 hydrate, which was considered as sufficient to theoretically illustrate the exchange concept under phase field theory. This will of course not reproduce the absolute minimum in free energy for a mixed hydrate in which CH4 occupies portions of the small cavities and increases stability over pure CO2 hydrate. The expression for free energy

gradients with respect to mole fraction, pressure and temperature is:

$$G_H^{EXP} = G^{EQ} + \sum_r \left.\frac{\partial G_H}{\partial x_r}\right|_{P,V,T,x_{i\neq r}} (x_r^{act} - x_r^{EQ}) + \left.\frac{\partial G_H}{\partial P}\right|_{T,V,\vec{x}} (P^{act} - P^{EQ}) + \left.\frac{\partial G_H}{\partial T}\right|_{P,V,\vec{x}} (T^{act} - T^{EQ}) \quad (2)$$

Here G_H^{EXP} is the free of hydrate away from equilibrium. G^{EQ} is free energy at equilibrium. In the earlier work [6] the mass balance of a hydrate is given by:

$$x_w + x_c + x_m = 1 \quad (3)$$

Which is of course being conserved inside the integration of the free energy functional but in the contour maps of the free energy of supersaturation with respect to concentrations different levels of concentration supersaturations in different directions (water, CO2, CH4) is not conserved and has to be evaluated as orthonormal gradient effects outside of equilibrium. In simple terms that means:

$$\left(\frac{\partial x_z}{\partial x_r}\right)\begin{cases}0, z \neq r\\ 1, z = r\end{cases} \quad (4)$$

Where z and r both represent any of the components of the hydrate: water, methane, and carbon dioxide. This is just means that the mole fractions are all independent. Using equation (1) we simply take the derivative with respect to one of the mole fractions (r=m,c, or w):

$$\frac{\partial G_H}{\partial x_r} = x_c\frac{\partial \mu_c^H}{\partial x_r} + x_m\frac{\partial \mu_m^H}{\partial x_r} + x_w\frac{\partial \mu_w^H}{\partial x_r} + \mu_c\frac{\partial x_c}{\partial x_r} + \mu_m\frac{\partial x_m}{\partial x_r} + \mu_w\frac{\partial x_w}{\partial x_r},$$

The mole fraction derivatives in above equation simply collapse by using equation (4) for mole fraction independence to get:

$$\frac{\partial G_H}{\partial x_r} = x_c\frac{\partial \mu_c^H}{\partial x_r} + x_m\frac{\partial \mu_m^H}{\partial x_r} + x_w\frac{\partial \mu_w^H}{\partial x_r} + \mu_r\frac{\partial x_r}{\partial x_r} \quad (5)$$

It was previously shown [4] that the chemical potential of a guest molecule can be approximated to a high degree of accuracy and in gradient terms:

$$\mu_k^H = A\ln(x_k) + B, \quad \frac{\partial \mu_k^H}{\partial x_r} = \{0, r \neq k\} \quad (6)$$

Where k and r both represents any of the components of the hydrate (CO2, CH4 & water). For the gradient due to a guest molecule, these simplifications lead to:

$$\frac{\partial G^H}{\partial x_k} = x_k\frac{\partial \mu_k^H}{\partial x_k} + \mu_k^H \quad (7)$$

For water, the form has two more terms:

$$\frac{\partial G_H}{\partial x_w} = \sum_{r=m,w,c} x_r\frac{\partial \mu_r^H}{\partial x_w} + \mu_w^H \quad (8)$$

The chemical potential of a guest in the hydrate μ_k^H from [2] is:

$$\mu_k^H = \Delta g_{kj}^{inc} + RT\ln(h_{kj}) \quad (9)$$

Where Δg_{kj}^{inc} is the Gibbs free energy of inclusion of guest molecule k in cavity j, h_{kj} the cavity partition function of component k in cavity j, the universal gas constant is R and T is temperature. The derivative of equation (9) with respect to an arbitrary molecule r is:

$$\frac{\partial \mu_k^H}{\partial x_k^H} = \frac{\partial \Delta g_{kj}^{inc}}{\partial x_r^H} + \frac{\partial\left(RT\ln(h_{kj})\right)}{\partial x_r^H} \quad (10)$$

The first term of equation (10), the stabilization energy is either evaluated as the Langmuir constant or using harmonic oscillator approach [2]. In either case it is assumed to be approximately of temperature and pressure. Omitting the first term of (10) and approximating impacts of guest-guest interactions to be zero we arrive at:

$$\frac{\partial \mu_k^H}{\partial x_k^H} = \frac{RT}{h_{kj}}\frac{\partial h_{kj}}{\partial x_r^H} \quad (11)$$

The validity of omitting guest-guest interactions may be questionable for some systems even though it is omitted in most hydrate equilibrium codes or empirically corrected for. Extensions for corrections to this can be implemented at a later stage.

The chemical potential of water:

$$\mu_w^H(T,P,\vec{\theta}) = \mu_w^{0,H}(T,P_0) - \sum_j RTv_j\ln\left(1 + \sum_k h_{kj}\right) \quad (12)$$

Where $\mu_w^{0,H}$ is the chemical potential of water in an empty hydrate structure, the first sum is taken over both small and large cavities, the second sum are over the components k in the cavity j. Here v_j is the number of type-j cavities per water molecule. Hydrate structure I contains 3 large cavities and 1 small cavity per 23 water molecules, $v_l = {}^3/_{23}$ and $v_s = {}^1/_{23}$. The paper by Kvamme & Tanaka [3] provides the empty hydrate chemical potential as polynomials in inverse temperature, the Gibbs free energies of inclusion, and

chemical potential of pure water, $\mu_w^{pure}(T)$. The derivative for the above equation with respect to an arbitrary molecule r results in:

$$\frac{\partial \mu_w^H}{\partial x_r} = \frac{\partial \mu_w^{0,H}}{\partial x_r} - \frac{\partial}{\partial x_r}\left(\sum_j RT v_j \ln\left(1 + \sum_k h_{kj}\right)\right)$$

$$\frac{\partial \mu_w^H}{\partial x_r} = -RT \sum_j v_j \frac{\partial}{\partial x_r}\left(\ln\left(1 + \sum_k h_{kj}\right)\right)$$

$$\frac{\partial \mu_w^H}{\partial x_r} = -RT \sum_j v_j \left[\frac{\sum_k \frac{\partial h_{kj}}{\partial x_r}}{\left(1 + \sum_k h_{kj}\right)}\right] \quad (13)$$

From equations (11) and (13), the derivative of the partition function can be evaluated from the equation that relates the filling fraction to the partition function:

$$h_{kj} = \frac{\theta_{kj}}{1 - \sum_i \theta_{kj}} \quad (14)$$

Where θ_{kj} is the filling fraction of the components k in the cavity j. But it is easiest to recast everything in terms of mole fraction because of the basic assumption of mole fraction independence:

$$\theta_{kj} = \frac{x_{kj}}{v_j x_w} \quad (15)$$

Since mass conservation is not used, the usual form of $1 - x_T$ is not considered. This is substituted into equation (16) and we get:

$$h_{kj} = \frac{\frac{x_{kj}}{v_j x_w}}{1 - \sum_i \frac{x_{ij}}{v_j x_w}}$$

$$h_{kj} = \frac{x_{kj}}{x_w v_j - \sum_i x_{kj}} \quad (16)$$

Now we can take the derivative with respect to an arbitrary component r and then equation (16) is used to eliminate the sums, we get:

$$\frac{h_{kj}}{\partial x_r} = \frac{1}{x_w v_j - \sum_i x_{ij}} \frac{\partial x_{kj}}{\partial x_r} - \frac{x_{kj}}{\left(x_w v_j - \sum_i x_{ij}\right)^2}\left(v_j \frac{\partial x_w}{\partial x_r} - \sum_i \frac{\partial x_{ij}}{\partial x_r}\right)$$

$$\frac{h_{kj}}{\partial x_r} = \frac{h_{kj}}{x_{kj}} \frac{\partial x_{kj}}{\partial x_r} - \frac{{h_{kj}}^2}{x_{kj}}\left(v_j \frac{\partial x_w}{\partial x_r} - \sum_i \frac{\partial x_{ij}}{\partial x_r}\right) \quad (17)$$

The first thing that must be dealt with the cavity mole fractions as a function of total mole fraction of a component:

$$x_k = \sum_j x_{kj} \quad (18)$$

Since the derivative of one mole fraction with respect to another is independent, the mole fraction in the cavity is also independent:

$$\frac{\partial x_{kj}}{\partial x_r} \begin{cases} 0, k \neq r \text{ or } r = w \\ 1, k = r \end{cases} \quad (19)$$

If $r = w$, then the derivative has to be zero because the mole fraction of the guest are independent of the mole fraction of water. Now equation (17) is simplified by using equation (18) and equation (19):

$$\frac{h_{kj}}{\partial x_w} = \frac{h_{kj}}{x_{kj}} \frac{\partial x_{kj}}{\partial x_w} - \frac{{h_{kj}}^2}{x_{kj}}\left(v_j \frac{\partial x_w}{\partial x_w} - \sum_i \frac{\partial x_{ij}}{\partial x_w}\right)$$

$$\frac{h_{kj}}{\partial x_w} = -\frac{{h_{kj}}^2 v_j}{x_{kj}} \quad (20)$$

$$\frac{h_{kj}}{\partial x_p} = \frac{h_{kj}}{x_{kj}} \frac{\partial x_{kj}}{\partial x_p} - \frac{{h_{kj}}^2}{x_{kj}}\left(v_j \frac{\partial x_w}{\partial x_p} - \sum_i \frac{\partial x_{ij}}{\partial x_p}\right)$$

$$\frac{h_{kj}}{\partial x_p} = \frac{h_{kj}}{x_{kj}} \frac{\partial x_{kj}}{\partial x_p} + \frac{{h_{kj}}^2}{x_{kj}} \frac{\partial x_{pj}}{\partial x_p} \quad (21)$$

Where p is an arbitrary guest molecule, k is also a guest molecule. These can be the same or different. If k and p are the same molecule, this gradient still exist and the "cross terms" are still able to be found even if there is independency in the mole fractions. $\frac{dx_{kj}}{dx_k}$ is calculated by starting with the equation (18) which is the basic definition of the mole fraction of the cavities and how they relate to the total mole fraction of the component. The total methane mole fraction x_m, is the sum of the mole fraction in the large cavities x_{ml}, and the mole fraction in the small cavities x_{ms}:

$$x_m = x_{ml} + x_{ms} \quad (22)$$

From discussions it is assumed that there is a constant ratio between the partition functions and between different cavities of the same component. This is defined as A:

$$A \equiv \frac{h_{ml}}{h_{ms}} \tag{23}$$

The partition function can be written in terms of the filling fraction as shown in equation (14). Using equation (14), equation (15), equation (23) and assuming that the filling fraction of CO2 in large cavities is zero we get:

$$A = \frac{\frac{\theta_{ml}}{1-\theta_{ml}-\theta_{cl}}}{\frac{\theta_{ms}}{1-\theta_{ms}}} = \frac{\theta_{ml}}{\theta_{ms}}\left(\frac{1-\theta_{ms}}{1-\theta_{ml}-\theta_{cl}}\right)$$

$$A = \frac{\frac{x_{ml}}{v_l x_w}}{\frac{x_{ms}}{v_s x_w}}\left(\frac{1-\frac{x_{ms}}{v_s x_w}}{1-\frac{x_{ml}}{v_l x_w}-\frac{x_{cl}}{v_l x_w}}\right) \tag{24}$$

This Simplifies to:

$$A = \frac{x_{ml}}{x_{ms}}\left(\frac{v_s x_w - x_{ms}}{1-\frac{x_{ml}}{v_l x_w}-\frac{x_{cl}}{v_l x_w}}\right)$$

$$x_{ml}[-v_l x_w] + x_{ms}[A v_l x_w - A x_{cl}] + x_{ms} x_{ml}[1-A] = 0 \tag{25}$$

Taking derivative of above equation with respect to total methane mole fraction:

$$[-v_s x_w]\frac{\partial x_{ml}}{\partial x_m} + [A v_l x_w - A x_{cl}]\frac{\partial x_{ms}}{\partial x_m} + x_{ml}[1-A]\frac{\partial x_{ms}}{\partial x_m} + x_{ms}[1-A]\frac{\partial x_{ml}}{\partial x_m} = 0$$

$$[x_{ms}[1-A] - v_s x_w]\frac{\partial x_{ml}}{\partial x_m} + \left[A v_l x_w - A x_{cl} + x_{ml}[1-A]\right]\frac{\partial x_{ms}}{\partial x_m} \tag{26}$$

Substitutions were made to simplify the above equation and get it into a simpler form:

$$X = x_{ms}(1-A) - v_s x_w$$

$$Y = A v_l x_w - A x_{cl} + x_{ml}(1-A)$$

$$X\frac{\partial x_{ml}}{\partial x_m} + Y\frac{\partial x_{ms}}{\partial x_m} = 0 \tag{27}$$

Taking the derivative of equation (22) with respect to the total mole fraction of methane and simplification results in:

$$\frac{\partial x_{ml}}{\partial x_m} + \frac{\partial x_{ms}}{\partial x_m} = \frac{\partial x_m}{\partial x_m} = 1$$

$$\frac{\partial x_{ml}}{\partial x_m} = -\frac{Y}{X-Y}$$
$$\frac{\partial x_{ms}}{\partial x_m} = \frac{X}{X-Y} \tag{28}$$

Substituting the values of X and Y gives the final answer:

$$\frac{\partial x_{ml}}{\partial x_m} = \frac{A v_i x_w - A x_{cl} + x_{ml}(1-A)}{x_{ml}(1-A) + x_{ms}(1-A) - v_s x_w - A v_l x_w - A x_{cl}}$$
$$\frac{\partial x_{ml}}{\partial x_m} = \frac{x_{ms}(1-A) - v_s x_w}{x_{ml}(1-A) + x_{ms}(1-A) - v_s x_w - A v_l x_w - A x_{cl}} \tag{29}$$

$\partial G/\partial P$ is calculated by taking derivative of equation (1) with respect to pressure:

$$\frac{\partial G_H}{\partial P} = x_c\frac{\partial \mu_c^H}{\partial P} + x_m\frac{\partial \mu_m^H}{\partial P} + x_w\frac{\partial \mu_w^H}{\partial P} + \mu_c\frac{\partial x_c}{\partial P} + \mu_m\frac{\partial x_m}{\partial P} + \mu_w\frac{\partial x_w}{\partial P} \tag{30}$$

The chemical potential gradients with respect to pressure can be given by:

$$\frac{\partial \mu_r^H}{\partial P} = \bar{V}_r$$

Thus equation (30) can be written as:

$$\frac{\partial G_H}{\partial P} = x_c\overline{V}_c + x_m\overline{V}_m + x_w\overline{V}_w + \mu_c^H\frac{\partial x_c}{\partial P} + \mu_m^H\frac{\partial x_m}{\partial P} + \mu_w^H\frac{\partial x_w}{\partial P} \tag{31}$$

The sum of the molar volumes $(\overline{V}_c, \overline{V}_m, \overline{V}_w)$ is in fact the total clathrate molar volume:

$$\overline{V}^{clath} = x_c.\overline{V}_c + x_m.\overline{V}_m + x_w.\overline{V}_w \tag{32}$$

Using the above value of $\overline{V}^{clath}$ simplifies the equation (31) to:

$$\frac{\partial G}{\partial P} = \overline{V}^{clath} + \mu_c^H\frac{\partial x_c}{\partial P} + \mu_m^H\frac{\partial x_m}{\partial P} + \mu_w^H\frac{\partial x_w}{\partial P} \tag{33}$$

The mole fraction derivatives can be calculated from

equation of state but there is no change under this derivative so equation (33) rewritten as:

$$\left(\frac{\partial G}{\partial P}\right)_{T,V,\bar{x}} = \overline{V}^{clath} \tag{34}$$

The free energy gradient with respect to temperature comes from the same fundamental relationship as used for the chemical potential gradient:

$$\frac{\partial\left(\frac{G}{RT}\right)}{\partial T} = -\frac{\overline{H}}{RT^2} \tag{35}$$

As before this can be differentiated and solved for the gradient:

$$\frac{\partial\left(\frac{G}{RT}\right)}{\partial T} = -RT^2 \int_{T_0}^{T}\left[\frac{H_0(T_0,P) + \int_{T_0}^{\theta} C_{p_i} d\eta}{R\theta^2}\right] d\theta \tag{36}$$

The Gibbs free energy for the hydrate as a function of mole fractions is shown in fig. 5. The CO2 only enters the large cavities, at least under moderate condition, and CH4 will occupy portion of the small cavities. As hydrate can never be fully occupied, the surface is restricted by the full filling of the large cavities $xc + xm < 4/24$ and $xm < 1/27$ is for small cavities. In this figure, the large cavities are less occupied by carbon dioxide and the small cavities are fully occupied by methane.

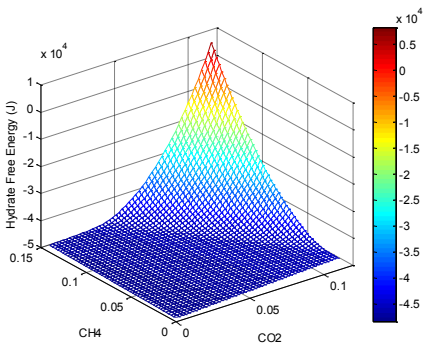

Figure 5: Hydrate free energy of mixed hydrate at 3°C and 40 bars.

The perturbation due to pressure temperature and composition gradients from equilibrium in hydrate Gibbs free energy is plotted in fig. 6.

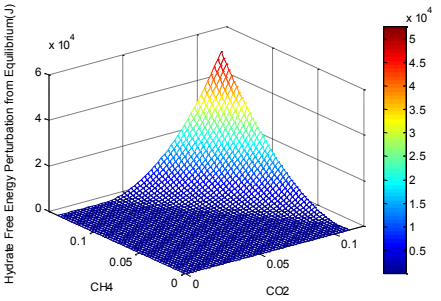

Figure 6: Perturbation due to pressure, temperature and composition gradients in hydrate free energy from equilibrium at 3°C and 40 bars.

III. Fluid Thermodynamics

The free energy of the fluid phase is assumed to have:

$$G_L^{Fluid} = \sum_{r=c,m,w} x_r \mu_r^{Fluid} \tag{37}$$

where μ_r^{Fluid} is the chemical potential of the fluid phase. The lower concentration of water in the fluid phase and its corresponding minor importance for the thermodynamics results in the following form of water chemical potential with some approximation of fugacity and activity coefficient:

$$\mu_w^{Fluid} = \mu_w^{ideal\ gas}(T,P) + RT\ln(y_w) \tag{38}$$

Where $\mu_w^{ideal\ gas}(T,P)$ chemical potential of water in ideal gas and y_w is the mole fraction of water in the fluid phase and can be calculated as:

$$y_w = \frac{x_w \gamma_w(T,P,\bar{x}) P_w^{sat}(T)}{\varphi_w(T,P,\bar{y})} \tag{39}$$

The vapour pressure can be calculated using many available correlations but one of the simplest is given in [6] as a fit to the simple equation:

$$\ln(P) = V_A - \frac{V_B}{T + V_C} \tag{40}$$

The temperature of the system is obviously available and $V_A = 52.703$, $V_B = -3146.64$ and $V_C = 5.572$. Further, the fugacity and the activity coefficient are approximated to unity merely because of the very low water content in fluid phase and its corresponding minor importance for the thermodynamics of the system. Hydrate formation directly from water in gas is not considered as significant within the systems discussed in this work. The water phase is close to unity in water mole fraction. Raoult's law is therefore accurate enough for our purpose. The chemical potential for the mixed fluid states considered as:

$$\mu_i^{Fluid} = \mu_i^{id.gas,pure} + RT\ln(y_i) + RT\ln\varphi_i(T,P,\bar{y}) \tag{41}$$

Where i represents CH4 or CO2. The fugacity coefficients of component i in the mixture is calculated using the classical SRK equation of state (EOS), [5]

$$\ln \varphi_i = (BB)_i(Z-1) - \ln(Z-B) - \frac{A}{B}((AA)_i - (BB)_i)\ln\left[1+\frac{B}{Z}\right] \quad (42)$$

Where Z is the compressibility factor of the phase and is calculated using the following cubic SRK EOS:

$$Z^3 - Z^2 + (A - B - B^2)Z - AB = 0 \quad (43)$$

Where,

$$A = \frac{\alpha a P}{R^2 T^2}$$

$$B = \frac{bP}{RT}$$

$$a = 0.427480\frac{R^2 T_c^2}{P_c}$$

$$b = 0.086640\frac{RT_c}{P_c}$$

$$\alpha = \left[1 + (0.48508 + 1.55171\omega - 0.15613\omega^2)\left(1 - \sqrt{T_r}\right)\right]^2$$

Where ω is the accentric factor of components. For mixture, the mixing rule with modification proposed by Soave [5] is used using the following formulations:

$$(\alpha a)_m = \sum\sum y_i y_j (\alpha a)_{ij}\ ;\ (\alpha a)_{ij} = \sqrt{(\alpha a)_i (\alpha a)_j}\left(1 - k_{ij}\right) \quad (44)$$

Where k_{ij} is the binary interaction parameter. Coutinho et al. [7] has proposed number of values for k_{ij} for CO2/CH4 system. Here we selected an average value $k_{ij} = k_{ji} = 0.098$ for unlike pairs of molecules and it is zero for alike pairs of molecules.

$$b_m = \sum_i y_i b_i \quad (45)$$

$(AA)_i$ and $(BB)_i$ in equation (42) are calculated as:

$$(AA)_i = \frac{2}{(\alpha a)_m}\left[\sum_j (\alpha a)_{ij}\right] \quad (46)$$

$$(BB)_i = \frac{b_i}{b_m} \quad (47)$$

IV. Aqueous Thermodynamics

The free energy of the aqueous phase can be written as:

$$G_L^{aqueous} = \sum_{r=c,m,w} x_r \mu_r^{aqueous} \quad (48)$$

The chemical potential $\mu_r^{aqueous}$ for components c (carbon dioxide) and m (methane) dissolved into the aqueous phase is described by nonsymmetric excess thermodynamics:

$$\mu_i = \mu_i^{\infty}(T) + RT\ln(x_i \gamma_i^{\infty}) + v_i^{\infty}(P - P_o) \quad (49)$$

μ_i^{∞} is the chemical potential of component i in water at infinite dilution, γ_i^{∞} is the activity coefficient of component i in the aqueous solution and v_i^{∞} is the partial molar volume of the component i at infinite dilution. The chemical potentials at infinite dilution as a function of temperature are found by assuming equilibrium between fluid and aqueous phases $\mu_i^{Fluid} = \mu_i^{aqueous}$. This is done at varying low pressures where the solubility is very low and the gas phase is close to ideal gas using experimental values for the solubility and extrapolating the chemical potential down to a corresponding value for zero concentration. The Henry's constants k_H are calculated for CH4 and CO2 using the expression proposed by Sander.[8]

$$k_H(T) = k_H^{\ominus} e^{\left(\frac{-\Delta_{soln}H}{R}\left(\frac{1}{T}-\frac{1}{T^{\ominus}}\right)\right)} \quad (50)$$

Where $T^{\ominus}$ is the reference temperature, which is equal to 298.15K. $\Delta_{soln}H$ is the enthalpy of dissolution and it is represented by the Clausius-Clapeyron equation[9] as:

$$\frac{d\ln k_H}{d(1/T)} = \frac{-\Delta_{soln}H}{R} \quad (51)$$

The values of $-(\mathrm{d}\ln[\mathrm{k\_H}])/\mathrm{d}(1/\mathrm{T})$ and $k_H^{\ominus}$ are given by Zheng et al.[10] and by Kavanaugh et al.[11] for CO2 and CH4 respectively which is shown in Table 1.

Table 1: Values of parameters.

Constants	CO2	CH4
$k_H^{\ominus}$ (M/atm)	0.036	0.0013
$-(\mathrm{d}\ln[\mathrm{k\_H}])/\mathrm{d}(1/\mathrm{T})$ (K)	2200	1800

The activity coefficient at infinite dilution γ_i^{∞} is calculated as:

$$\gamma_i^{\infty} = \frac{f_i^{\infty}}{k_H(T)} \tag{52}$$

Where,

$$f_i^{\infty} = e^{(-\beta\mu_i^{\infty})} \tag{53}$$

Where f_i^{∞} is the fugacity of component i, while μ_i^{∞} is calculated from [4]. The activity coefficient can be regressed by using the model for equilibrium to fit experimental solubility data. The chemical potential of water can be written as:

$$\mu_w = \mu_w^{pure\ liquid}(T) + RT\ln(1-x)\gamma_w + v_w(P - P_o) \tag{54}$$

where $\mu_w^{pure\ liquid}$ is pure water chemical potential and v_w is the molar volume of water. The strategy for calculating activity coefficient is given by Svandal et al.[4]. The Gibbs free energy for the liquid phase as function of mole fraction is shown in fig.7.

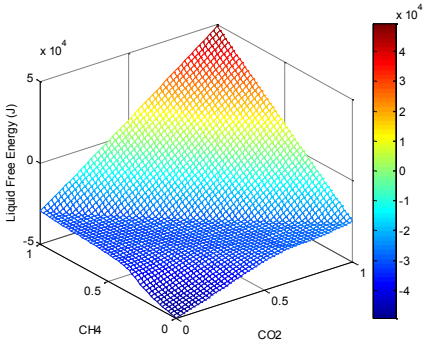

Figure 7: Liquid Gibbs free energy (J) as a function of the mole fraction of CH4 and CO2 at 3°C and 40 bars.

The aqueous and fluid phases are treated as a single common phase in the phase field theory approach. The smooth Gibbs free energy have constructed over the whole mole fraction domain of both CO2 and CH4 for this purpose.

V. Conclusion

Formulations of super saturation or undersaturation of hydrate in pressure, temperature and concentrations have been derived for a three component system of water, CO2 and CH4. Unlike earlier published approximations for mixed hydrate super saturation or sub saturation the expansions are rigorous to first order Taylor expansion and will as such also capture the total free energy minimum in mixed hydrate of CO2 and CH4. The results are implemented in Phase Field Theory model for the same system of three components and all possible surrounding fluid phases of these.

The Previously published results on absolute thermodynamics of hydrate also been used to illustrate the impact of molecular size on destabilization of the water clathrate. In particular it is demonstrated that a molecule like CO2 will stabilize the hydrate cages well but due to its size it will interfere with the movements of the water molecules constituting the cavity and cause a destabilization effect in the order of 1 kJ/mole at zero Celsius.

References

[1] J. H. van der Waals and J. C. Platteeuw, "Clathrate solutions," Advances in Chemical Physics, vol. 2, pp. 1–57, 1959.

[2] B. Kvamme, H. Tanaka, "Thermodynamic stability of hydrates for ethane, ethylene and carbon dioxide," J. Chem. Phys, vol. 99, pp. 7114 – 7119, 1995.

[3] V. T. John, G. D. Holder," Langmuir constants for spherical and linear molecules in clathrate hydrates. Validity of the cell theory," Journal of Physical Chemistry, Vol. 89: 3279, 1985.

[4] A. Svandal, T. Kuznetsova, B. Kvamme, "Thermodynamic properties and phase transitions in the H2O/CO2/CH4 system," Fluid Phase Equilibria, Vol. 246, pp. 177–184, 2006.

[5] G. Soave, "Equilibrium constant from a modified Redlich – Kwong equation of state,"Chemical Engineering Science, Vol. 27, pp. 1197 – 1203, 1972.

[6] R. C. Reid, J. M. Prausnitz, and T. K. Sherwood, "The Properties of Gases and Liquids," McGraw-Hill, Third Edition , 1977.

[7] J. A. P. Coutinho, G. M. Kontogeorgis, E. H. Stenby,"Binary interaction parameters for nonpolar systems with cubic equations of state: a theoretical approach 1. CO2/hydrocarbons using SRK equation of state," Fluid phase equilibria, Vol. 102, Issue 1, pp. 31 – 60, 1994.

[8] R. Sander,"Modeling Atmospheric Chemistry: Interactions between Gas-Phase species and liquid cloud/aerosol particles," Surv. Geophys, Vol. 20, Issue 1, pp. 1 – 31, 1999.

[9] J.C.M. Li,"Clapeyron Equation for Multicomponent Systems," Journal of Chemical Physics, vol. 25, pp. 572 – 574, 1956.

[10] D. Q. Zheng, T. M. Guo, and H. Knapp,"Experimental and modeling studies on the solubility of CO2, CHCIF2, CHF3, C2H2F4 and C2H4F2 in water and aqueous NaCL solutions under low pressure," Fluid Phase Equilib, Vol. 129, pp. 197 – 209, 1997.

[11] M. C. Kavanaugh, R. R. Trussell,"Design of aeration towers to strip volatile contaminants from drinking water," Vol. 72, pp. 684 – 692, 1980.

Paper 5

Mix Hydrate formation by CH4-CO2 exchange using Phase Field Theory with implicit Thermodynamics

M. Qasim, K. Baig, B. Kvamme and J. Bauman

International Journal of Energy and Environment, Volume 6, Issue 5, 2012, pp. 479-487

V

Mix Hydrate formation by CH4-CO2 exchange using Phase Field Theory with implicit Thermodynamics

M. Qasim, K. Baig, B. Kvamme and J. Bauman

***Abstract*—** Natural gas hydrates are ice-like structures composed of water and gas (mostly methane) molecules. They are found worldwide and contain huge amounts of bound methane. Therefore, it represent potentially vast and yet untapped energy resources. Hydrates from carbon dioxide are thermodynamically more stable than methane hydrate over large regions of condition. Mixed hydrates of structure I, in which methane occupies the small cavities are more stable than methane hydrate over all ranges of pressures and temperatures. The exchange of originally bound methane in hydrate with carbon dioxide is a great way to achieve two goals, the in situ release of hydrocarbon gas and a cleaner environment through safe storage of carbon dioxide. The resulting hydrate is a mix. Carbon dioxide can only replace methane in large cavities due to its size and therefore it forms mix methane-carbon dioxide hydrate with methane in the small cavities and a maximum theoretical exchange of 75% of the in situ methane. An improved thermodynamic model is implicitly implemented in phase field theory to study the kinetic rates due to the exchange process. A thin layer of water between methane hydrate and carbon dioxide is implemented in addition to the initial methane for a more realistic representation of a reservoir situation in which hydrate saturation is always lower than 100%. The nucleation on water-carbon dioxide interface is expected to be very slow compared to the growth rate. To trigger the carbon dioxide hydrate formation four small regions of carbon dioxide hydrate are placed on the water-carbon dioxide interface. The exchange process involves an initial dissociation of methane hydrate and the carbon dioxide will start forming hydrate. In term of Gibbs phase rule the system can theoretically reach equilibrium as limit if pressure and temperature is defined and the final hydrate is uniform. On the other hand the limited size of the system and the initial balance of masses of the three components methane, carbon dioxide and water will not make equilibrium possible in the model system. This implies also that kinetic rates of hydrate formation, hydrate reformation and dissociation will depend on composition of surrounding phases and corresponding free energies. This is also the expected situation in a porous media like a hydrate reservoir, in which the hydrate is in a stationary balance with fluids and typically kept trapped by layers of clay or shale. Phase field theory is a tool for evaluation of kinetic rates of different phase transitions as well as the relative impact of thermodynamic control and mass transport control. Heat transport is very rapid compared to mass transport and is neglected in this work.

***Keywords*—**Phase field theory, Natural gas hydrate, Hydrodynamics, Hydrate exchange.

I. Introduction

Gas hydrates are ice-like substances of water molecules encaging gas molecules called guest. Natural gas hydrates are dominated by methane and most naturally occurring hydrates are formed from biogenic sources. They form under high pressure and low temperature conditions within the upper hundred meters of the sub-seabed sediments [1]. Gas hydrate mostly exist in two crystalline structures structure I (sI) and structure II (sII). There may also rarely found a third type structure H denoted as sH. These structures vary in composition and types of cavities that constitutes the hydrate structure depending on the size of the guest molecule. The scope of this work is on hydrates with carbon dioxide (CO2) and methane (CH4) as guests. These two components both form the structure I hydrate and special focus will therefore be on this particular structure. Using the explanation by Sloan [22], structure I is a cubic crystalline in shape and formed with guest molecules having diameter between 4.2 and 6 Å, such as methane, carbon dioxide, ethane and hydrogen sulfide. One unit cell in it consists of 46 water molecules. It has two small and six large cages in one unit cell. The small cage has the shape of a 12 sided cavity with 12 pentagonal faces in each side and called pentagonal dodecahedron (5^{12}). The large cage has the shape of a 14 sided cavity (with 12 pentagonal faces and 2 hexagonal) faces and called tetradecahedron ($5^{12}6^2$). If all the cavities are filled with guest molecules the mole percent of water would be about 85%. Normally, not all cavities may found be completely occupied with guest molecules. Due to this very high water content hydrates look like snow or ice. They are also sometimes called as 'ice that burns' as shown in Fig. 1. It is natural to assume that hydrate properties may little depend on guest molecules due to their low content, but it is not the case. The most

Paper submitted November 25, 2011: Revised version submitted January 02, 2012. This work was supported financially by The Research Council of Norway through the projects: "subsurface storage of CO2 – Risk assessment, monitoring and remediation", Project number: 178008/I30, FME – SUCCESS, Project number: 804831, "CO2 injection for extra production", Project number: 801445, PETROMAKS project Gas hydrates on the Norwegian-Barents Sea-Svalbard margin (GANS, Norwegian Research Council) Project number: 175969/S30 and INJECT "subsurface storage of CO2", Project number: 805173.

M. Qasim, is with the University of Bergen, Post box 7800, 5020 Bergen, Allegt. 55 Norway. (e-mail: Muhammad.Qasim@ift.uib.no).

K. Baig, is with the University of Bergen, Post box 7800, 5020 Bergen, Allegt. 55 Norway. (e-mail: kba062@ift.uib.no).

B. kvamme[1], is with the University of Bergen, Post box 7800, 5020 Bergen, Allegt. 55 Norway (phone: +47-555-83310; e-mail: Bjorn.Kvamme@ift.uib.no).

J. Bauman is with the University of Bergen, Post box 7800, 5020 Bergen, Allegt. 55 Norway. (e-mail: Jordan.Bauman@ift.uib.no).

striking property of hydrate is that they can be formed and exist at temperatures higher than 0^0C if the pressure is high enough.

Fig.1 'Ice that burns', (Photo courtesy of: J. Pinkston and L. Stern / Us Geological Survey).

These gas hydrates are widely distributed in sediments along continental margins, and harbor enormous amounts of energy. Massive hydrates that outcrop the sea floor have been reported in the Gulf of Mexico [2]. Hydrate accumulations have also been found in the upper sediment layers of Hydrate ridge, off the coast of Oregon and a fishing trawler off Vancouver Island recently recovered a bulk of hydrate of approximately 1000kg [3]. Håkon Mosby Mud Volcano of Bear Island in the Barents Sea with hydrates is openly exposed at the ocean floor [4]. These are only few examples of the worldwide evidences of unstable hydrate occurrences that leaks methane to the oceans and eventually may be a source of methane increase in the atmosphere.

Hydrates of methane are not thermodynamically stable at mineral surfaces. From a thermodynamic point of view the reason is simply that water structure on hydrate surfaces are not able to obtain optimal interactions with surfaces of calcite, quarts and other reservoir minerals. The impact of this is that hydrates are separated from the mineral surfaces by fluid channels. The sizes of these fluid channels are not known and are basically not even unique in the sense that it depends on the local fluxes of all fluids in addition to the surface thermodynamics. Stability of natural gas hydrate reservoirs therefore depends on sealing or trapping mechanisms similar to ordinary oil and gas reservoirs. Many hydrate reservoirs are in a dynamic state where hydrate is leaking from top by contact with groundwater/seawater which is under saturated with respect to methane and new hydrates form from deeper gas sources.

Global energy needs and climate stress from greenhouse gases require new sources of energy and the management of CO2 emissions. Natural gas hydrate provides a great solution being a potential source of energy and reduction of CO2 emissions. Methane can be recovered by number of ways like depressurization, heating and injection of another gas. The scope of this work deals with the kinetic rates of CO2 injection into methane hydrate. This process is a favorable way to store a greenhouse gas (CO2) for long period of time and enables the ocean floor to remain stabilized even after recovering the methane gas [10]. Because, of the size CO2 can only fit into large cavities and it will force methane in large cavities to release. This exchange is a solid phase exchange and therefore in result the new hydrate formed is a mix CO2/CH4 hydrate which is thermodynamically more stable than CH4 hydrate over substantial regions of pressure and temperature.

Gas hydrates have great capacity to store gases [5-7] and several investigations of potential for using hydrate phase for storage and transport have been conducted even though the hydrates are not stable when exposed to new surroundings like for instance air. The storage of CO2 in reservoirs has already been established as a feasible alternative for reducing CO2 emissions into the atmosphere. Injection of produced CO2 from Sleipner oil and gas field into the Utsira formation was the first industrial CO2 aquifer storage project. A number of studies conducted for the Utsira storage. See for instance Xu and Preuss [8] and references therein. There are regions in the northern parts of North Sea and the Barents Sea suitable for CO2 storage which contains regions of pressure and temperature conditions which are within the CO2 hydrate stability regions. Kinetic rates for CO2 hydrate formation, as well as dissociation of CO2 hydrate towards under saturated water is therefore important in reservoir modeling of CO2 storage in those regions. There are also natural gas hydrates in those regions and storing CO2 in natural gas hydrate reservoirs may provide a win-win situation of safe long term CO2 storage in the form of hydrate and simultaneous release of natural gas.

In our studies we are more interested in the type of CO2 storage provided by the reservoirs that already contains natural gas hydrates. Mixed CO2 and methane hydrate, in which methane fills some portion of the small cavities, is significantly more stable than natural gas hydrates. Injecting CO2 into in situ natural hydrate results in the formation of CO2 hydrate by naturally replacing the originally bounded in-situ hydrocarbons and therefore, at the same time releases the hydrocarbons. ConocoPhillips has currently in May 2012 has completed working on a field trial on the Alaska North Slope together with the US Department of Energy (DOE project MH-06553) as a major funding agency for the project. Now they are focusing in evaluating the extensive test data. It is believed that the data achieved by this trial will be helpful to experimentally justify the theoretical works like the one presented in this article. The aim is to investigate the release methane through CO2 injection.

Theoretically, Phase field theory is the main tool to give a deep understanding into the kinetic rates involved during this exchange. This work has used the modified Phase Field Theory as illustrated by Qasim et al. [9]. This process strongly depends on the accurate thermodynamic model and therefore an improved thermodynamic model as in [15] is implemented along with modified Phase Field Theory.

II. Phase Field Model

Phase field theory model follows the formulation of

Wheeler et al. [11], which historically has been mostly applied to descriptions of the isothermal phase transition between ideal binary-alloy liquid and solid phases of limited density differences. The hydrodynamics effects and variable density were incorporated in a three components phase field theory by Kvamme et al. [12] through implicit integration of Navier stokes equation following the approach of Qasim et al.[9]. The phase field parameter ϕ is an order parameter describing the phase of the system as a function of spatial and time coordinates. The phase field parameter ϕ is allowed to vary continuously from 0 to 1 on the range from solid to liquid.

The solid state is represented by the hydrate and the liquid state represents fluid and aqueous phase. The solidification of hydrate is described in terms of the scalar phase field $\phi(x_1, x_2, x_3)$ where x_1, x_2, x_3 represents the molar fractions of CH4, CO2 and H2O respectively with obvious constraint on conservation of mass $\sum_{i=1}^{3} x_i = 1$. The field ϕ is a structural order parameter assuming the values $\phi = 0$ in the solid and $\phi = 1$ in the liquid [13]. Intermediate values correspond to the interface between the two phases. The starting point of the three component phase field model is a free energy functional [12],

$$F = \int d\underline{r} \left(\frac{\varepsilon_\phi^2}{2} T(\nabla\phi)^2 + \sum_{i,j=1}^{3} \frac{\varepsilon_{xi,j}^2}{4} T\rho\left(x_i \nabla x_j - x_j \nabla x_i\right)^2 + f_{bulk}(\phi, x_1, x_2, x_3, T) \right), \quad (1)$$

which is an integration over the system volume, while the subscripts i, j represents the three components, ρ is molar density depending on relative compositions, phase and flow. The bulk free energy density described as

$$f_{bulk} = WTg(\phi) + \left(1 - p(\phi)\right) f_S(x_1, x_2, x_3, T) + p(\phi) f_L(x_1, x_2, x_3, T) . \quad (2)$$

The phase field parameter switches on and off the solid and liquid contributions f_S and f_L through the function $p(\phi) = \phi^3(10 - 15\phi + 6\phi^2)$, and note that $p(0) = 0$ and $p(1) = 1$. This function was derived from density functional theory studies of binary alloys and has been adopted also for our system of hydrate phase transitions. The binary alloys are normally treated as ideal solutions. The free energy densities of solid and liquid is given by

$$f_S = G_S \rho_m^{hyd} , \quad (3)$$

$$f_L = G_L \rho_m^{L} . \quad (4)$$

The details of densities ρ_m^{hyd} and ρ_m^{L} can be found in Qasim et al. [14]. The hydrate free energy away from equilibrium G_S is calculated using the following equation:

$$G_S = G^{EQ} + \sum_r^{r=m,c,w} \frac{\partial G_S}{\partial x_r} dx_r + \frac{\partial G_S}{\partial P} dP + \frac{\partial G_S}{\partial T} dT . \quad (5)$$

Here G^{EQ} is the free energy at equilibrium. The free energy gradients with respect to mole fraction, pressure and temperature are $\frac{\partial G_S}{\partial x_r}$, $\frac{\partial G_S}{\partial P}$ and $\frac{\partial G_S}{\partial T}$ respectively. Where subscript r represents any of the components of the hydrate: methane, carbon dioxide and methane. The detail calculations of the free energy gradients can be found in Kvamme et al. [15]. The free energy of the liquid G_L is discussed in the following fluid and aqueous thermodynamic section.

The function $g(\phi) = \phi^2(1 - \phi^2)/4$ ensures a double well form of the f_{bulk} with a free energy scale $W = \left(1 - \frac{x_i}{v_m}\right) W_A + \frac{x_i}{v_m} W_B$ with $g(0) = g(1) = 0$, where v_m is the average molar volume of water. In order to derive a kinetic model we assume that the system evolves in time so that its total free energy decreases monotonically [13].

The usual equations of motion are supplemented with appropriate convection terms as explained by Tegze et al [16]. Given that the phase field is not a conserved quantity, the simplest form for the time evolution that ensures a minimization of the free energy is

$$\frac{\partial \phi}{\partial t} + (\vec{v}.\nabla)\phi = -M_\phi(\phi, x_1, x_2, x_3) \frac{\delta F}{\delta \phi} , \quad (6)$$

$$\frac{\partial x_i}{\partial t} + (\vec{v}.\nabla)x_i = \nabla.\left(M_{xi}(\phi, x_1, x_2, x_3) \nabla \frac{\delta F}{\delta xi}\right) , \quad (7)$$

where $\vec{v}$ is the velocity, $M_{xi} = x_i(1 - x_i)\frac{1}{RT} D$ and $M_\phi = \left(1 - \frac{x_i}{v_m}\right) M^A + \frac{x_i}{v_m} M^B$ are the mobilities associated with coarse-grained equation of motion which in turn are related to their microscopic counter parts. Where $D = D_S + (D_L - D_S)p(\phi)$ is the diffusion coefficient. The details are given elsewhere [12].

An extended phase field model is formulated to account for the effect of fluid flow, density change and gravity. This is achieved by coupling the time evolution with the Navier Stokes Equations. The phase and concentration fields associates hydrodynamic equation as described by Conti [17-19]

$$\frac{\partial \rho}{\partial t} = -\rho_m \nabla.\vec{v}, \qquad \rho \frac{\partial \vec{v}}{\partial t} + \rho(\vec{v}.\nabla)\vec{v} = \rho\vec{g} + \nabla.P. \quad (8)$$

Where $\vec{g}$ is the gravitational acceleration. ρ_m is the density of the system in hydrate (ρ_m^{Hyd}) and liquid (ρ_m^{L}). The detail for calculating these densities are already given by Qasim et al [14]. Further

$$P = \xi + \Pi. \quad (9)$$

is the generalization of stress tensor [17-20], ξ represents

non-dissipative part and Π represents the dissipative part of the stress tensor.

III. Fluid Thermodynamics

The free energy of the fluid phase is assumed to have

$$G_L = \sum_{i=1}^{3} x_i \mu_i^{Fluid}, \quad (11)$$

where μ_i^{Fluid} is the chemical potential of the ith component. The solubility of water is assumed to follow the Raoult's law. The lower concentration of water in the fluid phase and its corresponding minor importance for the thermodynamics results in the following form of water chemical potential with some approximation of fugacity and activity coefficient:

$$\mu_3^{Fluid} = \mu_3^{\infty} + RTln(y_3), \quad (12)$$

where μ_3^{∞} chemical potential of water at infinite dilution and y_3 is the mole fraction of water in the fluid phase. The chemical potential for the mixed fluid states is approximated as

$$\mu_i^{Fluid} = \mu_i^{SRK,pure} + RTln(y_3), \quad (13)$$

where i represents CH4 or CO2. The details are available in Svandal et al. [21].

IV. Aqueous Thermodynamics

The free energy of the aqueous phase assumed as

$$G_L = \sum_{i=1}^{3} x_i \mu_i^{aqueous}, \quad (14)$$

the chemical potential $\mu_i^{aqueous}$ of aqueous phase has the general form derived from excess thermodynamics

$$\mu_3^{H} = \mu_i^{\infty} + RTln(x_i \gamma_i^{\infty}) + v_i(P - P_0). \quad (15)$$

μ_i^{∞} is the chemical potential of component i in water at infinite dilution, γ_i^{∞} is the activity coefficient of component i in the aqueous solution in the asymmetric convention (γ_i^{∞} approaches unity in the limit of x becoming infinitely small). The chemical potentials at infinite dilution as a function of temperature are found by assuming equilibrium between fluid and aqueous phases$\left(\mu_3^{Fluid} = \mu_3^{aqueous}\right)$. This is done at low pressures where the solubility is very low, using experimental values for the solubility and extrapolating the chemical potential down to a corresponding value for zero concentration. The activity coefficient can be regressed by using the model for equilibrium to fit experimental solubility data. The chemical potential of water can be written as:

$$\mu_3 = \mu_3^{p} + RTln(1 - x)\gamma_3 + v_3(P - P_0), \quad (16)$$

where μ_3^{p} is pure water chemical potential. The strategy for calculating activity coefficient is given in Svandal et al. [21].

V. Results and Discussions

As an initial setup a structure I hydrate reservoir model is considered by inserting a thin water band between methane hydrate and CO2 liquid. This is a more realistic setup in comparison to the previous work [14]. The strip of water layer is shown as dark red strip around light red circular disk methane hydrate in Fig.2. This whole is then surrounded by CO2 liquid. It is believed that the CO2/CH4 exchange process will be faster due to higher diffusivity of CO2 in water and water in hydrate but all depends on the initial nucleation of CO2 hydrate on CO2 and water interface which is a very slow process. Therefore, four small regions of nucleation as CO2 hydrate of size 1Å×1Å are considered on the water and CO2 interface before running the simulation to let the things happen. These points are highlighted with white circles in Fig.2. The size of system is (150Å×150Å) with diameter of 60Å for circular hydrate. The temperature (276.15 K) and pressure (83.0 bar) remain constant in the system. The temperature and pressure condition is well inside the stability region of the guest molecules. The molar density of CO2 liquid is calculated using SRK equation of state. Hydrate density is calculated using the formulation by Sloan et al. [22].

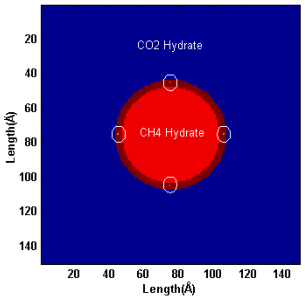

Fig.2 Initial picture of CH4 hydrate, water strip and liquid CO2 with 150Åx150Å size and a hydrate diameter of 60Å.

The simulation is run to 15.376 ns. The initial mole fraction of methane in hydrate is 0.14 is considered with the assumption that all small and large cavities are occupied by methane. Fig. 3 shows the initial density profile on the center line of the hydrate system passing through the hydrate. Many up-coming figures only show the profiles on the center line of the 2D-hydrate system passing through hydrate.

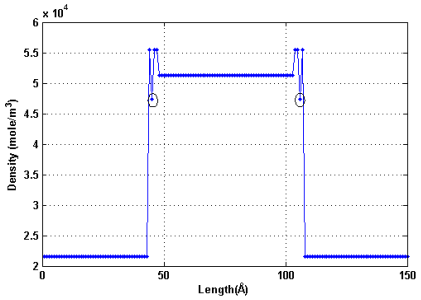

Fig.3 Density profile at time zero. Points encircled are the nucleation points and therefore CO2 hydrate density.

Methane hydrate initially starts to dissociate into the surrounding water. This is due to the driving force in terms of the change in chemical potential of methane in liquid phase and hydrate phase. This Phenomenon can be seen in Fig.4.

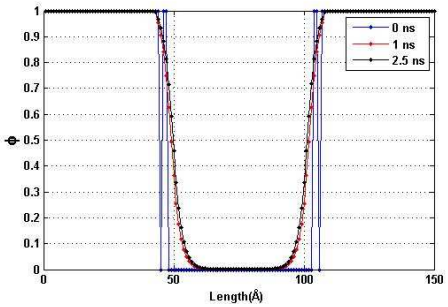

Fig.4. Phase Field parameter ϕ profile showing initial methane hydrate dissociation.

The CO2 starts penetrating into the methane hydrate as some empty spaces into the hydrate cavities are now available after some amount of methane has been released into the liquid phase. CO2 is assumed to only enter the large cavities of structure I due to its size. In Fig.5 both phase field parameter and CO2 profiles are plotted to exactly see the growth of CO2 in hydrate.

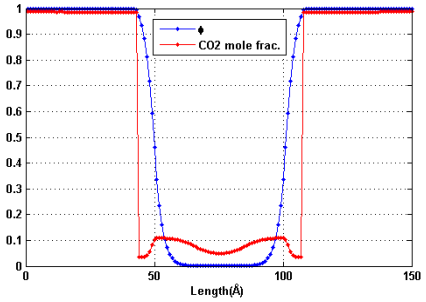

Fig.5. CO2 growth in methane hydrate at 2.5 ns.

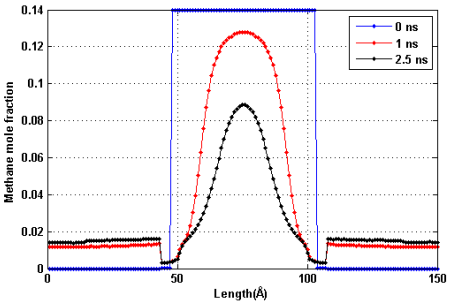

Fig.6. Methane drop inside hydrate and increase in surrounding with time.

Fig.6. shows the initial drop in methane concentration in hydrate. This is exactly can be seen in the methane flux profile in Fig.7. where dissolution rate drops quickly in first very few nano seconds.

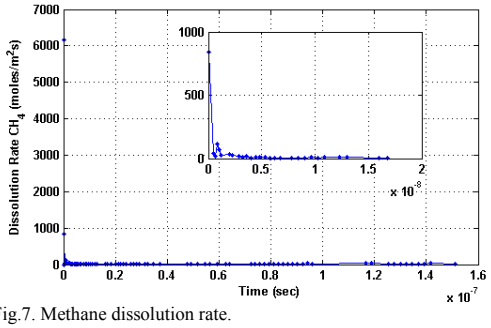

Fig.7. Methane dissolution rate.

To calculate the movement of methane from solid phase to liquid, the velocity on the interface is determined by tracking the ϕ values which is used to calculate the dissociation rate until 15.376 ns using the following equation from Sloan et al. [22]:

$$DR = SR \times \frac{\rho_{Hyd}}{M_G}\left(\frac{M_G}{M_G + 0.018 H_N}\right).$$

where DR is the dissociation rate (moles/m^{2}s), SR is hydrate radius shrinkage rate (m/s), ρ_{Hyd} is density of hydrate (kg/m^3), M_G is molar weight of the guest (kg/moles) and H_N is Hydrate number. The initial value of flux was high due to the initial relaxation of a system into a physically realistic interface.

Further, we give a figure (Fig.8) showing the mole fractions of methane and CO2 simultaneously. The figure shows mole fractions of both guests starts from the center to the wall of the system. Mole fractions of guests are given on three simulation times til 2.5 ns.

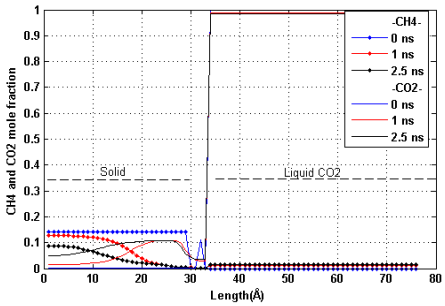

Fig.8. Methane and CO2 Mole fractions.

All these evidently shows that CO2 grows inside hydrate and the difference in chemical potentials inside and outside hydrate is the driving force while in similar way methane releases and leaving space for CO2.

Fig.9. shows direction arrows of velocity using velocity data in horizontal and vertical directions. The molecule movement outside the hydrate and towards the hydrate is clearly visible.

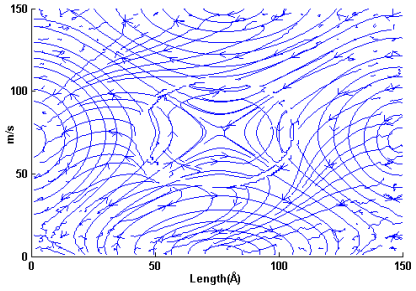

Fig.9. Direction arrows of flow at 2.5 ns.

The hydrate size is reduced because of methane dissociation until 2.5 nano seconds and then it start increasing till 12.57 ns due to reformation with CO2 penetration. This phenomenon is best explained by assistance of Fig.10, which illustrates the reformation process of CO2 hydrate, where the kinetics of the liquid CO2 from its liquid phase transformation to solid phase at different stages is plotted.

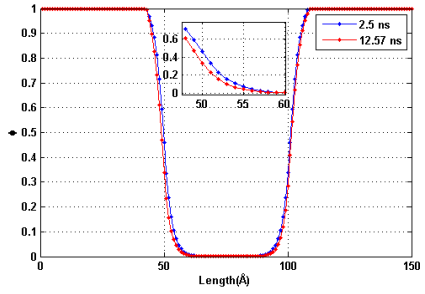

Fig.10. Hydrate reformation after initial dissociation due to CO2 penetration starting after 2.5 ns till 12.57 ns.

At the same time that is after 12.57 ns methane mole fraction also drops (see Fig.11) which initially was 0.14.

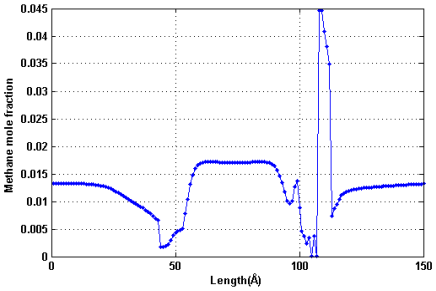

Fig.11. Methane mole fraction after 12.57 ns, drop in methane mole fraction is visible inside hydrate and increase elsewhere.

The in-out molecule movement is still continuing after 12.57 ns. A significant activity on the interface can still be observed. This can be observed by Fig.12 as well.

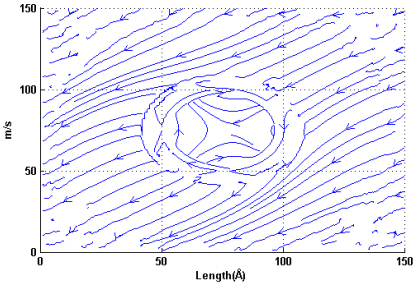

Fig.12. Flow profile after 12.57 ns, after full possible exchange.

The density profile is also transformed and after 12.57 ns the density of CO2 liquid drop as methane has penetrated and may have free gas in few places. This can be seen in Fig.13 and 14.

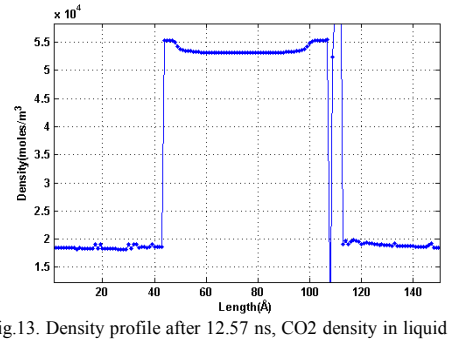

Fig.13. Density profile after 12.57 ns, CO2 density in liquid drops as methane has released after dissociation.

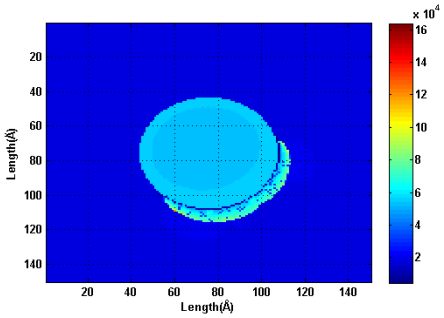

Fig.14. Density profile on whole 2D plane after 12.57 ns.

The increase of CO2 concentration inside hydrate is visible through Fig.15. The CO2 concentration is plotted along with Phase field parameter.

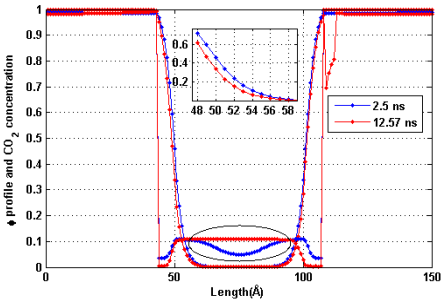

Fig.15. Combine plot of CO2 concentration and phase field parameter to see the hydrate reformation due to CO2 penetration in hydrate.

The area encircled clearly shows the growth of CO2 concentration inside hydrate and after 12.57 ns nearly 90 % of large cavities are filled with CO2. The hydrate at this time is not in stable condition and right after this time the hydrate starts dissociating again and in the matter of less than 3 ns the hydrate completely dissociates. The reason is the very low mole fraction of CO2 on the interface and access water. The CO2 exists in the range 0.3% to 0.8 % in water. Methane is even lower and is in the range of 0.1 % to 0.3 %. The corresponding chemical potential of CO2 in aqueous in the interface is from -3.2646E+04 j/mol to -3.4226E+04 j/mol respectively. On the other hand the mole fraction of CO2 inside the hydrate has raised up to 0.108 which means the chemical potential of CO2 in hydrate is -3.18450E+04 j/mol which is quite high then the chemical potential of CO2 in aqueous in the interface. This difference of free energy triggers the dissociation of hydrate. Fig. 16 gives a comparison of mole fractions of CO2 and water at 12.57 ns.

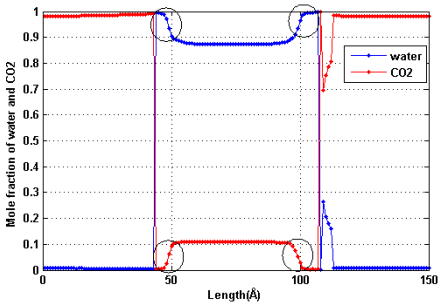

Fig.16. Water and CO2 mole fraction comparison after 12.57 ns.

The encircled regions shows a clearly that CO2 is very low in the interface in comparison to water. The methane is also very low in the same region as can be observed in Fig. 10. Once the dissociation starts the CO2 remain low as dissociation results more water and little CO2 to add in the interface. Fig. 17 clearly shows an even more drop in CO2 in interface after a very small time.

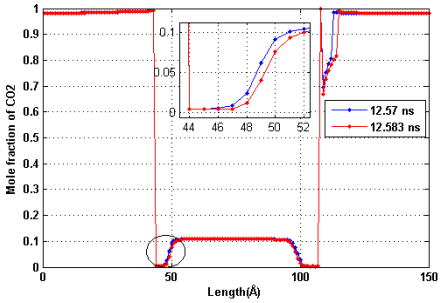

Fig. 17. CO2 mole fraction comparison 12.57 ns and 12.583 ns.

The encircled region is zoomed to clearly show the decrease in CO2 mole fraction in interface. On the other hand the water content grows more with time as suggested by Fig. 18.

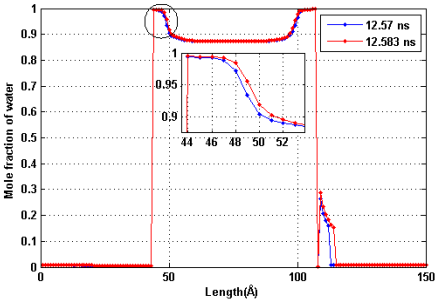

Fig. 18. Water mole fraction comparison 12.57 ns and 12.583 ns.

Again, the encircled region is zoomed to explain the growth of water on interface. This means that with time the CO2 drops and the water grows even more in interface and hence dissociation fasts with each passing time. That's the reason

why it results in a very rapid dissociation of the whole hydrate. For instance, the phase field parameter profiles are shown in Fig. 19 at 12.57 ns and 12.796 ns to show the rapid dissociation process.

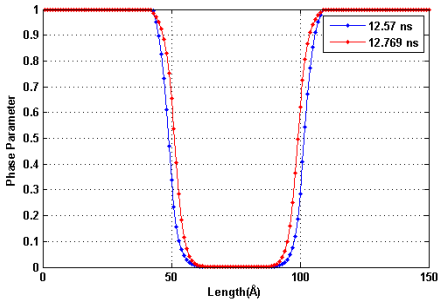

Fig. 19. Phase parameter comparison 12.57 ns and 12.769 ns.

The whole hydrate dissociates at 15.376 ns and phase parameter profile shows it in Fig. 20.

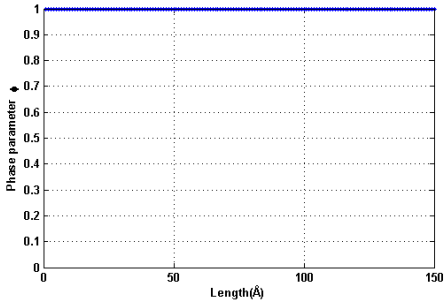

Fig. 20. Phase parameter at 15.376 ns showing full dissociation.

The CO2 and methane mole fractions are now very low in the previous hydrate region as expected, see Fig 21 and Fig.22.

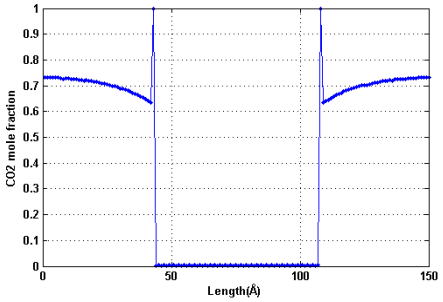

Fig.21. CO2 mole fraction after full dissociation.

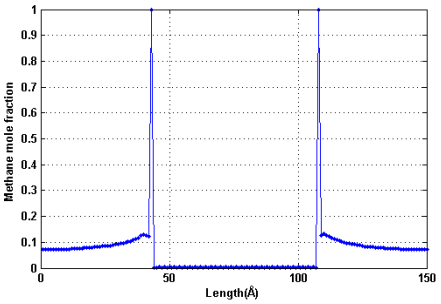

Fig.22. Methane mole fraction after full dissociation.

Phase field simulation with more appropriate description of thermodynamic model as well hydrodynamic [9] has been applied to model the exchange of CH4 with CO2 from natural gas hydrate at more realistic conditions corresponding to hydrates reservoir then in [14]. The data attained is useful in the modeling and optimization for the production of methane from hydrate reservoir as well as sequestration of CO2. As expected it was observed that the mole fraction of CO2 in the hydrate phase increases, while that of CH4 decreases with increasing time. It is also observed that the insertion of water band around methane hydrate speeds up the exchange process and hence CO2 hydrate reformation. After almost a 90 % exchange of CO2 with methane in large cavities the hydrate starts dissociating due to very low CO2 concentration in interface and high CO2 concentration inside the hydrate. The CO2 amount kept dropping during the dissociation and water kept rising on the interface which makes the dissociation very fast and in less than 3 ns the hydrates dissociates completely.

VI. Acknowledgment

This paper is a contribution to the Norwegian Research Council PETROMAKS project Gas hydrates on the Norwegian-Barents Sea-Svalbard margin (GANS, Norwegian Research Council Project No. 175969/S30).

References

[1] K. A. Kvenvolden, B. W. Rogers, "Gaia's breathglobal methane exhalations," Marine and Petroleum Geology, Vol.22, pp. 579-590, 2005.

[2] I. R. MacDonald, N. L. Guinasso, Jr. R. Sassen, J. M. Brooks, L. Lee, K. T. Scott, "Gas hydrate that breaches the sea floor on the continental slope of the Gulf of Mexico," pp. 699 – 702, 1994.

[3] G. Rehder, S. H. Kirby, W. B. Durham, L.A. Stern, E. T. Peltzer, J. Pinkston, P. G. Brewer, "Dissolution rates of pure methane hydrate and carbon-dioxide hydrate in undersaturated seawater at 1000-m depth," Geochimica et Cosmochimica Acta, Vol. 68, no. 2, pp. 285 – 292, 2004.

[4] A. V. Egorov, K. Crane, P. R. Vogt, A.N. Rozhkov, P. P. Shirshov, "Gas hydrates that outcrop on the sea floor: stability models," Geo-Marine Letters, Vol.19, pp. 68 – 75, 1999.

[5] A. Saji, H. Yoshida et al., "Fixation of carbondioxide by clathrate-hydrate," Energy Conversion and Management, Vol. 33, no. (5 – 8), pp. 643 – 649, 1992.

[6] A. Yamasaki, H. Teng et al., "CO2 hydrate formation in various hydrodynamics conditions," Gas Hydrates: Challenges for the Future, Vol. 912, pp. 235 – 245, 2002.

[7] J. W. Lee, M. K. Chun et al., "Phase equilibria and kinetic behavior of CO2 hydrate in electrolyte and porous media solutions: Application to

ocean sequestration CO2," Korean Journal of Chemical Engineering, Vol. 19, no. 4, pp. 673 – 678, 2002.
[8] T. Xu, J. A. Apps, K. Pruess, "Numerical simulation of CO2 disposal by mineral trapping in deep aquifers," Appl. Geochem., Vol. 19, pp. 917 – 936, 2004.
[9] M. Qasim, B. Kvamme, K. Baig, "Phase field theory modeling of CH4/CO2 gas hydrates in gravity fields," International Journal of Geology, Vol. 5, no. 2, pp. 48 – 52, 2011.
[10] K. Caldeira, M. E. Wickett, "Ocean model predictions of chemistry changes from carbon dioxide emissions to the atmosphere and ocean," J. Geophys. Res, pp. 110 – 112, 2005.
[11] A. A. Wheeler, W. J. Boethinger, G. B. McFadden, "Phase field model for isothermal phase transitions in binary alloys," Physical Review A, Vol. 45, pp. 7424 – 7439, 1992.
[12] B. Kvamme, A. Svandal, T. Buanes, T. Kuznetsova, "Phase field approaches to the kinetic modeling of hydrate phase transitions," AAPG Memoir, Vol. 89, pp. 758 – 769, 2009.
[13] A. Svandal, "Modeling hydrate phase transitions using mean field approaches," University of Bergen, pp. 1 – 37, 2006.
[14] M. Qasim, B. Kvamme, K. Baig, "Modeling dissociation and reformation of methane and carbon dioxide hydrate using Phase Field Theorey with implicit hydrodynamics," 7th International Conference on Gas Hydrates (ICGH 2011), Edinburgh, Scotland, United Kingdom, July 17 – 21, 2011.
[15] B. Kvamme, K. Baig, J. Bauman, P. H. Kivelä, "Thermodynamics and kinetic modeling of CH4/CO2 exchange in hydrates," 7th International Conference on Gas Hydrates (ICGH 2011), Edinburgh, Scotland, United Kingdom, July 17 – 21, 2011.
[16] G. Tegze, L. Gránásy, "Phase field simulation of liquid phase separation with fluid flow," Material science and engineering, vol. 413 – 414, pp. 418 – 422, 2005.
[17] M. Conti, "Density change effects on crystal growth from the melt," Physical Review, vol. 64, pp. 051601, 2001.
[18] M. Conti, M. Fermani, "Interface dynamics and solute trapping in alloy solidification with density change," Physical Review, vol. 67, pp. 026117, 2003.
[19] M. Conti, "Advection flow effects in the growth of a free dendrite," Physical Review, vol. 69, pp. 022601, 2004.
[20] K. Baig, M. Qasim, P. H. Kivelä, B. Kvamme, "Phase field theory modeling of methane fluxes from exposed natural gas hydrate reservoirs (in press)," American Institute of Physics, 2010.
[21] A. Svandal, T. Kuznetsova, B. Kvamme, "Thermodynamic properties and phase transitions in the H2O/CO2/CH4 system," Fluid Phase Equilibria, vol. 246, pp. 177 – 184, 2006.
[22] E. D. Sloan, C. A. Koh, "Clathrate hydrates of natural gases (3rd ed)," Boca Raton, FL: CRC Press, 2008.

Paper 6

Hydrate phase transition kinetics from Phase Field Theory with implicit hydrodynamics and heat transport

B. Kvamme, M. Qasim, K. Baig and P. H. Kivelä, J. Bauman

International Journal of Greenhouse Gas Control, Volume 29, 2014, pp. 263-278

VI

International Journal of Greenhouse Gas Control 29 (2014) 263–278

Contents lists available at ScienceDirect

International Journal of Greenhouse Gas Control

journal homepage: www.elsevier.com/locate/ijggc

Hydrate phase transition kinetics from Phase Field Theory with implicit hydrodynamics and heat transport

Bjørn Kvamme*, Muhammad Qasim, Khuram Baig, Pilvi-Helinä Kivelä, Jordan Bauman

University of Bergen, Department of Physics and Technology, Allégaten 55, N-5007 Bergen, Norway

ARTICLE INFO

Article history:
Received 23 August 2013
Received in revised form 6 May 2014
Accepted 6 August 2014

Keywords:
Hydrate
Thermodynamics
Non-equilibrium
Supersaturation
Kinetics
Carbon dioxide

ABSTRACT

Most hydrate that forms or dissociates are in situations of constant non-equilibrium. This is due to the boundary conditions and Gibbs Phase rule. At a minimum this leaves a hydrate with two adsorbed phases in addition to hydrate and fluids. One adsorbed phase is governed by the mineral surfaces and the other by the hydrate surface. With pressure and temperature defined by local conditions, hydrate formation will never be able to reach any state of equilibrium. The kinetics of hydrate formation and dissociation are a complex function of competing phase transitions. This requires kinetic theories that include minimization of free energy under constraints of mass and energy transport. Since phase transitions also change density, further constraints are given by fluid dynamics. In this work, we describe a new approach for non-equilibrium theory of hydrates together with a Phase Field Theory for simulation of phase transition kinetics. We choose a three component system of water, methane and carbon dioxide for illustration. Conversion of methane hydrate into carbon dioxide hydrate is a win–win situation of energy production combined with safe long term storage of carbon dioxide. Carbon dioxide is able to induce and proceed with a solid-state exchange, but is slow due to mass transport limitations. A faster process is the formation of new hydrate from injected carbon dioxide and residual pore water. This formation releases substantial heat. This assists in dissociating in situ methane hydrate, making the conversion progress substantially faster, because heat transport is very rapid in these systems. But conversion of liquid water into carbon dioxide hydrate, in the vicinity of the hydrate core will increase temperatures to some portions of the surface. The dissociating regions of the methane hydrate core will show a local decrease in temperature, due to extraction of heat for methane hydrate dissociation from surroundings. Another reason for heat transport implementation is that regions of the system that contains non-polar gas phase will have low heat conductivity and low heat convection. At this stage we apply a simplified heat transport model in which "lumped" efficient heat conductivity is used. We illustrate the theory on the conversion of methane hydrate to mix methane–carbon dioxide hydrate using three initial hydrate sizes: 150 Å × 150 Å, 500 Å × 500 Å and 5000 Å × 5000 Å. The hydrate cores used are spherical because it makes it easier to illustrate the impact of curvature. Symmetrical aspects simplifies the dependency to a two dimensional problem – although there are no such limitations in theory. The mineral surfaces are considered to be water wetting in these examples. It was observed that the smaller sizes convert to a more unstable mix hydrate for some periods of the simulation time, during which there were significant losses of the initial methane hydrate core. These instabilities are caused by local under saturated fluid phases around the hydrate core. Eventually a steady state progress was observed. The largest size system appeared to reach a steady state situation comparable faster than the two smaller systems.

1. Introduction

Natural gas hydrates are icelike crystalline compounds in which water serves as a host for different small non polar, or slightly polar, guest molecules. Industrial hydrate problems are mostly related to two of these structures, structure I and II, that forms hydrates with hydrocarbons up to butanes. In this work, we focus on hydrates of methane, carbon dioxide and mixtures of these. These components form structure I hydrates. The lowest symmetrical unit of this is a cubic cell with almost constant (Kvamme and Tanaka, 1995; Shpakov et al., 1997, 1998) average side lengths 12.01 Å for the region of industrial interest (above −70 °C) and natural

* Corresponding author. Tel.: +47 55583310; fax: +47 55583380.
E-mail address: bjorn.kvamme@ift.uib.no (B. Kvamme).

http://dx.doi.org/10.1016/j.ijggc.2014.08.003
1750-5836/

conditions on earth. Inside this unit crystal there are 46 water molecules constituting 6 large cavities and 2 small cavities. The large cavities are made from 24 water molecules arranged into the formation of 2 hexagonal faces and the rest as pentagonal faces. The small cavities are made from 20 water molecules forming pentagonal faces. Macroscopically, hydrates both look similar to ice and share some important properties of. An important distinction, however, is that hydrates can form also at temperatures above 0 °C depending on pressure. Another distinction from ice is the multi-component nature of the hydrate and its interaction with other phases. Hydrate formation from methane and water can happen in a number of ways. The most commonly discussed hydrate formation is on the interface between hydrate former phase and water (Kvamme and Tanaka, 1995), for which numerous experimental data are available (see for instance Koh and Sloan for a compilation (Koh and Sloan, 2008)). But hydrate can also form dissolved hydrate formers in water (Kvamme, 2002, 2003). Theoretically, hydrate can also form water dissolved in hydrate former phase (Kvamme et al., 2013a). Although more complete studies are needed to reveal whether that is realistic in view of mass transport limitations. Phase Field Theory is one theoretical method for investigating this (Qasim et al., 2011; Kvamme et al., 2004a, 2007, 2009, 2012a,b; Svandal, 2006; Tegze and Gránásy, 2005; Tegze et al., 2007). In addition, mineral surfaces will serve as adsorption sites for water as well as hydrate formers (Kvamme et al., 2012b; Cuong et al., 2012a,b). For the simplest case of one hydrate former this can give rise to at least three different hydrate formation cases: (1) water and hydrate former, both from adsorbed phase, form hydrate, (2) adsorbed water and hydrate fluid forms hydrate and (3) adsorbed hydrate former and water from fluid phase forms hydrate. It should be mentioned that the first layers of adsorbed water might have too low chemical potential to form hydrate, but few (2–4) water molecules outside will have chemical potentials suitable for hydrate formation (Kvamme et al., 2012b). If we sum up all phases for distribution of the two components methane and water it is easy to verify that these systems can generally not reach equilibrium (Gibbs's phase rule) in industrial situations or in nature, where pressure and temperature are normally given locally. Going even a step further in the analysis, it is also apparent that hydrates formed from different phases will result in different free energies. This can be visualized through Eq. (A.29) in the next section, in which the canonical partition function for the each cavity contains the chemical potential of the molecule inside that cavity (Kvamme and Tanaka, 1995), which at equilibrium would have to be equal to the chemical potential of the same molecule in the coexisting phase it came from. So even if the total system cannot reach equilibrium, the equality of chemical potentials at the (unreachable) asymptotic limit of equilibrium, are still driving forces during a process of hydrate formation. This will have impact on the hydrate filling and corresponding hydrate free energy.

In view of the above hydrate formation or dissociation, kinetics are very complex and not constantly going in one direction. Even if free energy change is negative and sufficiently negative to overcome the work involved in pushing the surrounding to give space for the growing hydrate, there could be gradients in free energy that involves positive free energy change. As an example consider formation of hydrate on a methane/pure water interface. After the hydrate has reached some thickness, the transport limitations through the hydrate film become substantial. If the initial water is pure, then hydrate will dissociate (Kvamme, 2002, 2003; Kvamme and Kuznetsova, 2004) again until a concentration of methane is in quasi equilibrium with the hydrate film. Similarly, on the methane side of the interface, in which the water content of the gas will be controlled by the chemical potential of water in hydrate (Kvamme et al., 2013a).

Injection of carbon dioxide into methane hydrate will lead to conversion of the in situ methane hydrate into a mixed hydrate in which carbon dioxide dominates occupation of the large cavities and methane fills some of the small cavities. The conversion is governed by two main mechanisms. Formation of new carbon dioxide from residual liquid water in the porous media releases heat that contributes to dissociation of surrounding methane hydrate. A second mechanism is direct solid-state exchange, which is substantially slower (Lee et al., 2003; Kuznetsova et al., 2012). This hydrate exchange is also feasible with injection of carbon dioxide and nitrogen mixtures as also demonstrated in a field pilot in Prudhoe Bay in the winter of 2012. Not all the result from this pilot has been published yet; although press release from Department of Energy states that the test was successful. The NETL web-page is continuously updated (National Energy Technology Laboratory, 2013).

In this work we discuss extension of the Phase Field Theory (Qasim et al., 2011; Kvamme et al., 2004a, 2007, 2009, 2012a,b; Svandal, 2006; Tegze and Gránásy, 2005; Tegze et al., 2007) to include hydrodynamics and heat transport. The first is needed if the dissociation of hydrate is more rapid than the solution of released methane into the surrounding water, so that methane bubbles form and affect the phase transition kinetics. Heat transport by hydrate dissociation is normally 2–3 orders of magnitude faster than mass transport in liquid water/hydrate system (Qasim et al., 2011; Kvamme et al., 2004a, 2007, 2009, 2012a,b; Svandal, 2006; Tegze and Gránásy, 2005; Tegze et al., 2007). Heat transport will, however, be slow though gas layers or gas bubbles. Implicit heat transport is obviously needed is the case where formation of new hydrate contributed to dissociation of original methane hydrate. For the fluid phases extensions to regions outside of equilibrium is quite trivial and the equations are given in Appendix 1 along with the equilibrium description for hydrate. The reason that these equations are included here are the use of chemical potentials and absolute thermodynamics (ideal gas as reference for all components in all phases). This is the most convenient choice sine it will avoid any need for shifting reference state during the free energy minimization which implicit in the Phase Field Theory (PFT) (Section 2). The extension of hydrate thermodynamics to outside equilibrium in all independent variable are accomplished using first order Taylor expansions as explained in Appendix 2. The reason these equations are included here is that the mole-fraction conservation is implicit in the PFT model and that gradients in all mole-fractions are treated as independent in the thermodynamic description. The PFT theory is described in Section 2 and examples of conversion of methane hydrate into carbon dioxide is used to illustrate the theory.

2. Phase Field Theory model

Generally the phase transition in a system follows two well defined physical processes, nucleation and growth. In addition some hydrate phase transitions shows a delay in the onset of massive growth, which is normally denoted as induction time. Nucleation is the unstable stage in which there is a competition of the free energy gain by the phase transition and the penalty of pushing old phases away in order to give room for the new phase. In this stage nuclei grow and decay as a function of different processes which induces some randomness to the system, like for instance diffusional transport of mass which by nature contain randomness element in direction versus location and orientations of growing nuclei. Within PFT modeling this is handled by subtracting the thermodynamic limits of the initial and final phase(s) from the free energy and adding a voice term which incorporates the impact on the system from the outside boundaries. See Gránásy

et al. (2003) and Svandal (2006) for more details on the nucleation modeling and corresponding parameters applied. The hydrate phase transitions described by Svandal (2006) (and papers included in the thesis) were homogenous hydrate growth from dissolved CO_2 in water. These systems were found to be essentially mass transport controlled due to fast heat transport through the liquid water phase. Critical nuclei diameter was found to be in the order of 2.5–3.0 nm, depending on thermodynamic driving force. Corresponding nucleation time is fast (nano to femtosecond) compared to a macro scale. Heterogeneous hydrate formation on the interface between a separate CO_2 phase and water will quickly nucleate a hydrate film that gradually grows slower and slower as mass transport through the hydrate film will strongly limit the support of building materials for continued hydrate growth. For methane above water at 83 bar and 4 °C this results in an induction time of close to 100 h (Kvamme et al., 2007). In this case the induction is caused by migration of methane along the plastic wall (CH_4 wettening) of the experimental compartment as well as rearrangements on the hydrate surfaces as dictated by the first and second laws of thermodynamics when free mass is not available. I.e., larger and more stable hydrate regions consume regions of higher free energy. The phenomena is in this sense very similar to observation in glass cells (water wettening) with water and different hydrocarbons (most studies with methane) as illustrated by numerous photographs of Makogan's book (Makogan, 1997). The systems studied in this work are totally different than any of these systems. The interface between an initial hydrate core and CO_2 liquid is in direct contact and the first few time steps rearrange the initial systems into an interface of gradual structure between fluid and hydrate of close to 1 nm thickness. Within these few time steps also regions of CO_2 hydrate establishes and practically the nucleation is within 1 ns needed to reconfigure the starting configuration (i.e., establishing an smooth interface from an initial sharp interface). This is also logical in the sense that building materials (water and CO_2) are readily available and in direct contact.

The effects of non-equilibrium thermodynamics on phase transition are incorporated by implementing the thermodynamic model implicitly into Phase Field simulation. The hydrodynamics effects and variable density were incorporated in a three components Phase Field Theory by Kvamme et al. (2004b) and Conti (2000) through implicit integration of Navier–Stokes equation following the approach of Qasim et al. (2011). The basic phase field model for two components is described/used by Wheeler et al. (1992) and other references (Gránásy et al., 2002, 2003, 2004; Tegze et al., 2006; Gránásy and Pusztai, 2002) and other references therein. The Phase Field Theory for three components is a straightforward extension of the basic theoretical model. The phase field parameter ϕ is an order parameter describing the phase of the system as a function of spatial and time coordinates. The phase field parameter ϕ is allowed to vary continuously from 0 to 1 on the range from solid to liquid.

The solid-state is represented by the hydrate and the liquid state represents fluid and aqueous phase. The solidification of hydrate is described in terms of the scalar phase field $\phi(x_1, x_2, x_3)$ where x_1, x_2, x_3 represents the molar fractions of CH_4, CO_2 and H_2O respectively with obvious constraint on conservation of mass $\sum_{i=1}^{3} x_i = 1$. The field ϕ is a structural order parameter assuming the values $\phi = 0$ in the solid and $\phi = 1$ in the liquid (Svandal, 2006). Intermediate values correspond to the interface between the two phases. The starting point of the three component phase field model is a free energy functional (Conti, 2000),

$$F = \int d\underline{r} \left(\frac{\varepsilon_\phi^2}{2} T(\nabla\phi)^2 + \sum_{i,j=1}^{3} \frac{\varepsilon_{xi,j}^2}{4} T\rho(x_i \nabla x_j - x_j \nabla x_i)^2 + f_{bulk}(\phi, x_1, x_2, x_3, T) \right) \quad (1)$$

which is an integration over the system volume, while the subscripts i, j represents the three components, ρ is molar density depending on relative compositions, phase and flow. The bulk free energy density described as:

$$f_{bulk} = WTg(\phi) + (1 - p(\phi)) f_S(x_1, x_2, x_3, T) + p(\phi) f_L(x_1, x_2, x_3, T) \quad (2)$$

The phase field parameter switches on and off the solid and liquid contributions f_S and f_L through the function $p(\phi) = \phi^3(10 - 15\phi + 6\phi^2)$, and note that $p(0) = 0$ and $p(1) = 1$. This function was derived from density functional theory studies of binary alloys and has been adopted also for our system of hydrate phase transitions. It might be modified by fitting profiles for hydrate/fluid interfaces derived from molecular simulations, but for the time being the profile is sufficiently representative. The binary alloys are normally treated as ideal solutions. The free energy densities of solid and liquid is given by

$$f_{bulk} = WTg(\phi) + (1 - p(\phi)) f_S(x_1, x_2, x_3, T) + p(\phi) f_L(x_1, x_2, x_3, T) \quad (3)$$

$$f_s = G_H \rho_m^H \quad (4)$$

$$f_L = G_L \rho_m^L \quad (5)$$

where the expressions for the free energy of hydrate in supersaturated (or undersaturated) states as functions of different thermodynamic variables are given through Eqs. (A.33)–(A.67) and the free energies of fluids are described in the first part of the paper from some fluid states and in references (Svandal et al., 2006b; Kvamme et al., 2004b; Wheeler et al., 1992; Gránásy et al., 2003) for other states. The details of densities ρ_m^{hyd} and ρ_m^L can be found in Qasim et al. (2011). Also note that a possible phase transition will only proceed unconditionally if the free energy change is negative, and more negative than the interface free energy barrier imposed by the interface work needed to give space for the new phase, and also all gradient in free energies results in negative free energy changes for the phase transition. Practically this latter condition implies that the system is supersaturated with respect to gradients of free energies in all thermodynamically independent variables for the system. If one or more gradients results in positive free energies and the phase transition will compete with other phase transitions.

The function $g(\phi) = \phi^2(1 - \phi^2)/4$ ensures a double well form of the f_{bulk} with a free energy scale $W = (1 - (x_i/v_m))W_A + (x_i/v_m)W_B$ with $g(0) = g(1) = 0$, where v_m is the average molar volume of water. In order to derive a kinetic model we assume that the system evolves in time so that its total free energy decreases monotonically (Svandal et al., 2006b; Kvamme et al., 2004b; Wheeler et al., 1992).

The usual equations of motion are supplemented with appropriate convection terms as explained by Tegze and Gránásy (2005) given that the phase field is not a conserved quantity, the simplest form for the time evolution that ensures a minimization of the free energy is:

$$\frac{\partial\phi}{\partial t} + (\vec{v} \cdot \nabla)\phi = -M_\phi(\phi, x_1, x_2, x_3) \frac{\delta F}{\delta \phi} \quad (6)$$

$$\frac{\partial x_i}{\partial t} + (\vec{v} \cdot \nabla)x_i = \nabla \cdot \left(M_{xi}(\phi, x_1, x_2, x_3) \nabla \frac{\delta F}{\delta xi} \right) \quad (7)$$

where $\vec{v}$ is the velocity, $M_{xi} = x_i(1-x_i)(1/RT)D$ and $M_\phi = (1-(x_i/v_m))M^A + (x_i/v_m)M^B$ are the mobilities associated with coarse-grained equation of motion which in turn are related to their microscopic counter parts. Where $D = D_S + (D_L - D_S)p(\phi)$ is the diffusion coefficient. The details are given elsewhere (Svandal, 2006; Kvamme et al., 2004b).

An extended phase field model is formulated to account for the effect of fluid flow, density change and gravity. This is achieved by coupling the time evolution with the Navier–Stokes Equations. The phase and concentration fields associates the hydrodynamic equation as described by Conti (2001, 2004) and with Conti and Fermani (2003).

$$\frac{\partial \rho}{\partial t} = -\rho_m \nabla \cdot \vec{v} \tag{8}$$

$$\rho \frac{\partial \vec{v}}{\partial t} + \rho(\vec{v} \cdot \nabla)\vec{v} = \rho\vec{g} + \nabla \cdot P \tag{9}$$

Where $\vec{g}$ is the gravitational acceleration. ρ_m is the density of the system in hydrate (ρ_m^{Hyd}) and liquid (ρ_m^L). Further

$$P = \square + \Pi \tag{10}$$

is the generalization of stress tensor (Conti, 2001, 2004; Conti and Fermani, 2003), $\square$ represents non-dissipative part and Π represents the dissipative part of the stress tensor.

For hydrate formation following water adsorption on rusty walls (Cuong et al., 2012a,b), heat transport is very fast compared to mass transport and not likely to have any significant rate limiting impact on the kinetic rates. Formation of hydrates inside bulk CO_2 (or inside CO_2/CH_4 fluid) heat transport rates may have an impact. For these cases we have, so far, extended our PFT code according to a simplified scheme as described below.

First consider the general thermodynamic relationship:

$$dH = \left(\frac{\partial H}{\partial T}\right)_{P,\vec{x}} dT + \left(V - T\left[\frac{\partial V}{\partial T}\right]_{P,\vec{x}}\right) dp \tag{11}$$

where the molar volume V, as well as the gradient of molar volume with respect to T, is very small for solids and condensed phases. The latter term is also exactly zero for ideal gas. So except for regions of high pressure gas the latter term is normally negligible. So for simplicity and, also considering other uncertainties which will be described below, the latter term is omitted as an approximation. Strictly speaking, it is not necessary since the volumetric terms are readily available from the solution of the equation of state used. The correction could be estimated but the latter term implies couplings to Navier–Stokes that would require some modifications in the integration algorithm.

The two primary contributions to heat transport are conduction and convection. For the systems that we consider the conduction term is the dominating one. A common approximation in hydrate modeling, as well as in interpretation of experimental data, is therefore to lump both these contributions into an "apparent" conductivity. Accordingly:

$$\dot{Q} = kA\ \Delta T \tag{12}$$

Where k is the "apparent" heat conductivity, A is the area for the heat transport and ΔT is the temperature difference. In the integrations of Eqs. (11) and (12), the 2 or 3 dimensional space in consideration is discretized into grid blocks. For each grid block the total molar enthalpy can be written as:

$$H_i = (1-\varphi_i)H_{S,i}(T, P, \vec{x}_{S,i}) + \varphi_i H_{L,i}(T, P, \vec{x}_{L,i}) \tag{13}$$

where subscript i is the index for grid block number and subscripts S and L denote hydrate and fluid respectively. These enthalpies are readily available from the individual thermodynamic models involved but are more conveniently evaluated directly from the free energy of each grid block using Eq. (1). From the first law of thermodynamics and combining Eqs. (11) and (12) we arrive at the simple result:

$$\left(\frac{\Delta H}{\Delta t}\right)_i = k_i A_i\ \Delta T_i \tag{14}$$

In discretized form for a chosen time step of the integration, Δt, and corresponding changes in enthalpy and temperature over a time step of progress. A_i is trivially given by the geometry of the grid block system and the dimensions of the system (3D or 2D simulation). We make no rigorous discussion on the most appropriate form of an average thermal conductivity of each grid block and have so far implemented the following average value:

$$k_i = (1-\varphi_i)k_{S,i}(T, P, \vec{x}_{S,i}) + \varphi_i k_{L,i}(T, P, \vec{x}_{L,i}) \tag{15}$$

in which a number of different correlations are available for gas mixtures in the fluid part of the latter term. For liquid water, part of the latter term values is fairly independent of pressure, and since solubility of CO_2 as well CH_4, is limited liquid water provides a fair approximation. For thermal conductivity of hydrate in the solid position of the grid block phase distribution, the value is almost insensitive to both pressures and compositions of the hydrate. Fixed values for $k_{S,i}$ and $k_{L,i}$ are $0.49\,W\,m^{-1}\,K^{-1}$ and $0.605\,W\,m^{-1}\,K^{-1}$ respectively (Henriet and Mienert, 1998). Mass transport is not limited in these systems, as explained in the first part of this section. Eqs. (13)–(15) will induce heterogeneous behavior since there is randomness in the rate of CO_2 hydrate formation around the initial CH_4 hydrate sphere. This randomness occurs during the initial transition from a sharp interface into a soft interface, which already results in varying amount of CO_2 hydrate as function of surface location. Part of this randomness is logical due to randomness in mass transport and mass rearrangement in creating the interface. But despite a very high resolution the amount of different phases in each grid volume that implies portions of initial CH_4 hydrate will vary locally around the hydrate core. But even if the hydrate core already had liquid water in between the CH_4 hydrate and CO_2 heterogeneous behavior would occur due to randomness in diffusional transport of water and CO_2 in the two directions, and corresponding variation in water/CO_2 ratio between different volume elements. As a consequence the amount of new CO_2 hydrate formed will vary with location.

3. Results

For hydrate inside water wetting mineral pore, hydrate will fill the inside of the pore and liquid water will surround the hydrate core. Injection of CO_2 into the pore will first displace some of the water surrounding the hydrate because the minerals will normally have a higher thermodynamic benefit from the water than the hydrate. But this depends, of course, on the wetting properties of the minerals. As an example, water adsorbed on hematite may have chemical potentials of 2–4 kJ/mole lower than liquid water under the same conditions (Kvamme et al., 2012b). If the mineral surface is CO_2 wetting, the larger portions of the in situ liquid water will surround the hydrate core in the pore. In this case, in situ free gas (if existing) will partly dissolve in the injected CO_2. The rate of dissolution depends on dissolution kinetic rates compared to flow dynamics and rates of CO_2 conversion into hydrate. The relative proportions of water surrounding the hydrate core independent on several additional factors. In the example used here to illustrate the theory, we have made one choice in which the mineral surfaces are water wetting. The degree of water wetting is not important for these examples since we focus on the exchange process on the hydrate core. Water wetting and possible impact on hydrate nucleation on growth can be included in terms of limits of chemical

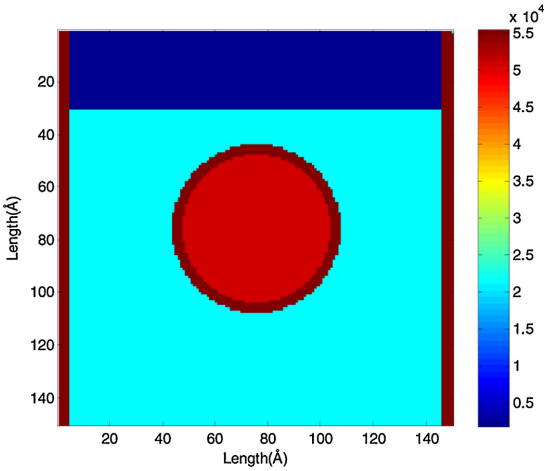

Fig. 1. Initial snap shot of density (mol/m^3) profile shows the initial distribution of phases and components for (150 Å × 150 Å) system; red disk in the center is CH_4 hydrate core, water regions are represented by maroon color, dark blue region is methane and rest is CO_2, similar distribution for other two 2D systems. (For interpretation of the references to color in this figure legend, the reader is referred to the web version of this article.)

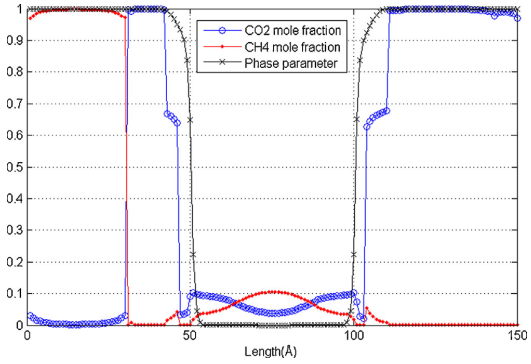

Fig. 2. CO_2 filling in hydrate while curve of methane mole fraction shows dissociation of methane, phase parameter curve to indicate hydrate and fluid phases.

potential of water toward sides of the simulations system assigned to be mineral sides. For the simulations as such the only impact would be that nucleation calculations toward the mineral surfaces is expected to be longer than the very fast nucleation which happens at the same time period as the interface changes from a sharp interface to a smooth interface. It is absolutely feasible to introduce that along the lines described by Kvamme et al. (2007) with additional data on chemical potential of adsorbed water as described by Kvamme et al. (2012b) and (Cuong et al., 2012a,b) for calcite.

With simulations on nano to micro scale in volume, it might be useful to investigate impact of size, at least to the level possible within reasonable simulation times. But also for the reason of sizes of CO_2 reservoirs relative to size of initial core and corresponding impact of changes in surrounding. Therefore, we investigate three different system sizes. The phenomena that we aim to investigate here is essentially one or maximum 2 dimensions in terms of kinetic dependency; at least for the simple crystal morphology that we use in our examples. In order to save CPU time, simulations are conducted in 2D. However, there are no constraints to this in the theory or the PFT code. As mentioned, there are two primary mechanisms involved in the conversion of methane hydrate into a mixed hydrate of carbon dioxide and methane in which some methane will occupy the small cavities. As an approximation we neglect filling of carbon dioxide in the small cavities since it is currently uncertain if this will be significant for rapid phase transitions in a dynamic reservoir flow environment.

The three 2D system sizes representing the sample pores sizes are 150 Å × 150 Å, 500 Å × 500 Å and 5000 Å × 5000 Å. The initial hydrate size varies in different systems, but all are disks in shape right at the center of the 2D systems. The radius of hydrate disk is 28 Å in smallest system, in slightly bigger system the radius is 114 Å and for the biggest system the radius is 1136 Å. The initial pure methane saturation is approximately 20% of the pore area. Small portions of water saturations are introduced around hydrate and as layers near the walls as illustrated in Fig. 1. This water is more or less the minimum interface thickness between liquid water and hydrate. The rest of the area is filled with injected CO_2 in pore. The initial distribution of components and phases are explained in Fig. 1.

Set-up for the smallest 2D system is illustrated in Fig. 1 for initial distribution of phases. This distribution is based on average liquid water saturation, free gas saturation and hydrate saturation of a real reservoir. The specific arrangement of initial phases is just an example and used for the purpose of illustrating the theory. Different set-ups will be investigated in subsequent papers. The same initial relative distribution of phases is also used for the larger systems. The model pore is a square shape of size 150 Å × 150 Å in Fig. 1 and sI structure hydrate is represented by circular region in red color right in center of the pore. The water saturation is represented with maroon color around hydrate in addition to the two strips adjacent to the walls. The upper blue strip is the methane saturation which is supposedly moved up by the injected CO_2 from its original position around the hydrate. The rest of the region shows the injected CO_2. The pressure is kept constant at 83 bar and the initial temperature is uniform and 277.15 K.

The CO_2–CH_4 molecular exchange process is driven by the lower energy state of CO_2 as the guest molecule in sI gas hydrate structures versus CH_4. This results in more favorable thermodynamics conditions of formation for the pure CO_2 versus pure CH_4 hydrates over large regions of pressures and temperatures. Mixed hydrate, in which CO_2 dominates occupation of large cavities and CH_4 dominates occupation of small cavities, is more stable at all conditions of temperature and pressure. The initial process is fast since that mechanism is dominated by rapid new formation of hydrate from the CO_2 and associated release of heat for dissociation of CH_4 hydrate. At later time for instance after 3 ns the simulation results clearly show as in Fig. 2 that the exchange process has started due to the favorable thermodynamics for CO_2 versus CH_4 hydrates.

CO_2 can penetrate in both small and large cages (Cuong et al., 2012b) but as mentioned before filling of CO_2 in the small cavities is ignored in this work. The large cavities are in 3:1 ratio with small cavities and therefore theoretically speaking 75% of methane can be replaced with CO_2 within the approximation of no CO_2 filling in small cavities. All the curves in Fig. 2, and in coming figures, show variation in parameters on the line starting from the boundary of the 2D geometry in Fig. 1 adjacent to blue methane region to the opposite boundary passing through the center of hydrate. This will show the variation in parameters in the pore with a single curve. The CO_2, CH_4 concentrations and phase field curves in Fig. 2 show that CO_2 has converted the interface water layer into hydrate and created a new interface dominated by CO_2 in favor of CH_4 with water and then started the (slow) solid-state conversion of the CH_4 hydrate core. The phase parameter, represented by the third curve in Fig. 2 is drawn here to show precisely the changes in mole fraction of CO_2 and CH_4 inside hydrate. The exchange will continue until

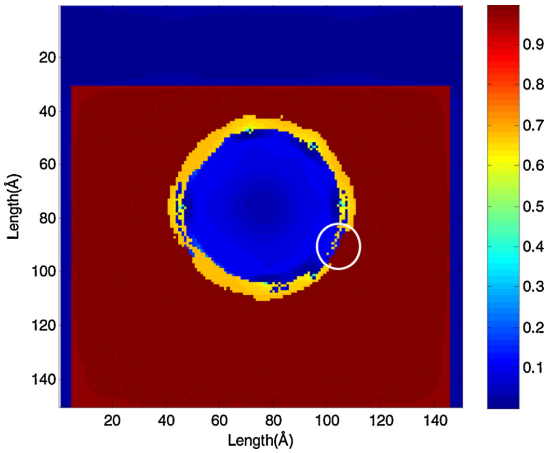

Fig. 3. CO_2 mole fraction in entire system after 3 ns, CO_2 starts to accumulate in outer regions of initial hydrate core forming mix hydrate in early stage of simulation time, few gaps are due to the dissociation of CH_4. The dark blue region adjacent to the wall and top of the system is showing the negligibly small amount of CO_2 concentration. (For interpretation of the references to color in this figure legend, the reader is referred to the web version of this article.)

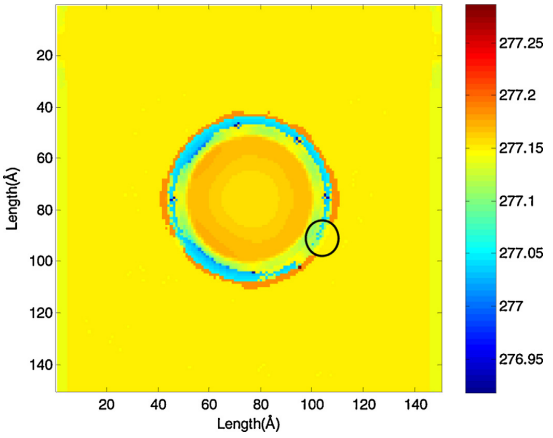

Fig. 4. Temperature profile in Kelvin in entire system after 3 ns, increase in temperature in the regions of mix hydrate formation and drops in methane dissociation regions.

almost all the methane in large cavities is exchanged with CO_2. The CO_2 sequestration in the entire pore can better be seen with the help of Fig. 3.

The encircled region in Fig. 3 shows one of the gaps in the CO_2 accumulation at the interface which is typically an escape region for dissociating methane mainly from the large cavities of hydrate. Other small gaps of hydrate dissociation can also be observed in Fig. 3. The formation of hydrate is an exothermic process and therefore results an increase in temperature in the hydrate formation area. The dissociation extracts heat since is an endothermic process. This is also observed in the temperature profile around the core, in which there are regions of increased temperature for formation of CO_2 hydrate. There are also regions of reduced temperature where hydrate dissociation extracts heat from the surroundings, as illustrated in Fig. 4. The encircled region in Fig. 4 is indicating one of the hydrate dissociating regions.

The average temperature changes as plotted in Fig. 5 illustrates that some heat for dissociation of the outer layers is even generated from the core after a larger temperature drop outside the encircled area in Fig. 4 have created a negative heat gradient in those regions and the inner parts of the core has cooled down slightly.

The temperature curve in Fig. 5 is again on the line starting from one wall to another passing through the center of hydrate. If the surrounding fluid is incapable of diluting the released methane within the time window of simulation time then methane will exist as a free gas near the interface. Note that the two components CH_4 and CO_2 are mutually soluble at these conditions according to the thermodynamics, but there are constraints on the solubility kinetics in terms of diffusivities compared to the impact of Navier–Stokes on the local variations in densities. The existence of free CH_4 dominated gas bubbles from released CH_4 can be observed in this example as shown in Fig. 6. A few regions of free gas are particularly expressed by encircling them within the fluid phase in Fig. 6. The mole fraction of methane in those regions varies in the range of 0.53–0.65.

The density of free gas increases with time proportional to dissolution of the released methane into the surrounding CO_2. Within these very small time scales, the dissolution of the CH_4 film into the CO_2 phase is limited, although relative dissolution rates are similar to the dissolution of the very small CH_4 gas bubbles. In particular in this specific example after 5.6 ns, most of the large cavities of hydrate are filled with CO_2 and methane is released into the surrounding fluids as illustrated in Fig. 7.

Due to under saturated water in the surrounding of the hydrate, the mixed hydrate could not be sustained and melted very quickly in the similar behavior as explained by Qasim et al. (2012). In parallel, another simulation was also run on slightly bigger pore size (500Å × 500 Å). It has a bigger circular hydrate right in the middle of planer geometry of pore with radius of 114 Å and bigger methane strip of 100 Å of width. As discussed by Svandal et al. (2006b) the diffusion is dependent on the curvature of the geometry. The smaller the curvature, the slower the diffusion of CO_2 into CH_4–hydrate. The bigger system therefore has more widely and fewer gaps in the temperature profile at the interface of hydrate Fig. 8.

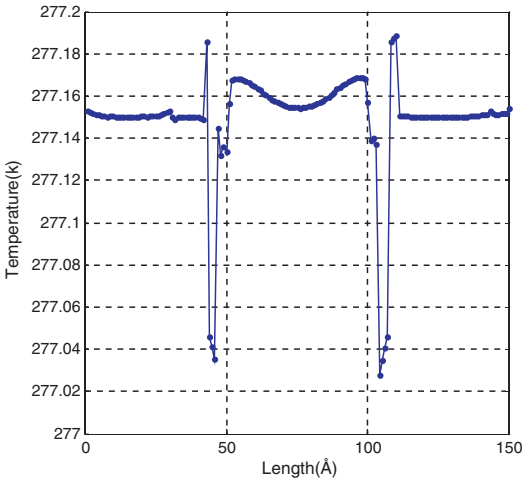

Fig. 5. Average temperature variation around and inside the core due to hydrate formation and dissociation after 3 ns.

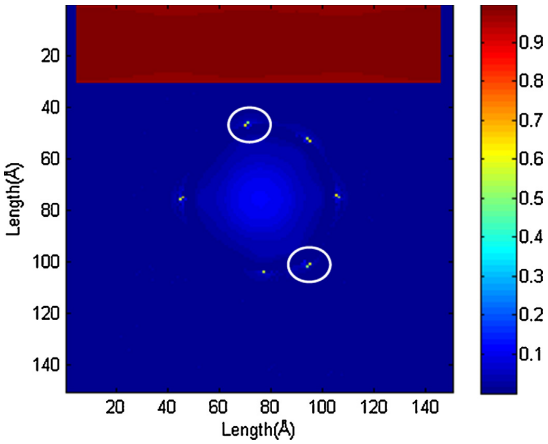

Fig. 6. Snapshot of methane mole fraction in entire system after 3 ns, two of the regions of methane bubbles from released methane near the interface are encircled. The bubbles are dynamically dissolving as can be seen from the methane mole fraction.

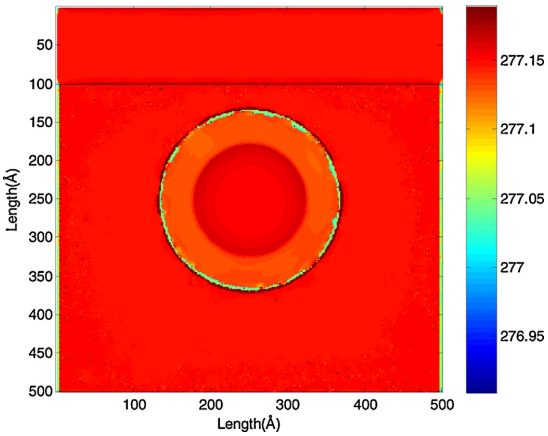

Fig. 8. Temperature (K) variation in initial stage of simulation, showing increased in temperature in the regions of mix hydrate formation and temperature drop in the methane dissociating regions.

The temperature variation shown in Fig. 8 is in the very initial stages of simulation time when the dissociation of CH_4 is rapid due to the formation of new CO_2 hydrate as the primary mechanism. Also, the original hydrate core is dissociating over substantial portions of the hydrate core. As the time progresses, the dissociation process slows down due to the slower direct conversion which is solid-state transport dominated. A more stable mixed hydrate is gradually forming as illustrated in Fig. 9. Reduction rate of hydrate has an asymptotic approach and reached a very low rate after 64 ns. At this time of the simulation, the size of the mixed hydrate is smaller than the original core.

At the same time that is after 64 ns the flux of dissociating methane also become negligibly small as shown in Fig. 10.

The dissolution rate of CH_4 presented in Fig. 10 is calculated using the formulation given by Koh and Sloan (2008) and used here in the similar way as by Qasim et al. (2012). The mole fraction of CH_4 and CO_2 given in Fig. 11 clearly suggests that, as per our assumption, CO_2 has occupied only large cavities while CH_4 has been dissociated out of them and most of the CH_4 is in only small cavities after 64 ns.

The surrounding fluid of the mix hydrate is not undersaturated with CO_2 in this example, unlike the smallest system, which triggered the dissociation of the mix hydrate. The filling of CO_2 in large cavities in the whole system can better be seen in Fig. 12.

To illustrate it further, we present another plot (Fig. 13) to be able to see the variations in CO_2 mole fraction more clearly and build up of CO_2 mole fraction happening inside hydrate.

The temperature curve after 64 ns is given in Fig. 14. Temperature has increased in the mix hydrate formation region while dropped on the interface due to dissociation of CH_4.

The evidences of methane bubble are also very obvious in Fig. 7. The arrow pointing toward the cloud at some distance around the hydrate core has many pixels with mole fraction of methane between 0.53 and 0.65. On the other hand the flow of methane into CO_2 fluid and CO_2 into methane is pretty controlled, symmetric all over CO_2/methane interface and slow as per Figs. 12 and 15.

The bigger system (5000Å × 5000 Å) behaves differently by achieving a stable mixed hydrate faster. This is illustrated in Figs. 16 and 17.

The simulation results for the largest system is only available up to 8.4 ns. Up until this time, only a partial part of the hydrate large cavities are filled with CO_2. It will take substantial CPU simulation time to complete the simulation until full exchange. The rate of CH_4 release, as illustrated in Fig. 17, clearly shows that methane is still released after 8.4 ns due to the exchange process in favor of CO_2

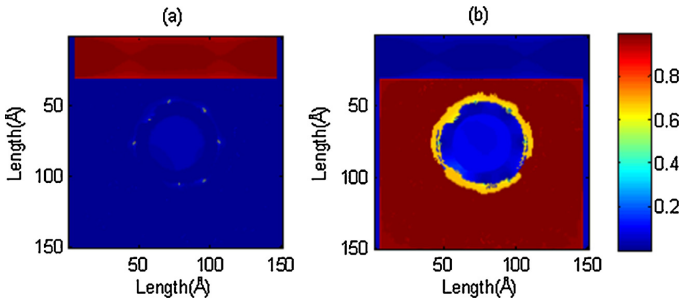

Fig. 7. Small system. (a) Methane and (b) carbon dioxide mole fraction in entire system after maximum exchange 5.6 ns (the time of largest mixed hydrate core). Density of free gas has also increased.

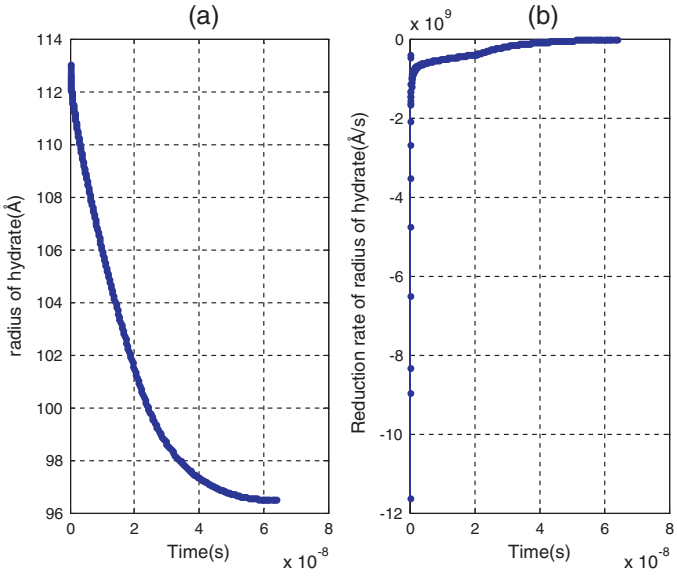

Fig. 9. Intermediate system (500Å × 500 Å) system: Radius of circular hydrate and its reduction rate shows convergence to a stable mixed hydrate as function of time.

occupation of large cavities. But the rate has decreased due to the slow solid-state exchange mechanism and the system seem to be entering a stationary slow progress.

The CO_2 mole fraction at 8.4 ns is illustrated in Fig. 18. Only a small portion near interface of hydrate is filled with CO_2. The behavior of the variation in temperature is similar to the system of size (500Å × 500 Å), see Fig. 19. A little jump in temperature, which is indicated by the arrow in Fig. 19 is on the interface of CO_2 and CH_4 fluid phases.

4. Discussion

The primary goal of this paper has been to illustrate a theoretical concept for studies of hydrate phase transition kinetics in multi-phase systems containing hydrate, water, free methane phase and carbon dioxide phases. The applied model systems applied are simplified in several ways. Crystal morphology certainly places a role in the kinetics in many ways. For instance, varying surface area, geometrical trapping in inclinements, and local gradients of free

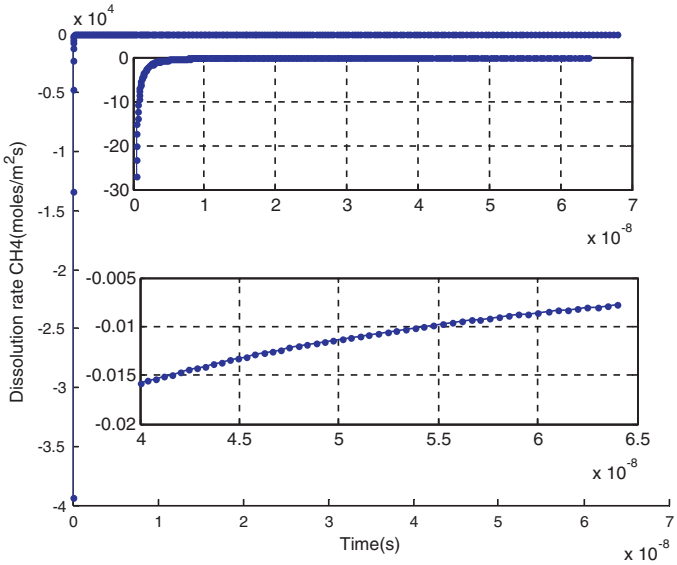

Fig. 10. The intermediate size (500Å × 500 Å) system: CH_4 dissolution rate shows the system approaching stability, the two figures inside are the zoomed regions of the curve.

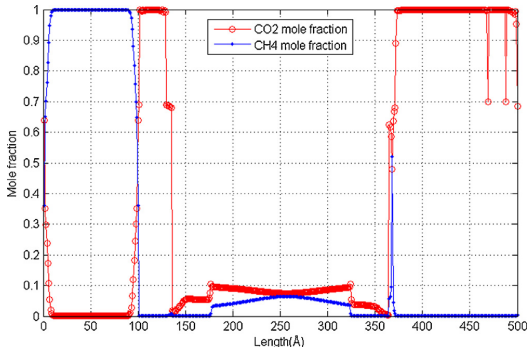

Fig. 11. CH_4 and CO_2 mole fraction after 64 ns of simulation time when the mix hydrate is stable and dissociation of methane has almost stopped.

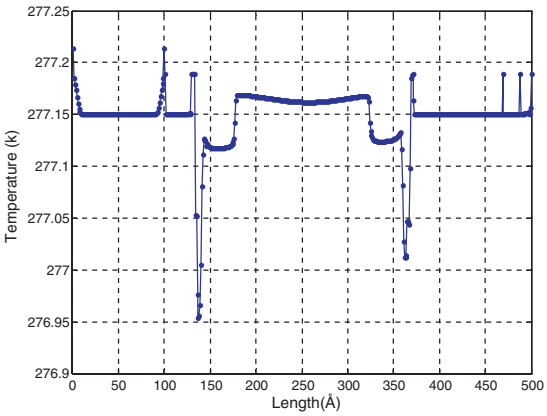

Fig. 14. Average temperature profile in the intermediate system (500Å × 500 Å). Temperature (K) curve after 64 ns (the time when the mixed hydrate is very stable).

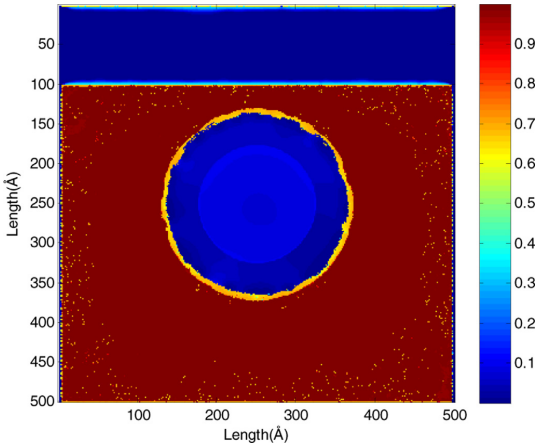

Fig. 12. Distribution of the CO_2 mole fraction in entire system after 64 ns.

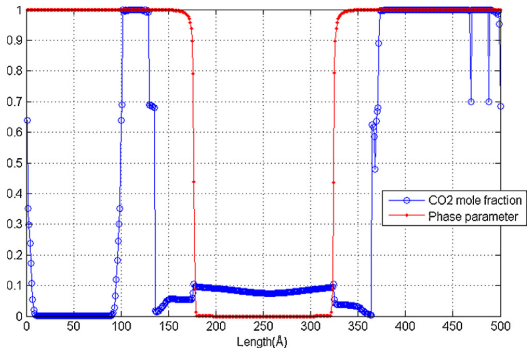

Fig. 13. Profiles for average CO_2 mole fraction and phase field parameter in hydrate after 64 ns (the time when mix hydrate is very stable). The number of un-occupied large cavities by CO_2 increases near to the center of the hydrate.

energies. This can surely be incorporated as demonstrated though our earlier publications in the reference list. A very thin film of free water around the hydrate was applied in all three system sizes used for illustration here. This is of course easy to vary in order to obtain a better picture of the two competing conversion mechanisms. The formation of new CO_2 hydrate will clearly dominate since mass transport through fluid phases dominates this mechanism, in contrast to solid-state conversion. There are two primary impacts of solid surfaces. Geometrically inclinements will reduce the mobility of components in some directions and provide more time for reorganization and accumulation of hydrate building blocks. This has been studied in different papers before and is a well known phenomena. The other important aspect is the adsorption of water and hydrate formers on mineral surfaces. This can result in different ways of creating new hydrate. For instance, from adsorbed guests and water or adsorbed water and surrounding guest molecules. Implementations of solid particles and/or solid walls have been demonstrated earlier, so the only additional features are inclusion

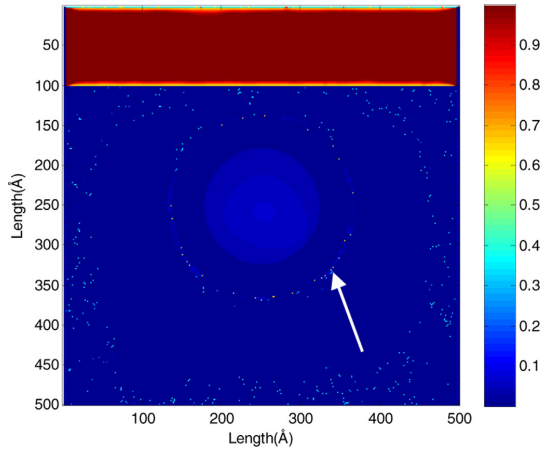

Fig. 15. Intermediate system. The appearance of methane bubbles with varying content of CO_2 as visualized by the color code to the right after 64 ns. Also dissolution into top and bottom of the upper methane layer. Periodic boundary condition so upper methane plume is in contact with bottom of simulation box.

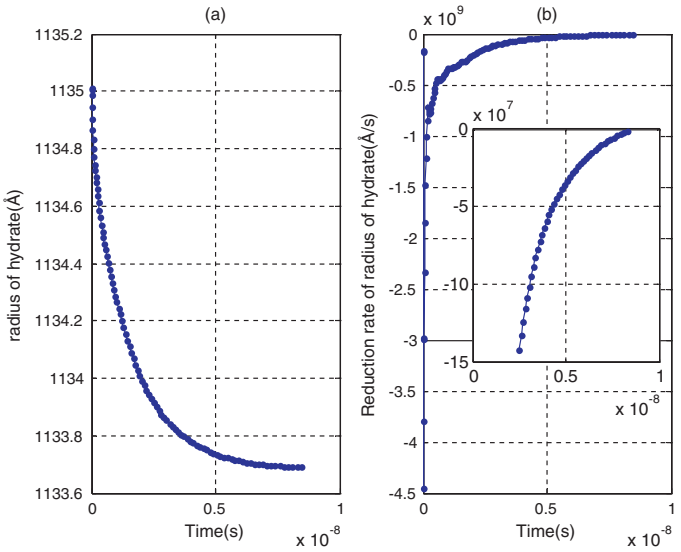

Fig. 16. Development of the hydrate core as function of time in the large simulation system (a): radius as function of time and (b) rate of radius reduction as function of time.

of thermodynamic properties. This can be accomplished through combinations of Quantum mechanics and Molecular dynamics simulations as discussed elsewhere (Kvamme et al., 2012b; Cuong et al., 2012b,c,d; Soave, 1972). Adsorbed structures of water on mineral surfaces, facing outside liquid water, typically cover 3–4 water layer. Therefore, even a simple extrapolation of adsorbed chemical potentials toward liquid water chemical potentials across a thickness in the order of 1.2 nm would at least be an approximate way of handling this. Of course, similar for adsorbed hydrate former molecules. The heat transport term is very over simplified, but over simplified in a similar way as many experimental groups interpret corresponding data. This was just applied temporarily in order to illustrate the qualitative features of possible impact of the coupled heat transport and phase transition dynamics. More rigorous results will be incorporated in future work along these lines.

Similarly, the mixing rules for heat conductivity. The theory can also be used for studying other hydrate production methods. Pressure reduction is fairly straightforward since pressure in the system can be reduced to any level. An additional heat transport term can be added directly to the heat transport for these directions relevant so as to imitate heat transport from the surroundings. Similar methods for studies of thermal stimulation method can be applied. Adding chemicals can also be included directly into the thermodynamic properties, either as changes in water properties or as added new components to the system. In view of possible extensions explained above, and given that hydrodynamics is already included, pore scale modeling of permeability and other reservoir flow properties are within reach.

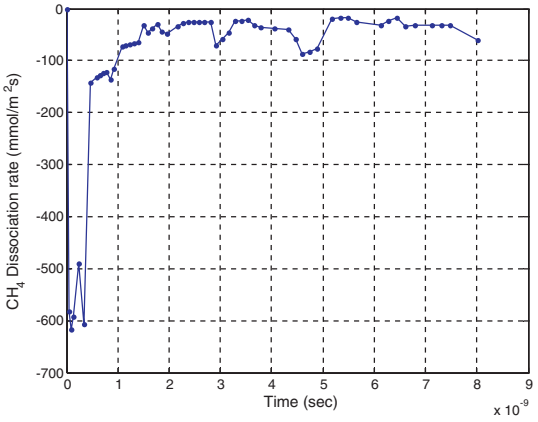

Fig. 17. Estimated methane release rate in the large system as function of time.

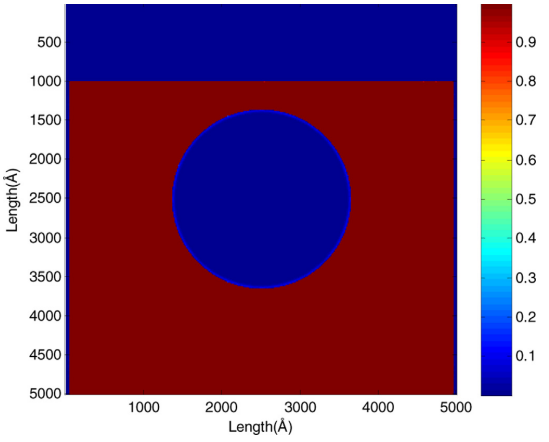

Fig. 18. Average CO_2 mole fraction in entire system after 8.4 ns as function of location in the large simulation system.

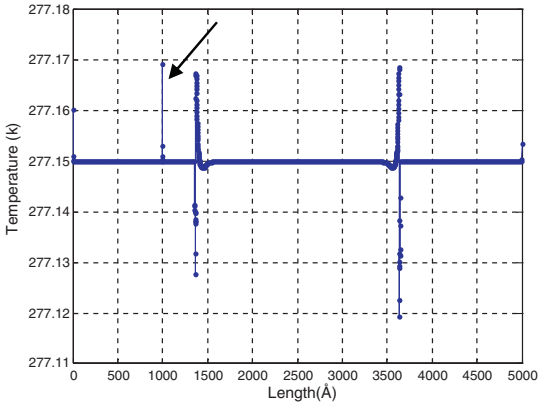

Fig. 19. Average temperature (K) as function of location in the simulation system after 8.4 ns for the large simulation system.

5. Conclusion

We have proposed Phase Field Theory models for studies of complex hydrate phase transitions. These include competing phase transitions of hydrate formation and hydrate dissociation that is relevant for non-equilibrium hydrate systems encountered in nature. We also presented a first order expansion of non-thermodynamics for hydrate outside of equilibrium. This, unlike earlier simplified approximations, makes rigorous extensions to include fillings of carbon dioxide and methane in all cavities of structure I hydrate. The expansion will also be valid for other hydrate structures, with appropriate modifications of structure specific characteristics. All thermodynamic properties are calculated based on absolute thermodynamics (ideal gas reference state) for consistency across all possible phase boundaries. There are no available nanoscales experiments that can be used to verify theoretical estimates so different model systems have been applied for illustrations.

Three sizes of square 2D model systems have been used to illustrate the theory, 150 Å × 150 Å, 500 Å × 500 Å and 5000 Å × 5000 Å. These systems all consist of an initial spherical core of CH_4 hydrate surrounded by a thin film of liquid water and CO_2 outside, with an additional water along two walls and a CH_4 plume at the top. As expected, the initial process is fast in all three systems since it is dominated by rapid formation of new CO_2 hydrate and subsequent dissociation of CH_4 hydrate from released heat. The exchange process from CH_4 hydrate over to mixed CO_2/CH_4 hydrate is faster in the smaller systems than the larger one. This is in accordance with the results reported by Svandal et al. (Conti, 2004), which also showed similar diffusion rate dependency of the curvature of the initial hydrate core. But the smaller systems lost relatively more portion of the initial hydrate core before reaching the maximum mix hydrate core. The smallest system reached almost full exchange in 5.6 ns. After that the mixed hydrate could not sustain its stability and dissociated completely due to undersaturated surrounding water. The larger systems, on other hand, behaved differently. The slightly larger system (500 Å × 500 Å) reached exchange after 64 ns with substantially less loss of hydrate core compared to initial size hydrate core. After this time, the reduction rate of the hydrate core was very low, due to the solid-state exchange dominated mechanism at this stage. The resulting mixed hydrate that was formed is significantly more stable than the smallest system. The largest system behaves even more promising and the reduction rate very quickly approaches small rates characteristic for solid rate transport mechanism.

Strategies for inclusion of mineral surfaces are outlined and will be investigated in future studies for theoretical investigation of the impact of mineral surfaces of hydrate phase transitions. Pore scale modeling of different reservoir transport parameters is other possible future directions outlined. Pore scale modeling of permeability is one specific example of future directions outlined. In a more general sense, the theory will be useful as basis for development of more simplified kinetic models for industrial applications and hydrates in porous media. This is because the theory provides very detailed information on the possible impacts of the different kinetic contributions to the overall kinetic rates of hydrate formation and dissociation in non equilibrium systems.

Acknowledgements

We acknowledge the grant and support from the Research Council of Norway through the following projects: SSC-Ramore, “Subsurface storage of CO_2 – Risk assessment, monitoring and remediation”, Research Council of Norway, project number: 178008/I30, FME-SUCCESS, Research Council of Norway, project number: 804831, PETROMAKS, “CO_2 injection for extra production”, Research Council of Norway, project number: 801445.

Appendix 1. Equilibrium thermodynamics

The theory for equilibrium thermodynamics is based on revised adsorption theory due to Kvamme and Tanaka (1995) and van der Waals and Platteeuw (1959). The expression for chemical potential of water in hydrate is:

$$\mu_w^H = \mu_w^{O,H} - \sum_i RT\nu_i \ln\left(1 + \sum_f h_{ij}\right) \tag{A.1}$$

This equation is derived from the macro canonical ensemble under the constraints of constant amount of water, corresponding to an empty lattice of the actual structure. Details of the derivation are given elsewhere (Kvamme and Tanaka, 1995) and will not be repeated here. $\mu_w^{O,H}$ is the chemical potential for water in an empty hydrate structure and h_{ij} is the cavity partition function of component j in cavity type i. The first sum is over cavity types, and the second sum is over components j going into cavity type i. Here ν_i is the number of type i cavities per water molecule. For hydrate structure I, there are 3 large cavities and 1 small per 23 water molecules, $\nu_l = 3/23$ and $\nu_s = 1/23$. In the classical use of Eq. (1), the cavity partition functions are integrated under the assumption that the water molecules are fixed and normally also neglecting interactions with surrounding guest molecules. This may be adequate for small guest molecules with weak interactions. On the other hand, molecules like CO_2 are large enough to have a significant impact on the librational modes of the water molecules in the lattice. An alternative approach (Kvamme and Tanaka, 1995) is to consider the guest movements from the minimum energy position in the cavity as a spring, and evaluate the free energy changes through samplings of frequencies for different displacements in the cavity. A molecule like methane will, as expected, not have significant impact on the water movements (Kvamme and Tanaka, 1995). CO_2 on the other hand, will change the water chemical potential by roughly 1 kJ/mol at 0 °C when compared to the assumption of undisturbed fixed water molecules. The cavity partition function may thus be written as:

$$h_{ij} = e^{\beta(\mu_j^H - \Delta g_{ji}^{inc})} \tag{A.2}$$

Where Δg_{ji}^{inc} now is the effect of the inclusion of the guest molecule j in the cavity of type i, which as indicated above is the minimum interaction energy plus the free energy of the oscillatory movements from the minimum position. At hydrate equilibrium, the chemical potential is equal to that of the chemical potential of the guest molecule in its original phase (chemical potential of dissolved CO_2 or CH_4 for the case of hydrate formation from aqueous solution). Eq. (A.2) can be inverted to give the chemical potential for the guest as a function of the cavity partition function:

$$\mu_j^H = \Delta g_{ji}^{inc} + RT \ \ln h_{ij} \tag{A.3}$$

Eq. (A.3) is basically derived from an equilibrium consideration but may be used as an approximation for bridging chemical potential to composition dependency. The relation between the filling fraction, the mole fractions and the cavity partition function is:

$$\theta_{ji} = \frac{x_{ji}}{v_i(1-x_T)} = \frac{h_{ji}}{1+\sum_j h_{ji}} \tag{A.4}$$

Here x_T is the total mole fraction of all the guests. It is assumed that CO_2 can only fit into the larger cavities, and unless some other guest molecule is present, the small cavities will then all be empty. For a system with only one component occupying the large cavities, the chemical potential of the guest molecule would be reduced to:

$$\mu_w^H = \Delta g_{ji}^{inc} + RT \ \ln\left(\frac{\theta_{ji}}{1-\theta_{ji}}\right) \tag{A.5}$$

For methane, which can occupy both large and small cavities, a more cumbersome approach is needed. Initially assuming that chemical potential of methane in the two cavities is the same. This gives a proportional relation between the two partition functions independent on composition:

$$\frac{h_{ml}}{h_{ms}} = e^{((\Delta g_{ms}^{inc} - \Delta g_{ml}^{inc})/(RT))} = A \tag{A.6}$$

The mole fraction of methane, x_m, is the sum of the mole fraction in each cavity, i.e., large x_{ml} and small x_{ms}. The mole fractions are expressed in terms of the cavity partition function from Eq. (4):

$$x_{ms} + x_{ml} = x_m \tag{A.7}$$

$$\frac{h_{ms}}{1+h_{ms}}v_s + \frac{h_{ml}}{1+h_{ml}+h_{cl}}v_l = \frac{x_m}{1+x_T} = B \tag{A.8}$$

Here h_{ms}, h_{ml} and h_{cl} are the cavity partition functions of methane in small cavities, methane in large cavities and carbon dioxide in large cavities respectively. The denominator in the second term can be expressed in terms of the mole fraction and one of the partition functions from Eqs. (A.4) and (A.7):

$$1 + h_{ml} + h_{ms} \tag{A.9}$$

The partition function for CO_2 using Eq. (A.4) needs to be calculated as:

$$\frac{x_{cl}}{v_l(1-x_T)} = \frac{h_{cl}}{1+h_{ml}+h_{cl}}$$

Rearranging the above equation in term of h_{cl} gives:

$$h_{cl} = \frac{x_{cl}(1+h_{ml})}{v_l(1-x_T)-x_{cl}}$$

Inserting the value of h_{cl} in Eq. (A.9) which gives constant C:

$$1 + h_{ml} + h_{cl} = (1+h_{ml})\left(1 + \frac{x_{cl}}{v_l(1-x_T)-x_{cl}}\right) \tag{A.10}$$

$$C = 1 + \frac{x_{cl}}{v_l(1-x_T)-x_{cl}} \tag{A.11}$$

Using Eqs. (A.6), (A.10) and (A.11) results:

$$1 + h_{ml} + h_{cl} = (1+Ah_{ms})C \tag{A.12}$$

Eq. (A.8) can be written in terms of single partition function:

$$\frac{h_{ms}}{1+h_{ms}}v_s + \frac{Ah_{ms}}{(1+Ah_{ms})C}v_l = B \tag{A.13}$$

Now the Eq. (A.13) can be reduced to get second order equation:

$$(v_sCA + v_lA - BCA)h_{ms}^2 + (v_sC + v_lA - BCA - BC)h_{ms} - BC = 0 \tag{A.14}$$

Eq. (A.14) can be written in the form of second constant:

$$\begin{aligned} &a_1(h_{ms})^2 + a_2(h_{ms}) + a_3 = 0 \\ &a_1 = A(v_l + v_sC - BC) \\ &a_2 = v_sC + Av_l - BC(1+A) \\ &a_3 = -BC \end{aligned} \tag{A.15}$$

A.1. Fluid thermodynamic

The free energy of the fluid phase is assumed to have:

$$G_L^{Fluid} = \sum_{r=c,m,w} x_r \mu_r^{Fluid} \tag{A.16}$$

where μ_r^{Fluid} is the chemical potential of the fluid phase. The lower concentration of water in the fluid phase and its corresponding minor importance for the thermodynamics results in the following form of water chemical potential with some approximation of fugacity and activity coefficient:

$$\mu_w^{Fluid} = \mu_w^{ideal\ gas}(T,P) + RT\ \ln(y_w) \tag{A.17}$$

Where $\mu_w^{ideal\,gas}(T,P)$ chemical potential of water in ideal gas and y_w is the mole fraction of water in the fluid phase and can be calculated as:

$$y_w = \frac{x_w\gamma_w(T,P,\vec{x})P_w^{sat}(T)}{\varphi_w(T,P,\vec{y})} \tag{A.18}$$

The vapor pressure can be calculated using many available correlations but one of the simplest is given in Kvamme et al. (2013b) as a fit to the simple equation:

$$\ln(P) = V_A - \frac{V_B}{T+V_C} \tag{A.19}$$

The temperature of the system is obviously available and $V_A = 52.703$, $V_B = -3146.64$ and $V_C = 5.572$. Further, the fugacity and the activity coefficient are approximated to unity merely because of the very low water content in fluid phase and its corresponding minor importance for the thermodynamics of the system. Hydrate formation directly from water in gas is not considered as significant within the systems discussed in this work. A separate study reveals that hydrate formation from water dissolved in carbon dioxide may be feasible from a thermodynamic point of view (Kvamme et al., 2013b) but more questionable in terms of mass transport in competition with other hydrate phase transitions. The water phase is close to unity in water mole fraction. Raoult's law is therefore accurate enough for our purpose. The chemical potential for the mixed fluid states considered as:

$$\mu_i^{Fluid} = \mu_i^{id.gas,pure} + RT\ \ln(y_i) + RT\ \ln\varphi_i(T,P,\rightharpoonup y) \tag{A.20}$$

Where i represents CH_4 or CO_2. The fugacity coefficients of component i in the mixture is calculated using the classical SRK equation

of state (EOS) (Soave, 1972),

$$\ln \varphi_i = (BB)_i(Z-1) - \ln(Z-B) - \frac{A}{B}((AA)_i - (BB)_i)\ln\left[1+\frac{B}{Z}\right] \quad (A.21)$$

Where Z is the compressibility factor of the phase and is calculated using the following cubic SRK EOS:

$$Z^3 - Z^2 + (A - B - B^2)Z - AB = 0 \quad (A.22)$$

Where,

$$A = \frac{\alpha a P}{R^2T^2}$$

$$B = \frac{bP}{RT}$$

$$a = 0.427480\frac{R^2T_c^2}{P_c}$$

$$b = 0.086640\frac{RT_c}{P_c}$$

$$\alpha = [1 + (0.48508 + 1.55171\omega - 0.15613\omega^2)(1-\sqrt{T_r})]^2$$

Where ω is the acentric factor of components. For mixture, the mixing rule with modification proposed by Soave (1972) is used using the following formulations:

$$(\alpha a)_m = \sum\sum y_i y_j (\alpha a)_{ij}; (\alpha a)_{ij} = \sqrt{(\alpha a)_i(\alpha a)_j}(1-k_{ij}) \quad (A.23)$$

Where k_{ij} is the binary interaction parameter. Coutinho et al. (1994) has proposed number of values for k_{ij} for CO_2/CH_4 system. Here we selected an average value $k_{ij} = k_{ji} = 0.098$ for unlike pairs of molecules and it is zero for alike pairs of molecules.

$$b_m = \sum_i y_i b_i \quad (A.24)$$

$(AA)_i$ and $(BB)_i$ in Eq. (A.21) are calculated as:

$$(AA)_i = \frac{2}{(a\alpha)_m}\left[\sum_j (a\alpha)_{ij}\right] \quad (A.25)$$

$$(BB)_i = \frac{b_i}{b_m} \quad (A.26)$$

A.2. Aqueous thermodynamic

The free energy of the aqueous phase can be written as:

$$G_L^{aqueous} = \sum_{r=c,m,w} x_r \mu_r^{aqueous} \quad (A.27)$$

The chemical potential $\mu_r^{aqueous}$ for components c (carbon dioxide) and m (methane) dissolved into the aqueous phase is described by nonsymmetric excess thermodynamics:

$$\mu_i = \mu_i^{\infty}(T) + RT\ln(x_i\gamma_i^{\infty}) + v_i^{\infty}(P - P_o) \quad (A.28)$$

μ_i^{∞} is the chemical potential of component i in water at infinite dilution, γ_i^{∞} is the activity coefficient of component i in the aqueous solution and v_i^{∞} is the partial molar volume of the component i at infinite dilution. The chemical potentials at infinite dilution as a function of temperature are found by assuming equilibrium between fluid and aqueous phases $\mu_i^{Fluid} = \mu_i^{aqueous}$. This is done at varying low pressures where the solubility is very low and the gas phase is close to ideal gas using experimental values for the solubility and extrapolating the chemical potential down to a corresponding value for zero concentration. The Henry's constants k_H are calculated for CH_4 and CO_2 using the expression proposed by Sander (2009).

Table 1
Values of parameters.

Constants	CO_2	CH_4
$k_H^{\ominus}$ (M/atm)	0.036	0.0013
$-(d\ln(k\_H))/d(1/T)$ (K)	2200	1800

$$k_H(T) = k_H^{\ominus} e^{\{[(-\Delta_{soln}H)/R][(1/T)-(1/T^{\ominus})]\}} \quad (A.29)$$

Where $T^{\ominus}$ is the reference temperature, which is equal to 298.15 K. $\Delta_{soln}H$ is the enthalpy of dissolution and it is represented by the Clausius–Clapeyron equation (Li, 1956) as:

$$\frac{d\ \ln k_H}{d(1/T)} = \frac{-\Delta_{soln}H}{R} \quad (A.30)$$

The values of $-(d\ln(k\_H))/d(1/T)$ and $k_H^{\ominus}$ are given by Zheng et al. (1997) and by Kavanaugh and Trussell (1980) for CO_2 and CH_4 respectively which is shown in Table 1.

The activity coefficient at infinite dilution γ_i^{∞} is calculated as:

$$\gamma_i^{\infty} = \frac{f_i^{\infty}}{k_H(T)} \quad (A.31)$$

Where,

$$f_i^{\infty} = e^{(-\beta\mu_i^{\infty})}$$

Where f_i^{∞} is the fugacity of component i, while μ_i^{∞} is calculated from Svandal et al. (2006b). The activity coefficient can be regressed by using the model for equilibrium to fit experimental solubility data. The chemical potential of water can be written as:

$$\mu_w = \mu_w^{pureliquid}(T) + RT\ln(1-x)\gamma_w + v_w(P - P_o) \quad (A.32)$$

where $\mu_w^{pureliquid}$ is pure water chemical potential and v_w is the molar volume of water. The strategy for calculating activity coefficient is given by Svandal et al. (2006b).

Appendix 2. Thermodynamics outside of equilibrium

The Phase Field Theory (PFT) model presented in this work has dynamically varying local densities, temperatures and concentrations. The constraints on the system is the pressure. Unlike our earlier PFT models (Kvamme et al., 2007, 2012a) which were at constant temperature, the calculations of non-equilibrium thermodynamic (Kvamme et al., 2012a) properties are implemented implicit calculations in this version since the free energies of all co-existing phases change dynamically with local conditions and possibly competing phase transitions. We use examples based on conversion of CH_4 hydrate into CO_2 hydrate or mixed CO_2–CH_4 hydrate, which have two primary mechanisms. The first one is that CO_2 creates a new hydrate from free water in the porous media and the released heat dissociate the in situ CH_4 hydrate. This mechanism is primarily dominated by mass transport rates through fluid phases. A second mechanism is the direct conversion of the in situ CH_4 hydrate with the CO_2, which is a much slower solid-state phase transition. The first mechanism implies heat release as well as heat consumption and complex coupled behavior of mass and heat transport around the hydrate core is expected. Also note that fluid thermodynamics and aqueous thermodynamics outside of equilibrium is trivial in contrast to hydrate, for which the thermodynamic model is derived from statistical mechanics based on equilibrium between hydrate and fluid phases. For this reason, we expand the thermodynamic properties of hydrate by a first order Taylor-expansion. This is considered accurate enough since the rate limiting kinetic contributions are expected to be

in the mass transport according to earlier studies (Svandal, 2006; Kvamme et al., 2009; Kavanaugh and Trussell, 1980). First of all, note that the mass is conserved inside the Phase Field Theory. The thermodynamics have to be developed in terms of gradients in all directions (P, T, mole-fractions) without conservation of mole-fractions in order to obtain the appropriate relative local driving forces and also avoid double conservation constraints in the free energy minimalization. In this paper we limit ourselves to three components, where CH_4 is the additional component to CO_2 and water. This can be directly extended to more components though straightforward extensions of the equilibrium and supersaturation thermodynamics, and appropriate adjustment of the PFT. As the thermodynamic changes are outlined here the primary additional change in the PFT model is in the free energy of the thermal fluctuations (Svandal, 2006; Conti, 1997, 2000) as function of concentrations, which is mathematically trivial. Supersaturations of fluid phases are straightforward and not different from what we have published before (Svandal, 2006; Kvamme, 2003) and in the first part of this paper.

The Gibbs free energy of the hydrate phase is written as a sum of the chemical potentials of each component (Svandal, 2006; Kvamme, 2003)

$$G_H = \sum_r x_r \mu_r^H \tag{A.33}$$

where μ_r^H and x_r is chemical potential and mole fraction of component r respectively. G_H is the free energy of hydrate. In the earlier work due to Svandal et al. (2006a) a simple interpolation in mole-fractions was used between pure CH_4 hydrate and pure CO_2 hydrate, which was considered as sufficient to theoretically illustrate the exchange concept under Phase Field Theory. This will of course not reproduce the absolute minimum in free energy for a mixed hydrate in which CH_4 occupies portions of the small cavities and increases stability over pure CO_2 hydrate. The expression for free energy gradients with respect to mole fraction, pressure and temperature is:

$$G_H^{EXP} = G^{EQ} + \sum_r \left.\frac{\partial G_H}{\partial x_r}\right|_{P,V,T,x_{i\neq r}} (x_r^{act} - x_r^{EQ}) + \left.\frac{\partial G_H}{\partial P}\right|_{T,V,\vec{x}} \times (P^{act} - P^{EQ}) + \left.\frac{\partial G_H}{\partial T}\right|_{P,V,\vec{x}} (T^{act} - T^{EQ}) \tag{A.34}$$

Here G_H^{EXP} is the free energy of hydrate away from equilibrium and the superscripts EQ and act represent the corresponding states at equilibrium and actual states respectively. We are now seeking gradients in all directions, independent of mole-fraction conservation (sum of mole-fractions are conserved inside PFT). So in terms of supersaturation in mole-fractions these have to be evaluated as orthonormal gradient effects. In simple terms that means:

$$\frac{\partial x_z}{\partial x_r} = \begin{cases} 0, z \neq r \\ 1, z = r \end{cases} \tag{A.35}$$

Where z and r both represent any of the components of the hydrate: water, methane, and carbon dioxide. This is just means that the mole fractions are all independent. Using Eq. (A.33) we simply take the derivative with respect to one of the mole fractions ($r = m$, c or w) and the mole fraction derivatives are obtained using Eq. (A.35) for mole fraction independence, resulting in:

$$\frac{\partial G_H}{\partial x_r} = x_c \frac{\partial \mu_c^H}{\partial x_r} + x_m \frac{\partial \mu_m^H}{\partial x_r} + x_w \frac{\partial \mu_w^H}{\partial x_r} + \mu_r \frac{\partial x_r}{\partial x_r} \tag{A.36}$$

It was previously shown (Svandal, 2006) that the chemical potential of a guest molecule can be approximated to a high degree of accuracy and in gradient terms:

$$\mu_k^H = A \ln(x_k) + B, \ \frac{\partial \mu_k^H}{\partial x_r} = \{0, r \neq k\}. \tag{A.37}$$

Where k and r both represents any of the components of the hydrate (CO_2, CH_4 and water). For the gradient due to a guest molecule, these simplifications lead to:

$$\frac{\partial G_H}{\partial x_k} = x_k \frac{\partial \mu_k^H}{\partial x_k} + \mu_k^H \tag{A.38}$$

For water, the form has two more terms:

$$\frac{\partial G_H}{\partial x_w} = \sum_r x_r \frac{\partial \mu_r^H}{\partial x_w} + \mu_w^H \tag{A.39}$$

The chemical potential of a guest in the hydrate μ_k^H can be written as (Kvamme and Tanaka, 1995):

$$\mu_k^H = \Delta g_{kj}^{inc} + RT \ \ln(h_{kj}) \tag{A.40}$$

Where Δg_{kj}^{inc} is the Gibbs free energy of inclusion of guest molecule k in cavity j, h_{kj} the cavity partition function of component k in cavity j, the universal gas constant is R and T is temperature. The derivative of Eq. (A.40) with respect to an arbitrary molecule r is:

$$\frac{\partial \mu_k^H}{\partial x_r^H} = \frac{\partial \Delta g_{kj}^{inc}}{\partial x_r^H} + \frac{\partial (RT \ln(h_{kj}))}{\partial x_r^H} \tag{A.41}$$

The first term of Eq. (A.41), the stabilization energy is either evaluated as the Langmuir constant or using harmonic oscillator approach (Kvamme and Tanaka, 1995). In either case, it is assumed to be approximately of temperature and pressure. Omitting the first term of (A.41) and approximating impacts of guest–guest interactions to be zero we arrive at:

$$\frac{\partial \mu_k^H}{\partial x_r^H} = \frac{RT}{h_{kj}} \frac{\partial h_{kj}}{\partial x_r^H} \tag{A.42}$$

The validity of omitting guest–guest interactions may be questionable for some systems even though it is omitted in most hydrate equilibrium codes or empirically corrected for. Extensions for corrections to this can be implemented at a later stage.

The chemical potential of water:

$$\mu_w^H(T, P, \vec{\theta}) = \mu_w^{0,H}(T, P_0) - \sum_j RT \upsilon_j \ln\left[1 + \sum_k h_{kj}\right] \tag{A.43}$$

Where $\mu_w^{0,H}$ is the chemical potential of water in an empty hydrate structure, the first sum is taken over both small and a large cavity, the second one is over the components k in the cavity j. Here υ_j is the number of type-j cavities per water molecule. Hydrate structure I contains 3 large cavities and 1 small cavity per 23 water molecules, $\upsilon_l = 3/23$ and $\upsilon_s = 1/23$. The paper by Kvamme and Tanaka (1995) provides the empty hydrate chemical potential as polynomials in inverse temperature, the Gibbs free energies of inclusion, and chemical potential of pure water, $\mu_w^{pure}(T)$. The derivative for the above equation with respect to an arbitrary molecule r results in:

$$\frac{\partial \mu_w^H}{\partial x_r} = -RT \sum_j \upsilon_j \left[\frac{\sum_k \frac{\partial h_{kj}}{\partial x_r}}{1 + \sum_k h_{kj}}\right] \tag{A.44}$$

From Eqs. (A.42) and (A.44), the derivative of the partition function can be evaluated from the equation that relates the filling fraction to the partition function:

$$h_{kj} = \frac{\theta_{kj}}{1 - \sum_i \theta_{ij}} \tag{A.45}$$

Where θ_{kj} is the filling fraction of the components k in the cavity j. But it is easiest to recast everything in terms of mole fraction because of the basic assumption of mole fraction independence:

$$\theta_{kj} = \frac{x_{kj}}{\upsilon_j x_w} \tag{A.46}$$

Since mass conservation is not used, the usual form of $1 - x_T$ is not considered. This is substituted into Eq. (A.45) and we get:

$$h_{kj} = \frac{x_{kj}}{\upsilon_j x_w - \sum_i x_{ij}} \tag{A.47}$$

Now we can take the derivative with respect to an arbitrary component r and using Eq. (A.47) we get:

$$\frac{\partial h_{kj}}{\partial x_r} = \frac{h_{kj}}{x_{kj}} \frac{\partial x_{kj}}{\partial x_r} - \frac{h_{kj}^2}{x_{kj}} \left[\upsilon_j \frac{\partial x_w}{\partial x_r} - \sum_i \frac{\partial x_{ij}}{\partial x_r} \right] \tag{A.48}$$

The first thing that must be dealt with the cavity mole fractions as a function of total mole fraction of a component:

$$x_k = \sum_j x_{kj} \tag{A.49}$$

Since the derivative of one mole fraction with respect to another is independent, the mole fraction in the cavity is also independent:

$$\left(\frac{\partial x_{kj}}{\partial x_r} \right) = \begin{cases} 0, k \neq r \text{ or } r = w \\ 1, k = r \end{cases} \tag{A.50}$$

If $r = w$, then the derivative has to be zero because the mole fraction of the guest are independent of the mole fraction of water. Now Eq. (A.48) is simplified by using Eqs. (A.49) and (A.50):

$$\frac{\partial h_{kj}}{\partial x_w} = -\frac{h_{kj}^2 \upsilon_j}{x_{kj}} \tag{A.51}$$

$$\frac{\partial h_{kj}}{\partial x_p} = \frac{h_{kj}}{x_{kj}} \frac{\partial x_{kj}}{\partial x_p} + \frac{h_{kj}^2}{x_{kj}} \frac{\partial x_{pj}}{\partial x_p} \tag{A.52}$$

Where p is an arbitrary guest molecule, k is also a guest molecule. These can be the same or different. If k and p are the same molecule, this gradient still exist and the "cross terms" are still able to be found even if there is independency in the mole fractions. dx_{kj}/dx_k is calculated by starting with the Eq. (A.49) which is the basic definition of the mole fraction of the cavities and how they relate to the total mole fraction of the component. The total methane mole fraction x_m, is the sum of the mole fraction in the large cavities x_{ml}, and the mole fraction in the small cavities x_{ms}:

$$x_m = x_{ml} + x_{ms} \tag{A.53}$$

From discussions it is assumed that there is a constant ratio between the partition functions and between different cavities of the same component. This is defined as A:

$$A \equiv \frac{h_{ml}}{h_{ms}} \tag{A.54}$$

The partition function can be written in terms of the filling fraction as shown in Eq. (A.45). Using Eqs. (A.45), (A.46), (A.54) and assuming that the filling fraction of CO_2 in small cavities is zero we get:

$$A \equiv \frac{x_{ml}/(\upsilon_l x_w)}{x_{ms}/(\upsilon_s x_w)} \left[\frac{1 - (x_{ms}/(\upsilon_s x_w))}{1 - (x_{ml}/(\upsilon_l x_w)) - (x_{cl}/(\upsilon_l x_w))} \right] \tag{A.55}$$

This simplifies into:

$$x_{ml}[-\upsilon_s x_w] + x_{ms}[A\upsilon_l x_w - A x_{cl}] + x_{ms} x_{ml}[1 - A] = 0 \tag{A.56}$$

Taking derivative of above equation with respect to total methane mole fraction:

$$[x_{ms}(1 - A) - \upsilon_s x_w] \frac{\partial x_{ml}}{\partial x_m} + [A\upsilon_l x_w - A x_{cl} + x_{ml}(1 - A)] \frac{\partial x_{ms}}{\partial x_m} = 0 \tag{A.57}$$

Substitutions were made to simplify the above equation and get it into a simpler form:

$$\begin{aligned} X &= x_{ms}(1 - A) - \upsilon_s x_w \\ Y &= A\upsilon_l x_w - A x_{cl} + x_{ml}(1 - A) \\ X \frac{\partial x_{ml}}{\partial x_m} &+ Y \frac{\partial x_{ms}}{\partial x_m} = 0 \end{aligned} \tag{A.58}$$

Taking the derivative of Eq. (A.53) with respect to the total mole fraction of methane and simplification results in:

$$\begin{aligned} \frac{\partial x_{ml}}{\partial x_m} + \frac{\partial x_{ms}}{\partial x_m} &= \frac{\partial x_m}{\partial x_m} = 1 \\ \frac{\partial x_{ml}}{\partial x_m} &= -\frac{Y}{X - Y} \\ \frac{\partial x_{ms}}{\partial x_m} &= \frac{X}{X - Y} \end{aligned} \tag{A.59}$$

Substituting the values of X and Y gives the final answer:

$$\begin{aligned} \frac{\partial x_{ml}}{\partial x_m} &= -\frac{A\upsilon_l x_w - A x_{cl} + x_{ml}(1 - A)}{x_{ms}(1 - A) - \upsilon_s x_w - A\upsilon_l x_w - A x_{cl} + x_{ml}(1 - A)} \\ \frac{\partial x_{ms}}{\partial x_m} &= \frac{x_{ms}(1 - A) - \upsilon_s x_w}{x_{ms}(1 - A) - \upsilon_s x_w - A\upsilon_l x_w - A x_{cl} + x_{ml}(1 - A)} \end{aligned} \tag{A.60}$$

$\partial G_H/\partial P$ is calculated by taking derivative of Eq. (A.33) with respect to pressure.

$$\frac{\partial G_H}{\partial P} = x_c \frac{\partial \mu_c^H}{\partial P} + x_m \frac{\partial \mu_m^H}{\partial P} + x_w \frac{\partial \mu_w^H}{\partial P} + \mu_c \frac{\partial x_c}{\partial P} + \mu_m \frac{\partial x_m}{\partial P} + \mu_w \frac{\partial x_w}{\partial P} \tag{A.61}$$

Where the chemical potential gradients with respect to pressure can be given by:

$$\frac{\partial \mu_r^H}{\partial P} = \bar{V}_r \tag{A.62}$$

Thus Eq. (A.61) can be written as:

$$\frac{\partial G_H}{\partial P} = x_c \bar{V}_c + x_m \bar{V}_m + x_w \bar{V}_w + \mu_c^H \frac{\partial x_c}{\partial P} + \mu_m^H \frac{\partial x_m}{\partial P} + \mu_w^H \frac{\partial x_w}{\partial P} \tag{A.63}$$

The sum of the molar volumes ($\bar{V}_c$, $\bar{V}_m$, $\bar{V}_w$) is in fact the total clathrate molar volume:

$$\bar{V}^{clath} = x_c \cdot \bar{V}_c + x_m \cdot \bar{V}_m + x_w \cdot \bar{V}_w \tag{A.64}$$

Using the above value of $\bar{V}^{clath}$ simplifies the Eq. (A.63) to:

$$\frac{\partial G_H}{\partial P} = \bar{V}^{clath} + \mu_c^H \frac{\partial x_c}{\partial P} + \mu_m^H \frac{\partial x_m}{\partial P} + \mu_w^H \frac{\partial x_w}{\partial P} \tag{A.65}$$

The mole fraction derivatives can be calculated from equation of state but there is no change under this derivative so Eq. (A.65) can be rewritten as:

$$\left[\frac{\partial G_H}{\partial P} \right]_{T,V,\bar{x}} = \bar{V}^{clath} \tag{A.66}$$

The free energy gradient with respect to temperature comes from the same fundamental relationship as used for the chemical potential gradient:

$$-\frac{\partial}{\partial T}\left[\frac{G}{T}\right]_{P,\vec{x}} = \frac{\bar{H}}{T^2} \tag{A.67}$$

References

Conti, M., 1997. Phys. Rev. A 55 (1), 765.
Conti, M., 2000. Phys. Rev. E 61 (1), 642.
Conti, M., 2001. Phys. Rev. 64, 051601.
Conti, M., 2004. Phys. Rev. 69, 022601.
Conti, M., Fermani, M., 2003. Phys. Rev. 67, 026117.
Coutinho, J.A.P., Kontogeorgis, G.M., Stenby, E.H., 1994. Fluid Phase Equilib. 102, 31.
Cuong, P.V., Kvamme, B., Kuznetsova, T., Jensen, B., 2012a. Int. J. Energy Environ. 6, 301.
Cuong, P.V., Kvamme, B., Kuznetsova, T., Jensen, B., 2012b. Mol. Phys. 110, 1097.
Cuong, P.V., Kvamme, B., Kuznetsova, T., Jensen, B., 2012c. Mol. Phys. 110 (11–12), 1097.
Cuong, P.V., Kvamme, B., Kuznetsova, T., Jensen, B., 2012d. Int. J. Energy Environ. 6 (3), 301.
Gránásy, L., Börzsönyi, T., Pusztai, T., 2002. Phys. Rev. Lett. 88 (20), 206105.
Gránásy, L., Pusztai, T., 2002. J. Chem. Phys. 117, 10121.
Gránásy, L., Pusztai, T., Börzsönyi, T., Warren, J.A., Kvamme, B., James, P.F., 2004. Phys. Chem. Glass. 45, 107.
Gránásy, L., Pusztai, T., Jurek, Z., Conti, M., Kvamme, B., 2003. J. Chem. Phys. 119, 10376.
Henriet, J.P., Mienert, J., 1998. Geological Society of London (Special Publication No. 137).
Kavanaugh, M.C., Trussell, R.R., 1980. J. Am. Water Works Assoc. 72, 684.
Koh, C., Sloan, E.D., 2008. Chem. Indust.
Kuznetsova, T., Kvamme, B., Morrissey, K., 2012. An alternative for carbon dioxide emission mitigation: in situ methane hydrate conversion. International Conference of Computational Methods in Sciences and Engineering 1504, 772, http://dx.doi.org/10.1063/1.4771807.
Kvamme, B., 2002. Int. J. Offshore Polar Eng. 12, 256.
Kvamme, B., 2003. Int. J. Offshore Polar Eng. 13, 1.
Kvamme, B., Baig, K., Qasim, M., Bauman, J., 2013a. Int. J. Energy Environ. 7 (1), 1.
Kvamme, B., Gránásy, L., Pusztai, T., Tegze, G., Kuznetsova, T., 2004a. CO_2 hydrate formation in aqueous solutions: phase field theory of nucleation and growth. In: Proceedings from AAPG Hedberg Research Conference "Natural gas hydrates: energy resource potential and associated geologic hazards", Vancouver, September 12–16.
Kvamme, B., Graue, A., Aspenes, E., Kuznetsova, T., Gránásy, L., Tóth, G., Pusztai, T., Tegze, G., 2004b. Phys. Chem. Chem. Phys. 6, 2327.
Kvamme, B., Graue, A., Kuznetsova, T., Buanes, T., Ersland, G., 2007. Int. J. Greenh. Gas Contr. 1/2, 236.
Kvamme, B., Kuznetsova, T., 2004. Fluid Phase Equilib. 217 (2), 95.
Kvamme, B., Kuznetsova, T., Kivelæ, P.H., 2012a. Phys. Chem. Chem. Phys. (in press).
Kvamme, B., Kuznetsova, T., Kivelæ, P.H., 2012b. Phys. Chem. Chem. Phys. 14, 4410.
Kvamme, B., Kuznetsova, T., Kivelæ, P.H., Bauman, J., 2013b. Phys. Chem. Chem. Phys. 15 (6), 2063.
Kvamme, B., Svandal, A., Buanes, T., Kuznetsova, T., 2009. AAPG Memoir 89, 758.
Kvamme, B., Tanaka, H., 1995. J. Phys. Chem. 99, 7114.
Lee, H., Seo, Y., Seo, Y.T., Moudrakovski, I.L., Ripmeester, J.A., 2003. Angew. Chem. Int. Ed. 42, 5048.
Li, J.C.M., 1956. J. Chem. Phys. 25, 572.
Makogan, Y., 1997. Hydrates of hydrocarbons. Penn Well, Tulsa.
National Energy Technology Laboratory, 2013. The National Methane Hydrates R&D Program, http://www.netl.doe.gov/technologies/oil-gas/FutureSupply/MethaneHydrates/projects/DOEProjects/DOE-Project_toc.html
Qasim, M., Baig, K., Kvamme, B., Bauman, J., 2012. Int. J. Energy Environ. 6 (5), 479.
Qasim, M., Kvamme, B., Baig, K., 2011. Int. J. Geol. 5 (2), 48.
Sander, R., 2009. Surv. Geophys. 20, 1.
Shpakov, V.P., Tse, J.S., Kvamme, B., Belosludov, V.R., 1997. Chimia v interesah ustoichivogo razvitia 6, 16.
Shpakov, V.P., Tse, J.S., Kvamme, B., Belosludov, V.R., 1998. Chem. Phys. Lett. 282, 107.
Soave, G., 1972. Chem. Eng. Sci. 27, 1197.
Svandal, A., 2006. Ph.D. thesis, University of Bergen.
Svandal, A., Kuznetsova, T., Kvamme, B., 2006a. Fluid Phase Equilib. 246, 177.
Svandal, A., Kvamme, B., Gràbàsy, L., Pusztai, T., Buanes, T., Hove, J., 2006b. J. Cryst. Growth 287, 486.
Tegze, G., Gránásy, L., 2005. Mater. Sci. Eng. 413–414, 418.
Tegze, G., Gránásy, L., Kvamme, B., 2007. Phys. Chem. Chem. Phys. 9, 3104.
Tegze, G., Pusztai, T., Tóth, G., Gránásy, L., Svandal, A., Buanes, T., Kuznetsova, T., Kvamme, B., 2006. J. Chem. Phys. 124, 234710.
van der Waals, J.H., Platteeuw, J.C., 1959. Adv. Chem. Phys. 2 (1), 1.
Wheeler, A.A., Boethinger, W.J., McFadden, G.B., 1992. Phys. Rev. A 45, 7424.
Zheng, D.Q., Guo, T.M., Knapp, H., 1997. Fluid Phase Equilib. 129, 197.

Paper 7

Impact of water film thickness on kinetic rate of mixed hydrate formation during injection of CO2 into CH4 hydrate

K. Baig, B. Kvamme, T. Kuznetsova, and J. Bauman

AIChE Journal, Volume 61, Issue 11, 2015, pp. 3944–3957

VII

Impact of Water Film Thickness on Kinetic Rate of Mixed Hydrate Formation During Injection of CO_2 into CH_4 Hydrate

Khuram Baig, Bjørn Kvamme, Tatiana Kuznetsova, and Jordan Bauman
Dept. of Physics and Technology, University of Bergen, NO-5020 Bergen, Norway

DOI 10.1002/aic.14913
Published online July 14, 2015 in Wiley Online Library (wileyonlinelibrary.com)

In this work, nonequilibrium thermodynamics and phase field theory (PFT) has been applied to study the kinetics of phase transitions associated with CO_2 injection into systems containing CH_4 hydrate, free CH_4 gas, and varying amounts of liquid water. The CH_4 hydrate was converted into either pure CO_2 or mixed CO_2—CH_4 hydrate to investigate the impact of two primary mechanisms governing the relevant phase transitions: solid-state mass transport through hydrate and heat transfer away from the newly formed CO_2 hydrate. Experimentally proven dependence of kinetic conversion rate on the amount of available free pore water was investigated and successfully reproduced in our model systems. It was found that rate of conversion was directly proportional to the amount of liquid water initially surrounding the hydrate. When all of the liquid has been converted into either CO_2 or mixed CO_2—CH_4 hydrate, a much slower solid-state mass transport becomes the dominant mechanism. © 2015 American Institute of Chemical Engineers *AIChE J*, 61: 3944–3957, 2015

Keywords: natural gas hydrates, nonequilibrium thermodynamics, mixed hydrate, phase field theory

Introduction

Natural gas hydrates are ice-like crystalline compounds in which water serve as a host for different small nonpolar, or slightly polar guest molecules. Natural gas hydrates occur both onshore in permafrost regions and continental margin sediments consisting mainly of fine-grained clay minerals and organic fragments. The majority of natural gas hydrate deposits existing around the world are found in fine-grained sediments characterized by low-hydrate saturation, which can be explained by very small pore size and low permeability of clay-rich sediments that hinder mobility of both water and gas, components essential for formation of hydrate. Gas hydrates mostly occur in sand units and are largely absent from mud sequences.[1–3]

Permafrost gas hydrate occurrences have been identified in sand-rich deposits in on-shore and near-shore environments, with gas hydrate deposits in Alaska and Canada being the typical examples. Analysis of well log data[4] and pore water geochemistry[5] indicates a very level of hydrate saturation at the Mount Elbert site (about 60–75%), which can be attributed to pre-existing free gas and presence of high conductivity faults.[6]

Natural gas hydrates are dominated by biogenic sources of methane. Indeed, according to Michael et al.,[7] as much as 99% of all gas hydrate deposits may be of biogenic origin. In contrast to natural gas of thermogenic origin, biogenic methane is very pure and contains only tiny amounts of heavier hydrocarbons. In this work, we, therefore, focus on hydrates of methane and carbon dioxide and their mixtures, known to form hydrates of structure I.[8,9]

Hydrate formation from methane and water can follow a number of different pathways. The most commonly discussed route is hydrate formation on the interface between the hydrate-former phase and water.[8] Numerous experimental data are available in literature (see, for instance, Koh and Sloan[10] for a compilation), though it should be pointed that the bulk of data[10] comes from dissociation point measurements, where hydrate is kept at a controlled pressure and slowly increasing temperature.

But hydrate can also form from hydrate formers dissolved in water[11,12] and (theoretically) from water dissolved in the hydrate-former phase,[13] although more comprehensive analysis is still needed to decide whether the latter route is realistic under mass- and heat-transport limitations. Earlier theoretical studies[14–21] indicate that the critical hydrate nucleus will be about 2.5–3 nm in size, which would require around a hundred of water molecules to come together within a very dilute mixture in natural gas or carbon dioxide. Even then, the excess heat of hydrate formation will be rather difficult to dispose of, since both natural gas and carbon dioxide are thermal insulators.

Mineral surfaces[13,22,23] will serve as adsorption sites for water and hydrate formers, which can give rise to at least three different formation scenarios even in the simplest case: (1) water and hydrate former, both from adsorbed phase, form hydrate, (2) adsorbed water and hydrate fluid forms hydrate, and (3) adsorbed hydrate former and water from fluid phase forms hydrate. Considering all the possible phases relevant for hydrate formation, hydrate dissociation, and hydrate reformation (CH_4 hydrate over to CO_2 hydrate or mixed CO_2/CH_4 hydrate), it will be impossible to satisfy the Gibbs phase rule

Correspondence concerning this article should be addressed to B. Kvamme at Bjorn.Kvamme@ift.uib.no

and for the system to achieve equilibrium. But even in this case, the equality of chemical potentials at the asymptotic equilibrium limit will still provide the driving forces during hydrate formation that will affect the hydrate filling and corresponding hydrate free energy.

Since the system will be generally unable to reach equilibrium, the dynamic situation will be governed by the combined first and second laws of thermodynamics under mass- and heat-transport constraints. This indicates that a proper analysis of competing phase transitions will required some sort of free energy minimization scheme. The phase field theory (PFT)[14–21] is a theoretical method very well suited for this task. It should be mentioned that the first layers of adsorbed water might have too low chemical potential to form hydrate but few (2–4) water molecules outside will have chemical potentials suitable for hydrate formation.[22]

Injection of carbon dioxide into methane hydrate will lead to conversion of in situ methane hydrate into a mixed hydrate where carbon dioxide dominates the large cavities and methane fills a fraction of the small cavities. This rate of this conversion is governed by two main mechanisms. Formation of new carbon dioxide hydrate from residual pore water will release heat that contributes to dissociation of surrounding methane hydrate. A second mechanism is a substantially slower direct solid-state exchange.[24,25] This hydrate exchange is also feasible with injection of carbon dioxide and nitrogen mixtures, as demonstrated by the Prudhoe Bay field pilot project in the winter of Ref. 26.

In this work, we use an extended version of PFT[14–21] incorporating both hydrodynamics and heat transport, developed and discussed in detail elsewhere.[14–50] The need to include the hydrodynamic effects arises when the rate of hydrate dissociation is so high that released methane is unable to dissolve fully into the surrounding water and forms bubbles affecting phase transition kinetics. Transport of heat released by hydrate will normally be 2–3 orders of magnitude faster than mass transport in a liquid water/hydrate system.[14–21] Heat transport will, however, be slow through gas layers or gas bubbles. Implicit treatment of heat transport will, therefore, be necessary when formation of new hydrate contributes to dissociation of original methane hydrate. Extension of thermodynamic properties to regions outside of equilibrium is quite trivial for the fluid phases, with the pertinent equations provided in the next section along with the equilibrium hydrate treatment. We then proceed to extend the hydrate thermodynamics beyond the equilibrium region using Taylor expansion of the first order.

Equilibrium thermodynamics

The theory for equilibrium thermodynamics is based on revised adsorption theory by Kvamme and Tanaka[8] and van der Waals and Platteeuw.[27] The expression for chemical potential of water in hydrate is

$$\mu_w^{\mathrm{H}} = \mu_w^{\mathrm{O,H}} - \sum_i RT v_i \ln\left(1+\sum_j h_{ij}\right) \tag{1}$$

This equation is derived from the macrocanonical ensemble under the constraints of constant amount of water, corresponding to an empty lattice of the actual structure. Details of the derivation are given elsewhere (Kvamme and Tanaka[8]) and will not be repeated here. $\imath_w^{\mathrm{O,H}}$ is the chemical potential for water in an empty hydrate structure and h_{ij} is the cavity partition function of component j in cavity type i. The first sum is over cavity types, and the second sum is over components j going into cavity type i. Here v_i is the number of type i cavities per water molecule. For hydrate Structure I, there are three large cavities and one small per 23 water molecules, $v_{\mathrm{l}} = 3/23$ and $v_{\mathrm{s}} = 1/23$. In the classical use of Eq. 1, the cavity partition functions are integrated under the assumption that the water molecules are fixed and normally also neglecting interactions with surrounding guest molecules. This may be adequate for small guest molecules with weak interactions. Conversely, molecules like CO_2 are large enough to have a significant impact on the librational modes of the water molecules in the lattice. An alternative approach[8] is to consider the guest movements from the minimum energy position in the cavity as a spring, and evaluate the free energy changes through samplings of frequencies for different displacements in the cavity. A molecule like methane will, as expected, not have significant impact on the water movements.[8,51] CO_2, conversely, will change water chemical potential by roughly 1 kJ/mole at 0°C when compared to the assumption of undisturbed fixed water molecules. The cavity partition function may thus be written as

$$h_{ij} = \mathrm{e}^{\beta\left(\mu_j^H - \Delta g_{ji}^{\mathrm{inc}}\right)} \tag{2}$$

where Δg_{ji}^{inc} now is the effect of the inclusion of the guest molecule j in the cavity of type i, which as indicated above is the minimum interaction energy plus the free energy of the oscillatory movements from the minimum position. At hydrate equilibrium, the chemical potential is equal to that of the chemical potential of the guest molecule in its original phase (chemical potential of dissolved CO_2 or CH_4 for the case of hydrate formation from aqueous solution). Equation 2 can be inverted to give the chemical potential for the guest as a function of the cavity partition function

$$\mu_j^{\mathrm{H}} = \Delta g_{ji}^{\mathrm{inc}} + RT \ln h_{ij} \tag{3}$$

Equation 3 is basically derived from an equilibrium consideration but may be used as an approximation for bridging chemical potential to composition dependency. The relation between the filling fraction, the mole fractions and the cavity partition function is

$$\theta_{ji} = \frac{x_{ji}}{v_i(1-x_{\mathrm{T}})} = \frac{h_{ji}}{1+\sum_j h_{ji}} \tag{4}$$

here x_{T} is the total mole fraction of all the guests. It is assumed that CO_2 can only fit into the larger cavities, and unless some other guest molecule is present, the small cavities will then all be empty. For a system with only one component occupying the large cavities, the chemical potential of the guest molecule would be reduced to

$$\mu_w^{\mathrm{H}} = \Delta g_{ji}^{\mathrm{inc}} + RT \ln\left(\frac{\theta_{ji}}{1-\theta_{ji}}\right) \tag{5}$$

For methane, which can occupy both large and small cavities, a more cumbersome approach is needed. Initially assuming that chemical potential of methane in the two cavities is the same. This gives a proportional relation between the two partition functions independent on composition

$$\frac{h_{m\mathrm{l}}}{h_{m\mathrm{s}}} = e^{\left(\frac{\Delta g_{m\mathrm{s}}^{\mathrm{inc}} - \Delta g_{m\mathrm{l}}^{\mathrm{inc}}}{RT}\right)} = A \tag{6}$$

The mole fraction of methane x_m is the sum of the mole fraction in each cavity, that is, large $x_{m\mathrm{l}}$ and small $x_{m\mathrm{s}}$. The

mole fractions are expressed in terms of the cavity partition function from Eq. 4

$$x_{ms}+x_{ml}=x_m \tag{7}$$

$$\frac{h_{ms}}{1+h_{ms}}v_s+\frac{h_{ml}}{1+h_{ml}+h_{cl}}v_l=\frac{x_m}{1+x_T}=B \tag{8}$$

here h_{ms}, h_{ml}, and h_{cl} are the cavity partition functions of methane in small cavities, methane in large cavities, and carbon dioxide in large cavities, respectively. The denominator in the second term can be expressed in terms of the mole fraction and one of the partition functions from Eqs. 4 and 7

$$1+h_{ml}+h_{ms} \tag{9}$$

The partition function for CO_2 using Eqs. 4 needs to be calculated as:

$$\frac{x_{cl}}{v_l(1-x_T)}=\frac{h_{cl}}{1+h_{ml}+h_{cl}}$$

Rearranging the above equation in term of h_{cl} gives:

$$h_{cl}=\frac{x_{cl}(1+h_{ml})}{v_l(1-x_T)-x_{cl}}$$

Inserting the value of h_{cl} in Eq. 9, which gives constant C

$$1+h_{ml}+h_{cl}=(1+h_{ml})\left(1+\frac{x_{cl}}{v_l(1-x_T)-x_{cl}}\right) \tag{10}$$

$$C=1+\frac{x_{cl}}{v_l(1-x_T)-x_{cl}} \tag{11}$$

Using Eqs. 6, 10, and 11 results

$$1+h_{ml}+h_{cl}=(1+Ah_{ms})C \tag{12}$$

Equation 8 can be written in terms of single partition function

$$\frac{h_{ms}}{1+h_{ms}}v_s+\frac{Ah_{ms}}{(1+Ah_{ms})C}v_l=B \tag{13}$$

Equation 13 can be simplified to yield a second-order equation

$$(v_sCA+v_lA-BCA)h_{ms}^2+(v_sC+v_lA-BCA-BC)h_{ms}-BC=0 \tag{14}$$

Equation 14 can be written in the form of second constant

$$a_1(h_{ms})^2+a_2(h_{ms})+a_3=0 \tag{15}$$

$$a_1=A(v_l+v_sC-BC)$$

$$a_2=v_sC+Av_l-BC(1+A)$$

$$a_3=-BC$$

Fluid thermodynamic

The free energy of the fluid phase is assumed to have

$$G_L^{Fluid}=\sum_{r=c,m,w}x_r\mu_r^{Fluid} \tag{16}$$

where μ_r^{Fluid} is the chemical potentials of the fluid phase components. The lower concentration of water in the fluid phase and its corresponding minor importance for the thermodynamics results in the following form of water chemical potential with some approximation of fugacity and activity coefficient

$$\mu_w^{Fluid}=\mu_w^{ideal\ gas}(T,P)+RT\ln(y_w) \tag{17}$$

where $\mu_w^{ideal\ gas}(T,P)$ chemical potential of water in ideal gas and y_w is the mole fraction of water in the fluid phase and can be calculated as

$$y_w=\frac{x_w\gamma_w(T,P,\bar{x})P_w^{sat}(T)}{\varphi_w(T,P,\bar{y})} \tag{18}$$

The vapor pressure can be calculated using many available correlations but one of the simplest is given in Refs. 29 and 54 as a fit to the simple equation

$$\ln(P)=V_A-\frac{V_B}{T+V_C} \tag{19}$$

The temperature of the system is obviously available and $V_A=52.703$, $V_B=-3146.64$, and $V_C=5.572$. Further, the fugacity and the activity coefficient are approximated to unity merely because of the very low-water content in fluid phase and its corresponding minor importance for the thermodynamics of the system. Hydrate formation directly from water in gas is not considered as significant within the systems discussed in this work. A separate study reveals that hydrate formation from water dissolved in carbon dioxide may be feasible from a thermodynamic point of view[29] but more questionable in terms of mass transport in competition with other hydrate-phase transitions. The water phase is close to unity in water mole fraction. Raoult's law is, therefore, accurate enough for our purpose. The chemical potential for the mixed fluid states considered as

$$\mu_i^{Fluid}=\mu_i^{id.gas,\ pure}+RT\ln(y_i)+RT\ln\varphi_i(T,P,\bar{y}) \tag{20}$$

where i represents CH_4 or CO_2. The fugacity coefficients of component i in the mixture is calculated using the Soave–Redlich–Kwong (SRK) equation of state (EOS)[15,30,51]

$$\ln\varphi_i=(BB)_i(Z-1)-\ln(Z-B)-\frac{A}{B}\left((AA)_i-(BB)_i\right)\ln\left[1+\frac{B}{Z}\right] \tag{21}$$

where Z is the compressibility factor of the phase and is calculated using the following cubic SRK EOS

$$Z^3-Z^2+\left(A-B-B^2\right)Z-AB=0 \tag{22}$$

where

$$A=\frac{\alpha aP}{R^2T^2}$$

$$B=\frac{bP}{RT}$$

$$a=0.427480\frac{R^2T_c^2}{P_c}$$

$$b=0.086640\frac{RT_c}{P_c}$$

$$\alpha=\left[1+\left(0.48508+1.55171\omega-0.15613\omega^2\right)\left(1-\sqrt{T_r}\right)\right]^2$$

where ω is the accentric factor of components. For mixture, the mixing rule with modification proposed by Soave[30] is used using the following formulations

$$(\alpha a)_m=\sum\sum y_iy_j(\alpha a)_{ij};\ \ (\alpha a)_{ij}=\sqrt{(\alpha a)_i(\alpha a)_j}\left(1-k_{ij}\right) \tag{23}$$

where k_{ij} is the binary interaction parameter. Coutinho et al.[31] has proposed a number of values for k_{ij} for CO_2/CH_4 system.

Here, we selected an average value $k_{ij} = k_{ji} = 0.098$ for unlike pairs of molecules, and it is zero for alike pairs of molecules

$$b_m = \sum_i y_i b_i \tag{24}$$

$(AA)_i$ and $(BB)_i$ in Eq. 21 are calculated as

$$(AA)_i = \frac{2}{(a\alpha)_m}\left[\sum_j (a\alpha)_{ij}\right] \tag{25}$$

$$(BB)_i = \frac{b_i}{b_m} \tag{26}$$

Aqueous Thermodynamic. The free energy of the aqueous phase can be written as

$$G_{\mathrm{L}}^{\mathrm{aqueous}} = \sum_{r=c,m,w} x_r \mu_r^{\mathrm{aqueous}} \tag{27}$$

The chemical potential μ_r^{aqueous} for components c (carbon dioxide) and m (methane) dissolved into the aqueous phase is described by nonsymmetric excess thermodynamics

$$\mu_i = \mu_i^{\infty}(T) + RT\ln\left(x_i\gamma_i^{\infty}\right) + v_i^{\infty}(P - P_o) \tag{28}$$

μ_i^{∞} is the chemical potential of component i in water at infinite dilution, γ_i^{∞} is the activity coefficient of component i in the aqueous solution and v_i^{∞} is the partial molar volume of the component i at infinite dilution. The chemical potentials at infinite dilution as a function of temperature are found by assuming equilibrium between fluid and aqueous phases $\mu_i^{Fluid} = \mu_i^{\mathrm{aqueous}}$. This is done at varying low pressures where the solubility is very low and the gas phase is close to ideal gas using experimental values for the solubility and extrapolating the chemical potential down to a corresponding value for zero concentration. The Henry's constants k_{H} are calculated for CH_4 and CO_2 using the expression proposed by Sander[32]

$$k_{\mathrm{H}}(T) = k_{\mathrm{H}}^{\ominus}\mathrm{e}^{\left(\frac{-\Delta_{\mathrm{soln}}H}{R}\left(\frac{1}{T}-\frac{1}{T^{\ominus}}\right)\right)} \tag{29}$$

where $T^{\ominus}$ is the reference temperature, which is equal to 298.15 K. $\Delta_{\mathrm{soln}}H$ is the enthalpy of dissolution, and it is represented by the Clausius–Clapeyron equation[33] as

$$\frac{d\ln k_H}{d(1/T)} = \frac{-\Delta_{\mathrm{soln}}H}{R} \tag{30}$$

The values of $-(d\ \ln[k_H])/d(1/T)$ and $k_{\mathrm{H}}^{\oplus}$ are given by Zheng et al.[34] and by Kavanaugh and Trussell[35] for CO_2 and CH_4, respectively, which is shown in Table 1. The activity coefficient at infinite dilution γ_i^{∞} is calculated as

$$\gamma_i^{\infty} = \frac{f_i^{\infty}}{k_{\mathrm{H}}(T)} \tag{31}$$

where

$$f_i^{\infty} = \mathrm{e}^{\left(-\beta\mu_i^{\infty}\right)}$$

where f_i^{∞} is the fugacity of component i, while μ_i^{∞} is calculated from Ref. 37. The activity coefficient can be regressed using the model for equilibrium to fit experimental solubility data. The chemical potential of water can be written as

$$\mu_w = \mu_w^{\text{pure liquid}}(T) + RT\ln(1-x)\gamma_w + v_w(P - P_o) \tag{32}$$

where $\mu_w^{\text{pure liquid}}$ is pure water chemical potential and v_w is the molar volume of water. The strategy for calculating activity coefficient is given by Svandal et al.[36]

Table 1. Values of Parameters

Constants	CO_2	CH_4
$k_{\mathrm{H}}^{\ominus}$ (M/atm)	0.036	0.0013
$-(d\ \ln[k_H])/d(1/T)$(K)	2200	1800

Thermodynamics outside of equilibrium

The PFT model presented in this work have dynamically varying local densities, temperatures and concentrations, and the constraints on the system is the pressure. Unlike our earlier PFT models,[21,51] which were kept at constant temperature, the calculations of nonequilibrium thermodynamic[15] properties are implemented implicit calculations into the PFT model in this version since the free energies of all coexisting phases change dynamically with local conditions and possibly competing phase transitions. We use examples based on conversion of CH_4 hydrate into CO_2 hydrate or mixed CO_2—CH_4 hydrate, which have two primary mechanisms. The first one is that CO_2 creates a new hydrate from free water in the porous media and the released heat dissociate the in situ CH_4 hydrate. This mechanism is primarily dominated by mass-transport rates through fluid phases. A second mechanism is the direct conversion of the in situ CH_4 hydrate with the CO_2, which is a much slower solid-state-phase transition. The first mechanism implies heat release as well as heat consumption and complex coupled behavior of mass and heat transport around the hydrate core is expected. Also note that fluid thermodynamics and aqueous thermodynamics outside of equilibrium is trivial in contrast to hydrate, for which the thermodynamic model is derived from statistical mechanics based on equilibrium between hydrate and fluid phases. For this reason, we expand the thermodynamic properties of hydrate by a first-order Taylor-expansion. This is considered accurate enough since the rate-limiting kinetic contributions are expected to be in the mass transport according to earlier studies.[16,17,35] First of all note that the mass is conserved inside the PFT. The thermodynamics have to be developed in terms of gradients in all directions (P, T, mole-fractions) without conservation of mole-fractions in order to obtain the appropriate relative local driving forces and also avoid double conservation constraints in the free enrgy minimalization. In this article, we limit ourselves to three components, where CH_4 is the additional component to CO_2 and water. This can be directly extended to more components though straightforward extensions of the equilibrium and supersaturation thermodynamics, and appropriate adjustment of the PFT. As the thermodynamic changes are outlined here the primary additional change in the PFT model is in the free energy of the thermal fluctuations[16,37,38] as function of concentrations, which is mathematically trivial. Supersaturations of fluid phases is straightforward and not different from what we have published before[12,16] and in the first part of this article.

The Gibbs free energy of the hydrate phase is written as a sum of the chemical potentials of each component[12,16]

$$G_{\mathrm{H}} = \sum_r x_r \mu_r^{\mathrm{H}} \tag{33}$$

where μ_r^{H} and x_r is chemical potential and mole fraction of component r, respectively. G_{H} is the free energy of hydrate. In the earlier work by Svandal,[16] a simple interpolation in mole-fractions was used between pure CH_4 hydrate and pure CO_2 hydrate, which was considered as sufficient to

theoretically illustrate the exchange concept under PFT. This will of course not reproduce the absolute minimum in free energy for a mixed hydrate in which CH_4 occupies portions of the small cavities and increases stability over pure CO_2 hydrate. The expression for free energy gradients with respect to mole fraction, pressure, and temperature is

$$G_{\mathrm{H}}^{\mathrm{EXP}} = G^{\mathrm{EQ}} + \sum_r \left.\frac{\partial G_{\mathrm{H}}}{\partial x_r}\right|_{P,V,T,x_{i\neq r}} \left(x_r^{\mathrm{act}} - x_r^{\mathrm{EQ}}\right) + \left.\frac{\partial G_{\mathrm{H}}}{\partial P}\right|_{T,V,\vec{x}} \left(P^{\mathrm{act}} - P^{\mathrm{EQ}}\right) + \left.\frac{\partial G_{\mathrm{H}}}{\partial T}\right|_{P,V,\vec{x}} \left(T^{\mathrm{act}} - T^{\mathrm{EQ}}\right) \tag{34}$$

here $G_{\mathrm{H}}^{\mathrm{EXP}}$ is the free energy of hydrate away from equilibrium and the superscripts, EQ and act, represent the corresponding states at equilibrium and actual states, respectively. We are now seeking gradients in all directions, independent of mole-fraction conservation (sum of mole-fractions are conserved inside PFT). So in terms of super saturation in mole-fractions, these have to be evaluated as orthonormal gradient effects. In simple terms that means

$$\frac{\partial x_z}{\partial x_r} = \begin{cases} 0, & z \neq r \\ 1, & z = r \end{cases} \tag{35}$$

where z and r both represent any of the components of the hydrate: water, methane, and carbon dioxide. This is just means that the mole fractions are all independent. Using Eq. 33, we simply take the derivative with respect to one of the mole fractions ($r = m, c$, or w) and the mole fraction derivatives are obtained using Eq. 35 for mole fraction independence, resulting in

$$\frac{\partial G_{\mathrm{H}}}{\partial x_r} = x_c \frac{\partial \mu_c^{\mathrm{H}}}{\partial x_r} + x_m \frac{\partial \mu_m^{\mathrm{H}}}{\partial x_r} + x_w \frac{\partial \mu_w^{\mathrm{H}}}{\partial x_r} + \mu_r \frac{\partial x_r}{\partial x_r} \tag{36}$$

It was previously shown[16] that the chemical potential of a guest molecule can be approximated to a high degree of accuracy and in gradient terms

$$\mu_k^{\mathrm{H}} = A\ln(x_k) + B, \quad \frac{\partial \mu_k^{\mathrm{H}}}{\partial x_r} = \{0, r \neq k\} \tag{37}$$

where k and r both represents any of the components of the hydrate (CO_2, CH_4, and water). For the gradient due to a guest molecule, these simplifications lead to

$$\frac{\partial G_{\mathrm{H}}}{\partial x_k} = x_k \frac{\partial \mu_k^{\mathrm{H}}}{\partial x_k} + \mu_k^{\mathrm{H}} \tag{38}$$

For water, the form has two more terms

$$\frac{\partial G_{\mathrm{H}}}{\partial x_w} = \sum_r x_r \frac{\partial \mu_r^{\mathrm{H}}}{\partial x_w} + \mu_w^{\mathrm{H}} \tag{39}$$

The chemical potential of a guest in the hydrate μ_k^{H} can be written as (Kvamme and Tanaka[8])

$$\mu_k^{\mathrm{H}} = \Delta g_{kj}^{\mathrm{inc}} + RT\ln\left(h_{kj}\right) \tag{40}$$

where $\Delta g_{kj}^{\mathrm{inc}}$ is the Gibbs free energy of inclusion of guest molecule k in cavity j, h_{kj} the cavity partition function of component k in cavity j, the universal gas constant is R and T is temperature. The derivative of Eq. 40 with respect to an arbitrary molecule r is

$$\frac{\partial \mu_k^{\mathrm{H}}}{\partial x_r^{\mathrm{H}}} = \frac{\partial \Delta g_{kj}^{\mathrm{inc}}}{\partial x_r^{\mathrm{H}}} + \frac{\partial\left(RT\ln\left(h_{kj}\right)\right)}{\partial x_r^{\mathrm{H}}} \tag{41}$$

The first term of Eq. 41 is the stabilization energy, which can be evaluated either via the Langmuir constant or using the harmonic oscillator approach.[8] In either case, it can be safely assumed to be a function of only temperature and pressure. Omitting the first term of Eq. 41 and disregarding the impact of guest–guest interactions, one will arrive at

$$\frac{\partial \mu_k^{\mathrm{H}}}{\partial x_r^{\mathrm{H}}} = \frac{RT}{h_{kj}} \frac{\partial h_{kj}}{\partial x_r^{\mathrm{H}}} \tag{42}$$

The wisdom of omitting guest–guest interactions may be questionable in certain cases, even though they are either ignored or empirically corrected for by the majority of hydrate equilibrium codes (the latter can be implemented at a later stage).

The chemical potential of water

$$\mu_w^{\mathrm{H}}\left(T, P, \vec{\theta}\right) = \mu_w^{0,\mathrm{H}}(T, P_0) - \sum_j RT\upsilon_j \ln\left[1 + \sum_k h_{kj}\right] \tag{43}$$

where $\mu_w^{0,\mathrm{H}}$ is the chemical potential of water in an empty hydrate structure, the first sum is taken over both small and a large cavity, the second one is over the components k in the cavity j. Here υ_j is the number of type- j cavities per water molecule. Hydrate structure I contains three large cavities and one small cavity per 23 water molecules, $\upsilon_{\mathrm{l}} = \frac{3}{23}$ and $\upsilon_{\mathrm{s}} = \frac{1}{23}$. The paper by Kvamme and Tanaka[8] provides the empty hydrate chemical potential as polynomials in inverse temperature, the Gibbs free energies of inclusion, and chemical potential of pure water $\mu_w^{\mathrm{pure}}(T)$. The derivative for the above equation with respect to an arbitrary molecule r results in

$$\frac{\partial \mu_w^{\mathrm{H}}}{\partial x_r} = -RT \sum_j \upsilon_j \left[\frac{\sum_k \frac{\partial h_{kj}}{\partial x_r}}{1 + \sum_k h_{kj}}\right] \tag{44}$$

From Eqs. 42 and 44, the derivative of the partition function can be evaluated from the equation that relates the filling fraction to the partition function

$$h_{kj} = \frac{\theta_{kj}}{1 - \sum_i \theta_{ij}} \tag{45}$$

where θ_{kj} is the filling fraction of the components k in the cavity j. But it is easier to recast everything in terms of mole fraction because of the basic assumption of mole fraction independence

$$\theta_{kj} = \frac{x_{kj}}{\upsilon_j x_w} \tag{46}$$

since mass conservation is not used, the usual form of $1 - x_{\mathrm{T}}$ is not considered. This is substituted into Eq. 45 and we get

$$h_{kj} = \frac{x_{kj}}{\upsilon_j x_w - \sum_i x_{ij}} \tag{47}$$

Now we can take the derivative with respect to an arbitrary component r and using Eq. 47, we get

$$\frac{\partial h_{kj}}{\partial x_r} = \frac{h_{kj}}{x_{kj}} \frac{\partial x_{kj}}{\partial x_r} - \frac{h_{kj}^2}{x_{kj}} \left[\upsilon_j \frac{\partial x_w}{\partial x_r} - \sum_i \frac{\partial x_{ij}}{\partial x_r}\right] \tag{48}$$

The first thing that must be dealt with the cavity mole fractions as a function of total mole fraction of a component

$$x_k = \sum_j x_{kj} \tag{49}$$

since the derivative of one mole fraction with respect to another is independent, the mole fraction in the cavity is also independent

$$\left(\frac{\partial x_{kj}}{\partial x_r}\right) = \begin{cases} 0, & k \neq r \text{ or } r = w \\ 1, & k = r \end{cases} \tag{50}$$

If $r = w$, then the derivative has to be zero because the mole fraction of the guest are independent of the mole fraction of water. Now Eq. 48 is simplified using Eqs. 49 and 50

$$\frac{\partial h_{kj}}{\partial x_w} = -\frac{h_{kj}^2 \upsilon_j}{x_{kj}} \tag{51}$$

$$\frac{\partial h_{kj}}{\partial x_p} = \frac{h_{kj}}{x_{kj}}\frac{\partial x_{kj}}{\partial x_p} + \frac{h_{kj}^2}{x_{kj}}\frac{\partial x_{pj}}{\partial x_p} \tag{52}$$

where p is an arbitrary guest molecule and k is also a guest molecule. These can be the same or different. If k and p are the same molecule, this gradient still exist and the "cross terms" are still able to be found even if there is independency in the mole fractions. $\frac{dx_{kj}}{dx_k}$ is calculated by starting with the Eq. 49, which is the basic definition of the mole fraction of the cavities and how they relate to the total mole fraction of the component. The total methane mole fraction x_m, is the sum of the mole fraction in the large cavities x_{ml}, and the mole fraction in the small cavities x_{ms}

$$x_m = x_{ml} + x_{ms} \tag{53}$$

From discussions, it is assumed that there is a constant ratio between the partition functions and between different cavities of the same component. This is defined as A

$$A \equiv \frac{h_{ml}}{h_{ms}} \tag{54}$$

The partition function can be written in terms of the filling fraction as shown in Eq. 45. Using Eqs. 45, 46, 54 and assuming that the filling fraction of CO_2 in small cavities is zero, we get

$$A \equiv \frac{\frac{x_{ml}}{\upsilon_l x_w}}{\frac{x_{ms}}{\upsilon_s x_w}}\left[\frac{1-\frac{x_{ms}}{\upsilon_s x_w}}{1-\frac{x_{ml}}{\upsilon_l x_w}-\frac{x_{c1}}{\upsilon_l x_w}}\right] \tag{55}$$

This simplifies into

$$x_{ml}[-\upsilon_s x_w] + x_{ms}[A\upsilon_l x_w - A x_{c1}] + x_{ms}x_{ml}[1-A] = 0 \tag{56}$$

Taking derivative of above equation with respect to total methane mole fraction

$$[x_{ms}(1-A) - \upsilon_s x_w]\frac{\partial x_{ml}}{\partial x_m} + [A\upsilon_l x_w - A x_{c1} + x_{ml}(1-A)]\frac{\partial x_{ms}}{\partial x_m} = 0 \tag{57}$$

Substitutions were made to simplify the above equation and get it into a simpler form:

$$\begin{aligned} X &= x_{ms}(1-A) - \upsilon_s x_w \\ Y &= A\upsilon_l x_w - A x_{c1} + x_{ml}(1-A) \\ X\frac{\partial x_{ml}}{\partial x_m} + Y\frac{\partial x_{ms}}{\partial x_m} &= 0 \end{aligned} \tag{58}$$

taking the derivative of Eq. 53 with respect to the total mole fraction of methane and simplification results in

$$\begin{aligned} \frac{\partial x_{ml}}{\partial x_m} + \frac{\partial x_{ms}}{\partial x_m} &= \frac{\partial x_m}{\partial x_m} = 1 \\ \frac{\partial x_{ml}}{\partial x_m} &= -\frac{Y}{X-Y} \\ \frac{\partial x_{ms}}{\partial x_m} &= \frac{X}{X-Y} \end{aligned} \tag{59}$$

substituting the values of X and Y gives the final answer:

$$\begin{aligned} \frac{\partial x_{ml}}{\partial x_m} &= -\frac{A\upsilon_l x_w - A x_{c1} + x_{ml}(1-A)}{x_{ms}(1-A) - \upsilon_s x_w - A\upsilon_l x_w - A x_{c1} + x_{ml}(1-A)} \\ \frac{\partial x_{ms}}{\partial x_m} &= \frac{x_{ms}(1-A) - \upsilon_s x_w}{x_{ms}(1-A) - \upsilon_s x_w - A\upsilon_l x_w - A x_{c1} + x_{ml}(1-A)} \end{aligned} \tag{60}$$

$\frac{\partial G_H}{\partial P}$ is calculated by taking derivative of Eq. 33 with respect to pressure

$$\frac{\partial G_H}{\partial P} = x_c\frac{\partial \mu_c^H}{\partial P} + x_m\frac{\partial \mu_m^H}{\partial P} + x_w\frac{\partial \mu_w^H}{\partial P} + \mu_c\frac{\partial x_c}{\partial P} + \mu_m\frac{\partial x_m}{\partial P} + \mu_w\frac{\partial x_w}{\partial P} \tag{61}$$

where the chemical potential gradients with respect to pressure can be given by

$$\frac{\partial \mu_r^H}{\partial P} = \bar{V}_r \tag{62}$$

Thus, Eq. 62 can be written as

$$\frac{\partial G_H}{\partial P} = x_c\bar{V}_c + x_m\bar{V}_m + x_w\bar{V}_w + \mu_c^H\frac{\partial x_c}{\partial P} + \mu_m^H\frac{\partial x_m}{\partial P} + \mu_w^H\frac{\partial x_w}{\partial P} \tag{63}$$

The sum of the molar volumes ($\bar{V}_c$, $\bar{V}_m$, $\bar{V}_w$) is in fact the total clathrate molar volume

$$\bar{V}^{\text{clath}} = x_c.\bar{V}_c + x_m.\bar{V}_m + x_w.\bar{V}_w \tag{64}$$

using the above value of $\bar{V}^{\text{clath}}$ simplifies the Eq. 64 to

$$\frac{\partial G_H}{\partial P} = \bar{V}^{\text{clath}} + \mu_c^H\frac{\partial x_c}{\partial P} + \mu_m^H\frac{\partial x_m}{\partial P} + \mu_w^H\frac{\partial x_w}{\partial P} \tag{65}$$

The mole fraction derivatives can be calculated from EOS but there is no change under this derivative so Eq. 66 can be rewritten as

$$\left[\frac{\partial G_H}{\partial P}\right]_{T,V,\vec{x}} = \bar{V}^{\text{clath}} \tag{66}$$

The free energy gradient with respect to temperature comes from the same fundamental relationship as used for the chemical potential gradient

$$-\frac{\partial}{\partial T}\left[\frac{G}{T}\right]_{P,\vec{x}} = \frac{\bar{H}}{T^2} \tag{67}$$

PFT model

The effects of nonequilibrium thermodynamics on phase transition are incorporated by implementing the thermodynamic model implicitly into phase field simulation. The hydrodynamics effects and variable density were incorporated in a three components PFT by Kvamme et al.[39] through implicit integration of Navier–Stokes equation following the approach of Qasim et al.[14] The basic phase field model for two components is described/used by Wheeler et al.[40] and other references[41–45] and other references therein. The PFT for three components is a straightforward extension of the basic theoretical model. The phase field parameter ϕ is an order parameter describing the phase of the system as a function of spatial and time coordinates. The phase field parameter ϕ is allowed to vary continuously from 0 to 1 on the range from solid to liquid.

The solid state is represented by the hydrate, and the liquid state represents fluid and aqueous phase. The solidification of

hydrate is described in terms of the scalar phase field ϕ (x_1, x_2, x_3) where $x_1, x_2,$ and x_3 represents the molar fractions of CH_4, CO_2, and H_2O, respectively, with obvious constraint on conservation of mass $\sum_{i=1}^{3} x_i = 1$. The field ϕ is a structural order parameter assuming the values $\phi = 0$ in the solid and $\phi = 1$ in the liquid.[16] Intermediate values correspond to the interface between the two phases. The starting point of the three component phase field model is a free energy functional[14]

$$F = \int d\underline{r} \left(\frac{a_\phi^2}{2} T(\nabla\phi)^2 + \sum_{i,j=1}^{3} \frac{a_{xi,j}^2}{4} T\rho(x_i \nabla x_j - x_j \nabla x_i)^2 + f_{\text{bulk}}(\phi, x_1, x_2, x_3, T) \right) \tag{68}$$

which is integration over the system volume, while the subscripts i, j represents the three components, ρ is molar density depending on relative compositions, phase, and flow. The bulk free energy density described as

$$f_{\text{bulk}} = WTg(\phi) + (1 - p(\phi)) f_S(x_1, x_2, x_3, T) + p(\phi) f_L(x_1, x_2, x_3, T) \tag{69}$$

The phase field parameter switches on and off the solid and liquid contributions f_S and f_L through the function $p(\phi) = \phi^3 \left(10 - 15\phi + 6\phi^2\right)$, and note that $p(0) = 0$ and $p(1) = 1$. This function was derived from density functional theory studies of binary alloys and has been adopted also for our system of hydrate-phase transitions. It might be modified by fitting profiles for hydrate/fluid interfaces derived from molecular simulations but for the time being the profile is sufficiently representative. The binary alloys are normally treated as ideal solutions. The free energy densities of solid and liquid is given by

$$f_{\text{bulk}} = WTg(\phi) + (1 - p(\phi)) f_S(x_1, x_2, x_3, T) + p(\phi) f_L(x_1, x_2, x_3, T) \tag{70}$$

$$f_s = G_H \rho_m^H \tag{71}$$

$$f_L = G_L \rho_m^L \tag{72}$$

where the expressions for the free energy of hydrate in a super saturate (or an undersaturated) state as functions of different thermodynamic variables are given through Eqs. 33–68, and the free energies of fluids are described in the first part of the article from some fluid states and in references[36,39,41,42] for other states. The details of densities ρ_m^{hyd} and ρ_m^L can be found in Qasim et al.[14] Also note that a possible phase transition will only proceed unconditionally if the free energy change is negative, and more negative than the interface free energy barrier imposed by the interface work needed to give space for the new phase, and also all gradient in free energies results in negative free energy changes for the phase transition. Practically, this latter condition implies that the system is supersaturated with respect to gradients of free energies in all thermodynamically independent variables for the system. If one or more gradients result in positive free energies and the phase transition will compete with other phase transitions.

The function $g(\phi) = \phi^2 \left(1 - \phi^2\right)/4$ ensures a double well form of the f_{bulk} with a free energy scale $W = \left(1 - \frac{x_i}{v_m}\right) W_A + \frac{x_i}{v_m} W_B$ with $g(0) = g(1) = 0$, where v_m is the average molar volume of water. In order to derive a kinetic model we assume that the system evolves in time so that its total free energy decreases monotonically.[36,39,41]

The usual equations of motion are supplemented with appropriate convection terms, as explained in Tegze and Grαnαsy[18]; given that the phase field is not a conserved quantity, the simplest form for the time evolution that ensures a minimization of free energy is

$$\frac{\partial\phi}{\partial t} + (\vec{v}.\nabla)\phi = -M_\phi(\phi, x_1, x_2, x_3) \frac{aF}{a\phi} \tag{73}$$

$$\frac{\partial x_i}{\partial t} + (\vec{v}.\nabla) x_i = \nabla . \left(M_{xi}(\phi, x_1, x_2, x_3) \nabla \frac{aF}{axi} \right) \tag{74}$$

where $\vec{v}$ is the velocity, $M_{xi} = x_i(1 - x_i)\frac{1}{RT} D$ and $M_\phi = \left(1 - \frac{x_i}{v_m}\right) M^A + \frac{x_i}{v_m} M^B$ are the mobilities associated with coarse-grained equation of motion which in turn are related to their microscopic counter parts; $D = D_S + (D_L - D_S) p(\phi)$ is the diffusion coefficient. Additional details can be found elsewhere.[16,39]

We have formulated an extended version of the phase field model, which takes into account the effects of fluid flow, density change, and gravity. This is achieved by coupling the time evolution with the Navier–Stokes Equations. The phase and concentration fields associate hydrodynamic equation as described by Conti and coworkers[46–48]

$$\frac{\partial\rho}{\partial t} = -\rho_m \nabla.\vec{v} \tag{75}$$

$$\rho \frac{\partial\vec{v}}{\partial t} + \rho(\vec{v}.\nabla)\vec{v} = \rho\vec{g} + \nabla.P \tag{76}$$

where $\vec{g}$ is the gravitational acceleration. ρ_m is the density of the system in hydrate $\left(\rho_m^{Hyd}\right)$ and liquid $\left(\rho_m^L\right)$. Further

$$P = \Xi + \Pi \tag{77}$$

is the generalization of stress tensor,[46–48] Ξ represents non-dissipative part and Π represents the dissipative part of the stress tensor.

For hydrate formation following water adsorption on rusty walls,[22,23] heat transport is very fast compared to mass transport and not likely to have any significant rate-limiting impact on the kinetic rates. Formation of hydrates inside bulk CO_2 (or inside CO_2/CH_4 fluid) heat-transport rates may have an impact. For these cases, we have so far extended our PFT code according to a simplified scheme as described below.

First consider the general thermodynamic relationship

$$dH = \left(\frac{\partial H}{\partial T}\right)_{P,\vec{x}} dT + \left(V - T\left[\frac{\partial V}{\partial T}\right]_{P,\vec{x}} \right) dp \tag{78}$$

where the molar volume V, as well as the gradient of molar volume with respect to T, is very small for solids and condensed phases. The latter term is also exactly zero for ideal gas. So except for regions of high-pressure gas, the latter term is normally negligible. So for simplicity and also in view of other uncertainties which will be described below the latter term is omitted as an approximation. Strictly speaking, it is not necessary since the volumetric terms are readily available from the solution of the EOS used. The correction could be estimated but the latter term implies couplings to Navier–Stokes that will require some modifications in the integration algorithm.

The two primary contributions to heat transport are conduction and convection. For the systems that we consider, the

conduction term is the dominating. A common approximation in hydrate modeling, as well as in interpretation of experimental data, is therefore, to lump both these contributions into an "apparent" conductivity. Accordingly

$$\dot{Q} = kA\Delta T \tag{79}$$

where k is the "apparent" heat conductivity, A is the area for the heat transport and ΔT the temperature difference. In the integrations of Eqs. 79 and 80, the 2-D or 3-D space in consideration is discretized into grid blocks, and for each grid block, the total molar enthalpy can be written as

$$H_i = (1-\varphi_i)H_{S,i}\left(T,P,\vec{x}_{S,i}\right)+\varphi_i H_{L,i}\left(T,P,\vec{x}_{L,i}\right) \tag{80}$$

where subscript i is the index for grid block number and subscripts S and L denote hydrate and fluid, respectively. These enthalpies are readily available from the individual thermodynamic models involved but are more conveniently evaluated directly from the free energy of each grid block using Eq. 69. From the first law of thermodynamics and combining Eqs. 79 and 80, we arrive at the simple result

$$\left(\frac{\Delta H}{\Delta t}\right)_i = k_i A_i \Delta T_i \tag{81}$$

In discretized form for a chosen time step of the integration, Δt, and corresponding changes in enthalpy and temperature over a time step of progress. A_i is trivially given by the geometry of the grid block system and the dimensions of the system (3-D or 2-D simulation). We make no rigorous discussion on the most appropriate form of an average thermal conductivity of each grid block and have so far implemented the following average value[51]

$$k_i = (1-\varphi_i)k_{S,i}\left(T,P,\vec{x}_{S,i}\right)+\varphi_i k_{L,i}\left(T,P,\vec{x}_{L,i}\right) \tag{82}$$

in which a number of different correlations are available for gas mixtures in the fluid part of the latter term. For liquid water part of the latter term, values are fairly independent of pressure, and since solubility of CO_2 as well CH_4, is limited liquid water provides a fair approximation. Thermal conductivity for hydrate in the solid position of the grid block phase distribution, the value is almost insensitive to both pressures and compositions of the hydrate. Fixed values for $k_{S,i}$ and $k_{L,i}$ are available elsewhere.[52]

Results

The injection of CO_2 into the pore will first displace some of the water surrounding the hydrate due to the minerals normally having a higher thermodynamic affinity for water than hydrate. But this will, of course, depend on the mineral wetting properties. As an example, first few layers of water adsorbed on hematite may have chemical potentials lower by 2–4 kJ/mole than that of liquid water.[13] If the mineral surface is CO_2-wetting, then a greater fraction of the in situ liquid water will surround the hydrate core inside the pores. In this case, the in situ free gas (if existing) will partially dissolve in the injected CO_2. The rate of dissolution will depend on dissolution kinetic rates compared to flow dynamics and rates of CO_2 conversion into hydrate. The rate of CO_2 conversion into hydrate is depends on the diffusion of CO_2 into the porous medium, which would depend on the properties of the medium such as pore sizes, pore connections, and porosity.[53] The 3-D bond pore network model presented by Mu et al.[53] showed that diffusivity increases with mean pore diameter when the pore size is less than 1 μm as a result of the Knudsen effect, with a very strong dependence of effective diffusivity on pore size (which is due to nanoscale to microscale impact of interactions between solid and fluid on energy and entropy generation as well as stress). The increased hydrate formation due to increased diffusion rate of CO_2 into the nanoscale pore size is observed by Adeyemo et al.[54] The relative fraction of water surrounding the hydrate core is of course dependent on several additional factors, but in the example used here for illustration purposes, we have chosen to have water-wetting mineral surface. The degree of water wetting is not important for these examples since thermodynamics of fluids adsorbed on mineral surfaces is not yet implemented but quite feasible along the lines described by Kvamme et al.[21] with additional data on chemical potential of adsorbed water as described by Cuong et al.[22,23] for calcite.

Conversion of CH_4 hydrate over to CO_2 hydrate may proceed via two primary mechanisms. The direct solid-state conversion will be slow, since its rate is related to solid-state diffusivity of CH_4 and CO_2 inside hydrate. The second mechanism implies that injected CO_2 is able to form a new hydrate together with free water surrounding hydrate (and of course also with adsorbed water). Heat released by hydrate formation will contribute to dissociation of in situ CH_4 hydrate. This effect could be expected to enhance the conversion rate as the amount of water surrounding the initial CH_4 hydrate core increases. The larger volume of liquid water around the hydrate would mean greater contact area between it and the CO_2, which would also facilitate the formation of new hydrate. This second mechanism will not be limited by heat transport since the rate of heat transport is 2–3 orders of magnitude faster than that of mass transport[16] through liquid water and hydrate. Conversely, heat transport through the CO_2 phase will be comparatively slow. This factor will, therefore, facilitate heat transfer from the CO_2 hydrate formation region toward the in situ CH_4 hydrate. Liquid-state diffusivity associated with mass transport to and from the hydrate surface will be orders of magnitude faster than the solid-state transport. The second mechanism is, therefore, expected to utterly dominate as long as there is any free water left around the CH_4 hydrate. We, therefore, have considered three different thicknesses of injected CO_2 to study the relative impact.[55]

To save CPU time, simulations are conducted in 2-D although there are no constraints to this in the theory or the PFT code. Two-dimensional is also sufficient for the simple crystal morphology that we are using in our examples at this stage. As mentioned, there are two primary mechanisms involved in the conversion of methane hydrate into a mixed hydrate of carbon dioxide and methane in which some methane will occupy the small cavities. As an approximation, we neglect filling of carbon dioxide in the small cavities since it is so far uncertain if this will be significant for rapid phase transitions in a dynamic reservoir flow environment. The thermodynamic stabilization from CO_2 filling in large is also uncertain since the cavity partition functions for CO_2 in small cavities are extremely small and in molecular dynamics simulations, using different well-known interaction models for CO_2, the hydrate dissociates fast. These are so far unpublished results. So even though experimental evidence may suggest that CO_2 might be trapped in small cavities, it does not necessary imply that chemical potential of hydrate water will be lowered by this occupancy. On the contrary, it might even result in large

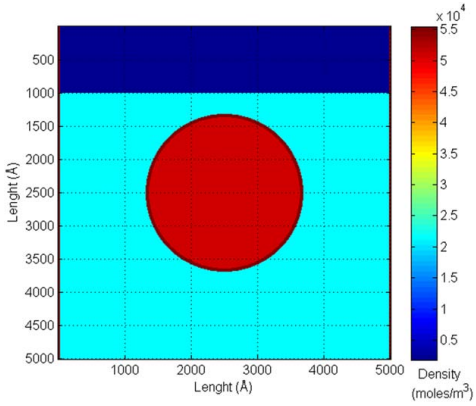

Figure 1. Initial snapshot of density (moles/m^3) profile shows the initial distribution of phases and components for (5000 Å × 5000 Å) system; red disk in the center is CH_4 hydrate core, water regions are represented by maroon color, dark blue region is methane, and rest is CO_2, Similar distribution for other two 2-D systems.

[Color figure can be viewed in the online issue, which is available at wileyonlinelibrary.com.]

CO_2 molecule hindering water liberations. Even a spherical CO_2 model in large cavity will interfere with some water liberational frequencies.[8] The chemical potential for water is roughly 1 kJ/mole at 273 K higher when water movement is accounted for by molecular dynamics simulations compared to the Langmuir constant integration using a fixed water lattice.[8] The difference is likely to be substantially worse for the small cavity. So given that it is uncertain if CO_2 is actually trapped in small cavities in significant amounts under the dynamic situations, we focus on we approximate to zero filling of CO_2 in small cavities.

The three 2-D systems of size 5000 Å × 5000 Å representing the sample pores size. The initial hydrate saturation was same for all systems, with hydrate cores represented by disks of radius 1136 Å located at the center of the 2D systems. The initial pure methane saturation is approximately 20% of the pore area. Water strips of varying thickness (5, 50, and 70 Å) are introduced around the hydrate core, with the rest of the system saturated with CO_2 to represent two different amounts of free water surrounding the hydrate and corresponding different water/CO_2 contact areas. A sample system is shown in Figure 1.

The distribution of phases and components shown in Figure 1 is based on average liquid water saturation, free gas saturation, and hydrate saturation of a real reservoir. Thickness of water film around the hydrate core shown in Figure 1 is 50 Å as an example. The model pore is a square shape of size 5000 Å × 5000 Å in Figure 1 and sI Structure hydrate is represented by circular region in red color right in center of the pore. The water saturation is represented with maroon color around hydrate in addition to the two strips adjacent to the walls. Considering the injection of CO_2 has moved methane up from its original position around the hydrate is, therefore, represented by the upper dark blue strip. The rest of the region shows the injected CO_2. The pressure is kept constant at 83 bars and the initial temperature is uniform and 277.15 K. These conditions have been used in this initial study since these conditions were applied in a number of experiments conducted in ConocoPhillips laboratory in Bartlesville over more than a decade. See for instance Kvamme and coworkers,[19,21] for examples and description of the experimental setup. Comparison with these experimental data will also require inclusion of realistic mineral surfaces, and that is a future goal.

The existence of free water and CO_2 liquid form a new CO_2 hydrate and as a result releases heat as shown in Figure 2. Heat released here is a dominating factor in the fast initial dissociation of methane hydrate and as a result allowing a faster initial exchange process. The second, dominating factor in the initial dissociation process is the lower energy state of CO_2 as the guest molecule in sI gas hydrate structures vs. CH_4. This results in more favorable thermodynamics conditions of formation for the pure CO_2 vs. pure CH_4 hydrates over large regions of pressures and temperatures, while mixed hydrate in which CO_2 dominates occupation of large cavities and CH_4

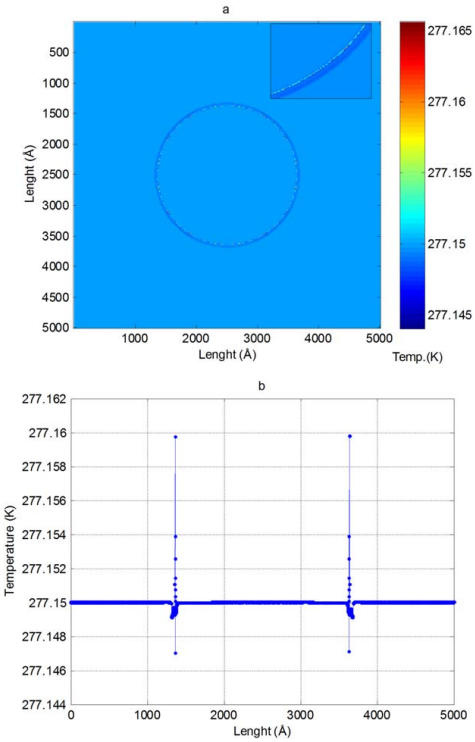

Figure 2. (a) Snapshot of temperature in kelvin shows an increased around the CH_4 hydrate due to formation of CO_2 hydrate, color bar is associated with (a) representing temperature in kelvin. For a more clear insight, a region at interface is highlighted and zoomed in. (b) Temperature curve from one end to another passing through center of CH_4 hydrate.

[Color figure can be viewed in the online issue, which is available at wileyonlinelibrary.com.]

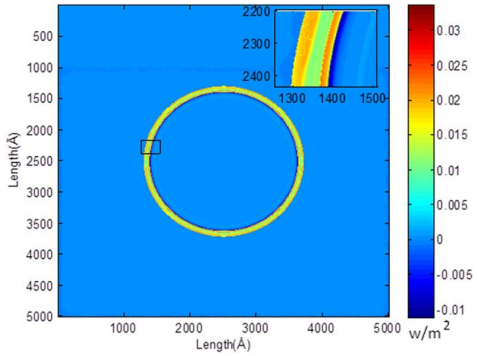

Figure 3. Heat flux profile.

[Color figure can be viewed in the online issue, which is available at wileyonlinelibrary.com.]

dominates occupation of small cavities is more stable at all conditions of temperature and pressure.

The formation of hydrate is an exothermic process and, therefore, result an increase in temperature in the area of new CO_2 hydrate formation, as shown in Figure 2a. Heat transport through CO_2 region is slow which will, therefore, also facilitate the heat being transported from the CO_2 hydrate formation region toward the in situ CH_4 hydrate as shown in Figure 3. The calculation details are given in Appendix.

The encircled region in Figure 2a is also show gaps in the increasing temperature regions at the interface which are typically escape regions for dissociating methane mainly from the large cavities of hydrate. The dissociation extracts heat since it is an endothermic process. Hydrate dissociation extracts heat from the surroundings which is illustrated in Figures 2a, b by regions of reduced temperature.

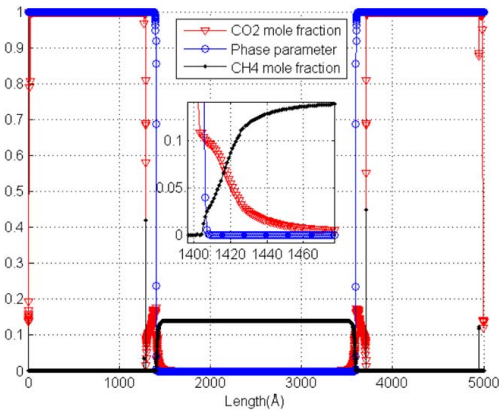

Figure 4. CO_2 filling in hydrate while curve of methane mole fraction shows dissociation of methane, phase parameter curve to indicate hydrate and fluid phases.

The zoomed graph is showing the clear picture of exchange process. [Color figure can be viewed in the online issue, which is available at wileyonlinelibrary.com.]

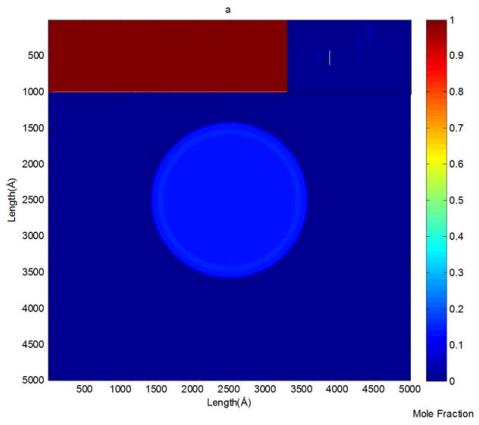

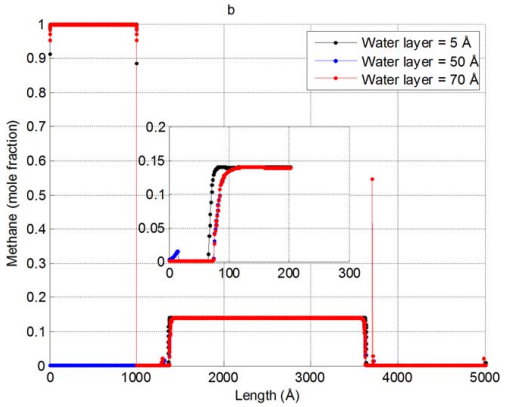

Figure 5. Snapshot of methane mole fraction in entire system after 4.84 ns.

(a) Methane mole fraction across the system after 4.84 ns for the system with water thickness 70 Å. A region at the interface is highlighted and zoomed in to show methane as free gas. (b) A comparison of methane mole fraction after 4.84 ns of three examples. [Color figure can be viewed in the online issue, which is available at wileyonlinelibrary.com.]

All the curves in Figure 4 and in coming figures show variation in parameters along the line starting from the boundary of the 2-D geometry in Figure 1 adjacent to blue methane region to the opposite boundary passing through the center of hydrate. This will show the variation in parameters in the pore with a single curve. The CO_2, CH_4 concentrations, and phase field curves in Figure 4 show that CO_2 has converted the interface water layer into hydrate and created a new interface dominated by CO_2 in favor of CH_4 with water and then started the (slow) solid-state conversion of the CH_4 hydrate core. The phase parameter is represented by the third curve in Figure 4 is drawn here to show precisely the changes in mole fraction of CO_2 and CH_4 inside hydrate.

Due to dissolution kinetics, the surrounding CO_2 will not be able to dissolve the released methane within the time window of simulation time. Methane will, therefore, exist as free gas bubbles near the interface and then gradually increasing in

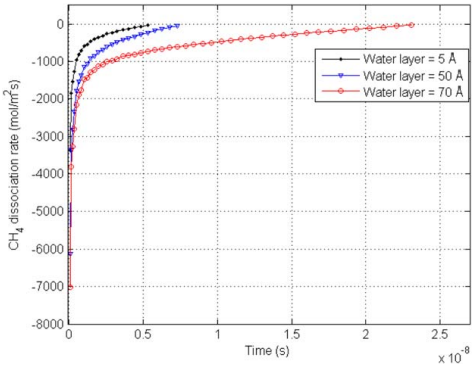

Figure 6. A comparison of estimated methane release rate in three systems.

[Color figure can be viewed in the online issue, which is available at wileyonlinelibrary.com.]

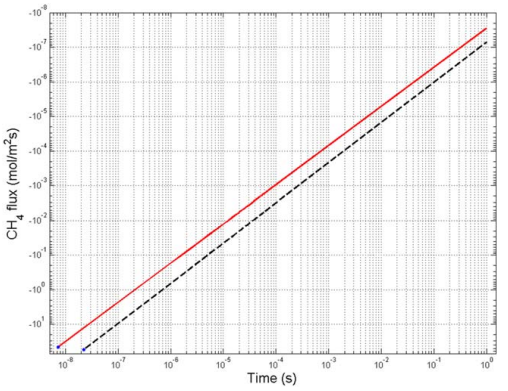

Figure 7. Extrapolation of CH_4 flux into experimental time-scale.

The solid red line represents simulation with 50-Å water thickness and dashed black line is for simulation with 70-Å water thickness around hydrate core. [Color figure can be viewed in the online issue, which is available at wileyonlinelibrary.com.]

CO_2 content. CH_4 and CO_2 are mutually soluble at these conditions according to the thermodynamics but there are constraints on the solubility kinetics in terms of diffusivities compared to the impact of Navier–Stokes on the local variations in densities. The existence of free CH_4-dominated gas bubbles from released CH_4 can be observed in this example as shown in Figure 5. Some few regions of free gas are particularly expressed by encircling them within the fluid phase in Figure 5. The mole fraction of methane in those regions varies in the range of 0.4–0.65. The system with the larger water layer thickness around initial hydrate has more methane at interface after a particular simulation time. The larger water layer ensures a higher dissociation rate of methane from hydrate due to a larger amount of new CO_2 hydrate being formed per unit time and rapid heat transport inward toward the hydrate core and slow heat transport into surrounding CO_2 phase. A comparison of dissociation rates of methane is presented in Figure 6 to emphasize this picture.

The simulation results covered a limited time interval due to computational restrictions, with only a fraction of the large cavities being filled with CO_2. Achieving a full exchange will require substantially longer simulation runs even when using a supercomputer with relatively high parallelization. The rate of CH_4 release, as illustrated in Figure 6, clearly shows that methane was still being released even toward the end of the simulations, though with the rate did decrease as the amount of free liquid water diminished due to transition to the slow solid-state exchange mechanism. All of the systems appear to enter a stationary slow progress dominated by solid-state exchange. To illustrate this, the numeric results were extrapolated to experimental time as the interface in these simulations is perfectly follows the power law, which is proportional to square root of time showing a diffusion control process (Figure 7). The dissociation rate by second mechanism is orders of magnitude faster than solid-state transport, which is illustrated in Table 2.

As expected, a system with the thinnest liquid water layer entered the slow-exchange stage faster than systems with more free water available to create new CO_2 hydrate. The difference in transition of rates between the heat supply mechanism vs. the solid-state transport is illustrated in Figure 8. These results will have significant practical implications; the conclusion that initial saturation of free water capable of producing new CO_2 hydrate will be a critical dynamic factor for conversion of in situ CH_4 hydrate into CO_2 and mixed CO_2/CH_4 hydrate being of utmost importance. And since the rate of heat absorption related to dissociation of CH_4 hydrate will be controlled and rate-limited by mass transport across the liquid water/hydrate interface, there will be a kinetic balance involved as well. Given that it is the interface that provides the most favorable site for hydrate formation from injected CO_2 and pore water, pore blockage can occur fast due to relatively thin but mechanically strong interface hydrates will potentially be able to trap liquid water and CO_2. This impact can be reduced by several additives. The high hydrate saturations typical for Alaska may, therefore, not be ideal for the conversion method, although CO_2/N_2 injection will work (Ignik Sikumi gas hydrate field trial[26]) and would perform better with a different completion type (separate injection and production wells) since the CH_4—CO_2—nitrogen exchange will result in a beneficent gas density gradient between injection and production sites.

Conclusions

The exchange of CH_4 with CO_2 in the hydrate will be controlled by two primary mechanisms. The fastest one will involve creation of new CO_2 hydrate. This new hydrate can nucleate from phases adsorbed on mineral surfaces, existing

Table 2. CH_4 Dissociation Rates

	Simulation 2 with water thickness 50 Å		Simulation 3 with water thickness 70 Å	
Time (s)	1.6 e −010	1	1.6 e −010	1
Dissociation rates (mol/m^{2}s)	3.365 e +003	2.858 e −008	3.815 e +003	7.249 e −008

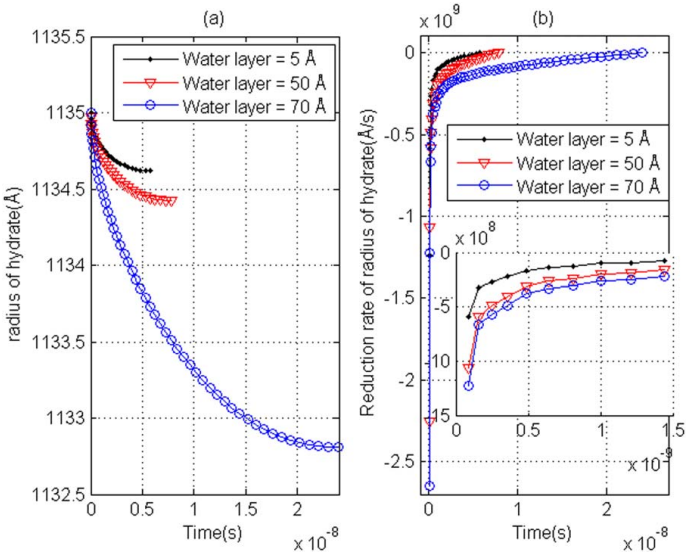

Figure 8. Development of the mix CH_4/CO_2 hydrate core as function of time three examples.

(a) Radius as function of time and (b) rate of radius reduction as function of time. [Color figure can be viewed in the online issue, which is available at wileyonlinelibrary.com.]

hydrate, or interface between liquid water and CO_2. Heat released by hydrate created from water surrounding the hydrate core will be mainly transported through water and existing hydrate since the surrounding CO_2 can be considered a thermal insulator, given its heat-transport rate is extremely small compared to liquid water and hydrate. In practice, this would mean that kinetic rate of this mechanism will be determined by the rate of liquid-state mass transport. This will be in contrast to a second, much slower mechanism, whose rate is proprotional to that of solid-state transport of molecules through hydrate.

We have applied a PFT developed and discussed in more detail through our previous studies[14–21] to investigate and analyze these complex hydrate phase transitions. Three examples of square 2-D model systems identical in size (5000 Å × 5000 Å) and having the same initial spherical CH_4 hydrate core (radius of 1136 Å) but differing in water film thickness around the hydrate core have been simulated to illustrate our approach. The initial conversion process has proven to be fast in all three systems as expected, since this stage is dominated by rapid formation of new CO_2 hydrate and subsequent dissociation of CH_4 hydrate facilitated by released heat of formation. The thickness of the water film was shown to strongly affect the rate of exchange, which increased with the thickness. The availability of free water facilitates the formation of new CO_2 hydrate, which results in release of heat and, therefore, promotes a faster dissociation of initial CH_4 hydrate core, eventually raising the exchange rate. After the free water has been consumed, the exchange rate is governed by solid-state transport, with all three systems observed to reach the same asymptotic limit accordingly.

ACKNOWLEDGMENTS

The authors acknowledge the grant and support from Research Council of Norway through the following projects: SSC-Ramore, "Subsurface storage of CO_2 - Risk assessment, monitoring and remediation", Research Council of Norway, project number: 178008/I30, FME-SUCCESS, Research Council of Norway, project number: 804831, PETROMAKS, "CO_2 injection for extra production", Research Council of Norway, project number: 801445, STATOIL through contract 4502354080 and Research Council of Norway, project number: 224857.

Literature Cited

1. Tsuji Y, Fujii T, Hayashi M, Kitamura R, Nakamizu M, Ohbi K, Saeki T, Yamamoto K, Namikawa T, Inamori T, Oikawa N, Shimizu S, Kawasaki M, Nagakubo S, Matsushima J, Ochiai K, Okui T. Methane-hydrate occurrence and distribution in the eastern Nankai trough, Japan: findings of the Tokai-oki to Kumano-nada methane-hydrate drilling program. In: T. Collett, A. Johnson, C. Knapp, and R. Boswell, editors. *Natural Gas Hydrates – Energy Resource Potential and Associated Geologic Hazards*. AAPG Memoir 89. 2009:228–249.
2. Boswell R, Collett TS. Current perspectives on gas hydrate resources. *Energy Environ Sci*. 2011;4:1206–1215.
3. Boswell R, Collett T, McConnell D, Frye M, Shedd B, Mrozewski S, Guerin G, Cook A, Godfriaux P, Dufrene R, Roy R, Jones E. *Joint Industry Project Leg II Discovers Rich Gas Hydrate Accumulations in Sand Reservoirs in the Gulf of Mexico, Fire in the Ice*, US Department of Energy, Office of Fossil Energy. National Energy Technology Laboratory. 2009;9:1–5.
4. Lee MW, Collett TS. In-situ gas hydrate hydrate saturation estimated from various well logs at the Mount Elbert Gas Hydrate Stratigraphic Test Well, Alaska North Slope. *Mar Petroleum Geol*. 2011;28:439–449.
5. Torres ME, Collett T, Rose K, Sample JC, Agena W, Rosenbaum E. Pore fluid geochemistry from the Mount Elbert Gas Hydrate Stratigraphic Test Well, Alaska North Slope. *Mar Petroleum Geol*. 2011;28:332–342.
6. Dai S, Lee C, Santamarina JC. Formation history and physical properties of sediments from the Mount Elbert Gas Hydrate Stratigraphic Test Well, Alaska North Slope. *Mar Petroleum Geol*. 2011;28:427–438.
7. Michael DM, Arthur HJ, Villiam PD. *Economic Geology of Natural Gas Hydrate*. Dordrecht: Springer, 2006.
8. Kvamme B, Tanaka H. Thermodynamic stability of hydrates for ethane, ethylene, and carbon dioxide. *J Phys Chem*. 1995;99:7114–7119.

9. Shpakov VP, Tse JS, Kvamme B, Belosludov VR. Elastic moduli calculation and instability in structure I methane clathrate hydrate. *Chem Phys Lett*. 1998;282:107–114.
10. Koh C, Sloan ED. *Clathrate Hydrates of Natural Gases; Chemical Industries*, 3rd ed. CRC Press/Taylor & Francis, 2008.
11. Kvamme B. Initiation and growth of hydrate from nucleation theory. *Int J Offshore Polar Eng*. 2002;12:256–262.
12. Kvamme B. Droplets of dry ice and cold liquid CO_2 for self transport to large depths. *Int J Offshore Polar Eng*. 2003;13:1–8.
13. Kvamme B, Kuznetsova T, Kivelæ PH. Adsorption of water and carbon dioxide on Hematite and consequences for possible hydrate formation. *Phys Chem Chem Phys*. 2012;14:4410–4424.
14. Qasim M, Kvamme B, Baig K. Phase field theory modeling of CH_4/CO_2 gas hydrates in gravity fields. *Int J Geol*. 2011;5:48–52.
15. Kvamme B, Baig K, Qasim M, Bauman J. Thermodynamic and kinetic modeling of CH_4/CO_2 hydrates phase transitions. *Int J Energy Environ*. 2013;7:1–8.
16. Svandal A. Modeling Hydrate Phase Transitions Using Mean-field Approaches, PhD Thesis, University of Bergen, 2006.
17. Kvamme B, Svandal A, Buanes T, Kuznetsova T. Phase field approaches to the kinetic modeling of hydrate phase transitions. *AAPG Memoir*. 2009;89:758–769.
18. Tegze G, Grαnαsy L. Phase field simulation of liquid phase separation with fluid flow. *Mater Sci Eng*. 2005;413–414:418–422.
19. Kvamme B, Graue A, Aspenes E, Kuznetsova T, Grαnαsy L, Tóth G, Pusztai T, Tegze G. Kinetics of solid hydrate formation by carbon dioxide: phase field theory of hydrate nucleation and magnetic resonance imaging. *Phys Chem Chem Phys*. 2004;6:2327–2334.
20. Tegze G, Grαnαsy L, Kvamme B. Phase field modeling of CH_4 hydrate conversion into CO_2 hydrate in the presence of liquid CO_2. *Phys Chem Chem Phys*. 2007;9:3104–3111.
21. Kvamme B, Graue A, Buanes T, Kuznetsova T, Ersland G. Storage of CO_2 in natural gas hydrate reservoirs and the effect of hydrate as an extra sealing in cold aquifers. *Int J Greenhouse Gas Control*. 2007;1:236–246.
22. Cuong PV, Kvamme B, Kuznetsova T, Jensen B. The impact of short-range force field parameters and temperature effect on selective adsorption of water and CO_2 on calcite. *Int J Energy Environ*. 2012;6:301–309.
23. Cuong PV, Kvamme B, Kuznetsova T, Jensen B. Molecular dynamics study of calcite and temperature effect on CO_2 transport and adsorption stability in geological formations. *Mol Phys*. 2012;110:1097–1106.
24. Lee H, Seo Y, Seo YT, Moudrakovski IL, Ripmeester JA. Recovering methane from solid methane hydrate with carbon dioxide. *Angew Chem Int Ed*. 2003;42:5048–5051.
25. Kuznetsova T, Kvamme B, Morrissey K. An alternative for carbon dioxide emission mitigation: in situ methane hydrate conversion. *AIP Conf Proc*. 2012;1504:772–775.
26. The U.S. Department of Energy's National Energy Technology Laboratory (NETL). Ignik Sikumi Gas Hydrate Field Trial 2012. Available at: http://www.netl.doe.gov/research/oil-and-gas/methane-hydrates/co2_ch4exchange. Accessed September 25, 2014.
27. van der Waals JH, Platteeuw JC. Clathrate solutions. *Adv Chem Phys*. 1959;2:1–57.
28. Reid RC, Prausnitz JM, Sherwood TK. *The Properties of Gases and Liquids*, 3rd ed. McGraw-Hill, 1977.
29. Kvamme B, Kuznetsova T, Kivelæ PH, Bauman J. Can hydrate form in carbon dioxide from dissolved water? *Phys Chem Chem Phys*. 2013;15:2063–2074.
30. Soave G. Equilibrium constants from a modified Redlich-Kwong equation of state. *Chem Eng Sci*. 1972;27:1197–1203.
31. Coutinho JAP, Kontogeorgis GM, Stenby EH. Binary interaction parameters for nonpolar systems with cubic equations of state—a theoretical approach. 1. CO_2 hydrocarbons using SRK equation of state. *Fluid Phase Equilib*. 1994;102:31–60.
32. Sander R. Modeling atmospheric chemistry: interactions between gas-phase species and liquid cloud/aerosols particles. *Surv Geophys*. 1999;20:1–31.
33. Li JCM. Clapeyron equation for multicomponent systems. *J Chem Phys*. 1956;25:572–574.
34. Zheng DQ, Guo TM, Knapp H. Experimental and modeling studies on the solubility of CO_2, $CHCLF_2$, CHF_3, $C_2H_2F_4$ and $C_2H_4F_2$ in water and aqueous NACL solutions under low-pressures. *Fluid Phase Equilib*. 1997;129:197–209.
35. Kavanaugh MC, Trussell RR. Design of aeration towers to strip volatile contaminants from drinking water. *J Am Water Works Assoc*. 1980;72:684–692.
36. Svandal A, Kuznetsova T, Kvamme B. Thermodynamic properties and phase transitions in the H2O/CO2/CH4 system. *Fluid Phase Equilib*. 2006;246:177–184.
37. Conti M. Solidification of binary alloys: thermal effects studied with the phase-field model. *Phys Rev A*. 1997;55:765–771.
38. Conti M. Thermal and chemical diffusion in the rapid solidification of binary alloys. *Phys Rev E*. 2000;61:642–650.
39. Kvamme B, Svandal A, Buanes T, Kuznetsova T. *Phase Field Approaches to the Kinetic Modeling of Hydrate Phase Transitions*, Vancouver, BC, Canada, September 12–16, 2004.
40. Wheeler AA, Boethinger WJ, McFadden GB. Phase field model for isothermal phase transitions in binary alloys. *Phys Rev A*. 1992;45:7424–7439.
41. Gránásy L, Pusztai T, Jurek Z, Conti M, Kvamme B. Phase field theory of nucleation in the hard sphere liquid. *J Chem Phys*. 2003;119:10376–10382.
42. Gránásy L, Pusztai T, Börzsönyi T, Warren JA, Kvamme B, James PF. Nucleation and polycrystalline solidification in binary phase field theory. *Phys Chem Glasses*. 2004;45:107 - 115.
43. Tegze G, Pusztai T, Tóth G., Gránásy L, Svandal A, Buanes T, Kuznetsova T, Kvamme B. Multiscale approach to CO_2 hydrate formation in aqueous solution: phase field theory and molecular dynamics. Nucleation and growth. *J Chem Phys*. 2006;124:234710.
44. Gránásy L, Börzsönyi T, Pusztai T. Nucleation and bulk crystallization in binary phase field theory. *Phys Rev Lett*. 2002;88:206105–206108.
45. Gránásy L, Pusztai T. Diffuse interface analysis of crystal nucleation in hard-sphere liquid. *J Chem Phys*. 2002;117:10121–10124.
46. M. Conti. Density change effects on crystal growth from the melt. *Phys Rev E*. 2001;64:051601.
47. Conti M, Fermani M. Interface dynamics and solute trapping in alloy solidification with density change. *Phys Rev E*. 2003;67:026117.
48. Conti M. Advection flow effects in the growth of a free dendrite. *Phys Rev E*. 2004;69:022601.
49. Circone S, Stern LA, Kirby SH, Durham WB, Chakoumakos BC, Rawn CJ, Rondinone AJ, Ishii Y. CO_2 hydrate: synthesis, composition, structure, dissociation behavior, and a comparison to structure I CH_4 hydrate; Lawrence Livermore National Laboratory. *J Phys Chem*. 2003;107:5529–5539.
50. Qasim M, Baig K, Kvamme B, Bauman J. Mix hydrate formation by CH_4-CO_2 exchange using phase field theory with implicit thermodynamics. *Int J Energy Environ*. 2012;6:479–487.
51. Qasim M. Microscale Modeling of Natural Gas Hydrates in Reservoirs, PhD Thesis, University of Bergen, 2013.
52. Haq BU. 1998. Natural gas hydrates: searching for the long-term climatic and slope-stability records. In: J.-P. Henriet and J. Mienert, editors. *Gas Hydrates: Relevance to World Margin Stability and Climate Change. Geological Society*, London, Special Publications, 137:303–318.
53. Mu D, Liu ZS, Huang C, Djilali N. Determination of the effective diffusion coefficient in porous media including Knudsen effects. *Microfluidics Nanofluidics*. 2008;4:257–260.
54. Adeyemo A, Kumar R, Linga P, Ripmeester J, Englezos P. Capture of carbon dioxide from flue or fuel gas mixtures by clathrate crystallization in a silica gel column. *Int J Greenhouse Gas Control*. 2010;4:478–485.
55. Kvamme B, Qasim M, Baig K, Kivelä PH, Bauman J. Hydrate phase transition kinetics from phase field theory with implicit hydrodynamics and heat transport. *Int J Greenhouse Gas Control*. 2014;29:263–278.
56. Asgeirsson LS, Ghajar AJ. Prediction of thermal conductivity and viscosity for some fluids in the near-critical region. *Chem Eng Commun*. 1986;43:165–184.
57. Sharqawy MH, Lienhard VJH, Zubair SM. Thermophysical properties of seawater: a review of existing correlations and data. *Desalination Water Treat*. 2010;16:354–380.
58. Todd B, Young JB. Thermodynamic and transport properties of gases for use in solid oxide fuel cell modelling. *J Power Sources*. 2002;110:186–200.

Appendix

Heat flux profile is calculated using the conduction equation:

$$\frac{q}{A} = -k\Delta T$$

$$\vec{q} = -(T_{t+dt} - T_t)\sum\nolimits_{i=\mathrm{CH_4},\mathrm{CO_2},\&\mathrm{water}} x_i k_i$$

where $\vec{q}$ is the heat flux in units W/m^2. k_i is the thermal conductivity of component i in W/mK and subscript i represents

components CO_2, CH_4, and H_2O. ΔT is the change in temperature at different time in kelvin (K) and x_i is the mole fraction of component i and subscript i represents components CO_2, CH_4, and H_2O.

A1: Thermal conductivity of liquid CO_2[56]

$$k_{CO_2} = a_1+b_1\rho+c_1\rho^2+d_1\rho^3+e_1\left[T^*\left(1+\frac{0.9\rho^{*^{2.86}}}{T^*}\right)\right]^{-0.6}\rho_r^{0.5} \tag{A1}$$

where

$$a_1 = -4.406180\times10^{-2}$$
$$b_1 = 5.981447\times10^{-4}$$
$$c_1 = -1.331925\times10^{-6}$$
$$d_1 = 1.022006\times10^{-9}$$
$$e_1 = 2.739334\times10^{-3}$$
$$T^* = |\frac{T-T_c}{T_c}|$$
$$\rho^* = |\frac{\rho-\rho_c}{\rho_c}|$$

T, is the temperature in kelvin (K)
The critical temperature of CO_2, $T_C = 304.21\ (K)$
The critical density of CO_2, $\rho_c = 4.64\times10^2\left(\frac{kg}{m^3}\right)$
The reduced density, $\rho_r = 0.95$,
ρ, is the liquid CO_2 density in kg/m^3

A2: Thermal conductivity of pure water[58]

$$k_{H_2O} = \sum_{i=1}^{4} a_i\left(\frac{T}{300}\right)^{b_i} \tag{A2}$$

where

$$a_1 = 0.80201$$
$$a_2 = -0.25992$$
$$a_3 = 0.10024$$
$$a_4 = -0.032005$$
$$b_1 = -0.32$$
$$b_2 = -5.7$$
$$b_3 = -12$$
$$b_4 = -15$$

T, is the temperature in kelvin (K)

A3: Thermal conductivity of CH_4[58]

$$k_{CH_4} = 0.01\sum_{i=0}^{6} c_i\tau^i \tag{A3}$$

where

$$c_0 = 0.4796$$
$$c_1 = 1.8732$$
$$c_2 = 37.413$$
$$c_3 = -47.440$$
$$c_4 = 38.251$$
$$c_5 = -17.283$$
$$c_6 = 3.2774$$
$$\tau = \frac{T}{1000}$$

T, is the temperature in kelvin (K)

Manuscript received Sep. 29, 2014, and revision received May 7, 2015.